Synthetic and structural aspects of unsaturated organic ligands

Ooi, Li-Ling

Award date:
2003

Awarding institution:
University of Bath

SYNTHETIC AND STRUCTURAL ASPECTS OF UNSATURATED ORGANIC LIGANDS

submitted by Li-ling Ooi

for the degree of PhD

of the University of Bath

2003

ProQuest LLC
789 East Eisenhower Parkway
P.O. Box 1346
Ann Arbor, MI 48106-1346

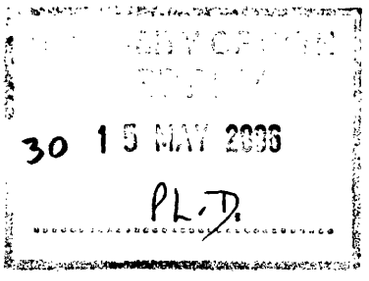
30 15 MAY 2006
PL.D.

Abstract

The first two chapters primarily review and discuss the background and applications of single crystal X-ray crystallography and microwave-assisted synthetic methods, both being the underlying techniques of this work.

Chapter 1 details single crystal X-ray crystallography from the initial discovery of X-rays to the background theory and applications of X-rays in crystallography. Synchrotron radiation and discussions on solid state interactions such as hydrogen bonding and graphitic packing are also included in this chapter.

Microwave-assisted synthesis in Chapter 2 is on the background, theory, development and applications of microwaves in the area of chemical synthesis.

Chapter 3 is broadly divided in to two parts; the first is on the background, results and discussions on the reactions of $Os_3(\mu\text{-}H)_2(CO)_{10}$ with some unsaturated alkyne ligands which affect novel cyclisations in the ligand while the second part concentrates on the microwave-assisted synthesis of some high nuclearity ruthenium clusters.

The chemistry of 2,2':6'2''-terpyridine is detailed in Chapter 4, including a section on solid-state luminescence measurements and a structural study on a new polymorph of 2,2':6'2''-terpyridine.

The reactions of the lanthanides with a variety of unsaturated nitrogen heterocycles (2,2':6'2''-terpyridine, 2,4,6-tris(2-pyridyl)-1,3,5-triazine and 1,10-phenanthroline) are discussed in Chapter 5. The structural variety of the lanthanide complexes observed across the series are also based on the varying configurations of the counterions (thiocyanates, nitrates and mixed thiocyanate-nitrates). Also included in this chapter are solid-state luminescence studies on some of the lanthanide complexes and a discussion on some coordination polymers of La^{3+} synthesised during the course of this work.

Chapter 6 details the experimental techniques and synthetic methods by which the results of the preceding chapters are obtained.

The Appendices consist of the crystal structure data, other crystals solved as part of the X-ray service and a list of publications to date.

Acknowledgements

A multitude of thanks and most heartfelt gratitude to my supervisor Prof. Paul R. Raithby, whose untiring support, never-ending patience and seemingly never-ending belief in me has made all this work and very much more possible.

Many many thanks to members of the Raithby group, past and present, who have made my time at Bath truly memorable. Special thanks to Louise and Hazel for the many unforgettable afternoon tea breaks, long meaningful conversations and 'favourite' Daresbury trips – couldn't have done it without you both!

A very big thank you is due to Dr Mary F. Mahon for her endless support, help and advice and to Dr Simon J. Teat for the many long late nights and wonderfully distracting pool games at Daresbury and many thanks also to Dr Simon A. Cotton from Uppingham School for synthesising some of the lanthanide crystals and for valuable discussions.

I am also profoundly grateful to my family for their indefatigable support and encouragement and to Jin Aik – without you the days would be a lot longer and much more dreary and I would probably talk to myself a lot more.

List of Tables

List of Figures

List of Structures I

Crystal structures discussed in Chapter 3: Ruthenium and Osmium Carbonyl Clusters

No.	Molecular Formula	Molecular Structure	Crystal Code
1	$Os_3(\mu\text{-}H)(CO)_{10}\{(\mu\text{-}\eta\text{-}(C_4H_3S)(C_8H_4S)\}$	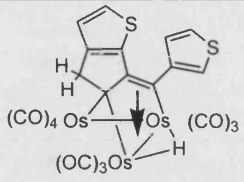	h01prr5
2	$Os_3(\mu\text{-}H)(CO)_9\{(\mu_3\text{-}\eta^3\text{-}(C_4H_3S)(C_8H_4S)\}$	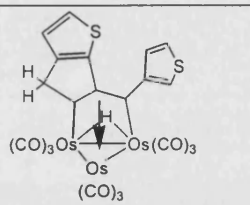	K01prr36
3	$Os_3(\mu\text{-}H)(CO)_{10}\{(\mu\text{-}\eta\text{-}(C_4H_3S)(C_8H_4S)\}$	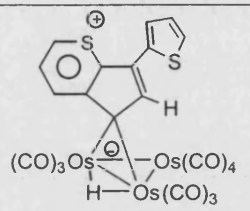	Lpc 2.36c
4	$Os_3(\mu\text{-}H)(CO)_{10}\{(\mu_3\text{-}\eta^2\text{-}\eta^1\text{-}\eta^1\text{-}(SC_7H_4)C(SC_4H_3)\}$	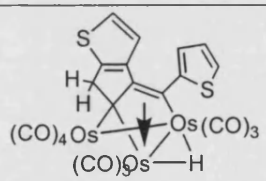	Lpc 2.36a
5	$Os_3(\mu\text{-}H)(CO)_9\{(\mu_3\text{-}\eta^3\text{-}(C_4H_3S)(C_8H_4S)\}$	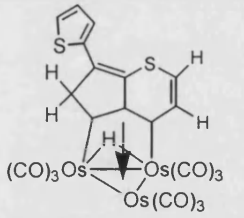	K01prr62
6	$Os_3(\mu\text{-}H)_2(CO)_9\{(\mu_3\text{-}\eta^1\text{-}\eta^1\text{-}(C_4H_3S)(C_8H_3S)\}$	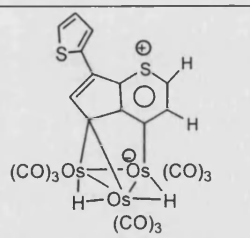	K02prr3
7	$Os_3(\mu\text{-}H)(CO)_9\{(\mu_3\text{-}\eta^3\text{-}(C_4H_3S)(C_8H_4S)\}$	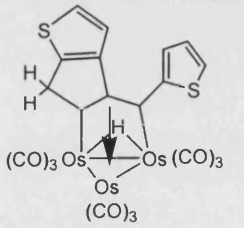	K02prr1

8	$Os_3(\mu\text{-}H)(CO)_{10}(O_2CCF_3)$	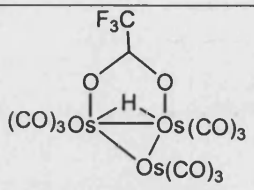	K01prr61
9	C14 H7 F3 O S2	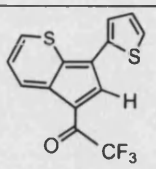	Bath 34
10	$Ru_6(\mu_6\text{-}C)(\mu\text{-}CO)(CO)_{13}[\eta^6\text{-}(C_6H_5)CH_3]$	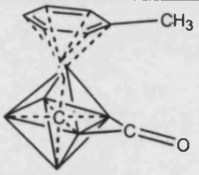	K02prr21
11	$Ru_6(\mu_6\text{-}C)(CO)_{17}$	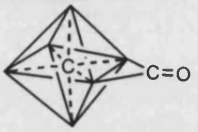	K03prr5
12	$Ru_3(\mu_2\text{-}CO)_2(CO)_8(bipy)$	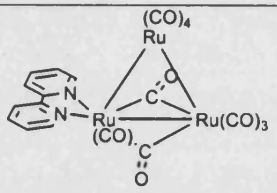	H03prr7

List of Structures II

Crystal structures discussed in Chapter 5: The Rare Earths

No.	Molecular Formula	Crystal Code
1	$La(terpy)(NCS)_3(MeOH)_3.2MeOH$	H01prr14
2	$La(terpy)_2(NCS)_3.MeOH$	H01prr12
3	$Nd(terpy)_2(NCS)_3$	Bath 41
4	$Eu(terpy)_2(NCS)_3$	K01prr13
5	$Eu(terpy)_2(NCS)_3.MeOH$	K01prr16
6	$[Er(terpy)_2(NCS)_2]^+[Er(terpy)(NCS)_4]^-.2EtOH$	K03prr12
7	$Ce(tptz)(NO_3)_3(H_2O).EtOH$	K01prr20
8	$Lu(tptz)(NO_3)_3(H_2O).EtOH$	H01prr24
9	$[Lu(tptz)(NO_3)_3.H_2O]. MeCN$	K02prr5
10	$[Lu(tptz)(NO_3)_3.(H_2O)_2]^+(NO_3)^-. 3MeOH$	K02prr15
11	$Ce(phen)_3(NCS)_3.EtOH$	H01prr11
12	$Dy(phen)_2(NCS)_3.EtOH](phen)$	H01prr10
13	$Tb(phen)_2(NCS)_2(NO_3)(MeOH)$	K01prr9
14	$Er(phen)_2(NCS)(NO_3)_3$	H02prr9
15	$Er(phen)_2(NO_3)_3$	H02prr1
16	$Pr(phen)_2(NO_3)_3$	K02prr7
17	$[La(O_2CPh)_3(CH_3OH)_3(H_2O)]_n$	Bath31
18	$[La(O_2CPh)_3(H_2O)_2.bipy]_n$	Bath 29

Table of Contents

CHAPTER I

PRINCIPLES OF X-RAY CRYSTALLOGRAPHY

1.0 Principles of X-Ray Crystallography

X-ray crystallography is a characterisation technique that helps to determine the molecular structure of a compound in the solid state. 'Structure' in this sense means the relative positions of the atoms or ions which make up the substance under study *i.e.* a geometrical description of bond lengths and angles, torsion angles, non-bonded distances and other quantities of interest.[1]

A crystal is made up molecular units in a regular arrangement repeated throughout the crystal in three dimensions. Discrete diffraction spots are a result of X-rays interacting with the molecular contents of the crystal when this regular three-dimensional array is present.

1.1 Discovery and Use of X-rays in Crystallography

X-rays were first discovered by W.C. Röntgen in 1895 as part of an experimental study on cathode-rays. However it was not until 1912, that Laue enlisted the help of two experimental physicists, Friedrich and Knipping to conduct an experiment on the diffraction of X-ray beams by crystals.[2]

The question of whether X-ray beams were waves or particles was one that baffled the physicists then. With their experiment, Laue, Friedrich and Knipping managed to prove that X-rays were waves while at the same time studying how radiation behaved through crystals. With the later development of quantum theory, it is now known that radiation can also behave as particles, and wave/ particle duality is allowed by this theory.

Although it was then known that X-rays were waves, the scientists could not explain the entire diffraction pattern that was recorded on the film placed opposite the source of the X-rays.

1.1.1 Laue Diffraction

The idea that X-rays could behave as waves was shown in the analogy that electron density in an atom is able to scatter X-rays in the fashion of wave fronts generated from slits in a grating.[3] The diffraction spots are a result of constructive interference while the empty space surrounding the spots is a product of destructive interference.

Von Laue's experiment showed that it was possible to obtain a diffraction pattern from a single stationary crystal using a wide range of wavelengths simultaneously.

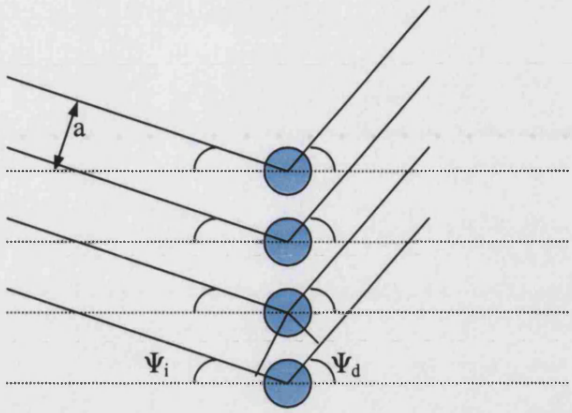

Figure 1.1.1 Representation of the Laue diffraction in one dimension

A one dimensional representation (Figure 1.1.1) shows that for X-rays to be scattered by two adjacent points, the path difference:

$$(a \sin\psi_i + a \sin\psi_d) = h\lambda$$

where ψ_i is the angle of the incident beam and ψ_d is the angle of the diffracted beam, a is the lattice spacing comparable to the wavelength λ, and h is the integer corresponding to the value of a.[4]

However, in three dimensions, three such equations (also known as the Laue conditions) need to be fulfilled where if a is an axis of the unit cell corresponding to h, then the cell axes b and c are relative to k and l respectively.

1.1.2 Bragg's Equation

W.H. Bragg is credited with the explaining diffraction images with a simple model. Braggs' theory was that in an appropriate orientation of a crystal, the X-ray beam can be reflected from planes through the crystal. These sets of planes are of equal distance apart and these distances are related to the size of the repeating unit in the crystal.[2]

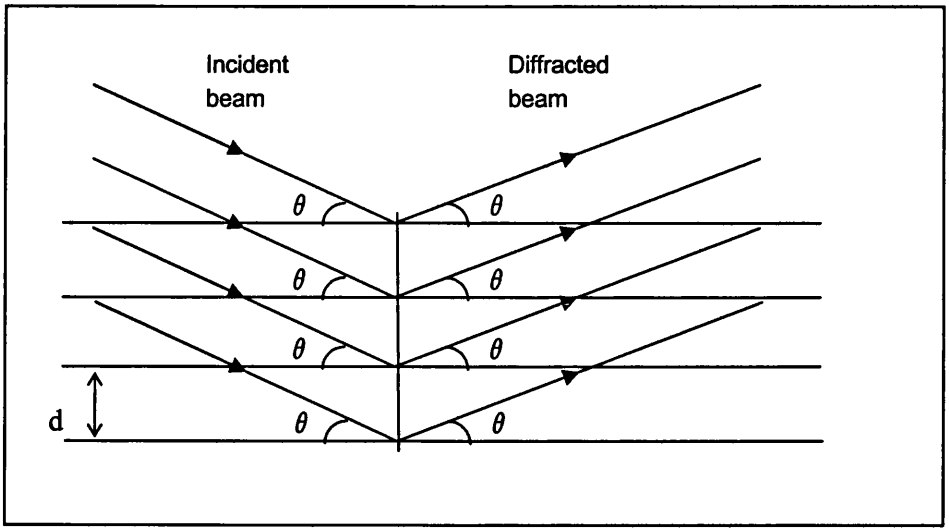

Figure 1.1.2 Bragg diffraction of x-ray beams by planes in a crystal.[2]

The angles at which diffraction takes place is explained by the Bragg equation:

$$n\lambda = 2d \sin \theta$$

In the equation, λ is given by the wavelength of the X-ray beam while *d* is the distance between the planes and θ is the angle at which the incident beam reaches the plane and is reflected again. This angle is also known as the Bragg angle, while n is the number of waves scattered by successive elements in the crystal plane.

Based on Bragg's idea, the incidence beam of a fixed wavelength X-ray will be reflected by planes in the crystal. The planes referred to in Bragg's theory are made up of planes passing through the atoms in a crystal. However, it is only in certain orientations that the waves from the X-ray will reinforce each other (i.e. satisfy the equation) while in other orientations they will not,[5] and it is this constructive and destructive interference that will produce a diffraction pattern of light and dark spots (reflections) on a film or a detector.

It should be remembered, however that Bragg's Law is a simplification of the process that occurs when x-rays interact with crystals. The true process is the diffraction of X-rays by the electron clouds around the atoms and not reflections from planes in the crystals.

1.2 Crystals and Crystal systems

Crystals of a particular element or compound tend to display a similar external morphology, with the same combination of plane faces and constant relative size, shapes and orientations.[6] Internally, crystals are made up of regular arrangements of small parallelapipeds, the concept of the *unit cell.*[2]

1.2.1 The Unit Cell and Bravais Lattices

The unit cell can be defined as the smallest repeating unit in a crystal. For any given array, a number of different choices for a unit cell may be made, however in practice, the simplest packing with angles closest to 90° is chosen and one that uses all the available symmetry of the lattice.

The unit cell is defined geometrically by the lengths of its edges, unit cell axes *a, b* and *c* and interaxial angles α (between *b* and *c*), β (between *a* and *c*) and γ (between *a* and *b*). Translational repetition of the unit cell in three dimensions generates the crystal lattice.[2] The unit cell is also considered to have lattice points at the eight vertices of the parallelepiped.

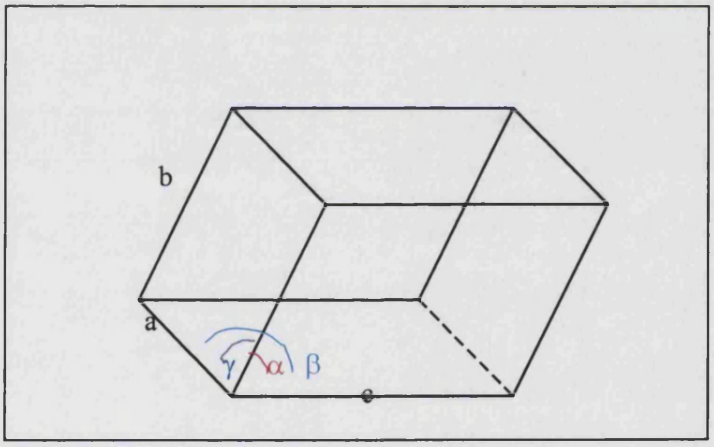

Figure 1.2.1 The unit cell

Due to constraints to the number of possible arrangements of the repeating parallelepipeds in three dimensions, only a certain number of symmetry combinations are possible when variations in unit cell lengths and angles are considered resulting in the 7 different crystal systems. This together with the various forms of centring in a lattice gives rise to the 14 different possible unit cell arrangements known as the Bravais lattices.

	Crystal System	Axes and Angles	Centering/ lattice types
1.	Cubic	a=b=c, $\alpha=\beta=\gamma$	P (primitive)
			I (body centred)
			F (face centred)
2.	Hexagonal	a=b≠c, $\alpha=\beta=90^\circ$ $\gamma=120^\circ$	P (primitive)
3.	Trigonal/ rhombohedral	a=b=c, $\alpha=\beta$ $\gamma\neq90^\circ$	P (primitive)
4.	Tetragonal	a=b≠c, $\alpha=\beta=\gamma$	P (primitive)
			I (body centred)
5.	Orthorhombic	a≠b≠c, $\alpha=\beta=\gamma=90^\circ$	P (Primitive)
			I (body centred)
			C (end centred)
			F (face centred)
6.	Monoclinic	a≠b≠c, $\alpha=\beta=90^\circ$ $\gamma\neq90^\circ$	P (primitive)
			C (end centred)
7.	Triclinic	a≠b≠c, $\alpha\neq\beta\neq\gamma\neq90^\circ$	P (primitive)

Table 1.2.1 The 7 crystal systems and 14 bravais lattices.

1.2.2 Symmetry Elements and Space Groups

Symmetry elements relate the ordered molecules in a crystal lattice to each other by means of internal symmetry. The three types of symmetry elements are centre of symmetry, an axis of symmetry (rotation axes) and a plane of symmetry (mirror planes).[2] Glide planes and screw axes also occur as a result of translational symmetry combined with either reflection or rotation.

The lattices must conform to the symmetry of the crystal and these possible symmetry combinations give rise to 230 *space groups*.

1.3 The Reciprocal Lattice

The lattice of the diffraction pattern is, by mathematical relationship, the reciprocal of the lattice of the original scattering object, in this case the atoms in the crystal.

The relationship between the crystal lattice vectors and the reciprocal lattice is simply that the reciprocal lattice is the resultant translation, perpendicular to that of the 'real' crystal while its lengths are all inversely proportional to that of the 'real' crystal as well.[3]

If the starred values are that of the reciprocal then:
$a.a^* = b.b^* = c.c^* = 1$

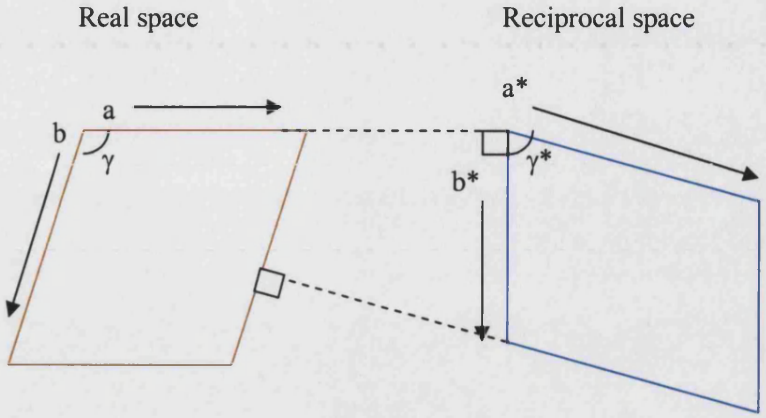

Figure 1.3.1 The relationship between real space and reciprocal space

1.4 Structure Factors and Their Relationship to the Phase Problem

X-rays are composed of many continuous individual waves. The phase relationship between these waves is maintained even when the scattering is affected by the electron density in the crystals. The amplitude of the beam can be found by a summation of the individual waves scattered in a particular direction while taking in to account their relative phases relative to an arbitrary origin.[3]

The relationship between the intensity of the X-rays and amplitude is given by

$$I \propto A^2$$

where I is intensity and A is the amplitude.

Each diffraction spot on a diffraction map consists of a combination of amplitude and phases and this is known as the structure factor, symbolised by F or F(hkl). In the case of atomic scattering, the intensity, I is also proportional to the square of the amplitude represented by $|F|^2$, where each value of |F| consists of a contribution from every atom in the unit cell. The structure factor is in essence a convolution of the electron density.

[*hkl* indices are also known as the Miller indices]

The phase problem arises because while it is possible to obtain structure factor amplitude, it is not the case with the relative phases or the phase angle, α.

Methods applied to solving the phase problem works by either deriving a trial structure or by calculating the approximate values of α for each reflection or by trying to find α directly (i.e. the Direct methods or the Patterson methods). It has been found that an electron density map is much more dependent on phase angles than on structure factor amplitudes and therefore it is more important to have correct phase angles than structure amplitudes.

Prior to the development of the Fourier method in crystal structure solution (*circa* 1930) each crystal was considered a problem of its own and had to be solved individually.[2]

The Fourier series consists essentially of converting a continuous wave function in to discrete values. It can be used to obtain an image of the contents of a crystal in three dimensions. The derivation of calculated amplitudes $|F_c|$ from the Fourier synthesis can be then directly compared with the observed amplitudes $|F_o|$. However, no such comparison can be made for the calculated phases.

The relationship between the structure factors and the actual scattering matter is represented by

$$\rho(xyz) = 1/V_c \sum_{\text{all hkl}} \Sigma \Sigma F(hkl)\exp[-2\pi i(hx + ky + lz)]$$

where $\rho(xyz)$ is the number of electrons per unit volume at any point x,y,z, V_c is the volume of the unit cell and F(hkl) is the structure factor for a particular set of indices.

1.4.1 Direct Methods

The direct methods approach to solving a crystal structre relies upon selecting the most important reflections in a diffraction pattern and working out the possible phase relationships between them.[1] From the best combinations, the Fourier transforms are calculated from the observed amplitudes and the trial phases. The Fourier map is then examined for recognisable features.[1]

Direct methods are based on the principle that as the intensities of reflections contain structural information (both amplitudes and phases) the electron density in a crystal cannot be negative and that the electron density is zero or close to zero except at actual atomic positions.

In three dimensions, this principle can be represented by

$$S(h_1k_1l_1)\, S(h_2k_2l_2) \approx S(h_1+h_2,\, k_1+k_2,\, l_1+l_2)$$

where S means "the sign of".

Phase determination is then carried out on "normalised structure factors", E, which is represented by

$$E \propto \frac{F}{\sqrt{\Sigma_i f_i}}$$

$$E \alpha \frac{F}{\sqrt{\Sigma f_i}}$$

where F is modified to take in to account the fall-off in individual scattering factors, f with the increasing scattering angle 2θ.

A statistical analysis of E values is then used to determine if the structure is centrosymmetric or non-centrosymmetric. This is then followed with the calculation of |E| values and the probability aspects of this |E| value being either positive or negative. Finally, a calculation of the E map enables the structure to be made out. The direct methods structure solution works best with structures that normally do not contain heavy atoms.

1.4.2 Patterson Synthesis

Although the Fourier transform gives the correct electron density map, it requires knowledge of the phases of all the reflections. The *Patterson synthesis* however uses the squared amplitudes which results in all the phases being zero. This produces the *Patterson map.*

Although the Patterson map looks like an electron density map, the peaks of electron density does not provide the actual positions of atoms in the structure, rather the Patterson map is a map of vectors between pairs of atoms in a structure.[1] The Patterson peaks show where atoms lie relative to each other but not where they lie relative to the origin.

Patterson methods are particularly suited to structures with heavy atoms because the Patterson peaks are proportional to the square of the atomic number of the atoms that contribute to a particular peak and vectors between the heavy atoms dominate the map. Once the heaviest atoms have been found, the rest of the atoms are found in relation to it. This is usually done by computing further Fourier difference maps.

1.5 Structure Refinement

Once some of the atoms have been found, the structure has to 'refined'. This is done by varying the numerical parameters that describe the structure in order to produce the 'best' agreement between the diffraction pattern calculated from the Fourier transform (F_c) and the observed diffraction pattern F_o.[1]

This best agreement is represented by R which generally measure the correctness of he structure. R is represented by:

$$R = \frac{\Sigma\{|F_o| - |F_c|\}}{\Sigma(|F_o|)}$$

Refinement of the structure is based on a statistical model known as the least-squares analysis, which defines the best fit between the two sets of data. Based on the least squares methods, a weighting scheme is used to determine the precision of measurement for each of the reflections.[7]

The weight assigned to each reflection is given by the equation:

$$\omega_i = \frac{1}{\sigma_i^2}$$

where σ_i is the standard deviation and ω_i is the variance. A more consistent way of obtaining σ_i is to make multiple measurements of the same value (reflection). However, as this is not always feasible an alternative weighting function based on plotting the mean of $|\Delta F_c|$ against the mean of $|F_o|$ for groups of reflections of similar magnitudes.[7]

The parameters to be refined are the ones describing the positions and vibrations of the atoms. Each atoms has three positional coordinates, *x, y, and z* and a displacement parameter *U*. A better fit to the collected data can be achieved by using more than one displacement parameter per atom (usually six: one for each axis and three cross-terms). This will allow the atom to vibrate freely by different amounts in different directions.[1] Therefore in total there are nine parameters to be refined for each atom.[7]

1.6 Constraints and Restraints

Constraints and restraints are methods with which certain parameters can be fixed to certain values, particularly to assist with difficult refinements.

A constraint is an exact mathematical relationship, which when applied ensures that not all the parameters can be freely or independently refined. It is absolutely rigid and therefore must be used with care to ensure that they are not inconsistent with the diffraction data. Unsuitable constraints will force other parameters to compensate and thereby introduce inaccuracies to the overall structure. Examples of constraints most commonly used are a) atom site occupancy factors, which, in a disordered structure is summed up to unity and b) the refinement of hydrogen atoms in which a 'riding model' is used to position the hydrogen atoms in an idealised geometry.

A restraint however, is an approximate target value for a particular parameter which can provide some extra information about a structure. It can be treated as an experimental observation and can be used with a weighting scheme applied to determine how closely the target value needs to be met. Restraints are most often applied to geometry and to atomic displacement parameters.

Determining a structure by x-ray crystallography

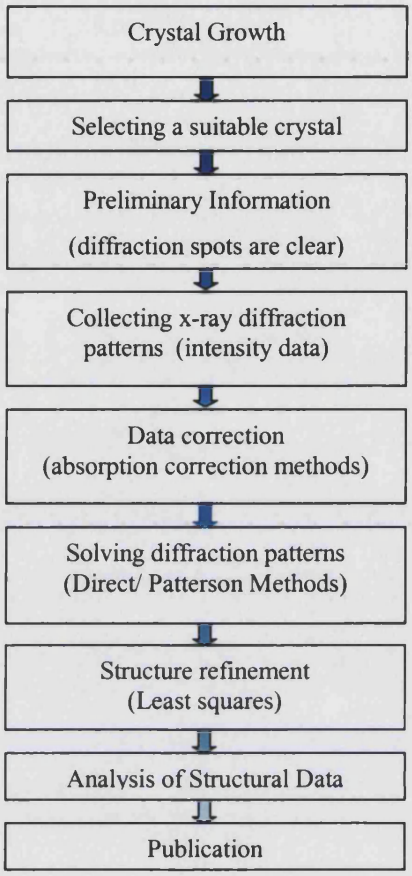

1.7 Data Collection

Nowadays, a vast number of single crystal X-ray diffraction experiments are performed on area detector diffractometers, however, prior to the now popular area detectors, four circle serial diffractometers were used. Area detectors were initially developed for the benefit of protein crystallographers and it was not until the mid-1990s that area detectors in small crystal fields started to take hold.[8] The theoretical applications for both types of diffractometers are based on the same principles of diffraction and Braggs' equation.

The charged-coupled device (CCD) is the type of detector now most commonly used in area detectors. The CCD is most typically used in the video and digital camera systems. It is essentially a semiconductor in which incident radiation produces electron-hole pairs; the electrons are trapped in potential wells and then read out as currents.

In order for data to be collected, the crystal first has to be mounted so that it can be moved and aligned. This is done by mounting the crystal on a goniometer head. The crystal is normally fixed or mounted on to a glass fibre that sits in a pip, fitted in to the top of the goniometer.[7]

Crystal selection and handling is normally carried out under a microscope where the crystals are placed on a glass slide and coated in a perflourinated ether oil. Once a crystal has been selected and mounted, it is then necessary to collect a short series of frames (*ca.* 10 frames). These frames are then used to determine the crystal orientation matrix and the unit cell parameters. It is also necessary to check the mosaic spread and the chi-squares or rocking curves which will be a more accurate measure of whether the crystal is suitable.

Once a single crystal suitable for diffraction is mounted on a diffractometer and held firmly in place, the crystal is rotated in the x-ray beam during the data collection process. Rotation of the crystal ensures that the maximum amount of data is collected, as three-dimensional data is compressed in to two dimensions.

1.8 Single Crystal X-ray Diffraction at the Synchrotron

Although single crystals are now solved routinely and with the development of area detectors, solutions can be obtained within the hour, chemists and crystallographers continuously push the boundaries, increasing the need for greater X-ray intensity.

Chemical crystallography has so far, largely relied on conventional sources of X-rays generators. However with the development of new technology, there has been the introduction of the rotating-anode generators and new forms of X-ray optics which work to focus and concentrate the rays can lead to an increase in the X-ray intensity output. This increase however is not dramatic and ranges from only 1 to 2 orders of magnitude compared to the conventional X-ray tubes.

1.8.1 What is Synchrotron Radiation

Synchrotron radiation was first observed as a by-product of particle accelerations. When particles (electrons and positrons) are accelerated in magnetic fields, electromagnetic radiation, occurring over a wide range of the whole spectrum, is emitted. It was recognised that this electromagnetic radiation could be utilised for many spectroscopic techniques.

Initially synchrotron radiation was exploited 'parasitically' from the particle accelerators designed for high energy physics, however, later, storage rings dedicated to the production of synchrotron radiation were built. Generally, storage rings make use of relativity to convert useless radio frequency energy in to useful electromagnetic waves and X-rays by means of a Doppler shift.[9]

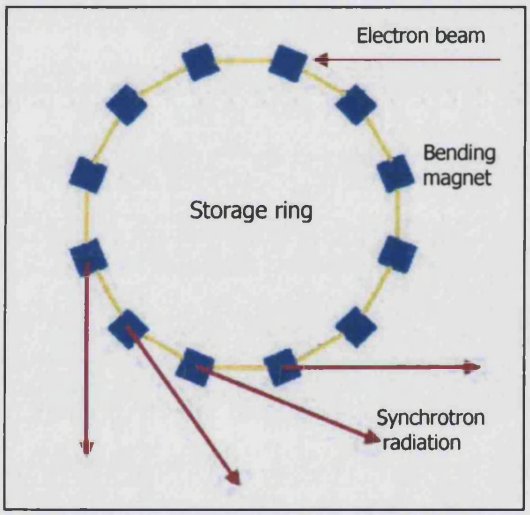

Figure 1.8.1 Schematic representation of a storage ring

A storage ring is essentially a circular arrangement of bending magnets (1.2 Tesla, or more) in which an electron (or positron) beam is made to move in a polygonal path. The electron beam consists of discrete bunches of electrons (not a continuous stream) injected in to the storage ring from a linear accelerator. This electron beam then moves in a high vacuum pipe. However, as the pipe is an imperfect vacuum, with residual gas molecules, this causes a steady decline in synchrotron radiation intensity, leading the beam to need to be 'refilled' with electrons.

As the electrons move through the storage ring, the bending magnets have magnetic fields perpendicular to the plane of the ring. This causes electrons to change directions (subjected to an inward radial acceleration) as they pass through the bending magnets. Electromagnetic radiation (ranging from infra-red to UV-visible to the soft X-ray region) is thus produced at a tangent to the orbit of the storage ring.

While the electromagnetic radiation emitted can be used for many spectroscopic techniques, crystallography requires X-rays for higher energy than that produced by the storage ring. A wiggler (wavelength shifter) is used for the purposes of extending the energy range and increasing the intensity of the electromagnetic radiation emitted. It works by causing extra synchrotron radiation emission from the electron path to 'wiggle' thereby shifting it to a higher photon energy (shorter wavelength). A set of three magnets (of high fields, approximately 5-6 Tesla) deflects the electron beam sending it around a curve then returning it to its original path.

A wiggler is currently in place at Station 9.8 in Daresbury Laboratories at the dedicated single-crystal facility. However, other devices that work in similar manners are multipole wigglers and undulators. Figure 1.8.2 shows the range of photon energy produced by the various devices.

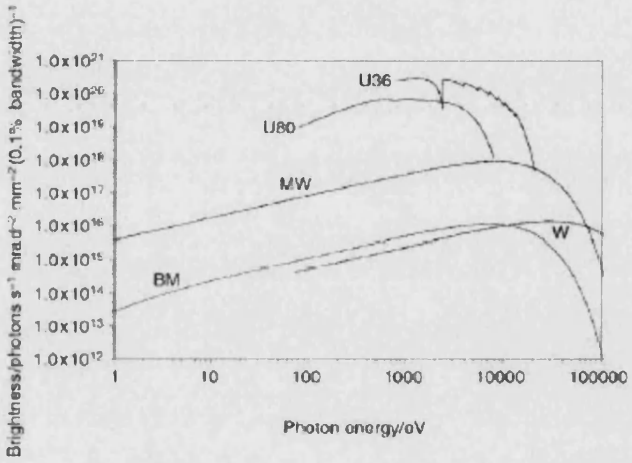

Figure 1.8.2 Synchrotron radiation emitted by various devices; BM: bending magnet; W: wigglers; MW: multipole wiggler; U80 and U36: undulators.[9]

1.8.2 The Need for Synchrotron Data

The challenges in crystallography come mainly from the difficulty in obtaining a sample that diffracts well and often these limitations are caused by small poor quality crystals. This problem is particularly acute in some areas of materials science where samples often include microporous solids and supramolecular assemblies where it is often extremely difficult to produce large enough crystals (1 mm^3) for a lab source of X-rays.

At the synchrotron, the higher flux (number of photos per second in a beam of radiation) and greater brightness and brilliance of the concentrated X-ray beam makes it possible solve the structures of materials that give micron-sized crystals, which on a lab source would not have produced an observable diffraction pattern.

Other advantages of the synchrotron include the availability of a wide range of wavelengths that can be tunable using various monochromators. Silicon or germanium is often used as the standard monochromator at which the wavelength is close to that of molybdenum radiation.

1.9 Polymorphism

A polymorph has been defined as 'a solid crystalline phase of a given compound resulting from the possibility of at least two different arrangements of the molecules of that compound in the solid state'.[10]

Polymorphism is simply known as the ability of a molecule to exist in more than one crystalline form. It is particularly common in organic compounds where different packing possibilities exist from the variations in intermolecular hydrogen bonding. Due to the variation in the physical arrangement of the molecules, the related polymorphs have different physical properties such as melting points, solubilities, hardness and densities.[11]

Although not much is known about the process of crystallisation, two key stages have been identified: a) the formation of a nucleus and b) the subsequent growth of the crystal.[10] The first stage, which is the least stable, is also associated with a free energy of activation,[11] this then finishes with the formation of the most stable product.[12]

1.10 Interactions in the Solid State

1.10.1 Hydrogen Bonding[13, 14]

Hydrogen bonds are non-covalent interactions and specifically involve donor-acceptor interactions where the donor is a coordinated hydrogen atom.

Hydrogen bond energies range from 15-40 kcal/mol^{-1} for strong bonds, 4-15 kcal/mol^{-1} for medium bonds and 1-4 kcal/mol^{-1} for weak bonds. Moderate and weak bonds have a wide spread of hydrogen bond lengths and bond angles in the crystalline state also showing a compromise with other packing forces.

Strong hydrogen bonds, also known as 'ionic hydrogen bonds' are often formed in groups where there is a deficiency of electron density in the donor group, O^{+}-H, N^{+}-H, or an excess of electron density in the acceptor group, F^{-}, O^{-}-H, O^{-}C, O^{-}P or N^{-}.

Meanwhile, moderate hydrogen bonds are mostly formed by neutral donor and acceptor groups such as O-H, N-H and O=C where donor atoms are electronegative relative to the hydrogen and the acceptor B have lone-pair unshared electrons. These 'normal' hydrogen bonds form important functions and are essential components of biological systems.

Weak hydrogen bonds are formed when the hydrogen atom is covalently bonded to a slightly more electroneutral atom relative to hydrogen. For example C-H, Si-H. It also occurs when the acceptor group has no lone-pairs but has π electrons such as C≡C or an aromatic system. These interactions are similar in energies and geometries to those of van der Waals complexes but can be differentiated from them by the direction of the A-H bond.

Quantities used to measure the geometry of the hydrogen bond are a) the A-H covalent bond length, b) the H---B hydrogen bond length and c) the A---B hydrogen bond distance. The bond angle is also defined by these parameters. It is only in strong hydrogen bonds that the angle is close to 180°, while in moderate and weak hydrogen bonds this angle deviates from linearity.

1.10.2 π-π Interactions

π-π interactions occur when attractive interactions between π-electrons and the σ-framework outweigh unfavourable contributions such as π-electron repulsions. It has been shown that although π-π interactions are controlled by electrostatic interactions, the major energetic contribution comes from other factors. Based on metal-porphyrin studies, Hunter and Sanders[15] found that the greater the intramolecular polarisation between the prophyrin and the metal, the stronger the π-π interaction between the porphyrins.

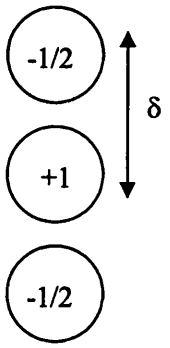

Figure 1.10.1 Model for an atom contributing one electron to the molecular π-system[15]

Based on Figure 1.10.1 each carbon atom in the π-system is considered to have a charge of +1 at the nucleus of the atom and two -1/2 charges at a distance, δ, above and below the plane of the π-system. Generally, π-π geometries are either repulsive or attractive.

In the face-to-face geometry (angle = 0, offset = 0) the repulsive forces are evident, however if one π-atom is rotated up to 90° relative to the other and one π-atom is offset laterally relative to the other there is an attractive band. Rotations between 0° and 90° can lead to attraction at small offsets in an edge-on arrangement. However for rotations between 90° and 180°, leading to repulsions at small offsets, this is again a face-to-face arrangement.[15]

In short, π-π repulsion dominates face-to-face stacked geometry while π-σ attraction dominates in edge-on or T-shaped geometries while the π-σ attraction also dominates in an offset π-stacked geometry. [15]

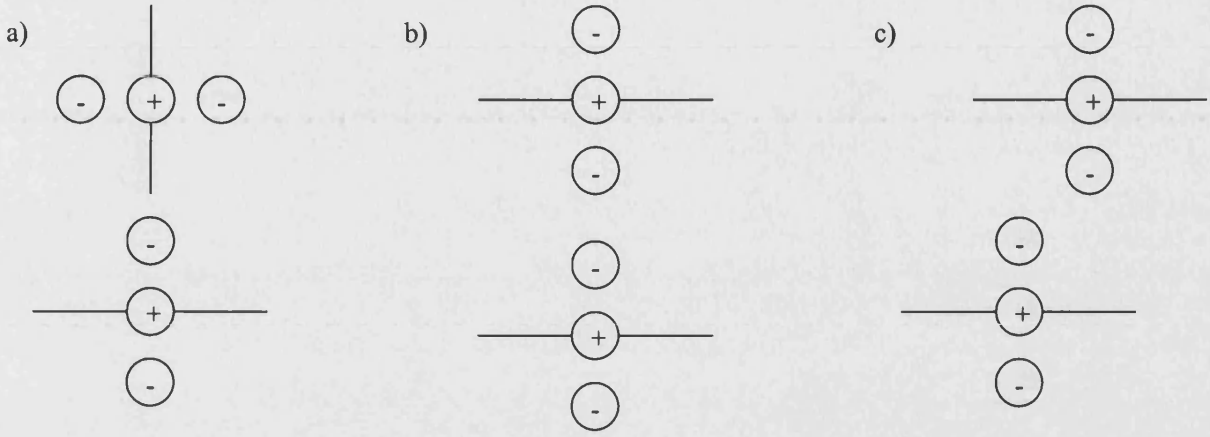

Figure 1.10.2 a) The edge-on or T-shaped geometry; b) The face-to-face geometry; c) the offset π-stacked geometry[15]

Apart from interactive motifs, aromatic compounds also form four basic types of stacking patterns. These are a) the herringbone motif where C···C nonbonded interactions are between nonparallel neighbouring molecules; b) the sandwich herringbone which is made up of sandwich type diads; c) the γ - motif in which the main C···C interactions are between parallel translated molecules; and finally d) the β-motif which is made up of graphitic planes characterised by strong C···C interactions.[16] Figure 1.10.3 shows the graphical representation of the four types of stacking motifs.

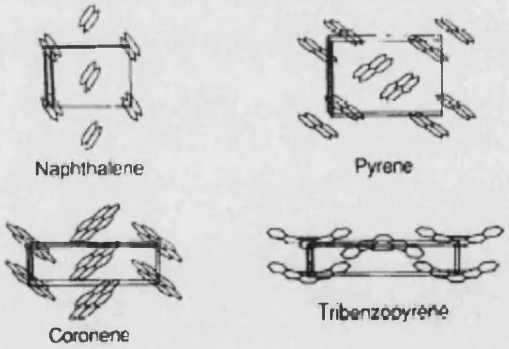

Figure 1.10.3 The four basic aromatic crystal packings as exemplified by naphthalene (herringbone), coronene (γ), pyrene (sandwich-herringbone) and tribenzopyrene (β).[16]

[1] W. Clegg, Crystal Structure Determination, Oxford Chemistry Primers,, 1998.

[2] H.S. Lipson, Crystals and X-Rays, Wykeham Publications, 1970.

[3] J.P. Glusker and K. N. Trueblood, Crystal Structure Analysis – A Primer, 2nd Ed., Oxford University Press, 1985.

[4] W. Clegg, Principles of X-ray Diffraction, The 8th BCA/CCG Intensive Teaching School in X-Ray Structure Analysis, 2000.

[5] A.J.C. Wilson, Elements of X-ray Crystallography, Addison-Wesley Publications,1980.

[6] J. Wormald, Diffraction Methods, Oxford Chemistry Series, 1973.

[7] G.H. Stout and L.H. Jensen, X-ray Structure Determination – A Practical Guide, The Macmillan Company, 1968.

[8] A.J. Blake, Data Collection in Practice, The 8th BCA/CCG Intensive Teaching School in X-Ray Structure Analysis, 2000.

[9] W. Clegg, *J. Chem. Soc., Dalton Trans.*, 2000, 3223-3232.

[10] J.D. Dunitz and J. Bernstein, *Acc. Chem. Res.* 1985, **28**, 193-200 and references therein.

[11] W.I. Cross, N. Blagden, R.J. Davey, *Crystal Growth and Design,* 2003, **3**, 151-158.

[12] N. Blagden, R.J. Davey, *Crystal Growth and Design*, 2003, advanced article: polymorph selection: challenges for the future.

[13] G.A. Jeffrey, An Introduction to Hydrogen Bonding, Oxford University Press, 1997.

[14] J.W. Steed and J. L. Atwood, *Supramolecular Chemistry*, John Wiley and Sons, 2000.

[15] C.A. Hunter and J.K.M. Sanders, *J. Am Chem. Soc.* 1990, **112**, 5525-5534.

[16] G.R.Desiraju and A.Gavezzotti, *Acta Cryst. B,* 1989, **45**, 473-382.

CHAPTER 2

MICROWAVE-ASSISTED CHEMICAL SYNTHESIS

2.0 Microwave –Assisted Chemical Synthesis

2.1 Introduction to Microwaves

Microwaves are short, non-ionising electromagnetic waves that travel at the speed of light. They occur in the region of electromagnetic spectrum between infrared radiation and radio frequencies, corresponding to wavelengths of 1cm to 1m (frequencies 30GHz – 300MHz).

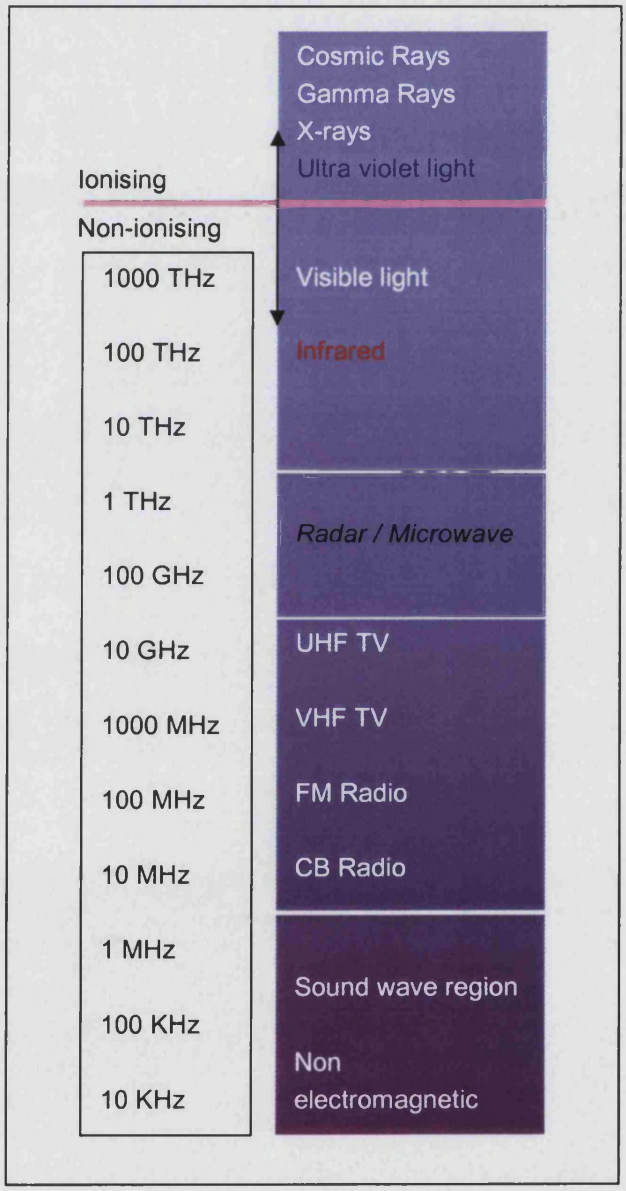

Figure 2.1.1 The Electromagnetic Spectrum

2.1.1 The History of Microwaves

Until the mid-18th century, although both electricity and magnetism were known and had been studied in detail, no one recognised the connection between the two. It was only in the early 19th century more and more physicists experimented with and tried to propose theories to explain electromagnetism. However, there were difficulties in proving the relationship between the two. Only in the 1860's after James Clerk Maxwell studied in depth the problems of electromagnetism, he managed to propose four equations, currently known as Maxwell's Equations that today form the essential laws of electrodynamics.[1]

$$\oint H \cdot dl = I + \varepsilon \frac{d}{dt} \iint E \cdot ds$$

Ampere's Law

$$\oint E \cdot dl = -\mu \frac{d}{dt} \iint H \cdot ds$$

Faraday's Law

$$\varepsilon \oiint E \cdot ds = \iiint q_v dv$$

Gauss' Law

$$\mu \oiint H \cdot ds = 0$$

The Fourth Equation

Figure 2.1.2 Maxwell's Equations[1]

Although the basis of microwaves was formed in the later part of the 19th century, it was only during the Second World War that microwave technology made great strides. This coincided with the need to be able to detect enemy vehicles; ships and planes - thus the birth of RADAR (**Ra**dio **D**etection **A**nd **R**anging).[2, 3]

Today, wavelengths between 1cm and 25cm are used for RADAR transmissions and the remaining range for telecommunications, while domestic and industrial microwave heaters are required to operate at fixed wavelengths of 12.2cm (2.45 GHz) or 33.3cm (900MHz).

The applications of microwave heating, in the form of the microwave oven were first discovered around 1946 by Dr. Percy Spencer, an engineer working at Raytheon Corporation, USA. While he was performing RADAR related experiments on the *magnetron**, he noticed that the candy in his pocket had melted. He later experimented with corn kernels, making popcorn and by placing an egg near the magnetron tube, he managed to make the egg cook and subsequently explode.[4]

Later, Spencer designed a metal box with an opening for microwave irradiation to be concentrated within it, building the first microwave oven.

*a magnetron is a diode-type electron tube used to produce microwave energy

2.1.2 Microwaves and Chemistry

The use of microwaves in chemistry is best summed up by Mingos[5] in his Tilden Lecture in 1991, 'microwave dielectric heating effect uses the ability of some liquids and solids to transform electromagnetic energy into heat and thereby drive chemical reactions'.

Although microwaves have been in use in chemistry since the mid-1970s, initially for moisture analysis and wet ashing and subsequently for microwave acid digestion, it was not until 1986, Gedye *et al.* and Giguere *et al.* reported the use of microwave ovens in organic chemical syntheses.[6,7] These early reports detailed a dramatic acceleration of organic reactions. (Further details in Section 2.4.1)

Subsequently, a wider use was found for microwave syntheses encompassing the synthesis of inorganic and organometallic complexes. Since then, developments in the field have included accelerated polymer synthesis and solid-state reactions of both organic and inorganic materials.

The use of microwave synthesis has been appealing due to several factors. Among them, the speed and efficiency offered over classical methods, particularly those involving long reflux and the ability to control the outcome, or the formation of the desired product. More recent developments in solid state microwave chemistry have led to chemical reactions performed on solid supports thereby reducing the need for solvents, making it more environmentally-friendly.

2.2 Principles of Microwave Functions

In order to fully utilise the potential of microwaves in chemical syntheses, it is necessary to understand how they work in correlation to the various chemical and physical properties of the materials / elements.

An important effect of microwaves on solvents is superheating in which solvents boil between 13-26°C above their normal boiling points at atmospheric pressure.[10] In simple terms superheating is understood to occur because microwaves are able to heat the solvent in a flask directly allowing it to reach a higher than usual temperature.[8]

Initially it was thought that there was a special 'microwave effect' that accelerated these reactions, however upon further investigation and rate reactions studies it was found that as with conventional chemical syntheses, microwave-enhanced reactions were also governed by the same fundamental principles of thermodynamics and kinetics.[9,10]

2.2.1 Microwave Heating

As stated earlier, microwaves are a form of electromagnetic waves. Material can be heated by energy from high frequency electromagnetic waves. This form of heating can occur due to the ability of an electric field to exert a force on charged particles.

When charged particles move through a material, a current is generated. However, if these charged particles are bound to certain regions, they will move until a counter force balances them and this causes what is known as dielectric polarisation.[5]

The electric component of microwaves is able to apply forces on charged particles that can cause them to start to migrate or rotate, and due to this movement further polarisation of already polar particles takes place.[11]

In essence, polarisation of molecules can occur when there is a distortion of the distribution of the electron cloud within the molecule or when there is a physical rotation of molecular dipoles.[12] There are four individual components that contribute to polarisation, given by the equation:

$$\alpha_t = \alpha_e + \alpha_a + \alpha_d + \alpha_i$$

α_t being the total polarisation and α_e is the electronic polarisation, α_a is the atomic polarisation occurring due to displacement of the nucleus, α_d is the dipolar (dielectric) polarisation and α_i is the interfacial polarisation (Maxwell-Wagner effect)[5]. Only two of these four factors, dipolar polarisation and interfacial polarisation contribute greatly to the dielectric heating effect as the frequencies at which they take place are comparable to microwave frequencies.[5]

2.2.1.1 Dielectric Polarisation

Dielectric polarisation is highly dependent on the dipole moments of the compounds, the higher the dipole moment of a molecule the greater it's contribution to the dielectric polarisation. This is because dielectric polarisation is dependent on the molecules ability to realign itself in line with the applied electrical field.[12]

These effects take place mainly in the liquid or gas phase, as in the solid form molecules are more constrained and unable to reorientate in an electric field. In the liquid form, molecules are able to rotate at a fairly high frequencies and can react to field reversals of up to 10^6 times a second at these rates, as the molecules are able to maintain pace with the field reversals they do not absorb any energy, hence to not heat up.

However, when the frequencies of the electric field are increased up to 10^{12}, when an electromagnetic field is applied, the molecules might be able to keep up with the speed of

field reversals, but the polarity (charges) lags behind.[5, 12] This is what causes the molecule to absorb energy from the electromagnetic waves and heat up. This can be summed up by the equation:

$$\tan\delta = \varepsilon'/\varepsilon''$$

where ε' is the dielectric constant, ε'' refers to dielectric loss and tan δ is the dielectric loss tangent.

The dielectric constant, ε', also known as the permittivity of a material,[12] describes the ability of the material to be polarised in an electric field[5] in other words, the charge storing capabilities of a material.[12] Molecules with large permanent dipoles also have large dielectric constants. A comparative example is the dielectric constant at 20°C for benzene, 2.3 and water, 80.4 (these values are relative to free space).[13]

Dielectric loss, ε'' is indicative of the efficiency for a material to convert electromagnetic energy in to heat, while the dielectric loss tangent, tan δ, defines the capability of a material to convert electromagnetic energy to heat at a given temperature and frequency.

The relationship between dielectric constant and dielectric loss is very much governed by microwave frequency. For water, as frequency is increased from 3×10^8 to 1×10^{10} Hz, the dielectric constant, ε' decreases while dielectric loss, ε'' increases.[5,11]

Dielectric heating rates are dependent on three factors[11]:

a) the value of tan δ
b) the size or quantity of the reaction mixture, and
c) the heat capacity of the medium.

If based on the frequency of microwaves, the maximum dielectric loss, ε'' occurs when frequencies reach 20GHz. However at this frequency, microwaves are only absorbed at a very short distance in to the material, this causes very low penetration of microwaves. Penetration depth, defined as the depth in to a material where the power falls to one half its value on the surface is approximately defined by:

$$D_p \propto \lambda_0 \sqrt{(\varepsilon'/\varepsilon'')}$$

where λ_0 is the wavelength of the microwave radiation.

2.2.1.2 Interfacial Polarisation

When conducting particles are incorporated in to a non-conductive medium, it results in a non-homogenous mixture with a dielectric constant that is frequency dependent. The dielectric loss is related to the build-up of charges between the interfaces of the two materials, also known as the Maxwell-Wagner effect.[5]

Wagner showed in the derivation of the equation (below) that the dielectric loss factor, ε_i'', is directly proportional to the product of the fraction v, of a material, the dielectric constant ε', and the frequency at maximum loss and inversely proportional to the conductivity, σ (Sm^{-1}) of the conductive phase. ω and τ represent the frequency and relaxation times, or the rate of build up and decay of polarisation respectively.

$$\varepsilon_i'' = \frac{9v\varepsilon' f_{max}}{1.8 \text{ v } 10^{10}\,\sigma} \quad \frac{(\omega\tau)}{(1+\omega^2\tau^2)}$$

2.2.2 Conduction Losses

Conduction losses are very much associated with interfacial polarisation. As the conductive phase is gradually more and more dispersed within the non-conducting medium, it reaches a point where the interactions between the individual conducting areas have to be taken in to account. In the Maxwell-Wagner model of a two layer capacitor, when this happens, the contribution of the excess conductive part is highly dependent on the d.c. conductivity.

Translated in to microwave terms, it clarifies the fact that in highly conductive liquids and solids (especially those containing vast amounts of salts), there is a point where conductive loss effects are larger than dipolar relaxation effects.[5] More simply put the addition of large amounts of salt to a material, does not greatly influence the dielectric constant or the permittivity of a material but has a marked effect on the dielectric losses.[11]

2.3 Effects of Microwave Heating

It has been established that the rise in temperature caused by microwave heating is very much dependent on the physical properties of liquid and solid samples. These are a) dielectric loss, b) specific heat capacity, c) the emissivity of the sample and, d) the strength of the applied field.[5]

The effects of microwave heating can be broadly divided in to thermal and non-thermal effects.[11]

2.3.1 Thermal Effects

Although thermal effects can be attributed to three main factors[5, 11] 'the superheating of solvents, the rapid achievement of reaction temperature and the efficient mixing and boundary effects', they do not necessarily work together congruously or simultaneously. Each factor can be manipulated to drive a reaction based on the reactants and its reaction medium.

For example, rapid heating effects can be used in the synthesis of zeolites and other ceramic processes to increase crystallinity.[11] Hot spots and surface effects, however, can be exploited to facilitate the synthesis of organometallic compounds, particularly when the heating of solids is required where dramatic decreases in reaction times have been reported.

The pressure cooker effect is believed to be the basis of the accelerations of reaction rates, as with early organic reactions that were often heated to high temperatures and high pressures. In the synthesis of Na-based zeolite A, it was found that under high power levels, the more condensed sodalite structure was obtained due to the higher temperatures and pressures.[5]

2.3.2 Non-thermal Effects

Non-thermal effects are often associated with microwave spectroscopy, carried out in the gas phase. However, in the early years of microwave chemistry, non-thermal effects were claimed to be the cause for significant rate enhancements. These non-thermal effects were also claimed to lower Gibbs energy of activation, which could occur through either the storage of microwave energy in the vibrational energy of a molecule (enthalpy effect) or by the alignment of molecules (entropy effect).[14]

The occurrence of non-thermal effects, at this stage of understanding seems highly unlikely, although it has not been completely ruled out due to the inability to explain the basis of some microwave reactions – specifically those related to polymers.[11]

2.4 Applications on Chemical Syntheses

Following Gedye's[6] and Giguere's[7] independent reports in 1986, on the fascinating results of microwave effects on some organic reactions, the development of other microwave applications on other aspects of chemistry including inorganic and organometallic chemistry, polymerisation reactions, solvent-free reactions even materials-based chemistry has grown tremendously.

For a microwave reaction to be effective, it is necessary for one or more of the components of the reaction to interact with microwaves. Often the easiest method is the use of an appropriate solvent. Based on the underlying theories of how microwaves work, any organic or inorganic solvent with a low molecular weight and a high dipole moment will couple effectively. Most common solvents include H_2O, MeOH and EtOH, this is followed by

MeCN, DMF and DCM. Non-polar organic solvents, however, such as benzene, chloroform and petroleum ethers do not couple effectively with microwaves.[5]

2.4.1 Organic Reactions

2.4.1.1 Enhancements of Organic Reactions

'Remarkable rate enhancements and dramatic savings in reactions times' were the words used to describe the pioneering reports by Gedye and his co-workers in the first organic microwave reactions.[6]

Both Gedye and Giguere used sealed Teflon vessels in a conventional microwave oven. Gedye's group studied four different types of organic reactions, optimising classical methods before comparing them with the microwave reactions. The four different types of reactions were a) the acid hydrolysis of benzamide to give benzoic acid, b) the permanganate oxidation of toluene also to produce benzoic acid, c) the esterification of benzoic acid with methanol, propanol and butanol and d) the S_N^2 reaction between sodium 4-cyanophenoxide and benzyl chloride to form 4-cyanophenyl benzyl ether. The results obtained are summarised in Table 2.4.1.

Reaction	Classical	Microwave	Rates (microwave) / Rates (classical)
Hydrolysis of benzamide to benzoic acid	1h, 90%	10 min, 99%	6
Oxidation of toluene to benzoic acid	25 min, 40%	5 min, 40%	5
Esterification of benzoic acid with methanol	8h, 74%	5 min, 76%	96
Esterification of benzoic acid with propanol	7.5h, 89%	18 min, 86%	25
Esterification of benzoic acid with n-butanol	1h, 82%	7.5 min, 79%	8
S_N^2 reaction; 4-cyanophenyl benzyl ether	12h, 72%	3 min, 74%	240
	16h, 89%	4 min, 93%	240

Table 2.4.1 Results of Gedye's Microwave Reactions[5, 6]

Meanwhile, Giguere's group studied a variety of reactions including Diels-Alder, Claisen and ene reactions. A summary of some of the results are listed in Table 2.4.1.

Reaction	Microwave	Literature	Control
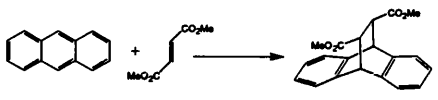	10 min, 87%, p-xylene, 160° < 187°C	72 h, 90%, dioxane, 101°C	4h, 67%, p-xylene, 138°C
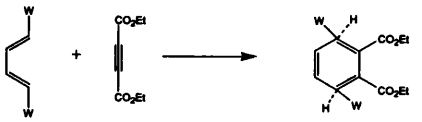	12 min, 55%, neat, 325° < 361°C	5h, 67%, neat, 150°C	5h, 67%, neat, 150°C
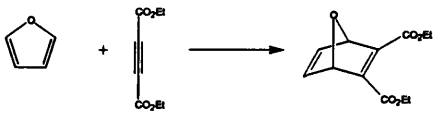	10 min, 66%, neat, 325° < 361°C	4h, 95%, neat, 100°C	4h, 68%, neat, 100°C
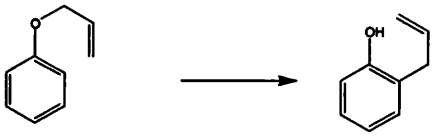	a) 10 min, 21% neat, 325° < 361°C b) 6 min, 92% DMF, 325° < 361°C	6h, 85%, neat, 220°C	6 min, 17%, neat, 320°C
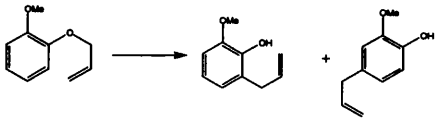	a) 12 min, 71%, neat, 370° < 400°C b) 5 min, 72%, DMF, 300°< 325°C c) 90 sec, 87%, N-methylformamide, 276°< 300°C	85 min, 85%, neat, 240°C	a) 45 min, 71%, neat, 265°C b) 12 min, 92%, neat, 320°C
	15 min, 62%, neat, 400°<425°C	12h, 85%, neat, 180°C	12h, 85%, neat, 180°C

Table 2.4.2 Results of Giguere's Microwave Reactions[5, 6]

The overall conclusion was that the vast increment in reaction rates was attributed mainly to the effects of pressure and superheating, the 'pressure-cooker' effect. It was also noted that although all experiments showed an increase in rates, it was in low-boiling solvent that the

effect was most striking,[6, 7] other contributing factors included container volume and the ratio of reaction volume to container volume.

Giguere's experiments also briefly showed the effect of solvent type on microwave reactions.[7] It was also noted that some literature methods differed significantly from the control reactions, indicating that the reported methods may not have been optimised. Temperature approximations were made by attaching sealed capillaries containing compounds of known melting points to the reaction vessels.

In the field of organic chemistry, the application of microwaves has grown to include the natural product racemisation and the synthesis of radiopharmaceuticals. An example of natural product racemisation is the transformation of (-)-vincadifformine to the more useful (+)-vincadiformine, which is a precursor of (+)-vincamine, an Eburnane alkaloid used in the treatment of cerebral insufficiency.[5, 15] While the lower reaction times with the use of microwaves in radiopharmaceuticals serves to ensure that there is less decay of radiation and less degradation of the reactants and of the products.

2.4.1.2 Inducing Specificity in Organic Reactions

The idea of being able to specifically induce the production of one product over another was achieved fairly early on in the history of microwave chemistry. Not long after his initial reports on rate enhancements of his organic reactions, Giguere together with Majetich[16] reported the capability of microwaves to enhance regioselectivity in the Diels-Alder reactions (see Figure 2.4.1). They surmised that the tricyclic products that were obtained reflected the kinetic instability of the ene adducts when superheating was employed.

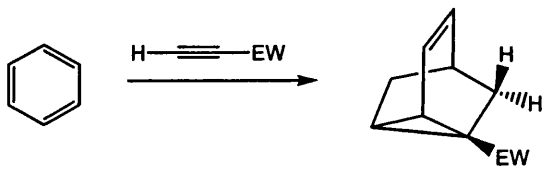

where EW = COOMe; COMe; COOH

Figure 2.4.1 Regioselective Synthesis in a Diels-Alder Reaction

More recently it was found that with proper control and different temperature regimes,[11] it is possible to control the isomeric ratios in the sulfonation of naphthalene.[17]

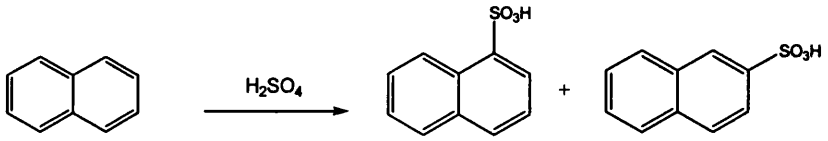

Figure 2.4.2 Isomeric Control in Sulfonation of Naphthalene

It was found that selectivity came directly from the change in heating rate (which in turn was induced by the change in microwave power). At high temperatures (~130°C), 2-naphthalene sulfonic acid is the major product compared to 1-naphthalene sulfonic acid.

2.4.1.3 Dry Organic Reactions (on Solid Supports)

As dielectric heating occurs directly, it is not always necessary for reactions to be performed in a solvent, especially if the reactions can be carried out on a matrix that has a large dielectric loss tangent and the reactants possess dipole moments.[11]
Solvent-free reactions also enable microwave reactions to be carried out in open vessels (test tubes, beakers and round bottomed flasks) avoiding the build-up of pressure[18] that often accompanies reactions in a solvent medium. The bulk temperature of these reactions is also lower although there may be occurrence of higher localised temperatures (hot spot effects). Such reactions in turn, reduce the problems often associated with solvent waste disposal and excess chemicals.

These reactions often consist of organic compounds adsorbed on the surface of inorganic oxides (e.g. alumina, silica or clay) that do not absorb microwaves. Some of the supports used include recyclable mineral oxides such as $Fe(NO_3)_3$-clay, $Cu(NO_3)_2$ – clay, NH_2OH-clay and $PhI(OAc)_2$-alumina in protection-deprotection, condensation, cyclisation, rearrangement, oxidation and reduction reactions. Varma[18] (1999) provides a comprehensive review of solvent-free organic syntheses, some examples are given below.

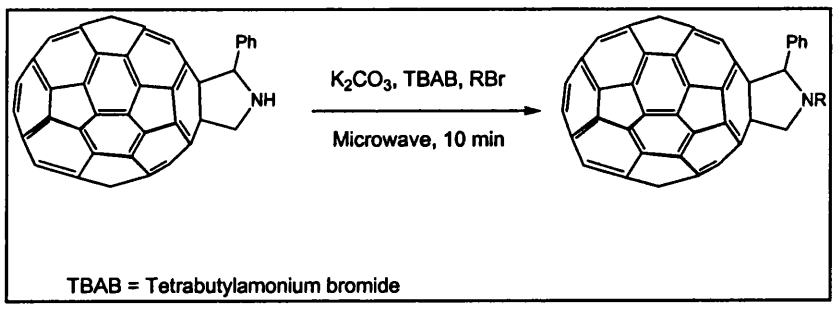

Figure 2.4.3 An N-Alkylation reaction using a Phase Transfer Reagent (TBAB)[18]

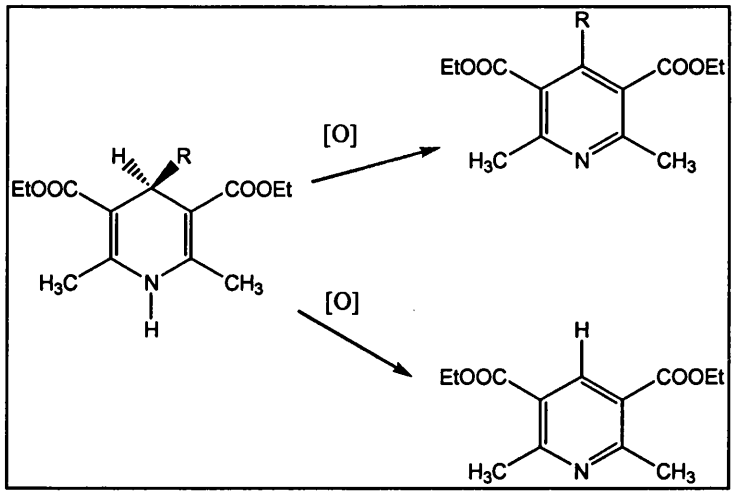

Figure 2.4.4 The Oxidative Dealkylation of 4-alkyl-1,4-dihydropyridines with MNO_2 on bentonite[11]

2.4.2 Inorganic and Organometallic Reactions

2.4.2.1 Enhancements of Inorganic Reactions

Following the successful application of microwave irradiation on organic synthesis, Mingos and his group subsequently experimented with the microwave synthesis of inorganic and organometallic compounds.

The challenges faced by inorganic synthetic chemists made microwaves appealing, particularly as transitional metal ions were often substitutionally-inert making the synthetic process problematic and often long and tedious.

Results from some of the reactions are summarised in Table 2.4.3[19]. The reactions were carried out on 0.2-1.0g scales in volumes of $15cm^3$ in sealed Teflon containers. In this case, Parr Microwave Acid Digestion Bombs were used in a conventional microwave oven.

Product*	Reaction mixture	Solvent	Microwave	Literature
$[Cr(DPM)_3]$	$CrCl_3.3H_2O$, urea, dipivalolylmethane	$EtOH/H_2O$	40s, 71%	24h
$[IrCl(CO)(PPh_3)_2]$	$IrCl_3.xH_2O$, PPh_3	DMF	45s, 70%	12h**
$[IrCl_3(9S3)]$	$IrCl_3.xH_2O$, 9S3	MeOH	16s, 98%	2h
$[Pt(Cl(terpy)]Cl.3H_2O$	K_2PtCl_4, terpy	H_2O	2 x 30s, 47%	24-100h
$[AuCl(terpy)]Cl_2.3H_2O$	$HAuCl_4$, terpy	H_2O	2 x 30s, 37%	24h
$[RuCl(CO)(bipy)_2]Cl$	$RuCl_3.xH_2O$, bipy	DMF	3 x 20s, 70%	168h
$[Ru(9S3)_2](PF_6)_2$	$RuCl_3.xH_2O$, 9S3	MeOH	6 x 25s, 49%	Cannot be synthesised directly

*DPM = 2,2,6,6-tetramethyl-3,5-heptadionato; 9S3 = 1,4,7-trithiacyclononane; terpy = 2,2';6',2''-terpyridine; bipy = 2,2'-dipyridyl.

** The reaction product was at times contaminated with $[IrCl_3(CO)(PPh_3)_2]$ which was reduced to $[IrCl(CO)(PPh_3)_2]$ with zinc in DMF.

Table 2.4.3 Results of Mingos's Inorganic Microwave Reactions

The large decrease in reaction times was also associated with the 'pressure cooker' effect, where pressure in the reaction vessels often approached 80 atm prior to completion[19] in comparison with long reflux times for conventional synthesis at 1 atm.

The efficiency of the reactions can also be attributed to the solvents used. The solvents selected all had high dielectric loss, being more efficient at transforming microwave energy in to heat.[19]

2.4.2.2 Solid State Inorganic Synthesis

Experimentation with the use of solid inorganic samples in the microwave has been somewhat limited. This may be due in part to the plasma discharges (electric arcing) that are known to occur when solid metal samples are heated in a microwave cavity. These discharges are caused by the large electric field gradients and often emit visible and sometimes dramatic electric discharges.[20]

However, attempts by Mingos demonstrated that it is possible to couple certain metal oxides, especially those with high dielectric loss tangents with microwaves. He and his co-workers[21] also showed that it was possible to at least reduce if not control the arcing to an acceptable level. They proposed the use of low microwave power; polar solvent with high viscosity and high boiling points (or use of higher pressures to increase the solvent boiling point) and efficient stirring. They also noted that arcing was largely dependent on the number of metal particles per unit volume.

Not all metals couple effectively with microwaves. For example,[22] while CaO, TiO_2, CeO_2, SnO, Al_2O_3, Pb_3O_4, Fe_2O_3, Cr_2O_3 and La_2O_3 do not absorb microwaves efficiently at 2.45 GHz, V_2O_5, ZnO, CuO, MnO_2, PbO_2 and WO_3 do. This strong absorption of microwaves

was reflected in dramatic heating effects. It was found that microwave heating of V_2O_5 and WO_3 was able to achieve temperatures in excess of 700°C and melt within one minute at 500W power level in a conventional microwave oven.[22] Thermal decomposition of PbO_2 to Pb_3O_4 (Yields in excess of 80%) showed that the temperature reached a maximum of approximately 200°C before falling even though the sample continued to be irradiated. It was proposed that the fall in temperature was because the product, Pb_3O_4, does not absorb microwaves efficiently.

In the synthesis of metal chalcogenides,[20] such as chromium sulfides and selenides, tantalum sulphide (TaS_2) and $FeCuS_2$ (chalcopyrites) it was found that although reaction times were reduced, this did not signify an increase in the actual rate of the reaction. The reduction in reaction times was mainly attributed to the rapid heating of the sample without heating of the reaction vessel or generating high vapour pressures. Ultimately the optimum synthetic route proposed, consisted of a combination of microwave and conventional heating thereby reducing the synthesis times from 6 to 3 days.

The reactions described above have mainly consisted of direct heating of particulate metal powders. There have also been methods in which insoluble metal powders have been heated in a solvent environment (thermohydrolysis). With the results achieved from this method, Stuerga[23, 24] and his co-workers have aptly named this 'microwave flash synthesis'.

Their reactions were carried out in a specially designed microwave reactor,[23] consisting of a microwave applicator associated with an autoclave (RAMO – *Reacteur Autoclave MicroOnde*). Its microwave generator used a continuous wave system with power up to 2 kW and an autoclave that was microwave transparent.

Results from the microwave flash synthesis of 'tin chloride in aqueous solutions' promised distinct advantages in the production of cassiterite compared with the usual sol-gel process, and conventional thermohydrolysis. A few seconds of microwave heating of the tin chloride solution led to nanosize tin oxide colloidal suspensions.

Using metal powder suspensions in solvents, Mingos and his co-workers[21] also showed that it was possible to complete such reactions using microwaves, although the use of microwaves did not necessarily result in any advantages over conventional heating. Results from the investigations are summarised in Table 2.4.4.

Reactants	Products	Time	Yield (Conventional) %
Cr + toluene + $AlCl_3$ + HCl + $Na(BPh_4)$	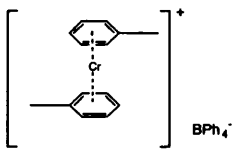	20 minutes	52 (51)
Al + toluene + $AlCl_3$ + $CrCl_3$ + $Na(BPh_4)$	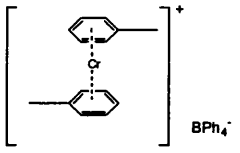	30 minutes	49 (53)
Al + benzene + $AlCl_3$ + $CrCl_3$ + $Na(BPh_4)$	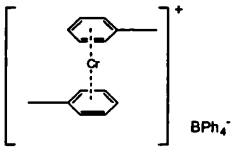	30 minutes	45
Cu/Zn + CH_2I_2 + oct-1-ene + I_2	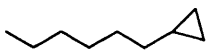	15 hours	52 (70)
Cu + *o*-iodonitrobenzene	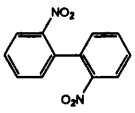	1.5 hours	65 (61)
Sn + HCl + 4-nitro-*o*-xylene	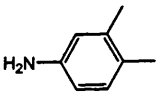	50 minutes	94 (97)
Zn + α,α'-dibromo-*o*-xylene + maleic acid dimethyl ester	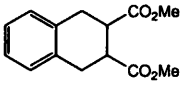	10 hours	0 (89, ultrasound)
Zn + 2-iodopropane + acetone + maleic acid dimethyl ester	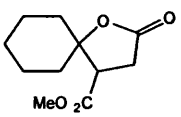	0.5 + 3 hours	64 (86)

Table 2.4.4 Reactions involving metal powder suspensions in solvents

2.4.3 Polymerisation Reactions

The ability of microwaves to enable reactions to reach high internal reaction temperatures, often at high pressures can also be exploited in the field of polymer chemistry. Examples of coupling polymerisations utilising microwaves were recently reported. Instead of conventional methods of polymer synthesis, which could range from 4 to 24 hours, it was found that using microwaves, it was possible to drive polymerisations to completion in approximately 10 minutes in a one-step, one pot fashion,[25] shown in Figure 2.4.5. The fast heating rates of microwave reaction have also led them to be used in polymer curing.[11]

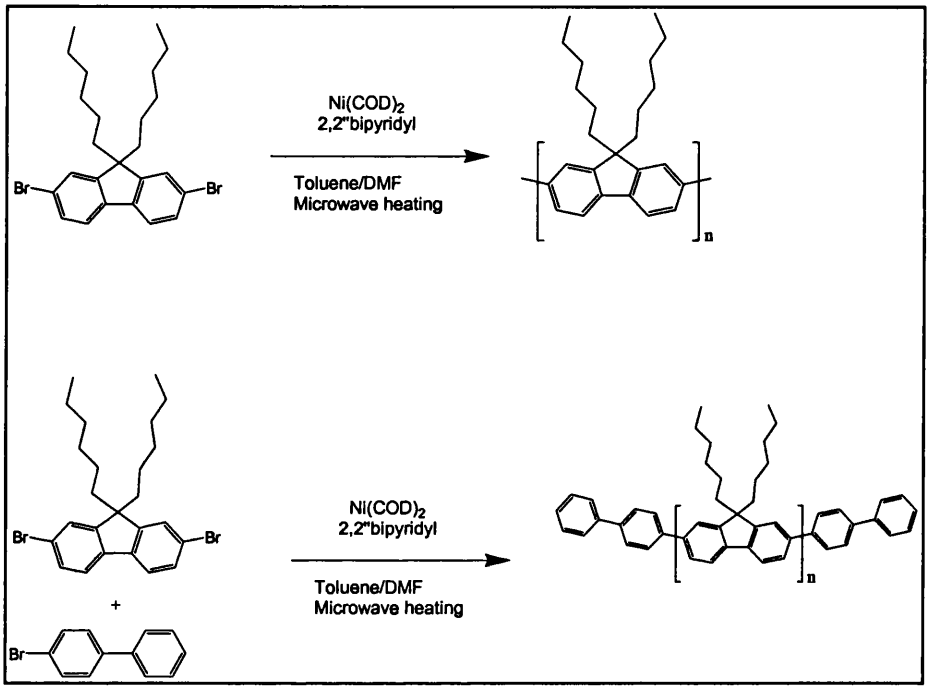

Figure 2.4.5 Synthesis of Poly-2,7-fluorenes[25]

2.5 Comparisons between Conventional Microwave Ovens and Focused Microwave Reactors

The reactions discussed above have mainly been performed in a conventional commercially available microwave oven or specially designed ovens. However, the results of the microwave synthesis in this theses have been performed in a Focused Microwave Reactor.

So far (August 03), there has only been one report in the literature on the use of a focused microwave reactor.[26] It was noted that with the use of a focused microwave reactor, reaction conditions could be more closely reproduced. A comparison between the two types of microwave ovens based on the synthesis of Ru(II) thiolato complexes is summarised in Table 2.5.1.

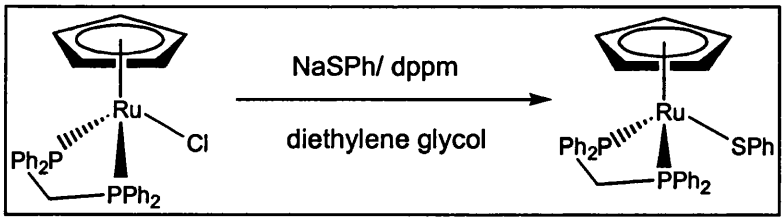

Figure 2.5.1 Synthesis of Ru(II) thiolato complexes

Microwave power	Reaction time; Yields (focused microwave)	Reaction time; Yields (conventional microwave)	Reaction time; Yields (conventional microwave)
100W	90s, 88%	>2mins, 8%	10 mins, 35%

Table 2.5.1 Results of Comparative Study between A Focused Microwave and a Conventional Microwave

Although it is likely that the general use of microwaves would dramatically decrease reaction times, Table 2.5.1 shows that the use of focussed irradiation is superior to the conventional microwave oven.[26]

2.6 Microwave Synthesis of High Nuclearity Ruthenium Clusters

The application of microwaves in this thesis is specifically related to the previously unexplored field of microwave synthesis of high nuclearity ruthenium clusters.

Some prior work related to cluster compounds has been reported. Mingos and Whitakker[20] studied in solid-state the synthesis of octahedral clusters of Mo, W, Nb and Ta. However, the reaction products from reduction or conproportionation (lower-oxidation state metal halides) reactions appeared to have very small dielectric loss tangents, as a result, the reactions slowed down once a proportion of the metal reagent had been reacted.

It was found that for metal clusters that were synthesised directly as salts, the heating characteristics were significantly better, making it possible to melt samples ($Na_4[Nb_6Cl_{12}]Cl_6$) under 1 minute at 300W microwave irradiation. With these higher density powders, lower power levels (150W) were required to heat the metal safely without arcing, however, as the reaction progressed, the formation of the products decreased the dielectric heating effect, making it necessary to increase the power levels.[20]

The use of microwaves in the synthesis high nuclearity ruthenium clusters puts to test all the fundamentals of microwave irradiation and a direct comparison can be made with the conventional synthetic methods of these clusters which involved lengthy thermolysis and pyrolysis of smaller clusters. The results are further discussed in Section 3.6.

---

[1] Electromagnetism, Maxwell's Equations, and Microwaves, Institute of Electrical and Electronics EngineersInstitute of Electrical and Electronics Engineers website. http://www.ieee-virtual-museum.org/exhibit/exhibit.php?taid=&id=159265&lid=1&seq=3 and links therein

[2] What is Radar and How Does it Work? http://www.ieee-virtual-museum.org/collection/tech.php?taid=&id=2345896&lid=1

[3] World War II: The Physicists' War http://www.ieee-virtual-museum.org/exhibit/exhibit.php?id=159265&lid=1&seq=6

[4] The History of the Microwave Oven http://www.gallawa.com/microtech/history.html

[5] D.M.P. Mingos and D.R. Baghurst, *Chem Soc. Rev.*, 1991, **20**, 1.

[6] R. Gedye, F. Smith, K. Westway, H. Ali, L. Baldisera, L. Laberge and J. Rousell, *Tetrahedron Lett.*, 1986, **27**, 279.

[7] R. Giguere, T.L. Bray, S.M. Duncan and G. Majetich, *Tetrahedron Lett.*, 1986, **27**, 4945.

[8] G. Whitakker, New Scientist, Feb. 1998, 157, *2123*, 28.

[9] K.D. Raner, C.R. Strauss, F. Vysjic and L. Mokbel, *J. Org Chem.*, 1993, **58**, 950.

[10] R. Laurent, A, Laporterie, J. Dubac, J. Berlan, S. Lefeuvre and M., Audhuy, *J. Org. Chem.* 1992, **57**, 7099.

[11] S.A. Galema, *Chem. Soc. Rev.*, 1997, **26**, 233.

[12] C. Gabriel, S. Gabriel, E.H. Frant, B.S.J. Halstead and D.M.P. Mingos, *Chem. Soc. Rev.*, 1998, **27**, 213.

[13] D.Q.M. Craig, Dielectric Analysis of Pharmaceutical Systems, Taylor and Francis, London, UK, 1995.

[14] R. Laurent, A. Lapoterie, J.Dubac, J. Berlan, S. Lefeuvre and M. Audhuy, *J. Org. Chem.*, 1992, **57**, 7099 and references therein.

[15] S. Takano, A. Kijima, T. Sugihara, S. Satah and K. Ogasawara, *Chem. Lett.*, 1989, 87.

[16] R.J.Giguere, A.M. Namen, G. Majetich and J, Defauw, *Tetrahedron Lett.*, 1987, 28, **52**, 6553.

[17] D.Stuerga, K. Gonon and M. Lallemant, *Tetrahedron*, 1993, 49, **28**, 6229.

[18] R.S. Varma, Green Chemistry, 1999, 43.

[19] D.R. Baghurt, S.R. Cooper, D.L. Greene, D.M.P. Mingos and S.M. Reynolds, *Polyhedron*,1990, 9, **6**, 893.

[20] A.G.Whittaker and D.M.P. Mingos, *J. Chem. Soc. Dalton Trans.*, 1995, 2073.

[21] A.G. Whittaker and D.M.P. Mingos, *J. Chem. Soc. Dalton Trans.*, 2002, 3967.

[22] D.R. Baghurst and D.M.P. Mingos, *J. Chem. Soc. Chem. Commun.*, 1988, 829.

[23] E. Michel, D. Stuerga and D. Chaumont, *Jour. Mater. Sci. Lett.*, 2001, **20**, 1593.

[24] T. Caillot, D. Aymes, D. Stuerga, N.Viart and G. Pourroy, *Jour. Mat. Sci.*, 2002, **37**, 5153.

[25] K.R. Carter, *Macromolecules*, 2002, 35, **18**, 6757.

[26] N. Kuhnert and T.N. Danks, *J. Chem. Research (S)*, 2002, 66.

CHAPTER 3

RUTHENIUM AND OSMIUM CARBONYL CLUSTERS: BACKGROUND, RESULTS AND DISCUSSIONS

3.0 Ruthenium and Osmium Carbonyl Clusters: Background, Results and Discussions

3.1 Definition of a Cluster

Cotton's classic description of a cluster defines it as 'a finite group of metal atoms that are held together mainly or at least to a significant extent, by bonds directly between metal atoms, even though some non-metal atoms may also be intimately associated with the cluster'.[1]

In the context of this theses, a cluster is defined as a conglomeration of three or more metal atoms with metal-metal bonds. Although the definition implies that there ought to be direct or substantial bonding between two metal atoms, it has been found that metal-metal bond lengths can vary by as much as 15% with the same formal metal-metal bond order.[2, 3] These extreme ranges are caused by metal-metal bonds being easily deformable as they are often the weakest bond in the molecule. This, however, is also compensated for, by favourable bonding and non-bonding as well as steric interactions between ligands.[4]

The variation in the bonding modes of clusters differs vastly from those found in the typical organometallic complexes. Table 3.1.1 briefly outlines the possible combinations of the bonding modes most commonly found in clusters.

μ (Bridging)	
μ or μ_2 edge-bridging	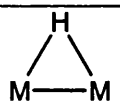
μ_3 capping a triangular face	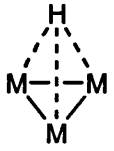
η (Hapticity)	
η^2	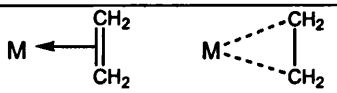
η^5	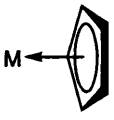
η^6	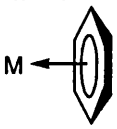

Table 3.1.1 A summary of binding modes in clusters.[21]

3.2 X-Ray Crystallography in Cluster Chemistry

Early metal carbonyl cluster chemistry was built upon simple mononuclear or polynuclear complexes of low molecularity. Based on what was known of the p-block elements, metal-metal bonds in transition metal compounds were believed to be of low stability. As the stability of M-M bonds in heavier p-block elements decreases with increasing atomic number going down the group, it was assumed that a similar decrease in stability would occur in transition metals.[5]

The earliest reports of metal clusters were those of $Co_2(CO)_8$,[6] $Fe_2(CO)_9$,[7] and $Fe_3(CO)_{12}$[8, 9] in the early 1900s. Early efforts in trying to provide a plausible structure of these early metal clusters often resulted in configurations that had no metal-metal bonds and maintained the inert gas configuration at the metal centres with the donation of an additional electron from the oxygens in an isocarbonyl bonding mode (Figure 3.2.1).[5] Thus early developments in cluster chemistry had very much been hindered by the challenges in identification and the accurate structural characterisation of metal clusters and their ligands.

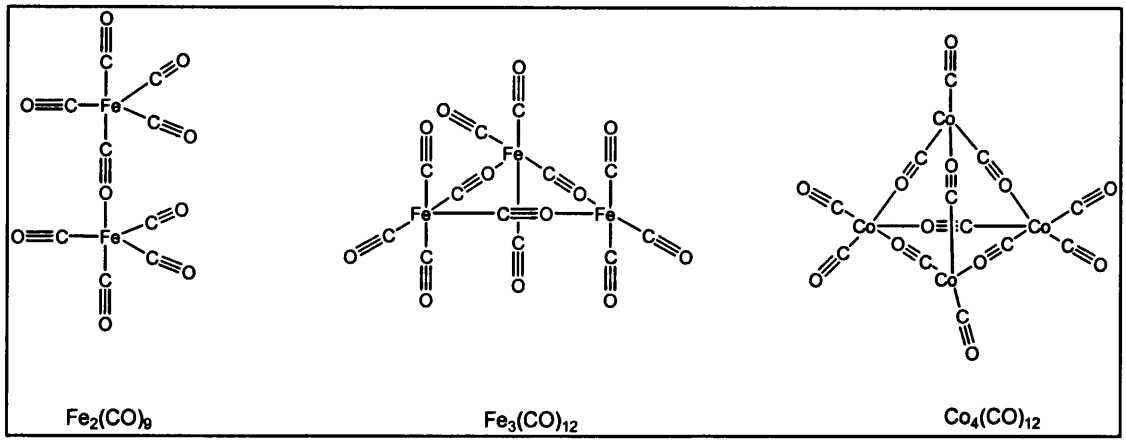

Figure 3.2.1 Proposed structures of metal carbonyls without metal-metal bonds[5]

Eventually, the use and application of X-ray crystallography became the ultimate determinant in cluster chemistry allowing the establishment the molecularity and correct formulation of metal clusters and their derivatives.[5] Although early X-ray crystallographic studies (1950s) contributed much, time scales were often the limiting factor with structure determination taking up to months and possibly years, compared to days even hours with current technology.

The only slight drawback to the high level of accuracy to which atomic positional parameters could be determined by X-rays are issues pertaining to the high absorption of X-rays by the heavy metal cluster core (especially by second and third row transition metals) and the difficulty in locating lighter atoms, particularly hydrogen atoms.[10, 11] Neutron diffraction has been successfully applied to hydrido cluster compounds [11, 12, 13] in efforts to locate interstitial hydrogen atoms, while indirect methods such as potential energy calculations, examination

of ligand polyhedral shell and the lengthening of metal-metal edges have also been employed.[10]

Although X-ray crystallography has become the foremost structural tool in cluster chemistry, it is by no means the sole technique in cluster identification. While X-ray crystallography provides a representation in the solid state, NMR and IR spectroscopy provides an insight in to the complex in solution. These methods also enable the monitoring of the progress of the reaction.[14] Mass spectrometry also became widely used as a quick tool for determining molecular weight in clusters. It is capable of providing an insight in to the number of carbonyls and organic ligands present, and sometimes even the number of metal atoms.[11]

Much of the earliest structural work was done by Lawrence Dahl, who determined the structures of $Rh_6(CO)_{16}$, and $Fe_3(CO)_{12}$. At that time, the iron complex aroused much interest and speculation arising from difficulties in verifying its solid state structure (further discussions in Section 3.2.1). Another landmark structure was that of $Fe_5(CO)_{15}C$, reported by Braye, Dahl, Hübel and Wampler in 1962[15] due to the presence of a carbide atom at the base of a square pyramidal array of iron atoms.[14]

3.2.1 The Effects of Ligands in Cluster Chemistry: A Structural Comparison of $Fe_3(CO)_{12}$ to $Ru_3(CO)_{12}$ and $Os_3(CO)_{12}$

It is of interest here to note the structural differences of the iron complex compared with the congener elements of ruthenium and osmium,[16] all with the general formula $M_3(CO)_{12}$. While all three elements form a triangular arrangement of the metal core, the main difference lies in the arrangement of the carbonyl ligands.

The core of the iron complex consists of a slightly distorted isosceles triangular arrangement, where a $Fe(CO)_4$ group is symmetrically coordinated by two Fe-Fe bonds to a $Fe_2(CO)_8$ fragment. Each metal atom of this $Fe_2(CO)_8$ fragment is then coordinated to three terminal and two μ_2-bridging carbonyls.

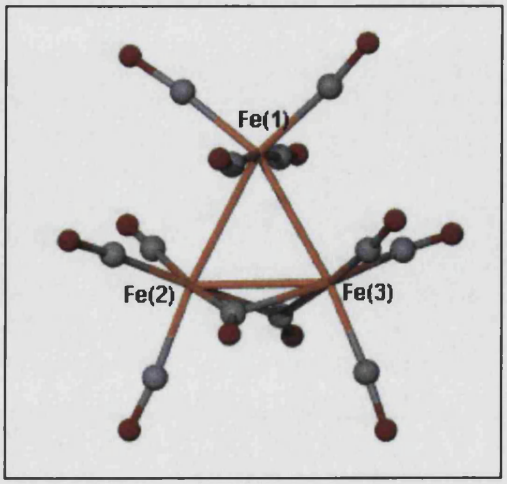

Figure 3.2.2 Crystal Structure of $Fe_3(\mu_2\text{-}CO)_2(CO)_{10}$[17]

Meanwhile, in the ruthenium and the osmium complexes, all carbonyl ligands are terminal with four carbonyl ligands bonded to each metal atom, two in the axial and two in the equatorial positions.[12] (refer to Figure 3.4.2 and Figure 3.5.1)

3.3 Types of Clusters

Maximum binding energies for transition metals often occur at approximately the centre of the transition metal series, which corresponds to the half filled d and s valence orbitals. However, in cluster compounds, it is the ligands surrounding the metal core that try to emulate this bonding situation. As a result,[2] cluster compounds of early transition metal elements are associated with π-donor ligands which can donate additional electrons to metal bonding molecular orbitals, while,

late transition metal cluster compounds often have π-acceptor ligands which can withdraw electron density from the cluster and depopulate the skeletal molecular orbitals (which would have otherwise been involved in metal-metal antibonding)

An important consideration in the formation of a cluster compound, is the formal oxidation state of the metal atoms involved. It is important that the metal has a low formal oxidation state to maximise metal-metal bonding effects, as a result, the π-donor or the π-acceptor character of the ligands have to be able to stabilise these low oxidation states.[2]

3.3.1 π-acceptor Clusters

A vast number of metal clusters of the late transition metals are of this type including the Osmium and Ruthenium clusters discussed in Section 3.5 and 3.6. In this range of clusters, carbon monoxide is the most effective and most widely used ligand. Its superiority as a ligand is largely due to its flexibility in which it can occupy terminal, edge-bridging or face-capping positions in a cluster, thereby contributing to the stabilisation of the low oxidation state cluster compounds.

Other π-acceptor ligands include isocyanides, nitric oxide, phosphines and polyenes such as cyclopentadienyl and benzene. While H^- is not strictly a π-acceptor ligand, many carbonyl and phosphine clusters compounds often have H^- as a ligand.[2]

3.3.2 π- donor Clusters

π-donor ligands such as O^{2-}, S^{2-}, Cl^- Br^-, I^- and OR^- are often associated with cluster compounds of the early transition metals. These commonly have oxidations states of +2 and +3. Table 3.3.1 summarises the number of electrons the ligand sets donate to a metal cluster.

Edge-bridging (μ_2)	
Two –electron donors:	O, S, Se
Three-electron donors:	SR, OR, PR_2 AsR_2 Cl, Br, I
Face Bridging (μ_3)	
Four-electron donors:	O,S, Se, Pr, AsR
Five-electron donors:	Cl, Br, I

Table 3.3.1 Electron-donating characteristics of Ligands in Metal Clusters[2]

3.4 Rationalising Clusters

When a cluster has been structurally determined, it is necessary to be able to rationalise the cluster in terms of the number of valence electrons available in the cluster. This process enables the understanding of the link between the structure and bonding properties of the cluster to be developed.[10]

3.4.1 Simple Electron Counting

The most basic form of electron counting assumes all metal atoms and ligands to be in the zero oxidation state. The total number of electrons is then calculated by adding the valence electrons of the metal atoms and the electrons donated by the ligands. The overall charge of the cluster is determined by adding or subtracting the appropriate number of electrons.[10] This method however, denotes nothing about how the bonding is.

3.4.2 The Effective Atomic Number (EAN) Rule

The 18-Electron Rule also known as the Effective Atomic Number (EAN) Rule forms the simplest arrangement in rationalising clusters. It is derived from the 18-electron counting rule for mononuclear organometallic complexes which is based on the fact that transition metals have nine valence atomic orbitals (AO's) 5*d*, 1*s* and 3*p* which can be used for metal-ligand bonds or for accommodating non-bonding electrons.[18]

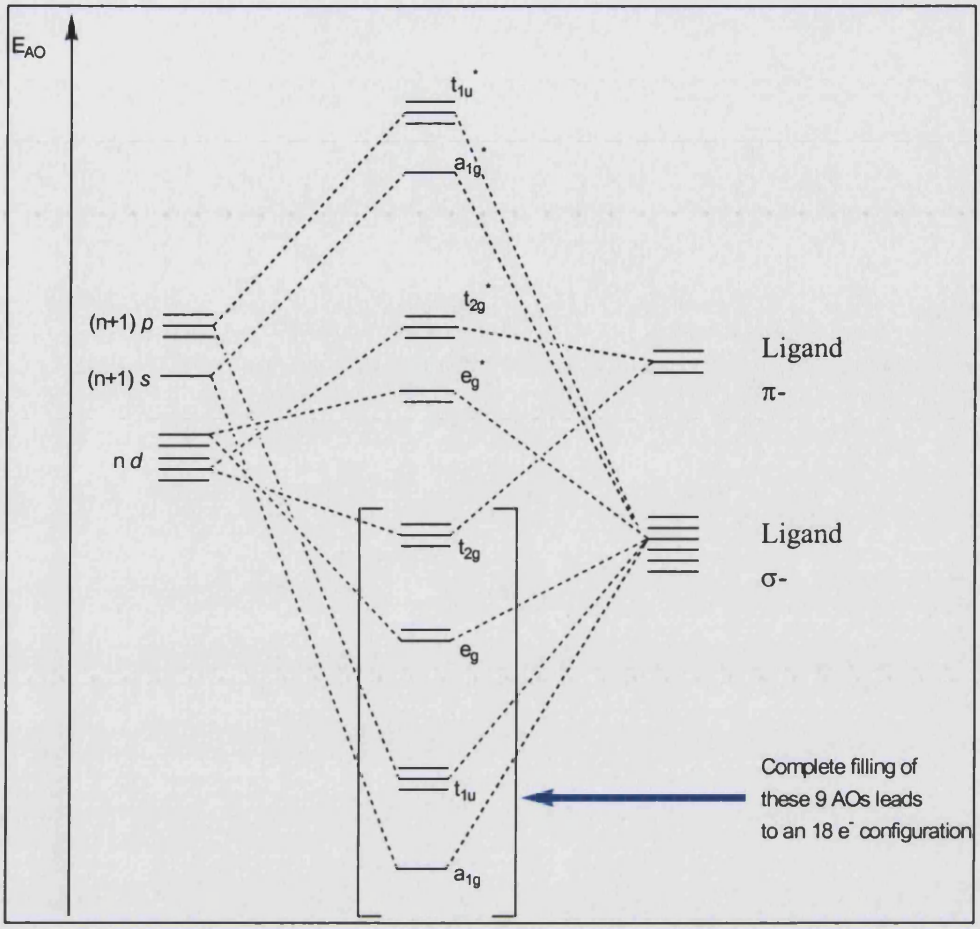

Figure 3.4.1 The EAN Rule for an octahedral metal complex

In applying the EAN rule to metal clusters, it is necessary to make two assumptions[10, 18]:
All nine AOs must be involved in either metal-metal bonding, metal-ligand bonding or used to accommodate non-bonding electrons, and,
Each metal atom at the vertex of a cluster is allocated one AO for each two-centre two-electron (2c-2e) bond it forms.

Based on these two rules, the number of metal-metal bonds from a lone ML_x unit can be related to the number, *v*, of electrons in the valence shell of the metal (including electrons contributed by the ligands), whereby the number of metal-metal bonds equals (18-*v*).[10]

In considering trinuclear complexes, with the formula $M_3(CO)_{12}$ (where M=Fe, Ru and Os): each ML_x unit, in this case $M(CO)_4$ unit has 16 valence electrons (eight electrons from the M and two each from each CO unit. In order to reach the necessary 18-electrons, each metal needs to form (18-16) 2 metal-metal bonds, in doing so each metal centre forms two 2c-2e bonds. The EAN rule, however, does not discriminate between the type of carbonyl ligands, whether they are bridging or terminal and based on this rule, no prediction can be made about the positions and the distributions of the carbonyl ligands (see Figure 3.4.2).[18]

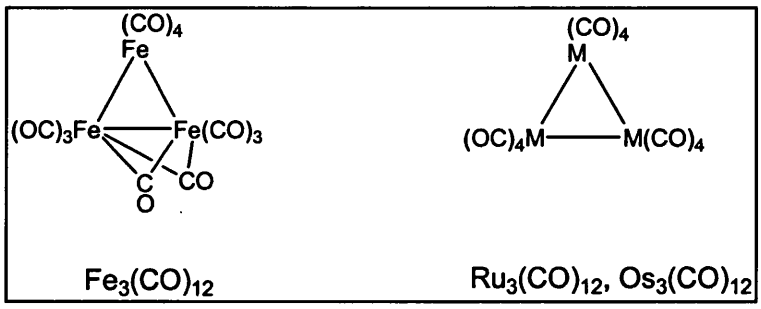

Figure 3.4.2 Examples of triangular tri-metal clusters

While the EAN rule works well from planar ring compounds and other low nuclearity geometries, it tends to break down when applied to higher nuclearity clusters (where $n \geq 6$). This is because of the assumption that the edges of a metal polyhedron corresponds to "normal" 2c-2e bonds is no longer appropriate. In the larger clusters, a delocalised bonding system where edges no longer correspond to bonds needs to be used.[10]

3.4.3 The Polyhedral Skeletal Electron Pair Theory (PSEPT)

The polyhedral skeletal electron pair theory (also known as Wade's Rules) was developed by Wade[19] and Mingos[20], initially to rationalise the shapes of boron hydride clusters, but have since found applications to the wide range of metal cluster chemistry.

The essence of this theory is based on the link between the polyhedral shapes of the cluster compounds and the numbers of electron pairs available to hold their skeletal atoms together. Like the EAN rules, it is also based on the assumption that each metal atom uses all of its nine valence shell AOs, however, instead of assuming two electrons at each of the two centre bonds (2c-2e) it allows the structure to be deduced from the total number of skeletal bond pairs.[18]

This theory is based on the core-geometry of a deltahedron*, from which other geometries can be derived. Starting with a *closo* geometry, which is closed deltahedron, the following derivatives are then related to it by the removal or one, two or three vertices, [21] as shown in Figure 3.4.3.

* A deltahedron is a polyhedron with triangular faces.

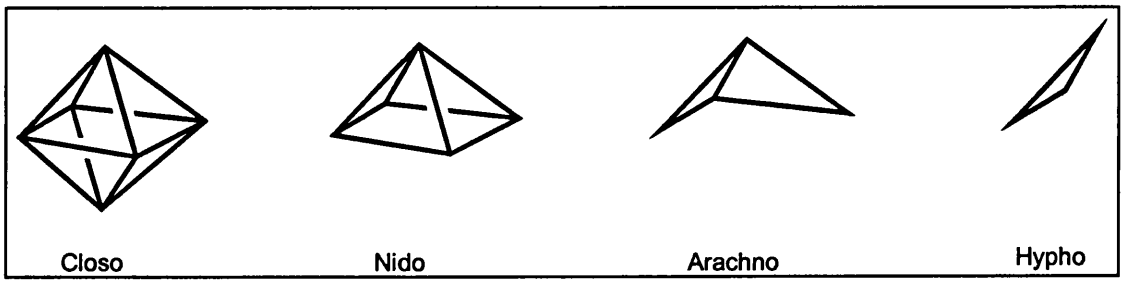

Figure 3.4.3 The relationship between *closo-, nido, arachno- and hypho-* clusters.[21]

3.5 Cluster-Assisted Reactions

Early cluster chemistry intrigued chemists, as the formation of a large metal core with numerous metal-metal bonds was initially considered to be highly unstable. Progress made, has since tried to explain and rationalise the formation of these clusters. Following on from that, reactions involving clusters, from the initial synthesis and kinetic studies on clusters to ligand transformations and cluster rearrangements has grown at an astounding pace.

3.5.1 The Chemistry of $Os_3(\mu\text{-}H)_2(CO)_{10}$

The chemistry of $Os_3(\mu\text{-}H)_2(CO)_{10}$ has been rich and varied due to its ability to remain unsaturated where other clusters have removed unsaturation through condensation by forming metal-metal bonds.[22] Based on the EAN rule, four metal-metal bonds are predicted for the tri-osmium cluster, proposing a formal double metal-metal bond at the double hydride-bridged edge (see Figure 3.5.1), which is shorter that of a 'single bond'. However, the so-called 'double bond' [between Os(2) and Os(3)] on this 46e$^-$ $Os_3(\mu\text{-}H)_2(CO)_{10}$ cluster is readily attacked by nucleophiles[23] and can undergo associative reactions under mild conditions,[22] while a conventional organic double bond would undergo attack by electrophiles.

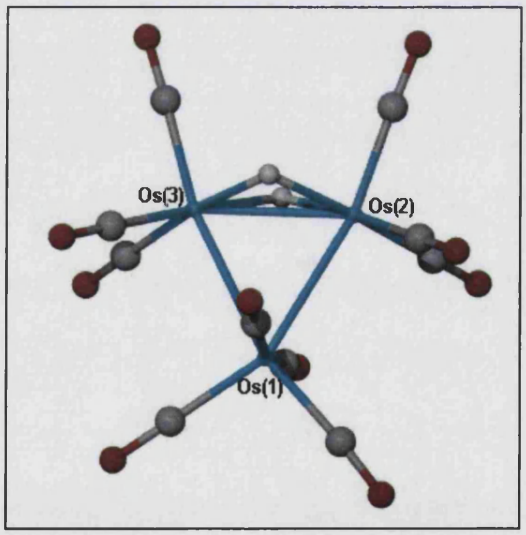

Figure 3.5.1 Crystal Structure of $Os_3(\mu\text{-}H)_2(CO)_{10}$[24]

Both neutron[24] and photoelectron [25] studies have identified the dihydride bridge as a four-centre, four-electron bond with a total of 46 electrons (8 from each osmium atoms, 2 from each carbonyl and 1 from each hydrogen).

Interpretations of the metal-metal overlap populations[25] suggest that while the the d-d overlap populations are equal for interactions between Os(2)-Os(3) and Os(1)-Os(2,3), the distributions of direct d-d- bonding is very different. This is because between the Os(1)-Os(2,3) atoms, the net d bonding is mainly between the e_g-orbitals while for the Os(2)-Os(3)

bonds it is the t_{2g}-type orbitals that contribute most to the overlap populations. It is the hydridic nature of the hydrogen atoms that causes a withdrawal of electrons from Os(2) and Os(3), thereby increasing the t_{2g}-t_{2g} bonding at the expense of the e_g-e_g bonding.

Reactions involving this cluster often proceeds via a shift of one bridging hydride in to a terminal position, thereby forming the 48e$^-$ $Os_3(\mu\text{-H})(CO)_{10}L$ cluster. Depending on its steric bulk, the incoming ligand then either occupies an axial or an equatorial site (see Figure 3.5.2). [22]

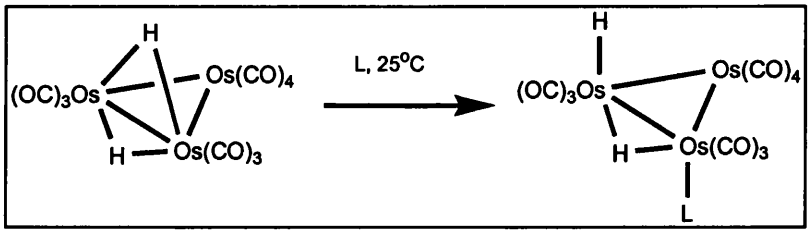

Figure 3.5.2 Associative Reactions of $Os_3(\mu\text{-H})_2(CO)_{10}$

3.5.2 Ligand Transformations – Thiolato Complexes

The pioneering work on the reactions of thiols with clusters began with iron carbonyls, when mercaptobenzothiazole was found to behave in an anomalous way.[26, 27] The product was subsequently identified as $Fe_3(\mu_3\text{-}S_2)(CO)_9$. Later, thiolato reactions involving ruthenium and osmium clusters led to the isolation of complexes with the general formula $M_3(\mu\text{-H})(\mu\text{-SR})(CO)_9$.[28, 29, 30]

Many of these reactions involving sulphur-based organic ligands were geared towards modelling surface reactions, such as those involving the coating of a metal surface. These have led on to studies aimed at modelling an improving the understanding of processes such as the desulphurisation of fossil fuels and the poisonous effects of sulphur on heterogeneous catalysts. [22]

While there has been much evidence that sulphide ligands are chemically reactive, there have also been established examples of sulphido trimetallic clusters that are extremely stable. In his review of cluster-assisted ligand transformations, Lavigne[22] provides an interesting and comprehensive review of some possible thiolato-transformations. An interesting example is given below.

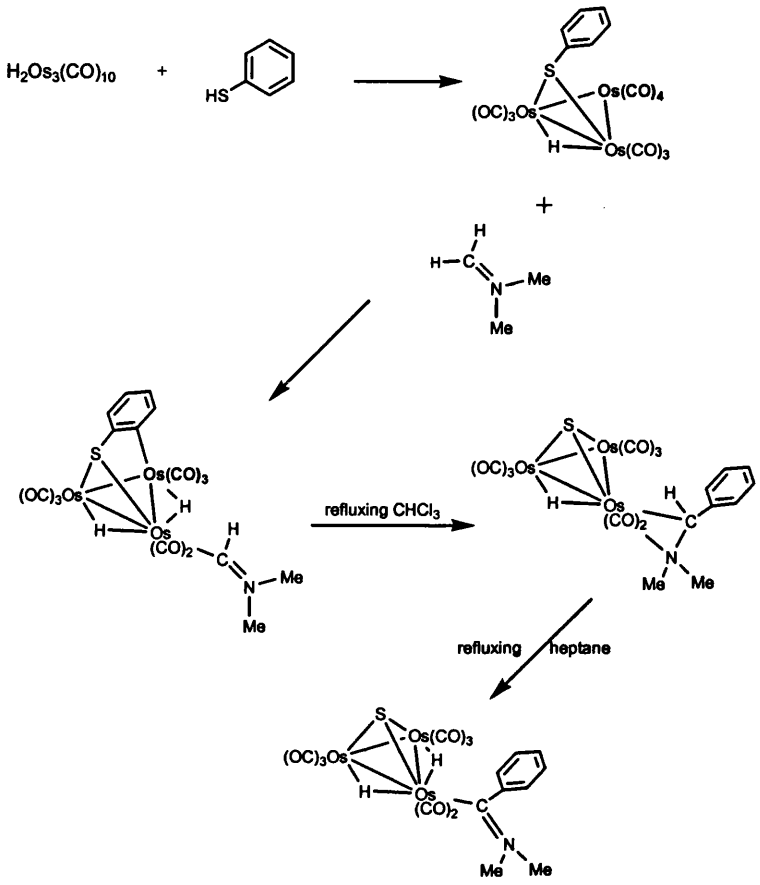

Figure 3.5.3 An example of thiolato ligand transformations on $Os_3(\mu\text{-}H)_2(CO)_{10}$

3.5.3 Ligand Transformations – Alkyne Cluster Complexes

Alkyne-reactions with metal clusters have generated much interest due to the variety of ligand transformations that can occur upon chelation to the metal core. These products are often unique structurally and have shown promise due to their unusual material properties,[11, 31, 32, 33] and their potential as precursors for nanoscale particles.[34]

However, some confusion can arise from comparing alkyne- and alkene- based reactions with clusters as both organic ligands, upon coordination to a cluster can lead to the formation of the same product. Cluster reactions with alkyne ligands can be broadly divided in to three categories; a) reactions in which the alkyne-ligand retains its original geometry upon coordination to the cluster; b) the alkyne-ligands link together to form complex organic units, and c) the formation of alkylidyne ligands formed by the rupture of the C-C triple bond.[11]

Figure 3.5.4 shows the various types of possible bonding modes of alkyne ligands upon coordination to trimetallic clusters.

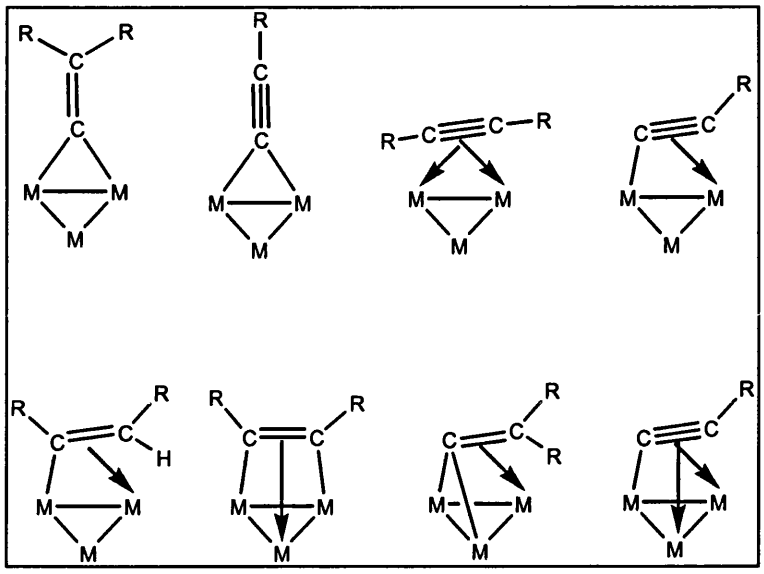

Figure 3.5.4 Various bonding modes of alkyne ligands in cluster complexes

The following subsections describe and discuss the results of reacting $Os_3(\mu\text{-}H)_2(CO)_{10}$ with 1,4-bis(3-thiophenyl)butadiyne and 1,3-bis(3-thiophenyl)butadiyne.

3.5.4 Synthesis of $Os_3(\mu\text{-}H)(CO)_{10}\{(\mu\text{-}\eta\text{-}(C_4H_3S)(C_8H_4S)\}$(1)

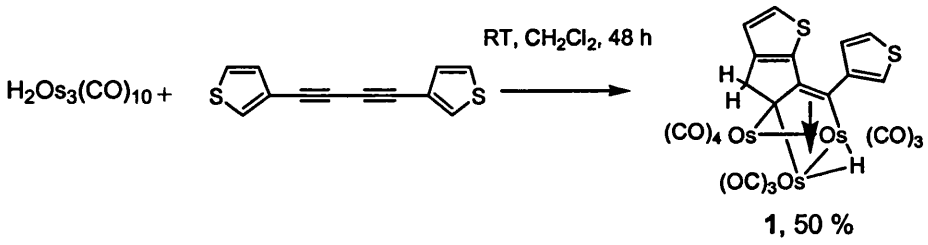

Figure 3.5.5 Reaction of $Os_3(\mu\text{-}H)_2(CO)_{10}$ and 1,4-bis(3-thiophenyl)butadiyne

Equimolar amounts of $Os_3(\mu\text{-}H)_2(CO)_{10}$ and 1,4-bis(3-thiophenyl)butadiyne were stirred in dichloromethane under nitrogen at room temperature for 48 hours. The resulting yellow solution was reduced under pressure and then separated by chromatography. Apart from a small amount of starting material, the major yellow product was identified using spectroscopy and single crystal X-ray diffraction as $[Os_3(\mu\text{-}H)(CO)_{10}\{(\mu\text{-}\eta\text{-}(C_4H_3S)(C_8H_4S)\}]$ (1), a 50-electron cluster, consistent with the metal-metal bonds.

3.5.4.1 Crystal Structure of $Os_3(\mu\text{-}H)(CO)_{10}\{(\mu\text{-}\eta\text{-}(C_4H_3S)(C_8H_4S)\}$(1)

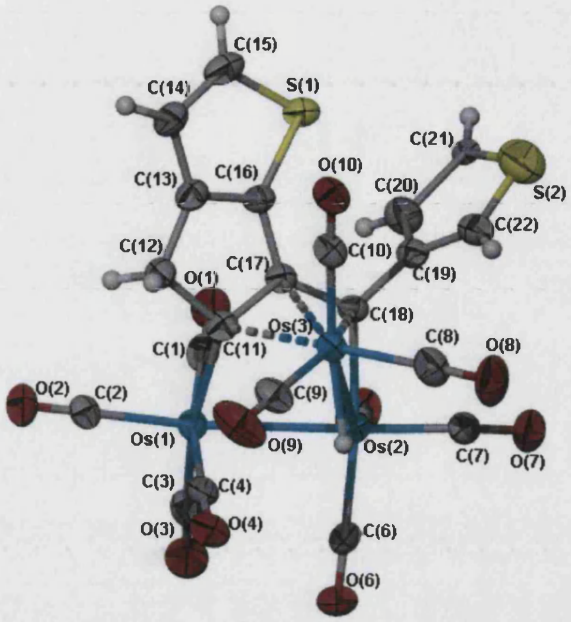

Figure 3.5.6 Structure of $Os_3(\mu\text{-}H)(CO)_{10}\{(\mu\text{-}\eta\text{-}(C_4H_3S)(C_8H_4S)\}$(**1**) showing atom-numbering scheme employed. Ellipsoids are drawn at 50% probability level.

The reaction of $Os_3(\mu\text{-}H)_2(CO)_{10}$ with 1,4-bis(3-thiophenyl)butadiyne yielded only one product $Os_3(\mu\text{-}H)(CO)_{10}\{(\mu\text{-}\eta\text{-}(C_4H_3S)(C_8H_4S)\}$(**1**) with no evidence of any other structural isomers. **1** crystallises in the *Monoclinic* space group *P* $2_1/c$ with four molecules in the asymmetric unit. The overall structure of the product is related to that of a series of cluster complexes derived from the cyclisation of diyenes with β-amino moieties.[53]

The core of the molecule consists of a triosmium cluster in an open triangular geometry with osmium-osmium bonds between Os(1)-Os(2) [2.8754(4)Å] and Os(2)-Os(3) [2.9112(4)Å], while the non-bonded Os(1)-Os(3) distance is 3.745Å. These Os-Os bond lengths lie within the range found in a plethora of other triosmium clusters,[5] the two bonded Os-Os distances being comparable to those in $Os_3(CO)_{12}$, 2.877(3)Å. There are also ten terminal carbonyls and a bridging hydride across the longest Os-Os bond. The Os(1)-Os(2)-Os(3) angle is fairly large at 80.647(11)°, compared with that in closed triangular clusters.

The alkyl carbons on the thiophene ligand have rearranged to form a five-membered ring fused to one of the thiophene rings. This rearranged ligand spans all three osmium atoms with bond lengths averaging 2.234 ± 0.069Å with the shortest between C(18)-Os(2) 2.153(7)Å and the longest at 2.322(8)Å between C(11)-Os(3). The carbon-carbon bonds on the ligand vary significantly, ranging from 1.343(12) Å to 1.583(11)Å which shows residual localization in the ring system, while the carbon-sulphur bonds average 1.688 ± 0.051Å.

The lone thiophene ring deviates from the plane of the fused rings by 82.80(24)°. [Plane 1: C(20)-C(21)-S(2)-C(22)-C(19); Plane 2: C(13)-C(14)-C(15)-S(1)-C(16)]

On the osmium atoms, the terminal carbonyl ligands are close to linear with angles ranging from 176.2(8)° to 179.2(8)°.

The slight variation of the ligand set of 1,4-bis(3-thiophenyl)butadiyne instead 1,4-bis(2-thiophenyl)butadiyne shows stark differences in the results of the ligand rearrangement. This is discussed in further detail in Section 3.5.5.

	Bond Lengths (Å)		**Bond Lengths (Å)**
Os(1)-Os(2)	2.8754(4)	C(11)-C(17)	1.428(11)
Os(2)-Os(3)	2.9112(4)	C(11)-C(12)	1.556(10)
C(11)-Os(1)	2.196(7)	C(12)-C(13)	1.503(11)
C(11)-Os(3)	2.322(8)	C(13)-C(16)	1.343(12)
C(17)-Os(3)	2.287(7)	C(13)-C(14)	1.433(11)
C(18)-Os(2)	2.153(7)	C(14)-C(15)	1.363(14)
C(18)-Os(3)	2.213(7)	C(15)-S(1)	1.735(10)
C(12)-C(13)	1.503(11)	C(16)-C(17)	1.470(10)
C(13)-C(16)	1.343(12)	C(16)-S(1)	1.718(8)
C(13)-C(14)	1.433(11)	C(17)-C(18)	1.428(11)
C(14)-C(15)	1.363(14)	C(19)-C(22)	1.356(12)
C(15)-S(1)	1.735(10)	C(19)-C(20)	1.408(12)
C(16)-C(17)	1.470(10)	C(20)-C(21)	1.583(11)
C(16)-S(1)	1.718(8)	C(21)-S(2)	1.622(8)
C(17)-C(18)	1.428(11)	C(22)-S(2)	1.675(9)

Table 3.5.1 Selected bond lengths for **1**

	Bond Angles (°)		**Bond Angles (°)**
Os(1)-Os(2)-Os(3)	80.647(11)	C(13)-C(12)-C(11)	103.1(6)
O(1)-C(1)-Os(1)	178.3(8)	C(16)-C(13)-C(14)	112.6(8)
O(2)-C(2)-Os(1)	178.9(7)	C(16)-C(13)-C(12)	111.0(7)
O(3)-C(3)-Os(1)	176.6(8)	C(14)-C(13)-C(12)	136.3(8)
O(4)-C(4)-Os(1)	178.5(8)	C(15)-C(14)-C(13)	111.3(8)
O(5)-C(5)-Os(2)	179.2(8)	C(14)-C(15)-S(1)	112.7(7)
O(6)-C(6)-Os(2)	178.6(9)	C(13)-C(16)-C(17)	110.6(7)
O(7)-C(7)-Os(2)	176.2(8)	C(13)-C(16)-S(1)	113.4(6)
O(8)-C(8)-Os(3)	178.6(9)	C(17)-C(16)-S(1)	135.7(6)
O(9)-C(9)-Os(3)	178.9(8)	C(11)-C(17)-C(18)	120.7(7)
O(10)-C(10)-Os(3)	178.4(8)	C(11)-C(17)-C(16)	108.4(7)

Table 3.5.2 Selected bond angles for **1**

3.5.4.2 Thermal decarbonylation of $Os_3(\mu\text{-H})(CO)_{10}\{(\mu\text{-}\eta\text{-}(C_4H_3S)(C_8H_4S)\}$(1) to yield 2

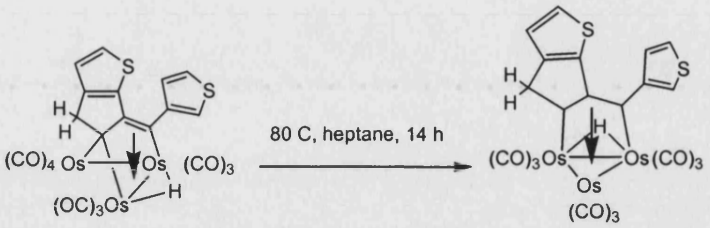

Figure 3.5.7 Thermal decarbonylation of $Os_3(\mu\text{-H})(CO)_{10}\{(\mu\text{-}\eta\text{-}(C_4H_3S)(C_8H_4S)\}$

$Os_3(\mu\text{-H})(CO)_{10}\{(\mu\text{-}\eta\text{-}(C_4H_3S)(C_8H_4S)\}$(**1**) was dissolved in heptane and heated for 14 hours under nitrogen. The resulting yellow solution was separated by chromatography and subsequently recrystallised from dichloromethane to yield pale yellow crystals characterised as $[Os_3(\mu\text{-H})(CO)_9\{(\mu_3\text{-}\eta^3\text{-}(C_4H_3S)(C_8H_4S)\}]$ (**2**).

2 was also formed when **1** was refluxed in toluene under hydrogen for 14 hours. The reaction mixture also contained some starting material, **1**, a small amount of $[Os_3(\mu\text{-H})_2(CO)_{10}]$, and a dark-brown decomposition product.

3.5.4.3 Crystal Structure of $Os_3(\mu\text{-H})(CO)_9\{(\mu_3\text{-}\eta^3\text{-}(C_4H_3S)(C_8H_4S)\}$ (2)

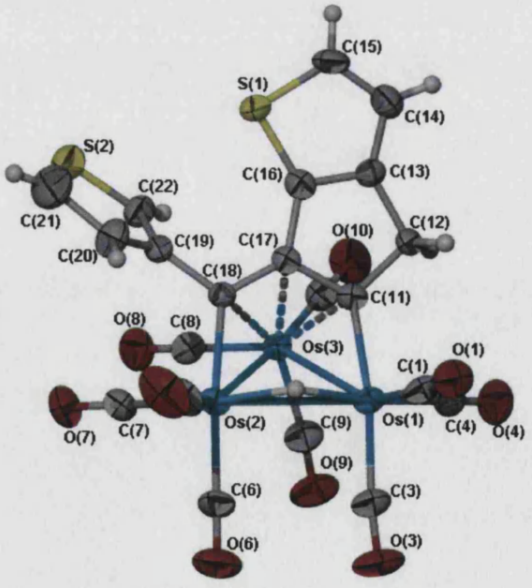

Figure 3.5.8 Structure of $Os_3(\mu\text{-H})(CO)_9\{(\mu_3\text{-}\eta^3\text{-}(C_4H_3S)(C_8H_4S)\}$ (**2**) showing atom-numbering scheme employed. Ellipsoids are drawn at 50% probability level. Disorder removed for clarity.

Upon heating, $Os(\mu\text{-}H)(CO)_{10}\{(\mu\text{-}\eta\text{-}(C_4H_3S)(C_8H_4S)\}$(1) loses a terminal carbonyl ligand and forms a closed core triosmium isosceles triangle to give the 48-electron cluster $[Os_3(\mu\text{-}H)(CO)_9\{(\mu_3\text{-}\eta^3\text{-}(C_4H_3S)(C_8H_4S)\}]$ (2) in quantitative yields. The ligand remains intact and coordinated to all three osmium atoms. The hydride ligand, as in **1**, also bridges the longest of the osmium-osmium bonds, Os(1)-Os(2), which is 2.9850(4)Å, while Os(1)-Os(3) and Os(2)-Os(3) distances are 2.8164(4)Å and 2.8158(4)Å respectively. All three of the Os-Os bond lengths now correspond to single bond values, but the two unbridged edges are shorter than those in (**1**), while the bridged edge is longer, consistent with the presence of a bridging hydride.[5, 23] The angles in the triangle are Os(3)-Os(1)-Os(2) 57.985(9)°, Os(3)-Os(2)-Os(1) 58.006(9)° and Os(2)-Os(3)-Os(1) 64.008(10)° respectively.

Bonds between the osmium and the coordinated ligand (osmium-carbon bonds) range from 2.054(7) to 2.348(7) Å compared to a smaller range of between 2.153(7) to 2.322(8) Å in **1**. While the carbon-carbon bonds of the ligand are comparable to those in **1**, ranging from the shortest at 1.328(17) Å [C(14)-C(15)] to 1.575(11)Å [C(20)-C(21)], there is a distinctly short carbon-sulphur bond between C(21) and S(2) at 1.585(9) Å. As in **1**, the lone thiophene ring also deviates significantly from the plane of the fused rings with dihedral angles of 64.72°. [Plane 1: C(19)-C(20)-C(21)-S(2)-C(22); Plane 2: C(16)-S(1)-C(15)-C(14)-C(13)] The C(21) and S(2) atoms of the thiophene ring are disordered over the two sites. Individual atomic sites were refined with 61%:39% occupancies and the atomic coordinates and displacement parameters tied together and summed to unity.

The terminal carbonyl ligands are all close to linear with the exception of C(3)-O(3)-Os(1) which is slightly bent at 173.6(1)°.

	Bond Lengths (Å)		**Bond Lengths (Å)**
Os(1)-Os(3)	2.8164(4)	C(17)-C(18)	1.406(9)
Os(1)-Os(2)	2.9850(4)	C(13)-C(14)	1.413(11)
Os(2)-Os(3)	2.8158(4)	C(11)-C(17)	1.449(10)
C(11)-Os(1)	2.054(7)	C(16)-C(17)	1.482(10)
C(11)-Os(3)	2.301(7)	C(18)-C(19)	1.507(9)
C(17)-Os(3)	2.348(6)	C(12)-C(13)	1.514(10)
C(18)-Os(2)	2.117(7)	C(11)-C(12)	1.536(10)
C(18)-Os(3)	2.308(7)	C(20)-C(21)	1.575(11)
C(14)-C(15)	1.328(13)	S(2)-C(21)	1.585(9)
C(13)-C(16)	1.376(11)	C(22)-S(2)	1.680(9)
C(19)-C(22)	1.391(12)	C(16)-S(1)	1.711(8)
C(19)-C(20)	1.401(11)	C(15)-S(1)	1.728(9)

Table 3.5.3 Selected bond lengths for **2**

	Bond Angles (°)		Bond Angles (°)
Os(3)-Os(1)-Os(2)	57.985(9)	O(6)-C(6)-Os(2)	177.3(10)
Os(3)-Os(2)-Os(1)	58.006(9)	O(7)-C(7)-Os(2)	179.4(9)
Os(2)-Os(3)-Os(1)	64.008(10)	O(8)-C(8)-Os(3)	179.7(9)
O(1)-C(1)-Os(1)	175.6(7)	O(9)-C(9)-Os(3)	175.0(9)
O(3)-C(3)-Os(1)	173.6(10)	C(16)-S(1)-C(15)	90.5(4)
O(4)-C(4)-Os(1)	175.8(8)	C(21)-S(2)-C(22)	100.1(4)
O(5)-C(5)-Os(2)	177.2(11)	C(20)-C(21)-S(2)	105.8(5)

Table 3.5.4 Selected bond angles for **2**

3.5.5 Synthesis of $Os_3(\mu\text{-H})(CO)_{10}\{(\mu\text{-}\eta\text{-}(C_4H_3S)(C_8H_4S)\}$ (3) and $Os_3(\mu\text{-H})(CO)_{10}\{(\mu_3\text{-}\eta^2\text{-}\eta^1\text{-}\eta^1\text{-}(SC_7H_4)C(SC_4H_3)\}$ (4a and 4b)

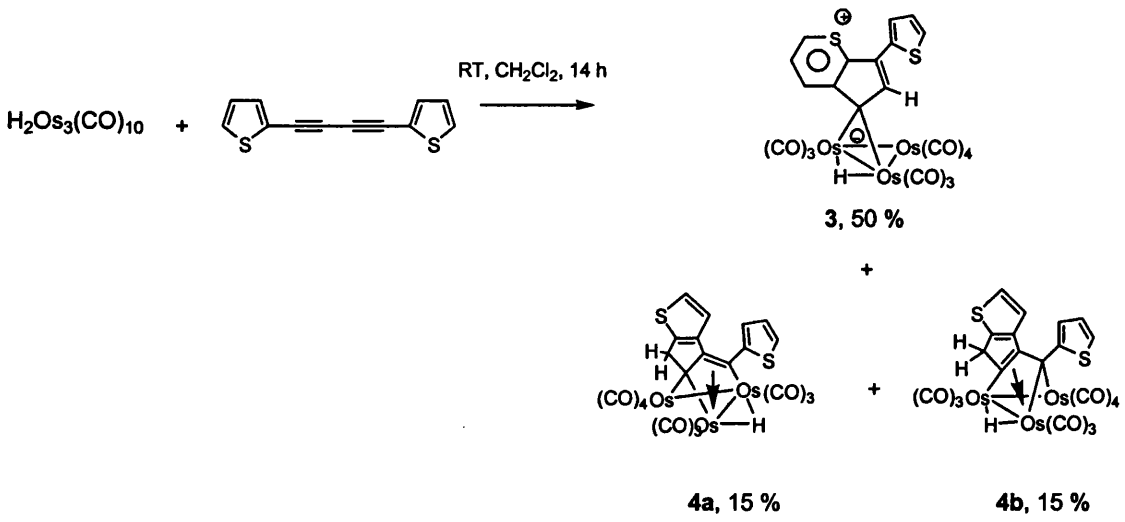

Figure 3.5.9 Reaction of $[Os_3(\mu\text{-H})(CO)_{10}]$ and 1,4-bis(2-thiophenyl)butadiyne

This reaction was based on literature methods,[35] where $Os_3(\mu\text{-}H_2)(CO)_{10}$ and 1,4-bis(2-thiophenyl)butadiyne were dissolved in dichloromethane and the resulting dark green solution was stirred at room temperature for 12 hours under nitrogen. The reaction mixture was separated by chromatography where the green main product, collected from the middle of the TLC plate was characterized as $[Os_3(\mu\text{-H})\ (CO)_{10}\{(\mu\text{-}\eta\text{-}(C_4H_3S)(C_8H_4S)\}]$ (**3**, yield 55 %) and a minor yellow band separated from the top of the TLC plate was identified as a pair of isomeric products, $[Os_3(\mu\text{-H})(CO)_{10}\{(\mu_3\text{-}\eta^2\text{-}\eta^1\text{-}\eta^1\text{-}(SC_7H_4)C(SC_4H_3)\}]$ (**4a** and **4b**) (combined yield 35%). Although this isomeric pair could not be separated chromatographically, they were able to be selectively crystallised yielding the crystal structure of the **4a**.

chromatographically, they were able to be selectively crystallised yielding the crystal structure of the **4a**.

While the structures of **3** and **4a** were able to be confirmed by single crystal X-ray crystallography, analysis of the remaining non-crystalline product **4b** is dependent on spectroscopic techniques which show a close resemblance between **4b** and **4a**. Markedly different IR spectra, and systematic shifts in the ^{1}H resonances throughout the NMR spectra suggests that these products are indeed structural isomers. In **4b**, it is likely that cyclisation similar to that in **4a**, has taken place, but the ligand insertion geometry to the metal framework is different. This would result in the travelling of the double bond in the tricarbon bridge, which could explain the observed shifts in the proton resonances, and in accordance with the recorded spectra, would not significantly affect the coupling constants. For **4b**, the free thiophenyl resonances are moved to higher frequencies (three double doublets 7.36–7.01 ppm) with respect to the corresponding values for **4a** (7.02–6.82 ppm), as well as the resonances from the newly formed substituted cyclopentathiophene ring (two doublets at 8.27 and 6.51 ppm for **4b** vs. 7.19 and 5.98 ppm for **4a**). The resonances from the two sp^3-protons in the five-membered ring give rise to two doublets centered at 3.76 and 3.48 ppm, with identical distortion and coupling constants as those observed for corresponding protons in **4a**. The observed low frequency (high field) shift most likely displays the vicinity of the double bond in the tricarbon bridge. The mechanistic route for the formation of these isomeric products remains ambiguous.

3.5.5.1 Crystal Structure of $Os_3(\mu\text{-H})\ (CO)_{10}\{(\mu\text{-}\eta\text{-}(C_4H_3S)(C_8H_4S)$ (3)

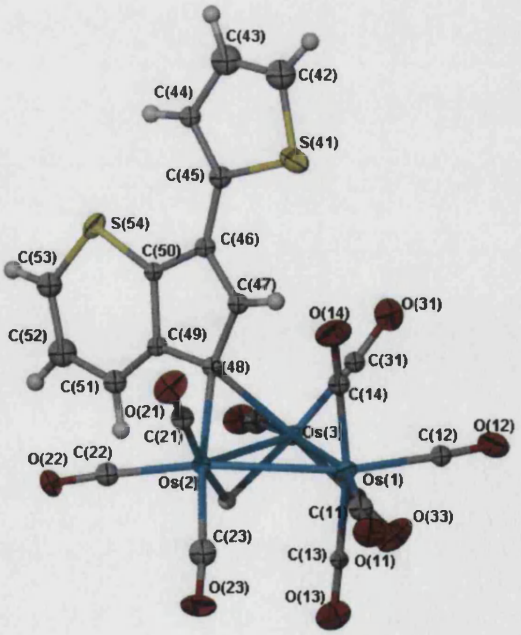

Figure 3.5.10 Structure of $Os_3(\mu\text{-H})\ (CO)_{10}\{(\mu\text{-}\eta\text{-}(C_4H_3S)(C_8H_4S)$ (**3**) showing atom-numbering scheme employed. Ellipsoids are drawn at 50% probability level.

The reaction between $[Os_3(\mu\text{-H})(CO)_{10}]$ and 1,4-bis(2-thiophenyl)butadiyne has effected a novel cyclisation of the bisthiophene ligand with the formation of a fused five-membered and six-membered ring. While the previous structural forms can be related to those in with the N-heterocyclic ligands,[53] this compound is unique.

The structure consists of a closed 48-electron triosmium core with ten terminal carbonyls, three each on Os(2) and Os(3) and four on Os(1), and a bridging hydride between the Os(2) and Os(3). The organic moiety lies perpendicular to the Os(2)-Os(3) axis with the ligand anchored via an alkylidene interaction from C(48) to Os(2) and Os(3) at almost equal distances of 2.25(2) and 2.26(2) Å for Os(2)-C(48) and Os(3)-C(48) respectively.

The six-membered ring is a product of ring expansion on one of the original thiophene ligands with bond lengths varying from 1.36(3) to 1.70(2) Å, with the carbon-sulphur bonds being equal. Unlike the earlier structures of **1** and **2**, the organic moiety in **3** is almost entirely planar with the dihedral angles between S(41)-C(42)-C(43)-C(44)-C(45) and C(46)-C(7)-C(48)-C(49)-C(50) at only 6.44(3)°.

The formation of this alkylidene complex is completely unprecedented, although there are publications in which five- and six-membered sulphur containing rings have been generated using iron and rhodium complexes.[26, 27] The ring expansion, via insertion of a carbon atom of the diyne backbone into the adjacent double bond of the thiophene ring, coupled with the ligand cyclisation, leads to a very novel product.

By comparison, the use of 1,4-bis(3-thiophenyl)butadiyne seems to completely prohibit the aromatic ring expansion upon coordination to $[H_2Os_3(CO)_{10}]$. It seems likely that in addition to the hydride transfer from the cluster core to the coordinating ligand, there is also a significant interaction of one of the thiophene sulphur atoms of 1,4-bis(2-thiophenyl)butadiyne with either the cluster core, or the alkyl carbons, which may trigger the ring expansion as observed for cluster **3**. In the case of 3-thienyl-substitution this pathway becomes unavailable, most likely due to the loss of suitable interaction geometry or distance.

The packing of the complex in the solid state, is governed by the ligand-ligand interactions which consists of a staggered π-π stacking interaction, shown in Figure 3.5.11. The centroid-centroid distances between the thiophene ring and the six-membered sulphur ring below it is at 3.773Å.

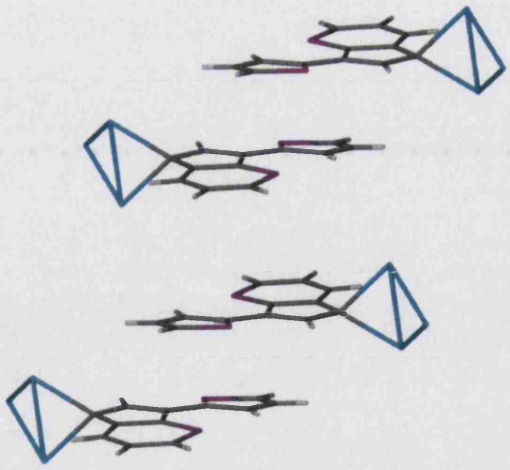

Figure 3.5.11 π-π interactions of the ligands

	Bond Lengths (Å)		**Bond Lengths (Å)**
Os(1)-Os(3)	2.881(2)	C(51)-C(52)	1.42(3)
Os(2)-Os(3)	2.777(3)	C(49)-C(50)	1.46(3)
Os(1)-Os(2)	2.879(3)	C(52)-C(53)	1.36(3)
Os(2)-C(48)	2.25(2)	C(53)-S(54)	1.69(2)
Os(3)-C(48)	2.26(2)	S(54)-C(50)	1.70(2)
C(46)-C(47)	1.36(3)	C(50)-C(46)	1.42(3)
C(47)-C(48)	1.43(3)	C(45)-C(46)	1.45(3)
C(48)-C(49)	1.44(3)	C(49)-C(51)	1.37(3)

Table 3.5.5 Selected bond lengths for **3**[35]

	Bond Angles (°)		**Bond Angles (°)**
Os(1)-Os(3)-Os(2)	61.14(7)	C(51)-C(52)-C(53)	124(2)
Os(2)-Os(1)-Os(3)	57.65(7)	C(52)-C(53)-S(54)	12492)
Os(1)-Os(2)-Os(3)	61.21(6)	C(53)-S(54)-C(50)	104(1)
Os(2)-C(48)-Os(3)	76.1(6)	C(46)-C(45)-C(44)	132(2)
C(47)-C(48)-C(49)	103(2)	C(46)-C(45)-S(41)	117.6(14)
C(48)-C(47)-C(46)	115(2)	C(45)-S(41)-C(42)	91.3(11)
C(48)-C(49)-C(50)	108(2)	S(41)-C(42)-C(43)	113(2)
C(48)-C(49)-C(51)	132(2)	C(42)-C(43)-C(44)	115(2)
C(49)-C(51)-C(52)	125(2)	C(43)-C(44)-C(45)	111(2)

Table 3.5.6 Selected bond angles for **3**[35]

3.5.5.2 Crystal Structure of $Os_3(\mu\text{-}H)(CO)_{10}\{(\mu_3\text{-}\eta^2\text{-}\eta^1\text{-}\eta^1\text{-}(SC_7H_4)C(SC_4H_3)\}$ (4a)

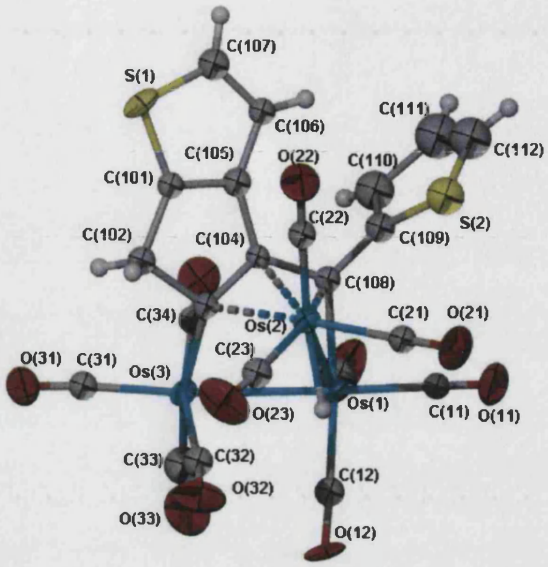

Figure 3.5.12 Structure of $Os_3(\mu\text{-}H)(CO)_{10}\{(\mu_3\text{-}\eta^2\text{-}\eta^1\text{-}\eta^1\text{-}(SC_7H_4)C(SC_4H_3)\}$ (**4a**) showing atom-numbering scheme employed. Ellipsoids are drawn at 50% probability level.

The metal core of **4a** consists of an open 50-electron triosmium unit, coordinated by a rearranged ligand system. The open triangular unit is also coordinated by ten terminal carbonyls and a bridging hydride between Os(1) and Os(2). The osmium-osmium distances are comparable to those in **3** at 2.867(2)Å between Os(1)- Os(3) and 2.905(2) between Os(1)-Os(2), while the non-bonded Os(2)-Os(3) distance is 3.748Å.

The ligand in this case, has rearranged in a manner similar to that in **1**, where a five-membered ring is fused to one of the thiophene rings. The transformed ligand bridges all three osmium atoms acting as a five electron donor. Bond lengths within the ligand range from 1.23(4)Å between C(111)-C(112) to1.70(2) between S(1)-C(107) and S(1)-C(101).

As in **1** and in **2**, the free thiophene ring is twisted away from the Os(2)-Os(3) axis to avoid the steric clash between this group and the protruding proton bound to C(106). The dihedral angle between C(109)-S(20-C(112)-C(111)-C(110) and C(101)-C(105)-C(106)-C(107)-S(1) is 87.83(2)°.

	Bond Lengths (Å)		**Bond Lengths (Å)**
Os(1)-Os(3)	2.867(2)	C(112)-C(111)	1.23(4)
Os(1)-Os(2)	2.905(2)	C(111)-C(110)	1.58(4)
Os(1)-C(108)	2.16(2)	C(110)-C(109)	1.58(2)
Os(3)-C(103)	2.15(2)	C(104)-C(105)	1.49(3)
Os(2)-C(103)	2.31(2)	C(105)-C(101)	1.37(3)
Os(2)-C(104)	2.28(2)	C(105)-C(106)	1.42(3)
Os(2)-C(108)	2.24(2)	C(106)-C(107)	1.36(3)
C(108)-C(109)	1.45(3)	S(1)-C(107)	1.70(2)
C(108)-C(104)	1.45(3)	S(1)-C(101)	1.70(2)
C(103)-C(104)	1.41(3)	C(101)-C(102)	1.53(3)
C(109)-S(2)	1.66(2)	C(102)-C(103)	1.61(3)
S(2)-C(112)	1.64(3)		

Table 3.5.7 Selected bond lengths for **4a**[35]

	Bond Angles (°)		**Bond Angles (°)**
Os(2)-Os(1)-Os(3)	80.98(5)	C(102)-C(101)-S(1)	134(2)
Os(2)-C(103)-Os(3)	114.0(9)	C(105)-C(101)-S(1)	112(2)
C(103)-C(104)-C(108)	121(2)	C(101)-S(1)-C(107)	92.5(10)
C(104)-C(108)-C(109)	120(2)	S(1)-C(107)-C(106)	113(2)
C(102)-C(103)-C(104)	107(2)	C(107)-C(106)-C(105)	111(2)
C(101)-C(102)-C(103)	100(2)	C(106)-C(105)-C(104)	141(2)
C(105)-C(101)-C(102)	114(2)	C(105)-C(104)-C(108)	126(2)

Table 3.5.8 Selected bond angles for **4a**[35]

3.5.6 Thermal decarbonylation of $Os_3(\mu\text{-}H)(CO)_{10}\{(\mu\text{-}\eta\text{-}(C_4H_3S)(C_8H_4S)\}$ to yield 4 and 5

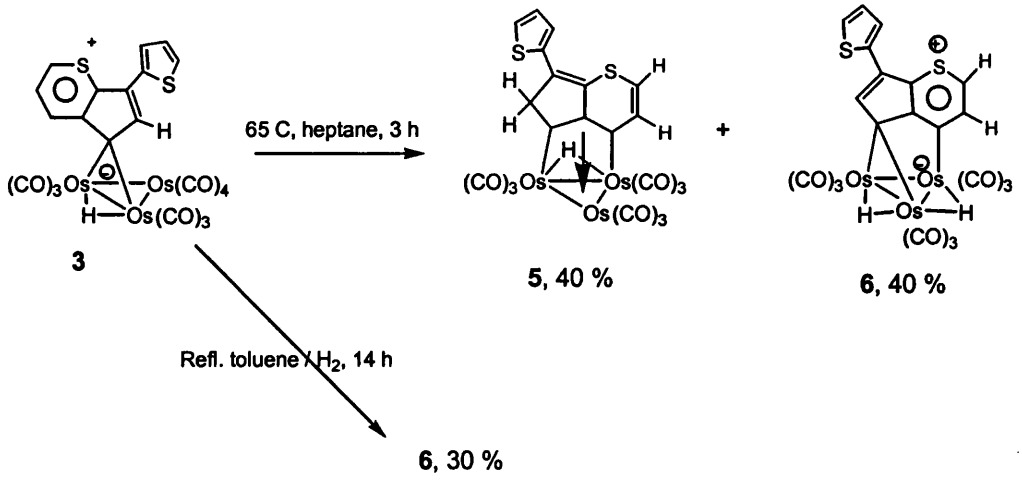

Figure 3.5.13 Thermal decarbonylation of $Os_3(\mu\text{-}H)(CO)_{10}\{(\mu\text{-}\eta\text{-}(C_4H_3S)(C_8H_4S)\}$

When $Os_3(\mu\text{-}H)(CO)_{10}\{(\mu\text{-}\eta\text{-}(C_4H_3S)(C_8H_4S)\}$(**3**) was heated at 65°C under nitrogen, in heptane for 3 hours an orange solution resulted. Separation by chromatography gave approximately equal amounts of orange and red products. The orange product (yield 40 %) (with a high Rf value,) was recrystallised from dichloromethane as a microcrystalline solid that was characterized by spectroscopic methods and single crystal X-ray diffraction as $[Os_3(\mu\text{-}H)(CO)_9\{(\mu_3\text{-}\eta^3\text{-}(C_4H_3S)(C_8H_4S)\}]$ (**5**). The second product yielded dark red crystals from the slow evaporation of a chloroform solution at –20°C and was characterised as $[Os_3(\mu\text{-}H)_2(CO)_9\{(\mu_3\text{-}\eta^1\text{-}\eta^1\text{-}(C_4H_3S)(C_8H_3S)\}]$ (**6**).

6 was also formed when **3** was refluxed in toluene under hydrogen for 14 hours. Some decomposition products and the starting dihydride cluster $Os_3(\mu\text{-}H)_2(CO)_{10}$ were also recovered.

3.5.6.1 Crystal structure of $Os_3(\mu\text{-}H)(CO)_9\{(\mu_3\text{-}\eta^3\text{-}(C_4H_3S)(C_8H_4S)\}$ (5).

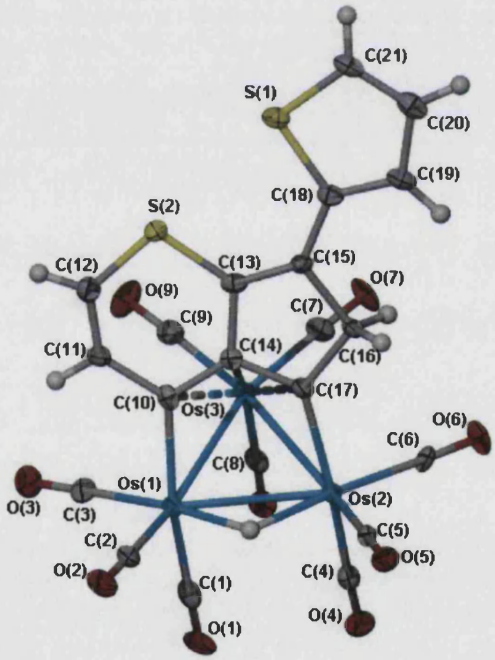

Figure 3.5.14 Structure of $Os_3(\mu\text{-}H)(CO)_9\{(\mu_3\text{-}\eta^3\text{-}(C_4H_3S)(C_8H_4S)\}$ (**5**) showing atom-numbering scheme employed. Ellipsoids are drawn at 50% probability level. Dichloromethane solvent omitted for clarity

The structure of **5** consists of a closed 48-electron triosmium triangular core with nine terminal carbonyls, one on each of the osmium atoms, a bridging hydride and the transformed organic ligand coordinated to all three metal atoms.

The Os-Os bonds are an average of 2.821 ± 0.083Å, with the hydride ligand bridging the longest, Os(1)-Os(2) which is 2.9036(4)Å. Meanwhile the bond angles range between 57.145(11)° and 62.960(12)°.

On the coordinated ligand, carbon-carbon bonds range from 1.275(12) between C(13)-C(15) to 1.527(12)Å between C(15)-C(16), while the carbon-sulphur bonds average 1.707 ± 0.044Å. The ligand is coordinated to the osmium core through five bonds ranging from 2.050(9)Å [C(17)-Os(2)] to 2.329(8)Å [C(10)-Os(3)]. As in **3**, the thiophene ring does not deviate significantly from the plane of the fused rings with dihedral angles between the two at only 5.30°. [Plane 1: S(1)-C(18)-C(190-C(20)-C(21); Plane 2: C(13)-C(14)-C(15)-C(16)-C(17)]

Meanwhile the osmium-carbonyl bond angles are close to linearity with the furthest deviation being 175.9(8)° for Os(2)-C(5)-O(5).

Figure 3.5.15 shows the packing of the complex in the solid state, which is governed by π-π interactions between the ligands also akin to that in **3**. The closest centroid-centroid interaction is also between the six-membered sulphur ring and the thiophene ring at 3.691Å.

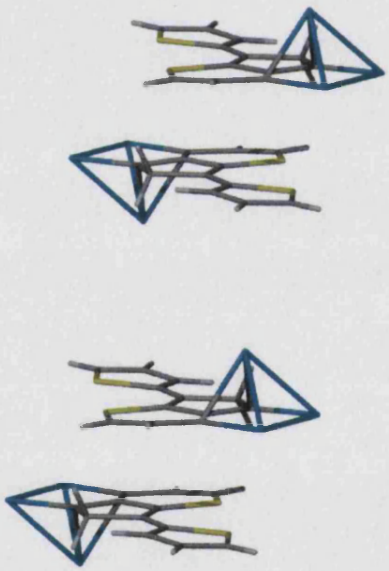

Figure 3.5.15 Packing diagram of **5**.

	Bond Lengths (Å)		**Bond Lengths (Å)**
Os(1)-Os(3)	2.7385(4)	C(14)-C(17)	1.415(12)
Os(1)-Os(2)	2.9036(4)	C(14)-Os(3)	2.306(8)
Os(2)-Os(3)	2.8202(5)	C(15)-C(18)	1.414(12)
C(10)-C(14)	1.389(12)	C(15)-C(16)	1.527(12)
C(10)-C(11)	1.467(12)	C(16)-C(17)	1.480(11)
C(10)-Os(1)	2.079(9)	C(17)-Os(2)	2.050(9)
C(10)-Os(3)	2.329(8)	C(17)-Os(3)	2.293(8)
C(11)-C(12)	1.324(13)	C(18)-C(19)	1.325(13)
C(12)-S(2)	1.688(10)	C(18)-S(1)	1.742(10)
C(13)-C(15)	1.275(12)	C(21)-S(1)	1.653(9)
C(13)-C(14)	1.453(12)	C(22)-Cl(2)	1.705(13)
C(13)-S(2)	1.744(9)	C(22)-Cl(1)	1.722(13)

Table 3.5.9 Selected bond lengths for **5**

	Bond Angles (°)		**Bond Angles (°)**
Os(3)-Os(1)-Os(2)	59.896(11)	O(9)-C(9)-Os(3)	178.4(9)
Os(3)-Os(2)-Os(1)	57.145(11)	C(21)-S(1)-C(18)	92.5(5)
Os(1)-Os(3)-Os(2)	62.960(12)	C(12)-S(2)-C(13)	100.8(5)
O(1)-C(1)-Os(1)	177.5(9)	C(17)-C(16)-C(15)	105.6(7)
O(2)-C(2)-Os(1)	177.0(9)	C(14)-C(17)-C(16)	103.6(7)
O(3)-C(3)-Os(1)	177.8(9)	C(15)-C(13)-C(14)	109.3(8)
O(4)-C(4)-Os(2)	176.0(8)	C(15)-C(13)-S(2)	127.4(7)
O(5)-C(5)-Os(2)	175.9(8)	C(14)-C(13)-S(2)	123.2(7)
O(6)-C(6)-Os(2)	178.0(9)	C(19)-C(18)-C(15)	125.8(9)
O(7)-C(7)-Os(3)	177.5(9)	C(19)-C(18)-S(1)	110.5(7)
O(8)-C(8)-Os(3)	177.9(8)	C(15)-C(18)-S(1)	123.7(7)

Table 3.5.10 Selected bond angles for **5**

3.5.6.2 Crystal structure of $Os_3(\mu\text{-}H)_2(CO)_9\{(\mu_3\text{-}\eta^1\text{-}\eta^1\text{-}(C_4H_3S)(C_8H_3S)\}$ (6).

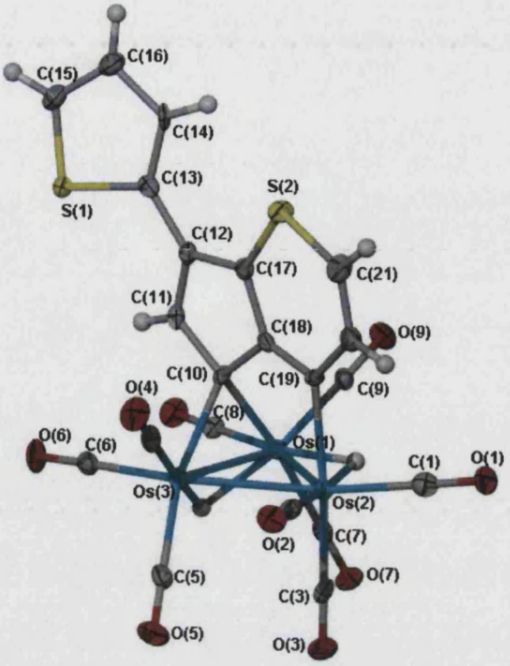

Figure 3.5.16 Structure of $Os_3(\mu\text{-}H)(CO)_9\{(\mu_3\text{-}\eta^3\text{-}(C_4H_3S)(C_8H_4S)\}$ (**6**) showing atom-numbering scheme employed. Ellipsoids are drawn at 50% probability level. Disorder and dichloromethane solvent omitted for clarity

The red product, **6**, was confirmed by X-ray crystallography to be $Os_3(\mu\text{-}H)_2(CO)_9\{(\mu_3\text{-}\eta^1\text{-}\eta^1\text{-}(C_4H_3S)(C_8H_3S)\}$. It consists of a closed triosmium triangular core with nine terminal carbonyls and two bridging hydrides between Os(1)- Os(2) and Os(1)-Os(3). The complex has also crystallised with a dichloromethane solvent molecule in the lattice. The osmium-osmium bonds average 2.888 ± 0.119Å with the hydrides on the longest [Os(1)-Os(2) 3.0238 (3)Å] and the shortest [Os(1)-Os(2) 2.7965(3)Å]of the osmium-osmium bonds. The terminal carbonyls on the osmiums are almost all linear with the average angle being 178.2 ± 0.7°.

The bis-thiophene ligand has undergone a transformation similar to that in **3** and **5**, which consists of a fused five-membered and six-membered sulphur ring linked by C(12)-C(13) 1.441 (9)Å to the thiophene ring. This transformed ligand lies almost perpendicular to the plane of the osmium triangle and is bound by C(10)-Os(1) 2.199(6)Å, C(10)-Os(1) 2.187(6)Å and C(19)-Os(2) 2.137(6)Å.

The atoms S(1) and C(14) in the lone thiophene ring are disordered over the two sites, and individual atomic sites were refined at 80%:20% occupancies and the atomic coordinates and displacement parameters tied together and summed to unity.

The carbon-carbon bonds in the fused rings average 1.41 ± 0.36 Å with the shortest bond between C(20)-C(21) 1.351(10)Å and the longest between C(10)- C(18) 1.46(9)Å, while the carbon-sulphur bonds are typical at 1.710(7) for S(2)-C(21) and 1.713(7) for S(2)-C(17).

	Bond Lengths (Å)		**Bond Lengths (Å)**
Os(1)-Os(3)	2.7965(3)	C(18)-C(19)	1.380(9)
Os(1)-Os(2)	3.0238(3)	C(19)-C(20)	1.422(9)
Os(2)-Os(3)	2.8445(3)	C(20)-C(21)	1.351(10)
Os(1)-C(10)	2.187(6)	C(13)-C(14)	1.357(13)
Os(2)-C(19)	2.137(6)	C(14)-C(16)	1.422(13)
Os(3)-C(10)	2.199(6)	C(15)-C(16)	1.336(11)
C(11)-C(12)	1.399(9)	S(2)-C(21)	1.710(7)
C(12)-C(17)	1.434(9)	S(2)-C(17)	1.713(7)
C(10)-C(11)	1.450(9)	S(1)-C(15)	1.671(8)
C(10)-C(18)	1.460(9)	S(1)-C(13)	1.733(7)
C(17)-C(18)	1.420(9)		

Table 3.5.11 Selected bond lengths for **6**

	Bond Angles (°)		**Bond Angles (°)**
Os(3)-Os(1)-Os(2)	58.357(8)	C(13)-C(14)-C(16)	116.4(8)
Os(3)-Os(2)-Os(1)	56.821(8)	C(16)-C(15)-S(1)	115.2(6)
Os(1)-Os(3)-Os(2)	64.822(9)	C(15)-C(16)-C(14)	108.5(7)
C(15)-S(1)-C(13)	92.2(4)	C(18)-C(17)-C(12)	109.8(6)
C(21)-S(2)-C(17)	101.2(3)	C(18)-C(17)-S(2)	122.8(5)
C(12)-C(11)-C(10)	112.1(6)	C(12)-C(17)-S(2)	127.3(5)
C(11)-C(12)-C(17)	105.7(6)	C(19)-C(18)-C(17)	125.6(6)
C(11)-C(12)-C(13)	126.9(6)	C(19)-C(18)-C(10)	125.8(6)
C(17)-C(12)-C(13)	127.4(6)	C(17)-C(18)-C(10)	108.3(6)
C(14)-C(13)-C(12)	132.3(7)	C(18)-C(19)-C(20)	119.9(6)
C(14)-C(13)-S(1)	107.6(6)	C(21)-C(20)-C(19)	123.5(6)
C(12)-C(13)-S(1)	120.0(5)	C(20)-C(21)-S(2)	126.9(6)

Table 3.5.12 Selected bond angles for **6**

3.5.6.3 Thermal decarbonylation of $Os_3(\mu\text{-}H)(CO)_{10}\{(\mu_3\text{-}\eta^2\text{-}\eta^1\text{-}\eta^1\text{-}(SC_7H_4)C(SC_4H_3)\}$ 4a and 4b to yield 7

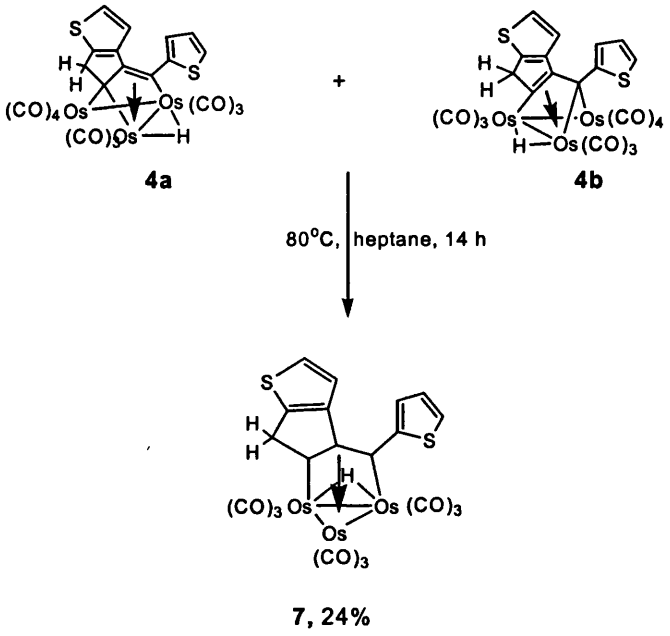

Figure 3.5.17 Thermal decarbonylation of $Os_3(\mu\text{-}H)(CO)_{10}\{(\mu_3\text{-}\eta^2\text{-}\eta^1\text{-}\eta^1\text{-}(SC_7H_4)C(SC_4H_3)\}$

When the isomeric mixture **4a** and **4b** was heated in heptane at 90°C for 27 hours, a single decarbonylated yellow product was formed (7mg, 24 %). This was characterised by spectroscopic and single crystal X-ray diffraction as $[Os_3(\mu\text{-}H)(CO)_9\{(\mu_3\text{-}\eta^3\text{-}(C_4H_3S)(C_8H_4S)\}]$ (7)

3.5.6.4 Crystal structure of $Os_3(\mu\text{-}H)(CO)_9\{(\mu_3\text{-}\eta^3\text{-}(C_4H_3S)(C_8H_4S)\}$(7)

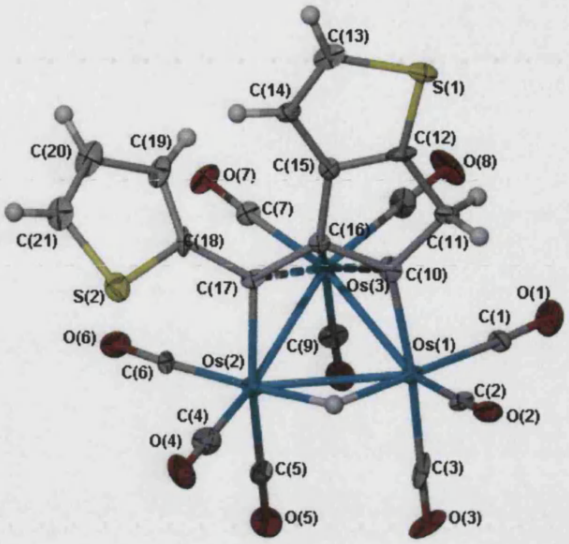

Figure 3.5.18 Structure of $Os_3(\mu\text{-}H)(CO)_9\{(\mu_3\text{-}\eta^3\text{-}(C_4H_3S)(C_8H_4S)\}$ (**7**) showing atom-numbering scheme employed. Ellipsoids are drawn at 50% probability level.

The crystal structure of **7** consists of a closed 48-electron triangle of osmium atoms coordinated to nine terminal carbonyls (three on each osmium atoms), a bridging hydride and the transformed ligand coordinated to all three osmium atoms.

The osmium-osmium bond lengths are 2.8005(7) [Os(2)-Os(3)], 2.8250(7) [Os(2)-Os(3)] and 2.9407(7) [Os(1)-Os(2)] respectively, with the hydride bridging the longest of the metal-metal bonds. Nearly all the terminal carbonyls are close to linear with the exception of O(2)-C(2)-Os(1) at 173.6(11)°.

The ligand is akin to that in both **4a** and **4b** with a fused five-membered ring and a thiophene attached through C(17)-C(18) [1.487(16)Å]to another thiophene ring. The ligand has bonds to all three osmium metals ranging from 2.072(12) for C(10)-Os(1) to 2.340(11) for C(17)-Os(3).

Within ligand, the carbon-carbon bonds average 1.43 ± 0.07Å with the shortest bonds between C(20)-C(21) at 1.33(2)Å and between C(12)-C(15) at 1.347(17)Å, while the longest bonds are C(10)-C(11) 1.512(17)Å and C(11)-C(12) at 1.511(16)Å. The carbon-sulphur bonds range from 1.694(12) to 1.757(13) Å for C(12)-S(1) and C(13)-S(1) respectively.

	Bond Lengths (Å)		**Bond Lengths (Å)**
Os(1)-Os(3)	2.8250(7)	C(13)-C(14)	1.350(19)
Os(1)-Os(2)	2.9407(7)	C(13)-S(1)	1.757(13)
Os(2)-Os(3)	2.8005(7)	C(14)-C(15)	1.423(17)
C(10)-Os(1)	2.072(12)	C(15)-C(16)	1.501(16)
C(10)-Os(3)	2.259(14)	C(16)-C(17)	1.420(17)
C(16)-Os(3)	2.326(12)	C(17)-C(18)	1.487(16)
C(17)-Os(2)	2.124(11)	C(18)-C(19)	1.395(18)
C(17)-Os(3)	2.340(11)	C(19)-C(20)	1.415(17)
C(10)-C(11)	1.512(17)	C(20)-C(21)	1.33(2)
C(11)-C(12)	1.511(16)	C(18)-S(2)	1.733(13)
C(12)-C(15)	1.347(17)	C(21)-S(2)	1.709(14)
C(12)-S(1)	1.694(12)		

Table 3.5.13 Selected bond lengths for **7**

	Bond Angles (°)		**Bond Angles (°)**
Os(3)-Os(2)-Os(1)	58.891(16)	C(14)-C(15)-C(16)	140.7(12)
Os(3)-Os(1)-Os(2)	58.077(16)	C(17)-C(16)-C(10)	123.6(11)
Os(2)-Os(3)-Os(1)	63.031(17)	C(17)-C(16)-C(15)	128.6(11)
C(12)-C(11)-C(10)	103.5(10)	C(10)-C(16)-C(15)	107.2(10)
C(15)-C(12)-C(11)	111.2(10)	C(19)-C(18)-C(17)	130.7(12)
C(15)-C(12)-S(1)	115.4(10)	C(19)-C(18)-S(2)	110.3(9)
C(11)-C(12)-S(1)	133.4(10)	C(17)-C(18)-S(2)	118.9(10)
C(14)-C(13)-S(1)	110.4(10)	C(18)-C(19)-C(20)	111.0(13)
C(13)-C(14)-C(15)	114.5(12)	C(21)-C(20)-C(19)	115.0(14)
C(12)-C(15)-C(14)	109.7(11)	C(20)-C(21)-S(2)	111.5(11)
C(12)-C(15)-C(16)	109.3(11)		

Table 3.5.14 Selected bond angles for **7**

3.5.7 Reaction of 3 with Trifluoroacetic acid to yield 8 and 9

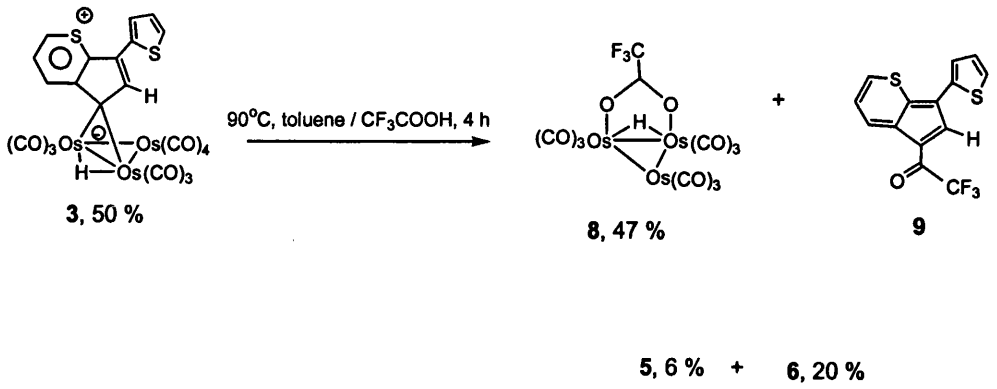

Figure 3.5.19 Reaction of 1 with trifluoroacetic acid

When triflouroacetic acid was added dropwise to a toluene solution of **3** and heated to 90°C under nitrogen, the resulting dark green mixture became a dark reddish-violet solution. Chromatographic separation of the mixture yielded small amounts of the expected decarbonylated clusters **5** (3 mg, 6.1 %), and **6** (10 mg, 20.5 %), as well as a yellow product (high Rf) characterized as $[Os_3(\mu\text{-}H)(CO)_{10}(O_2CCF_3)]$ (**8**) (21 mg, 47 %). A fourth, intensely deep blue coloured product **9** (10 mg) was separated from the bottom of the TLC plate. Spectroscopic analysis and single crystal X-ray diffraction identified the compound as the organic fragment cleaved from the parent cluster.

Ligand transformations upon anchorage to a cluster surface have yielded a wide variety of organic ligands. While these transformations have been useful in modelling surface reactions, the possibility of clusters to be used as catalysts has been proposed but has not actually found application due to the often hard bonds between the metal surfaces and the chelated ligands.

In an effort to simulate a clusters' function as a catalyst, attempts were made to cleave the coordinated thiopyrylium ligand from clusters **1** and **3**.

Initial thermal reactions under hydrogen, in the presence of aqueous NaOH, yielded only small amounts of the starting dihydride cluster $Os_3(\mu\text{-}H_2)(CO)_{10}$ and the stable decarbonylated clusters **2, 5** and **6**.

As bases did not produce the results hoped for, attempts were then carried out using concentrated hydrochloric acid in a dichloromethane solution based on reports that alkoxy bridge diols were successfully cleaved from a triosmium cluster.[36] This however proved to be inefficient even under mild heating.

When trifluoromethyl sulfonic acid was used in chloroform, the reaction proceed extremely rapidly, causing an immediate colour change from green to red and finally the formation of dark brown insoluble decomposition product which could not be further analysed.

Based on a successful cleavage reaction yielding $[HOs_3(CO)_{10}(OOCCF_3]$ from $[HOs_3(CO)_{10}(OSi\equiv)]$ in good yields,[37] **3** was reacted with an excess of CF_3COOH at 90°C. Small amounts of the decarbonylated clusters **5** and **6** were formed but the main products were $[Os_3(\mu\text{-}H)(CO)_{10}(O_2CCF_3)]$ (**8**) and an intensely coloured blue compound, subsequently identified as the thiophene-substituted cyclopentathiapuran derivative (**9**) cleaved from the parent cluster.

3.5.7.1 Crystal structure of $Os_3(\mu\text{-}H)(CO)_{10}(O_2CCF_3)$ (8)

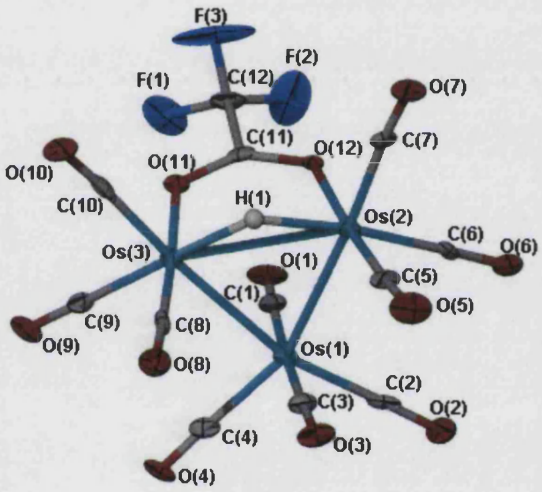

Figure 3.5.20 Structure of $Os_3(\mu\text{-}H)(CO)_{10}(O_2CCF_3)]$ (**8**) showing atom-numbering scheme employed. Ellipsoids are drawn at 50% probability level.

$Os_3(\mu\text{-}H)(CO)_{10}(O_2CCF_3)$ was formed as one of the major products from the successful cleavage of the organic moiety from the 48-electron triosmium cluster **3**. It consists as expected, of a closed triosmium core with a bridging hydride between the longest osmium-osmium bonds, Os(2)-Os(3) 2.9322(5)Å, and ten terminal carbonyl bonds, three each on Os(2) and Os(3) and four on Os(1). The angles within the metal core range from 53.861(12)° for Os(1)-Os(3)-Os(2) to 67.887(13)° for Os(2)-Os(1)-Os(3).

The trifluoroacetic acid moiety bridges the triangular osmium core with O(12) bound to Os(2) and O(11) bound to Os(3) at distances of 2.122(6) and 2.135(5)Å respectively.

The terminal carbonyls are almost all close to linear with Os-C-O angles averaging 177.02 ± 1.58Å.

	Bond Lengths (Å)		**Bond Lengths (Å)**
O(11)-Os(3)	2.122(6)	C(11)-O(12)	1.242(11)
O(12)-Os(2)	2.135(5)	C(11)-C(12)	1.522(12)
Os(1)-Os(2)	2.5560(4)	C(12)-F(3)	1.162(11)
Os(1)-Os(3)	2.6914(5)	C(12)-F(1)	1.273(11)
Os(2)-Os(3)	2.9322(5)	C(12)-F(2)	1.286(15)
C(11)-O(11)	1.238(11)		

Table 3.5.15 Selected bond lengths for **8**

	Bond Angles (°)		**Bond Angles (°)**
O(1)-C(1)-Os(1)	177.2(8)	O(9)-C(9)-Os(3)	178.3(9)
O(2)-C(2)-Os(1)	178.6(8)	O(10)-C(10)-Os(3)	175.6(9)
O(3)-C(3)-Os(1)	175.8(9)	C(11)-O(11)-Os(3)	123.1(6)
O(4)-C(4)-Os(1)	176.7(8)	C(11)-O(12)-Os(2)	124.2(6)
O(5)-C(5)-Os(2)	176.4(9)	F(3)-C(12)-C(11)	106.9(9)
O(6)-C(6)-Os(2)	179.3(8)	F(1)-C(12)-C(11)	117.0(9)
O(7)-C(7)-Os(2)	174.2(9)	F(2)-C(12)-C(11)	113.6(8)
O(8)-C(8)-Os(3)	178.1(8)		

Table 3.5.16 Selected bond angles for **8**

3.5.7.2 **Crystal structure of 9** (thiophene-substituted cyclopentathiapuran)

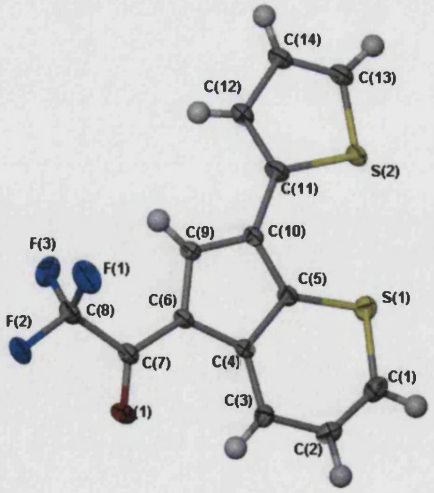

Figure 3.5.21 Structure of **9** showing atom-numbering scheme employed. Ellipsoids are drawn at 50% probability level.

The cleaved organic moiety consists of a thiophene ring coordinated to the fused five-membered and six-membered sulphur rings through C(10)-C(11) while the trifluoro acetic acid is reduced to a ketone and is linked to the fused rings through a single bond at C(7)-C(8) 1.578(3)Å.

A hydrogen bond interaction is observed between O(1)-H(2) (-x-1, 1-y,-z) at a distance of 2.461Å [C-O distances of 3.387Å] with a C-H-O angle of 174.12^{O} as shown in Figure 3.5.22.

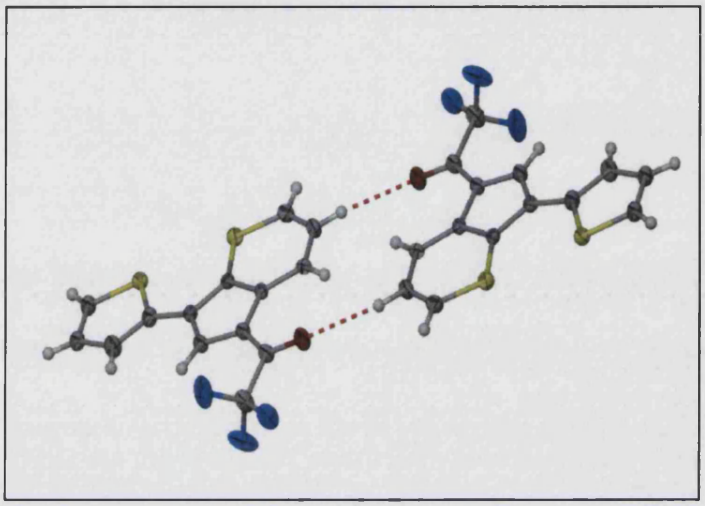

Figure 3.5.22 Hydrogen bond between O(1) and H(2)

Figure 3.5.23 shows the packing of the molecule in solid state where π-π interactions are observed between the planes of the aromatic ring systems. The shortest centroid-centroid distance, as shown in the figure is 3.573Å.

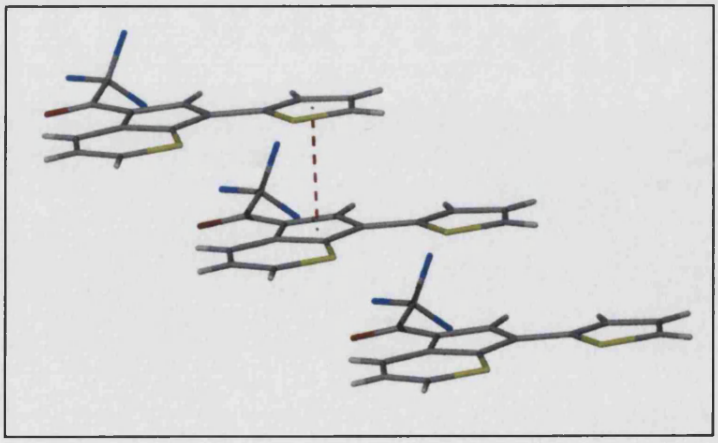

Figure 3.5.23 Packing diagram of **9**

	Bond Lengths (Å)		**Bond Lengths (Å)**
S(1)-C(1)	1.675(2)	F(1)-C(8)	1.338(3)
S(1)-C(5)	1.6935(19)	F(3)-C(8)	1.330(3)
S(2)-C(11)	1.736(3)	F(2)-C(8)	1.332(2)
S(2)-C(13)	1.692(3)	O(1)-C(7)	1.226(2)

Table 3.5.17 Selected bond lengths for **9**

	Bond Angles (°)		**Bond Angles (°)**
C(1)-S(1)-C(5)	103.72(10)	C(6)-C(7)-C(8)	117.05(18)
C(13)-S(2)-C(11)	92.32(12)	O(1)-C(7)-C(6)	126.5(2)
C(5)-C(10)-C(11)	128.48(18)		

Table 3.5.18 Selected bond angles for **9**

3.5.8 Conclusions

In the coordination of 2- and 3-thienyl substituted diynes to the unsaturated triosmium cluster $Os_3(\mu\text{-}H)_2(CO)_{10}$, it was found that the selection of the parent cluster, as well as the type of the heteroaryl endgroups in the diacetylene ligand, dictates the outcome of the reactions.

The aromatic endgroups are shown to undergo major transformations upon coordination to the triosmium core, including intramolecular cyclisations and formation of novel heteroaryl subunits.

Although the reaction mechanisms for the transformations remain unclear, it is likely that the availability of the sulphur atom for coordination to the metal centre, and the presence of the osmium bound bridging hydrides, are key factors which determine the type of the ligand transformation.

Following the common trend for triosmium clusters, compound **3** can be thermally decarbonylated to yield the osmium nonacarbonyl species **4** and **5**, which are not thermally interconvertible. Interestingly, the thermal reaction of **3** under hydrogen atmosphere yields cluster **6** selectively, associated with the formation of the dihydride carbonyl cluster $[Os_3(\mu\text{-}H)_2(CO)_{10}]$.

Intramolecular cyclisation reactions occurring when diynes are coordinated to unsaturated carbonyl clusters is well documented.[38, 39, 40] The ability to decoordinate such 'rearranged' ligands and the further understanding and elucidation of the reaction mechanism could lead to the development of new rational synthetic strategies aimed at producing novel organic chemicals.[41]

Our future research will involve the study of the reaction mechanisms of the ligand transformations observed, and exploring the possible synthetic and catalytic potential of the interactions between triosmium clusters and 1,4- substituted diynes. This may include attempts for Os-mediated, or -catalyzed, cyclizations of the heteroaryl-alkyl functionalities.

3.6 Microwave-assisted Synthesis of High-nuclearity Clusters

Pyrolytic and thermolytic methods have been extensively employed in the field of cluster chemistry, particularly in the synthesis of high nuclearity carbonyl clusters. These reactions are often carried out either in inert solvents or in the solid state under vacuum, often produced a wide range of products in which control of the reaction pathway was extremely difficult.[42, 43]

This section discusses the attempts and the results of microwave reactions carried out on $Ru_3(CO)_{12}$. The reactions were mainly based on previously reported thermolysis and pyrolysis reactions which yielded high nuclearity (Ru_6) clusters. The rationale behind the use of microwaves for synthesis lay mainly in the possibility that the use of microwaves could lead to drastically shortened reaction times and possibly increased yields.

Previously reported thermolysis and pyrolysis reactions were often carried out at over 250°C at high pressures over a number of days. The use of microwaves could induce a similar sort of pressure cooker effect at much decreased reactions times.

While it is hard to predict the products of thermolytic of pyrolytic reactions, an understanding of thermodynamic and kinetic effects can provide an insight in to the reactions.

There have been very few thermodynamic studies carried out on transition metal carbonyl clusters. However the enthalpy of disruption ΔH_D, for a cluster of the general formula $[M_m(CO)_n]$ where

$$M_m(CO)_n(g, 298K) \rightarrow m\ M(g, 298K) + n\ CO(g, 298K)$$

is defined as:

$$\Delta H_D = m\ \Delta H^\circ_f[M, g] + n\ \Delta H^\circ_f[CO, g] - \Delta H^\circ_f[M_m(CO)_n, g]$$

where [M, g] refers to metal atoms in their ground states.

It has been suggested that if clusters were described by the number of localised metal-CO terminal bonds (*T*), metal-CO bridging bonds (*B*) and metal-metal bonds (*M*) the mean bond enthalpy contributions of $\underline{T}$, $\underline{M}$ and $\underline{B}$ are related by[44, 45]:

$$2\underline{T} \approx 3\underline{M}\ (\text{cluster}) \approx 4\underline{B} \approx 2\underline{M}\ (\text{metal})$$

In the general synthesis of clusters, the following reaction has been proposed:

$$n ML_p \rightarrow M_nL_m + (pn - m)\ L$$

and a negative enthalpy is only expected when $x\underline{M}$(cluster) $\geq y\underline{T}$, where x is the number of metal-metal bonds formed and $y = (pn - m)$, the number of ligands lost in the process.
As $x \approx y$ (the number of x is close to the number of y) in most cases, then the enthalpy will be negative only when $\underline{M} > \underline{T}$. However, the positive entropy term in these reactions means that the free energy for cluster formation will be negative when $\underline{M}$ approaches $\underline{T}$. [45]

For example:

$$Os_3(CO)_{12} \xrightarrow{\text{heat}} Os_6(CO)_{18} + Os_5(CO)_{16} + Os_4(CO)_{13}$$

Kinetic factors can often influence the product formation and subsequently the chemical behaviour of cluster compounds. Both kinetic and thermodynamic effects reinforce each other to give a more extensive range of cluster compounds.

A comparison:

25°C, 20 atms

$$Fe_3(CO)_{12} + 3CO \longrightarrow 3Fe(CO)_5$$

160°C, 90 atms

$$Os_6(CO)_{18} + 3CO \longrightarrow Os_6(CO)_{21}$$

shows how kinetic and thermodynamic stabilities can influence the relative stabilities and reactivities of different clusters. The osmium complex does not degrade to form a mononuclear complex but incorporates additional CO ligands by adopting a more open skeletal geometry.[45]

3.6.1 Microwave Reaction of $Ru_3(CO)_{12}$ in Toluene : Ru_6 (μ_6-C)(μ-CO)$(CO)_{13}[\eta^6$ – $(C_6H_5)CH_3]$.

$Ru_3(CO)_{12}$ was stirred in toluene, prior to microwave irradiation at 300W for 60 minutes at 230°C. The resultant solution changed from bright orange to a deep red with a small amount of black precipitate and a shiny metallic precipitate on the tube walls, presumed to be metallic ruthenium. Workup on silica plates led to the recovery of a single deep red product obtained from the middle of the plate in 46.5% yield. This was subsequently identified by spectroscopic methods and single crystal X-ray diffraction as Ru_6 (μ_6-C)(μ-CO)$(CO)_{13}[\eta^6$ – $(C_6H_5)CH_3]$.

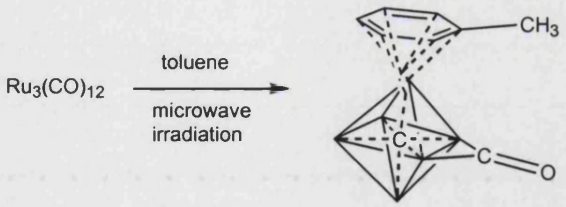

Figure 3.6.1 Reaction of $Ru_3(CO)_{12}$ in Toluene

This complex, together with other arene-substituted complexes of the general formula $Ru_6C(CO)_{14}$(arene) was first reported in 1968 (yields *ca.* 5-15%) when $Ru_3(CO)_{12}$ was refluxed in the 'appropriate' arene for 3-5 hours.[46] Along with the arene-substituted hexaruthenium clusters, tetranuclear hydrides, $H_2Ru_4(CO)_{13}$ and β-$H_4Ru_4(CO)_{12}$ were also recovered in this initial reaction. Unlike the early thermolysis reactions, however, this one-pot microwave reaction led to the isolation of only one product at much improved reactions times and greater yields.

3.6.1.1 Crystal Structure of $Ru_6(\mu_6\text{-C})(\mu\text{-CO})(CO)_{13}[\eta^6 - (C_6H_5)CH_3]$ (10)

The solid-state molecular structure of $Ru_6(\mu_6\text{-C})(\mu\text{-CO})(CO)_{13}[\eta^6 - (C_6H_5)CH_3]$, represented in Figure 3.6.2, consists of a regular octahedral array of Ru atoms with a crystallographically imposed mirror slicing through the centre of the molecule along C(9), C(12) and C(13) downwards consistent with the earlier reports.[47]

It crystallises in the orthorhombic space group P *nam* (non-standard setting of P *nma*), with Ru-Ru distances ranging from 2.8186(8) to 2.9622(7) Å. The Ru(4) edge is capped by the toluene ring with Ru-C distances ranging from 2.187(9) to 2.282(8)Å with an average of 2.240 ± 0.035 Å.

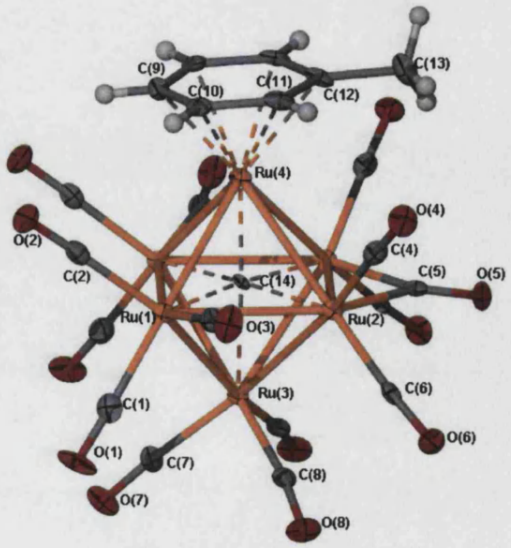

Figure 3.6.2 Structure of $Ru_6(\mu_6\text{-C})(\mu\text{-CO})(CO)_{13}[\eta^6 - (C_6H_5)CH_3]$ (**10**) showing atom-numbering scheme employed. Ellipsoids are drawn at 50% probability level.

The carbido ligand, C(14) has been noted to be slightly displaced from the geometric centre of the octahedron, placing it closer to the toluene-substituted Ru atom with a C(14)-Ru(4) distance of 1.925(7)Å compared to 2.092(7)Å between C(14) and Ru(3). This has also been noted as a feature corresponding to other arene-substitued hexaruthenium derivatives.[47]

While, the Ru(2)-Ru(2') edge is bridged by a symmetrical carbonyl ligand C(5)-O(5). The other non-bridging carbonyl ligands are all close to linear with the exception of Ru(1) -C(3)-O(3) at an angle of 168.1(6)° and Ru(2) -C(5)- O(5) at an angle of 136.7(2)°.

	Bond Lengths (Å)		**Bond Lengths (Å)**
Ru(1)-Ru(4)	2.8444(7)	C(12)-C(13)	1.499(12)
Ru(1)-Ru(3)	2.8509(8)	C(1)-Ru(1)	1.917(7)
Ru(1)-Ru(1)'	2.9442(8)	C(2)-Ru(1)	1.910(8)
Ru(1)-Ru(2)	2.9622(7)	C(3)-Ru(1)	1.927(6)
Ru(2)-Ru(2)'	2.8186(8)	C(4)-Ru(2)	1.878(6)
Ru(2)-Ru(4)	2.9017(8)	C(5)-Ru(2)	2.061(7)
Ru(2)-Ru(3)	2.9336(7)	C(6)-Ru(2)	1.885(7)
C(14)-Ru(4)	1.925(7)	C(7)-Ru(3)	1.900(9)
C(14)-Ru(1)	2.046(6)	C(8)-Ru(3)	1.917(6)
C(14)-Ru(2)	2.090(6)	C(9)-Ru(4)	2.187(9)
C(14)-Ru(3)	2.092(7)	C(10)-Ru(4)	2.235(6)
C(9)-C(10)	1.400(7)	C(11)-Ru(4)	2.255(6)
C(10)-C(11)	1.406(9)	C(12)-Ru(4)	2.282(8)
C(11)-C(12)	1.420(8)		

Table 3.6.1 Selected bond lengths for $Ru_6(\mu_6\text{-}C)(\mu\text{-}CO)(CO)_{13}[\eta^6-(C_6H_5)CH_3]$.

	Bond Angles (°)		**Bond Angles (°)**
Ru(4)-C(14)-Ru(1)	91.4(3)	O(2)-C(2)-Ru(1)	178.3(6)
Ru(4)-C(14)-Ru(2)	92.5(3)	O(3)-C(3)-Ru(1)	168.1(6)
Ru(2)'-C(14)-Ru(2)	84.8(3)	O(4)-C(4)-Ru(2)	177.0(5)
Ru(1)-C(14)-Ru(3)	87.1(2)	O(5)-C(5)-Ru(2)	136.7(2)
Ru(2)'-C(14)-Ru(3)	89.1(3)		

Table 3.6.2 Selected bond angles for $Ru_6(\mu_6\text{-}C)(\mu\text{-}CO)(CO)_{13}[\eta^6-(C_6H_5)CH_3]$.

3.6.2 Microwave Reaction of $Ru_3(CO)_{12}$ in Heptane: $Ru_6(\mu_6\text{-}C)(CO)_{17}$

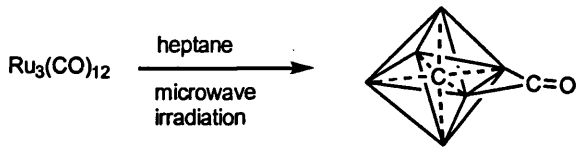

Figure 3.6.3 Microwave Reaction of $Ru_3(CO)_{12}$ in Heptane

A mixture of $Ru_3(CO)_{12}$ in heptane was irradiated in the microwave cavity in a three-step process. First, at 200W for 30 minutes at 80°C, then at 300W for 60 minutes at 150°C and finally the temperature was increased to 180°C and held for another 60 minutes. The reaction mixture changed from bright orange colour to deep red with a small amount of deep red precipitate and some orange starting material. The reaction mixture was concentrated under reduced pressure and separated by chromatography. The deep red product obtained from the middle of the plate was recrystallised from dichloromethane affording single crystals suitable for X-ray analysis. (Yield: 20mg, 73 %) The product was unambiguously identified as $Ru_6(\mu_6\text{-}C)(CO)_{17}$.

The first reported instance of this hexaruthenium cluster was as a by-product from the thermolysis of $Ru_3(CO)_{12}$ in arene solvents,[46, 48] and its crystal structure was first reported in 1969 based on data obtained from a Weissenburg rotational camera.. Later it was found that the cluster crystallises in two polymorphic forms, [49] in *Monoclinic* P $2_1/c$ and P 2/a. Optimisation of the reaction to yield $Ru_6(\mu_6\text{-}C)(CO)_{17}$ subsequently led to the reaction being carried out in an autoclave.[49, 50]

The above microwave reaction is based on autoclave reaction, with initial reactants and purging performed in a suitably adapted manner. The temperature of the microwave reaction was taken up step-wise in order to avoid the charring of the starting material and to try avoid the sudden build-up of pressure in the microwave reaction vessel, the comparable autoclave reaction was carried out at 30 atm.

3.6.2.1 Crystal Structure of $Ru_6(\mu_6\text{-}C)(CO)_{17}$ (11)

The complex molecule of $Ru_6(\mu_6\text{-}C)(CO)_{17}$ crystallises in the 'new'[49] *Monoclinic* space group $P2_1/n$. The ruthenium core consists of six Ru atoms bound together in an octahedral array with a central carbido atom and a symmetrically bridging carbonyl ligand in the equatorial plane.

The Ru-Ru bonds are typical, averaging 2.90 ± 0.04 Å with the shortest bond between Ru(4) and Ru(5) at 2.9373(8)Å and the longest at 2.9762(8) between Ru(2) and Ru(5).

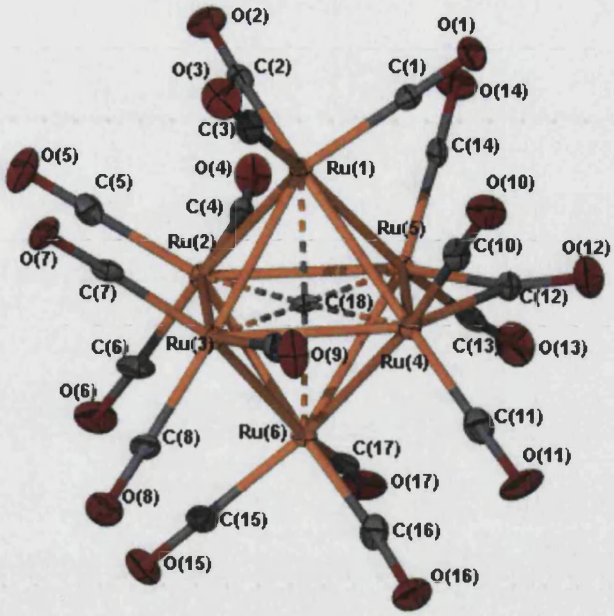

Figure 3.6.4 Structure of $Ru_6(\mu_6\text{-}C)(CO)_{17}$ (**11**) showing atom-numbering scheme employed. Ellipsoids are drawn at 50% probability level.

Unlike the toluene-substituted derivative, the carbido ligand in this cluster is situated at the geometric centre of the hexaruthenium cluster. Bond length variation between the ruthenium atoms and C(18) are very slight, ranging from 2.036(7) to 2.059(7)Å.

The majority of the carbonyl ligands are nearly linear ranging from Ru(6)-C(16)-O(16) 174.7(7) to Ru(4)-C(11)-O(11) 178.9(8)° with the exception of Ru(3)-C(9)-O(9) at 163.7(7)° and Ru(2)-C(4)-O(4) at 170.2(7)°.

By taking the bridging ligand as a reference, and the positions of the other carbonyl ligands in to account, this particular polymorph has been described as having a *cis-trans* conformation, as opposed to the *cis-cis* conformation for the other polymorph.[49]

The packing of $Ru_6(\mu_6\text{-}C)(CO)_{17}$ is said to be a head-to-tail linkage of two consecutive molecules (as shown in Figure 3.6.5) with the bridging carbonyl filling the space generated by tetragonal cavity made up of four terminal carbonyl ligands.[49]

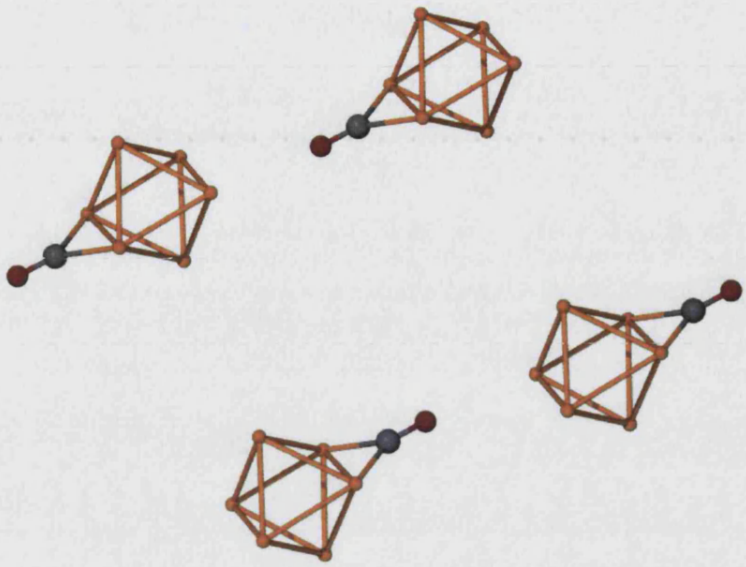

Figure 3.6.5 Packing diagram of $Ru_6(\mu_6\text{-}C)(CO)_{17}$ core and bridging ligand

	Bond Lengths (Å)		**Bond Lengths (Å)**
Ru(1)-Ru(5)	2.8832(8)	C(18)-Ru(6)	2.036(7)
Ru(1)-Ru(2)	2.8836(8)	C(18)-Ru(3)	2.047(7)
Ru(1)-Ru(4)	2.8872(8)	C(18)-Ru(1)	2.055(7)
Ru(1)-Ru(3)	2.8952(8)	C(18)-Ru(2)	2.057(7)
Ru(2)-Ru(6)	2.8602(8)	C(18)-Ru(5)	2.057(7)
C(8)-Ru(3)	1.900(8)	C(18)-Ru(4)	2.059(7)
C(11)-Ru(4)	1.904(9)	C(11)-O(11)	1.146(9)
C(12)-Ru(5)	2.057(8)	C(17)-O(17)	1.125(9)
C(12)-Ru(4)	2.082(8)	C(16)-O(16)	1.146(9)
C(13)-Ru(5)	1.885(8)	C(15)-O(15)	1.114(9)
C(14)-Ru(5)	1.877(8)	C(14)-O(14)	1.146(9)
C(15)-Ru(6)	1.939(8)	C(13)-O(13)	1.137(9)
C(16)-Ru(6)	1.902(8)	C(12)-O(12)	1.166(9)
C(17)-Ru(6)	1.920(9)		

Table 3.6.3 Selected bond lengths for $Ru_6(\mu_6\text{-}C)(CO)_{17}$

	Bond Angles (°)		**Bond Angles (°)**
O(9)-C(9)-Ru(3)	163.7(7)	O(12)-C(12)-Ru(4)	136.5(6)
O(2)-C(2)-Ru(1)	176.9(7)	Ru(6)-C(18)-Ru(3)	90.0(3)
O(3)-C(3)-Ru(1)	176.8(7)	Ru(6)-C(18)-Ru(1)	177.7(4)
O(4)-C(4)-Ru(2)	170.2(7)	Ru(3)-C(18)-Ru(1)	89.8(3)
O(17)-C(17)-Ru(6)	175.3(7)	Ru(5)-C(12)-Ru(4)	86.5(3)

Table 3.6.4 Selected bond angles for $Ru_6(\mu_6\text{-}C)(CO)_{17}$

3.6.3 Microwave Reaction of $Ru_3(CO)_{12}$ + 2:2'-bipyridine: $Ru_3(\mu_2\text{-}CO)_2(CO)_8(bipy)$

The microwave experiments described thus far are mainly concerned with comparing microwave effects to earlier methods of thermolysis and pyrolysis yielding high nuclearity clusters, however, the following reaction is a fairly typical ligand substitution cluster experiment, normally performed by a short reflux of the cluster with an appropriate ligand.

The reaction of $Ru_3(CO)_{12}$ with nitrogen heterocycles has been somewhat limited as harsh reactions conditions have often led to the break-up of the cluster. A suitable nitrogen-donor molecule however, could model the heterogeneously-catalysed hydrogenation of liquid fuels.[51] This reaction was based on previously reported methods carried out by refluxing $Ru_3(CO)_{12}$ and 2,2'-bipyridine in cyclohexane.[52]

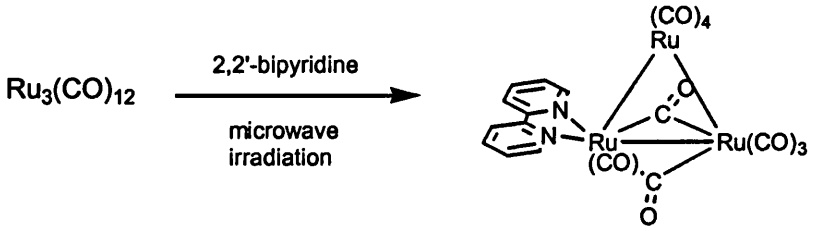

Figure 3.6.6 Microwave Reaction of $Ru_3(CO)_{12}$ + 2:2'-bipyridine: $Ru_3(\mu_2\text{-}CO)_2(CO)_8(bipy)$

The mixture was first stirred in cyclohexane for 15 minutes before a two-stage microwave-irradiation process when it was irradiated at 200W for 5 minutes at 50°C, and then at 300W for 10 minutes at 100°C. The solution changed from bright orange to a deep brown colour with a small amount of black precipitate. The reaction mixture was reduced under pressure and separated by chromatography and the reddish-brown product (yield: 36mg, 77.3 %) was recrystallised from dicholoromethane. Spectroscopic techniques and single crystal X-ray analysis identified the product as $Ru_3(\mu_2\text{-}CO)_2(CO)_8(bipy)$.

3.6.3.1 Crystal Structure of $Ru_3(\mu_2\text{-}CO)_2(CO)_8(bipy)$

$Ru_3(\mu_2\text{-}CO)_2(CO)_8(bipy)$ crystallises in the *Monoclinic* space group $P2_1/n$, consistent with previous reports.[52] It is analogous to the structure of $Fe_3(\mu_2\text{-}CO)_2(CO)_{10}$ (refer to Section 3.2.1) with two bridging carbonyls spanning one side of the metal triangle and a 2,2'-bipyridine ligand chelated to one ruthenium atom.

In this cluster the ruthenium core consists of an isosceles triangle with the shortest Ru-Ru bond being 2.7541(4) Å between Ru(1) and Ru(3), the Ru(1)-Ru(2) and Ru(2)-Ru(3) bonds are 2.8371(4) and 2.8517(4) Å respectively. The two bridging carbonyls bridge the shortest of the Ru-Ru bonds and are asymmetrically arranged.

The Ru-C bonds average 1.980 ± 0.092 Å with the shortest bond being 1.882(4) Å while the longest is 2.211(4) Å. Interestingly the shortest Ru-C bond is between Ru(3)-C(10) and it has been proposed that the short metal-carbon distance can be attributed to the high electron density at the metal atoms due to the presence of the chelating ligand and back-bonding by the terminal carbonyl ligand.[52]

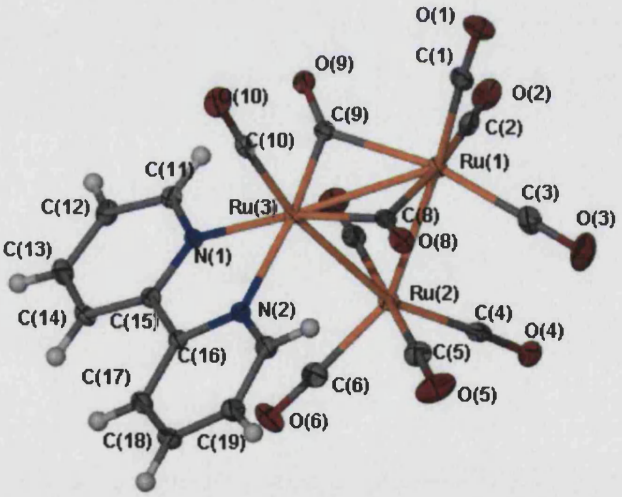

Figure 3.6.7 Structure of $Ru_3(\mu_2\text{-}CO)_2(CO)_8(bipy)$ (**12**) showing atom-numbering scheme employed. Ellipsoids are drawn at 50% probability level.

The asymmetry of the bridging carbonyl ligands is mainly due to the variation in metal-carbon bond lengths at C(9) with Ru(1)-C(9) and Ru(3)-C(9) distances at 2.211(4) and 1.959(4) Å compared to distance of 2.027(4) and 2.098(4)Å for the other Ru-C bridge.

The terminal carbonyl ligands on the ruthenium atoms are close to linear with ranges from 175.7(4)° to 179.2(4)° for Ru(1)-C(2)-O(2) and Ru(1)-C(3)-O(3) respectively.

It was also noted that the position of the bridging carbonyls are approximately *trans* to the bipy nitrogens. Based on the structurally related $Fe_2(\mu\text{-}CO)_2(CO)_5$(bipy) (where only one of the bridging carbonyls was *trans* to the chelating ligand) it was suggested that the ligand-chelated metal atom donates electron density to the μ-CO π^* orbitals, thereby enabling some electron density redistribution.[52]

In studying the crystal packing of the complex, it is interesting to note the staggered π-π interactions of the bipy ligand has a centroid-centroid distance of 3.743Å. The packing of $Ru_3(\mu_2\text{-}CO)_2(CO)_8$(bipy) as a whole in the solid state seems to largely be influenced by the packing effects of the ligand.

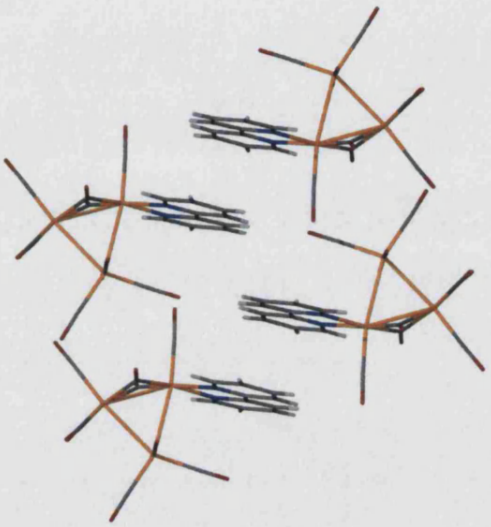

Figure 3.6.8 Packing effects of $Ru_3(\mu_2\text{-}CO)_2(CO)_8$(bipy)

	Bond Lengths (Å)		**Bond Lengths (Å)**
Ru(1)-Ru(3)	2.7541(4)	C(10)-O(10)	1.146(5)
Ru(1)-Ru(2)	2.8371(4)	C(11)-N(1)	1.349(5)
Ru(2)-Ru(3)	2.8517(4)	C(11)-C(12)	1.379(5)
N(1)-Ru(3)	2.188(3)	C(12)-C(13)	1.380(5)
N(2)-Ru(3)	2.184(3)	C(13)-C(14)	1.390(5)
C(1)-O(1)	1.134(5)	C(14)-C(15)	1.388(5)
C(2)-O(2)	1.130(5)	C(15)-N(1)	1.357(4)
C(3)-O(3)	1.129(5)	C(15)-C(16)	1.471(5)
C(4)-O(4)	1.134(5)	C(16)-N(2)	1.354(4)
C(5)-O(5)	1.131(5)	C(16)-C(17)	1.383(5)
C(6)-O(6)	1.133(5)	C(17)-C(18)	1.383(5)
C(7)-O(7)	1.128(5)	C(18)-C(19)	1.381(5)
C(8)-O(8)	1.174(4)	C(19)-C(20)	1.374(5)
C(9)-O(9)	1.174(4)	C(20)-N(2)	1.346(4)

Table 3.6.5 Selected bond lengths for $Ru_3(\mu_2\text{-}CO)_2(CO)_8$(bipy)

	Bond Angles (°)		**Bond Angles (°)**
Ru(3)-Ru(1)-Ru(2)	61.312(10)	O(4)-C(4)-Ru(2)	176.7(3)
Ru(1)-Ru(2)-Ru(3)	57.908(10)	O(5)-C(5)-Ru(2)	176.3(4)
Ru(1)-Ru(3)-Ru(2)	60.780(10)	O(6)-C(6)-Ru(2)	178.0(4)
Ru(3)-C(9)-Ru(1)	82.44(13)	O(7)-C(7)-Ru(2)	176.6(3)
Ru(3)-C(8)-Ru(1)	83.77(13)	O(8)-C(8)-Ru(3)	137.6(3)
O(1)-C(1)-Ru(1)	177.4(4)	O(8)-C(8)-Ru(1)	138.7(3)
O(2)-C(2)-Ru(1)	175.7(4)	O(10)-C(10)-Ru(3)	176.4(3)
O(3)-C(3)-Ru(1)	179.2(4)		

Table 3.6.6 Selected bond angles for $Ru_3(\mu_2\text{-}CO)_2(CO)_8(bipy)$

3.6.4 Conclusions

Microwave-assisted reactions particularly for the synthesis of higher nuclearity clusters have been found to be superior to the pyrolysis and thermolysis methods, previously used. It has also been found that ligand substitution experiments on clusters are also achievable using a microwave reactor.

However, the current set-up of the microwave reactor has some limiting factors in that the size and quantities of the reactions are limited by the size of the reaction vessels, in this case, 10ml tubes. In order to avoid an excessive build-up of pressure, the tubes are only filled to a maximum of 6 ml, although 5 ml of solvent is more commonly used. It is therefore necessary to run multiple runs of the same experiment in order to increase product yields.

Unfortunately due to systematic errors it is hard to ensure that each run is an exact duplicate of the prior one, although microwave settings are exactly the same.

It can be concluded that microwaves can be used as a quick alternative to conventional experiments that needed to be run over a course of several days, the factor of time can be cut down to a fraction of what it would have originally taken.

However, further investigations are necessary in order to understand better the multiple effects of microwave heating on the reactions of metal clusters.

[1] F.A. Cotton, *Quarterly Reviews (Chem. Soc. London)* 1966, **20**, 389

[2] D.M.P. Mingos and A.S. May, Structural and Bonding Aspects of Metal Cluster Chemistry, p. 11 – 114 in The Chemistry of Metal Cluster Complexes, D.F. Shriver, H.D. Kaesz and R.D. Adams, VCH Publishers, 1990. USA

[3] B.F.G. Johnson, J. Lewis, (Transition-Metal Molecular Cluster), *Adv. Inorg. Chem. Radiochem.*, **24**, 225.

[4] C.P. Horowitz, E.M. Holt and D.F. Shriver, *Inorg. Chem.*, 1984, **23**, 2491.

[5] J. Lewis and P. R. Raithby, *J. Organometallic Chem.* 1995, **500**, 227, and references therein.

[6] L.Mond, H.Hirtz and M.D.Coop, *J. Chem. Soc.* 1910, **997**, 798.

[7] J.Dewar and H.O. Jones, *Proc. R. Soc (London)*, 1905, **A76**, 558.

[8] J.Dewar and H.O. Jones, *Proc. R. Soc (London)*, 1907, **A79**, 66.

[9] W. Hieber, *Z. Anorg Chem.*, 1932, **204**, 165.

[10] S.M. Owen, *Polyhedron*, 1988, 7, **4**, 253.

[11] P.R. Raithby and M.J. Rosales, (Alkyne-substituted Trainsition Metal Clusters), *Adv. Inorg. Chem. Radiochem*, 1985, **29**, 169.

[12] P.R. Raithby, The Structure of Metal Cluster Compounds, Chap. 2, p. 5-193 in Transition Metal Clusters, Ed. B.F.G. Johnson, John Wiley and Sons, 1980, U.K.

[13] P.F. Jackson, B.F.G. Johnson, J. Lewis, P.R. Raithby, M. McPartlin, W.J.H. Nelson, K.D. Rouse, J, Allibon and S.A. Mason, *J. Chem Soc., Chem. Comm.*, 1980, 295.

[14] H.D. Kaesz and D.F. Shriver, Introduction p 1-6 in The Chemistry of Metal Cluster Complexes, D.F. Shriver, H.D. Kaesz and R.D. Adams, VCH Publishers, 1990. USA

[15] E.H.Braye, L.F. Dahl, W. Hübel and D.L. Wampler, *J. Am. Chem. Soc.*, 1962, **84**, 4633.

[16] C.H. Wei and L.F. Dahl, *J. Am. Chem. Soc.*,1969, **91**, 1351.

[17] F.A. Cotton and J.M. Troup, *J. Am. Chem. Soc.*, 1974, **96**, 4155.

[18] K. Wade, Some Bonding Considerations, Chap.3, p.193-225 in Transition Metal Clusters, Ed. B.F.G. Johnson, John Wiley and Sons, 1980, U.K.

[19] K.Wade, *Adv. Inorg. Chem. Radiochem.*, 1976, **18**, 1.

[20] D.M.P. Mingos, Nature Phys. Sci. (London) 1972, **236**, 99.

[21] C.E.Housecroft, Metal-metal Bonded Carbonyl Dimers and Clusters, Oxford Chemistry Primers, Oxford University Press, UK.

[22] G.Lavigne, Cluster-Assisted Ligand Transformations, p 201-302 in The Chemistry of Metal Cluster Complexes, D.F. Shriver, H.D. Kaesz and R.D. Adams, VCH Publishers, 1990. USA and references therein.

[23] L.P. Clarke, PhD Thesis: The Chemistry of Osmium and Ruthenium Diyene Clusters, 1997, Cambridge

[24] R.W. Broach, J.M. Williams, *Inorg Chem*, 1979, **18**, 314.

[25] D.E.Sherwood and M.B. Hall, *Inorg. Chem.*, 1982, **21**, 3458.

[26] W. Hieber and P. Spacu, *Z. Anorg, Allgem. Chem.*, 1937, **233**, 353.

[27] W. Hieber and C. Scharfenberg, *Ber,*. 1940, **73**, 1012.

[28] G.R. Crooks, B.F.G. Johnson and J. Lewis, *J. Chem. Soc. A,* 1969, 797.

[29] J.A. de Beer and R.J. Jaines, *J. Chem Soc. Chem. Commun.*, 1970, 288.

[30] T.A. Cresswell, J.A.K. Howard, F.G. Kennedy, S.A. R. Knox and H. Wadepohl, *J. Chem. Soc. Dalton Trans.*, 1981, 2220.

[31] P.Belanzoni, N. Re, A. Sgamellotti and C. Floriani, *J Chem. Soc. Dalton Trans.*, 1998, 1825 and references therein.

[32] M.I. Bruce, S.M. Pyke, N.N. Zaiyseva, B.W. Skelton, A.H. White, *Helv. Chim. Acta.*,2001, **84** 3197.

[33] M.I. Bruce, P.J.Low, N.N. Zaiyseva, S. Kahlal, J.-F. Halet, B.W. Skelton, A.H. White, *J Chem. Soc. Dalton Trans.*, 2000, 2939.

[34] M.I. Bruce, M.E. Smith, N.N. Zaiyseva, B.W. Skelton, A.H. White, *J. Organometallic Chem.*, 2003, **670**, 170.

[35] Lionel Clarke; PhD Thesis; The Chemistry of Osmium and Ruthenium Diyne Clusters; 1997; Cambridge.

[36] M.W. Lum and W.K. Leong, *J. Chem. Soc. Dalton,* 2001, 2476.

[37] D. Roberto, E. Lucenti, C. Roveda and R. Ugo, *Organometallics*, 1997, **16**, 5974.

[38] P, Blenkiron, C.D. Enright, N.J. Taylor, A.J. Carty, *Organometallics*, 1996, **485**, 219.

[39] M.I.Bruce, B.W.Skelton, A.H. White, N.N. Zaitseva, *Inorg. Chem. Commun.*, 1998, **1**, 134.

[40] C.S.-W. Laul, W.-T. Wong, *J. Chem. Soc., Dalton Trans.*, 1999, 2511.

[41] S.P. Tunik, V.D. Khirpoun, I.A. Balova, M.E. Borovitov, I.N. Domnin, E. Nordlander, M. Haukka, T.A. Pakkanen, D.H. Farrar, *Organometallics*, 2003, **22**, 3455.

[42] R.D. Adams, Systematics of the Synthesis of Transition metal Carbonyl, Clusters, p 121 in The Chemistry of Metal Cluster Complexes, D.F. Shriver, H.D. Kaesz and R.D. Adams, VCH Publishers, 1990. USA and references therein.

[43] M.D. Vargas and J.N. Nicholls, (High Nuclearity Carbonyl Clusters: Their Synthesis and Reactivity), *Adv. Inorg. Chem. Radiochem.*, **30**, 123.

[44] J.A. Connor, Thermochemical Estimation of Metal-to-Metal Bond Enthalpy Contributions in Clusters, Chap.5, p.345-390 in Transition Metal Clusters, Ed. B.F.G. Johnson, John Wiley and Sons, 1980, U.K.

[45] D.M.P. Mingos and D.J. Wales, Introduction to Cluster Chemistry, Prentice Hall Inc., 1990, USA.

[46] B.F.G. Johnson, R.D. Johnston and J. Lewis, *J. Chem. Soc.* (A), 1968, 2865.

[47] L.J. Farrugia, *Acta Cryst. C*, 1988, **44**, 997 and references therein.

[48] P.J. Dyson, *Adv. Organomet. Chem*, **43**, 43.

[49] D. Braga, F. Grepioni, P.J. Dyson, B.F.G. Johnson, P. Frediani, M. Bianchi and F. Piacenti, *J. Chem Soc Dalton. Trans.* , 1992, 2565.

[50] G.Freeman, S.L. Ingham, B.F.G. Johnson, M. McPartlin and I.J. Scowen, *J. Chem Soc Dalton. Trans* , 1997, 2705.

[51] M.C. Cifuentes, M.G. Humphrey, B.W. Skelton, A.H. White, *J. Organometallic Chem.*, 1996, **513**, 201.

[52] M.I. Bruce, M.G. Humphrey, M.R. Snow, E.R.T. Tiekink and R.C. Wallis, *J. Organometallic Chem.*, 1986, **314**, 311.

[53] S.P Tunik, V.D. Khripun, I.A. Balova, E. Nordlander, M. Haukka, T.A. Pakkanen, and P.R. Raithby, *Organometallics,* 2001, **20**, 3854.

CHAPTER 4

THE CHEMISTRY OF 2,2':6'2''-TERPYRIDINE AND ITS DERIVATIVES

4.0 The Chemistry of 2,2':6'2"-Terpyridine (Terpy) and Its Derivatives

Since its discovery in the 1930s, 2,2':6'2''-Terpyridine as a ligand has been widely used and applied to a large variety of reactions. Although it is not considered to be an 'old' ligand it has been extensively studied. It was first discovered as a by-product of an Fe(III) reaction with pyridine.

A recent search in the Cambridge Structural Database (v 5.24) gave a total of 606 complexes with terpyridine as a ligand, while terpyridine and its derivatives form a total of 911 complexes listed in the CSD.

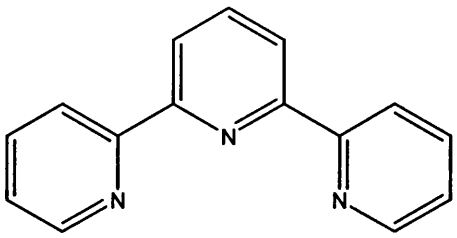

Figure 4.4.1.1 2,2':6'2''-terpyridine in the *cis-cis* conformation

4.1 Chemical Stabilisation

Terpyridine and its derivatives form a successful class of ligands due to its capability to work seamlessly with metal ions of a wide range of oxidation states. Constable[1] in his review of terpyridine chemistry describes it as a 'class of ligands that excels in all of these categories', in that it allows the stabilisation of oxidation states outside the conventional +2 or +3 of the transition metals, and allows for the deviation from the more common geometries of octahedral, tetrahedral and square-planar.

Terpyridine in its neutral form consists of three unprotonated basic sites at the nitrogen atoms, each contributing two nonbonding (n) electrons to the overall molecular structure,[2] while the π^* antibonding orbitals are delocalised on the pyridine rings.[3]

Stabilisation of metal-terpyridine complexes can occur through back-donation or backbonding where there is a transfer of electron density from a metal centre to ligands. This most commonly happens at a metal centre of low oxidation state with an excess of electron density on the metal atom. Stabilisation is achieved through the reduction of electron density by means of electron transfer to either ligand nonbonding or π antibonding orbitals.[1] High oxidation metal centres, however, are stabilised by the electron donation from strong σ or π donor ligands.

Terpyridine-based ligands are able to fulfil these roles ideally. These abilities can be explained by the filled highest occupied molecular orbital (HOMO) and a vacant lowest unoccupied molecular orbital (LUMO), which are of suitable energies for interaction with metal *d* orbitals.[4]

4.2 Bonding Geometries of Terpyridine

Factors that often influence the complexation geometries of monodentate ligands such as steric and electronic effects and crystal field stabilisation energy (CFSE) terms do not always hold for the larger polydentate ligands.

The geometries of complexes incorporating large polydentate ligands are often dictated by the configuration of the ligand; a planar pentadentate ligand cannot form octahedral complexes. In such cases, a compromise needs to be achieved between the geometry of the metal and that of the ligand, this often leads to an unusual or distorted geometry around the metal or a distortion of the ligand.[1] In extreme cases, it could cause a polydentate ligand to bind only through some of its potential sites, i.e. a mono- or bidentate terpyridine.

4.2.1 Monodentate and Bidentate

Although terpyridine is technically capable of being a monodentate and/or a bidentate ligand, it has often been assumed the formation of the monodentate and bidentate species occurs as transition intermediates towards to more stable tridentate form.

To date there has been little structural evidence to suggest that the formation of monodentate and bidentate forms are a common occurrence. The only reported structure of a bidentate terpyridine is that on two polymorphs of $[Ru(terpy)(CO)_2Br_2]$, one red and one yellow. The colour differences are believed to be caused by the orientation of the uncoordinated pyridine ring.[5]

Some work done in the 1960s-1970s with manganese and rhenium were thought to contain bidentate terpyridine ligands based on their vibrational spectra.[6, 7] Some work by Chapman *et al.*[8] have shown the existence of an on-off bidentate-tridentate equilibrium in $[Eu(terpy)_3]^{3+}$ in solution NMR studies. While Fréchette and co-workers[9] have established from proton NMR studies, that in the formation of $[La(terpy)_n]^{3+}$ (where n=1,2) terpyridine is partially free when the complex ions are formed.

4.2.2 Bridging

There have been very few examples of bridging terpyridine, most likely because the *cis-cis* conformation is the most ideal and most common geometry in complexation, although the *cis-trans* conformation is more energetically favourable to the occurrence of bridging. The closest example of bridging is based on the bidentate system of $[Ru(terpy)(CO)_2Br_2]$

mentioned earlier with a stacking interaction between the free pyridine ring and that on an adjacent molecule.

4.2.3 Tridentate

The tridentate chelating form of terpyridine is the most commonly reported and frequently the metal-ligand ratios are 1:1 and1:2. The 1:2 complexes are predominantly based on an octahedral geometry and frequently exhibit D_{2d} local symmetry.[1] It is however the larger ionic sphere of the lanthanides that more readily accommodates the formation of 1:3 terpyridine complexes with PF_6^- and BF_4^- often used as counterions. These will be discussed in further detail in Chapter 5.

The tridentate cis-cis conformation of a chelating terpyridine results in distortions of the ligand. In order to achieve an efficient coordination to a metal centre via tridentate chelation, it is necessary for terpyridine to adopt the cis-cis conformation. This leads to a considerable strain placed on the geometry of the free ligand. Constable in 1985[1] predicted that reduction of the interannular angle between the central and terminal pyridine rings was necessary for terpyridine to function as an efficient tridentate ligand.

Since then, the in-depth structural report terpyridine by Churchill *et al.*[10] and that of other numerous structural reports of new metal-terpyridine complexes have served to confirm this observation and will be discussed in greater detail in the following sections.

4.3 Ab Initio Quantum-Mechanical Calculations

Ab initio quantum mechanical calculations carried out on the possible conformations of terpyridine[11] show that the lowest energy configuration is the '*trans- trans*' form. The *cis-cis* conformation is least favourable due to a reduction in conjugation between the rings and destabilisation caused by repulsions between the two *ortho* hydrogen atoms.

However, these calculations were carried out on gas phase idealised molecules and the results (listed in Table 4.3.1) do not point towards a significant difference in the energies of each conformation.

Conformation	Energies
cis, cis	-737.798
cis, trans	-737.807
trans, trans	-737.818

Table 4.3.1: Results from quantum mechanics calculations of conformations of terpyridine. Energies in au (= 627.509 kcal mol^{-1}) [11]

4.4 Luminescence of Terpyridine

Early UV-visible absorption studies on terpyridine were carried out by Nakamoto[12] in 1960 while luminescence measurements were carried out a decade later by Fink and Ohnesorge.[2]

The luminescence and absorption studies, in solution at that time was very much complicated by acid-base properties of terpy which depending on the pH of the solution governed the formation of the neutral or slightly alkaline species, $[HTerpy]^+$ or even $[H_2Terpy]^{2+}$.

To further add to these difficulties were the various conformations of *cis-cis, cis-trans* and *trans-trans* all of which are believed to occur in solution.

As the nitrogens on the pyridine rings introduce non-bonding electron pairs in to the system these non-bonding electron pairs in N can be promoted by UV-vis absorption in to the antibonding π^* orbitals of the pyridine ring.[13,14]

Figure 4.4.1 and Table 4.4.1 are a summary of the luminescence properties of terpyridine in their various states.

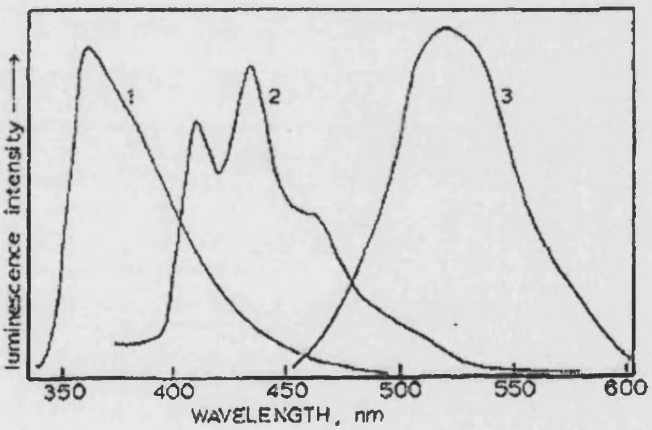

Figure 4.4.1 Fluorescence spectra of terpyridine[2]. 1. 1.0 x $10^{-5}M$ $[HTerpy]^+$ in $10^{-4}M$ HCl at 313 nm; 2.1.0 x 10^{-3} M Terpy in cyclohexane at 366nm; 3. 1.0 x $10^{-3}M$ $[H_2Terpy]^{2+}$ in 0.2M HCl at 313 nm

	Terpy **(alkaline/neutral)**	**$[HTerpy]^+$** **(slightly acidic pH 2-4)**	**$[HTerpy]^{2+}$** **(very acidic pH < 2)**
Colour of emission	Blue emission	Intense violet luminescence (313 nm excitation)	Low energy green emission (313 or 365 nm excitation)
Description of emission curve	Triple peaked - comparable to (mirror image of) absorption spectra	Long tail from UV to visible region -responsible for violet colour - sharp cut off in high energy absorption due to self absorption	Symmetrical Gaussian curve -suggestion of a single electronic transition
Transitions	Absorption curve suggests low intensity, lowest energy triple peaked $*\pi \leftarrow n$ absorption assignment. Emission spectra suggests the reverse transition when molecule returns to the ground state $*\pi \rightarrow n$	The emission is excited by the $\pi^* \leftarrow \pi$ absorption transitions The violet luminescence is the reverse transition of the absorption band assigned as $^1\pi^* \rightarrow \pi$	Known to exist in *cis-cis* conformations in the ground state. The yellow-green luminescence is also assigned as $^1\pi^* \rightarrow \pi$
Lifetime measurements	2±1 ns in cyclohexane and in absolute ethanol	2±1 ns in fluid solution	
Phosphorescence	Observed in solid state $T \rightarrow S$ phosphorescence of the rigid medium		A blue-green detectable after glow is assigned as phosphorescence with transitions of $^3\pi^* \rightarrow \pi$

Table 4.4.1 Luminescence of 2,2':2'6''-terpyridine in solution.

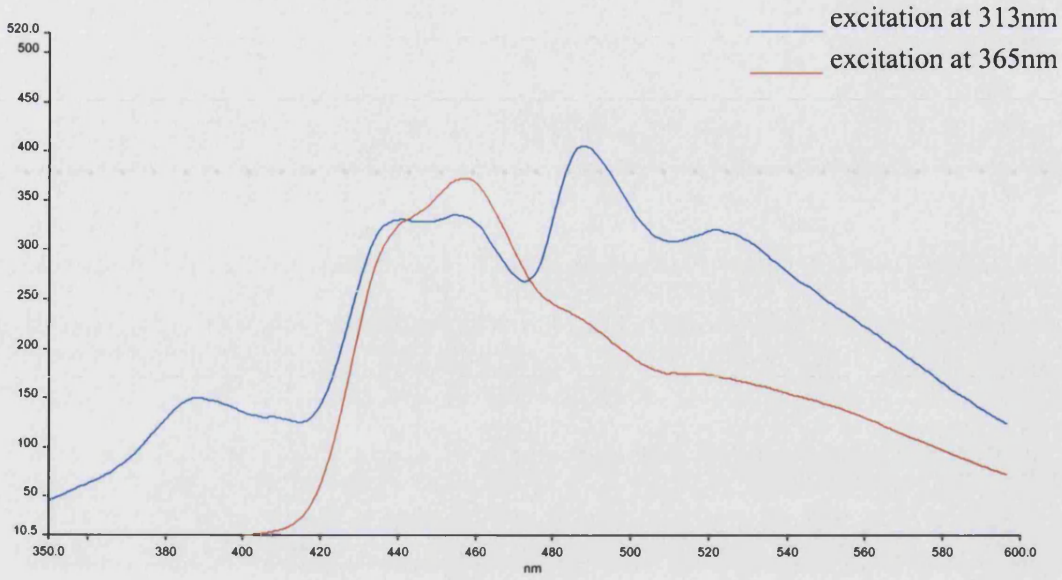

Figure 4.4.2 Fluorescence spectra of 2,2':2'6''-terpyridine in the solid state

Figure 4.4.2 shows the fluorescence spectra of terpy measured in the solid state at two excitation wavelengths, 313nm and 365nm respectively. Based on the luminescence studies of terpy in solution, the spectra excited at 365 nm is similar to that of $[HTerpy]^+$ in solution which has been assigned as $^1\pi^* \rightarrow \pi$ transition, while the triple peaked line of 313nm is comparable to that of neutral terpyridine which are assigned to the $^*\pi \rightarrow$ n transitions.

Solvent effects have been noted in the absorption studies carried out on neutral terpyridine with the solvent-structure relationships blurring as the solvent becomes more polar and consequently more hydrogen bonded. The shifts and the regions in which the luminescence (in solution) is emitted is very much pH dependent which is not a determining factor in solid-state measurements. Further work, however, needs to be done to confirm these transitions in the solid state.

4.5 Structural Study of Terpyridine

Apart from the solid-state luminescence measurements discussed above, a structural study was carried out on terpy. Interest in the use of terpy as a ligand stems mainly from its luminescent properties and the promise it shows as an encapsulating ligand for the lanthanides. Terpys ability to transfer charges to a metal centre is studied further in Chapter 5, in conjunction with the Lanthanides. It was also necessary for related work involving laser irradiation, to obtain the terpy structures at a series of different temperatures, detailed in the following sections.

The powdered form of 2,2':6'2'' terpyridine was obtained from Sigma-Aldrich and used without further purification. Single crystals suitable for X-ray analysis were obtained by slow evaporation of a hexane-toluene mixture that was vigorously heated and subsequently cooled to –18°C. A crystal of dimensions 0.50 x 0.25 x 0.20 mm^3 was mounted on a glass fibre and flash frozen to the data collection temperatures of 100(2)K, 150(2) K, 200(2)K and 250(2) K.

Identification code	k03prr4	k03prr3	k03prr1	k03prr2
Empirical formula	C30 H22 N6	C15 H11 N3	C15 H11 N3	C15 H11 N3
Formula weight	466.54	233.27	233.27	233.27
Temperature	250(2) K	200(2) K	150(2) K	100(2) K
Wavelength	0.71069 Å	0.71073 Å	0.71073 Å	0.71073 Å
Crystal system	Monoclinic	Monoclinic	Monoclinic	Monoclinic
Space group	P21/c	P21/c	P21/c	P2
Unit cell dimensions	a = 11.696(5) Å	a = 11.6994(2) Å	a = 11.7070(2) Å	a = 11.7139(2) Å
	b = 16.071(5) Å	b = 15.8843(3) Å	b = 15.7190(3) Å	b = 15.5770(3) Å
	c = 13.647(5) Å	c = 13.6337(2) Å	c = 13.6210(2) Å	c = 13.6051(3) Å
	α= 90.000(5)°.	α= 90°.	α= 90°.	α= 90°.
	β= 109.590(5)°.	β= 109.4290(10)°.	β= 109.2840(10)°.	β= 109.1210(10)°.
	γ = 90.000(5)°.	γ = 90°.	γ = 90°.	γ = 90°.
Volume	2416.7(16) Å3	2389.36(7) Å3	2365.93(7) Å3	2345.53(8) Å3
Z	4	8	8	8
Density (calculated)	1.282 Mg/m3	1.297 Mg/m3	1.310 Mg/m3	1.321 Mg/m3
Absorption coefficient	0.079 mm-1	0.080 mm-1	0.081 mm-1	0.081 mm-1
F(000)	976	976	976	976
Crystal size	0.50 x 0.25 x 0.20 mm3	0.50 x 0.25 x 0.20 mm3	0.50 x 0.25 x 0.20 mm3	0.50 x 0.25 x 0.20 mm3
Theta range for data collection	2.99 to 25.00°.	3.01 to 25.01°.	3.04 to 25.00°.	3.06 to 25.01°.
Index ranges	-13<=h<=13, -18<=k<=19, -15<=l<=16	-13<=h<=13, -18<=k<=18, -16<=l<=16	-13<=h<=13, -18<=k<=18, -16<=l<=16	-13<=h<=13, -17<=k<=18, -16<=l<=16
Reflections collected	24125	26661	27711	21460
Independent reflections	4236 [R(int) = 0.0616]	4201 [R(int) = 0.0589]	4148 [R(int) = 0.0481]	4119 [R(int) = 0.0469]
Completeness to theta = 25.00°	99.6 %	99.7 %	99.4 %	99.6 %
Absorption correction	Semi-empirical from equivalents	Semi-empirical from equivalents	Semi-empirical from equivalents	Semi-empirical from equivalents
Max. and min. transmission	1.084 and 0.933	1.112 and 0.905	1.029 and 0.943	0.9839 and 0.9605
Refinement method	Full-matrix least-squares on F2	Full-matrix least-squares on F2	Full-matrix least-squares on F2	Full-matrix least-squares on F2
Data / restraints / parameters	4236 / 0 / 325	4201 / 0 / 325	4148 / 0 / 325	4119 / 0 / 325
Goodness-of-fit on F2	1.208	1.205	1.148	1.159
Final R indices [I>2sigma(I)]	R1 = 0.0681, wR2 = 0.1420	R1 = 0.0548, wR2 = 0.1271	R1 = 0.0475, wR2 = 0.1195	R1 = 0.0471, wR2 = 0.1178
R indices (all data)	R1 = 0.0944, wR2 = 0.1544	R1 = 0.0750, wR2 = 0.1381	R1 = 0.0612, wR2 = 0.1279	R1 = 0.0570, wR2 = 0.1223
Largest diff. peak and hole	0.208 and -0.265 e.Å-3	0.253 and -0.319 e.Å-3	0.249 and -0.319 e.Å-3	0.204 and -0.311 e.Å-3

Table 4.5.1: Crystal data and structure refinement at variable temperature

4.5.1 Molecular description of 250K version

In contrast to the previously reported polymorph of terpy that crystallises in the *Orthorhombic* space group $P2_12_12_1$ with one molecule in the asymmetric unit,[10] we now report a new polymorph of 2,2':6'2'' terpyridine (terpy) that crystallises in the *Monoclinic* space group $P2_1/c$ with two molecules of terpy in the asymmetric unit. Both polymorphs adopt the energetically favourable '*trans-trans*' conformation.

The two terpy molecules are not planar with respect to each other, with corresponding centroid-centroid distances ranging from 3.710Å to 4.201Å (3.723Å) averaging 3.878Å.

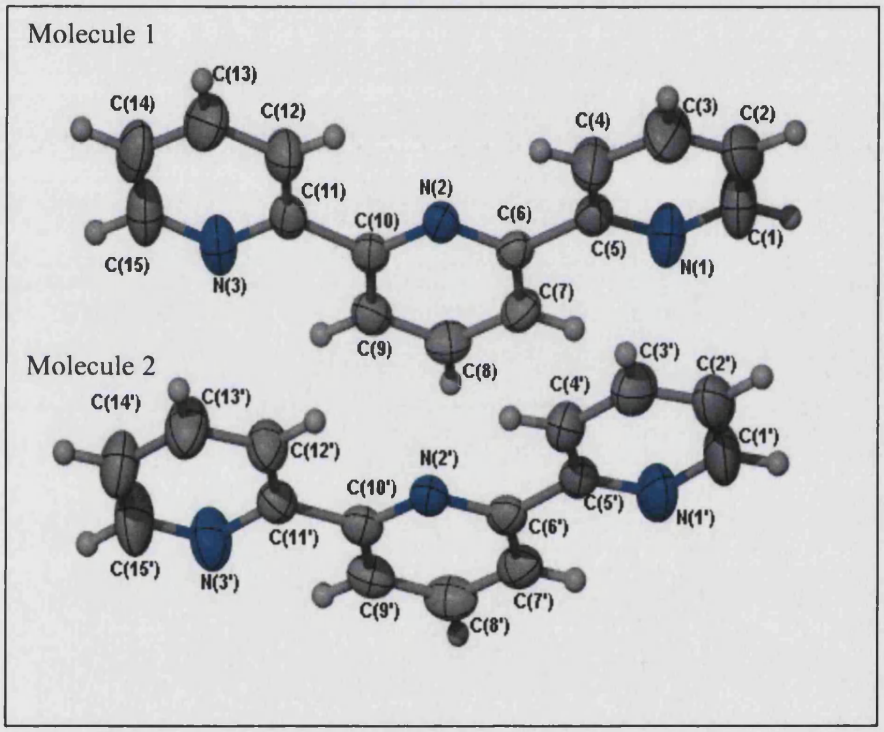

Figure 4.5.1: Structure of the two molecules of terpyridine showing the numbering scheme employed. Ellipsoids drawn at 50% probability.

The C-C bonds linking the rings are typical of single C-C bonds between sp^2 hybridised carbon atoms with C(5)-C(6) 1.492(3) Å, C(10)-C(11) 1.491(3) Å, C(5')-C(6') 1.486(3) Å and C(10')-C(11') 1.487(3) Å

Within the rings, the overall average C-N bonds are longer in molecule 2 compared to molecule 1. The C-N bonds in molecule 1 average 1.337 ± 0.006 Å with bonds involving N(2), in the central ring, being the longest; C(6)-N(2) 1.343 (2)Å and C(10)-N(2) 1.342(3)Å , while in molecule 2 the C-N bond length averages 1.342 ± 0.005 Å ranging from a low value of 1.335 (3)Å for C(15')-N(3') to a high value of 1.350(3)Å for C(1')-N(1'). Unlike

molecule 1, the longest C-N bonds in molecule 2 involve N(1') on the right ring of the molecule with C(1')-N(1') 1.350(3)Å and C(5')-N(1)' 1.345(3)Å.

This is in contrast with the single terpy molecule in the *Orthorhombic* polymorph[10] where the average C-N distances are 1.342 ± 13 Å with a low value of 1.317(7) Å and a high value of 1.353 (8)Å.

The C-C bonds within rings of the two molecules are not distinctly different, with average distances of 1.377 ± 0.011 Å (molecule 1) and 1.374 ± 0.012 (molecule 2). The C-C distances in molecule 1 range from 1.357(4) Å for C(1)-C(2) to 1.392(3) Å for C(9)-C(10) while in molecule 2 the shortest distance is for C(14')-C(15') 1.356(3) Å and the longest is C(9)-C(10) 1.390(3) Å.

As with the earlier reported structure[10] the angles involving the inter-ring C-C bonds can be divided in to two significant sets:- those involving a nitrogen atom and those only involving carbon atoms. Table 2 shows the selected angles with calculated averages and standard deviations.

Molecule 1	(°)	**Molecule 2**	(°)
C(4)-C(5)-C(6)	122.37(17)	C(4')-C(5')-C(6')	121.02(18)
C(7)-C(6)-C(5)	120.07(17)	C(7')-C(6')-C(5')	121.36(18)
C(12)-C(11)-C(10)	121.74(18)	C(12')-C(11')-C(10')	121.82(18)
C(9)-C(10)-C(11)	120.18(18)	C(9')-C(10')-C(11')	121.22(18)
Average	121.09	Average	121.36
Standard deviation	1.14	Standard deviation	0.34
N(3)-C(11)-C(10)	116.21(18)	N(3')-C(11')-C(10')	116.24(17)
N(2)-C(10)-C(11)	117.19(17)	N(2')-C(10')-C(11')	116.7(16)
N(2)-C(6)-C(5)	117.59(16)	N(2')-C(6')-C(5')	116.32(17)
N(1)-C(5)-C(6)	116.06(17)	N(1')-C(5')-C(6')	116.99(19)
Average	116.76	Average	116.56
Standard deviation	0.75	Standard deviation	0.35

Table 4.5.2: Selected bond angles involving inter-ring C-C bonds.

While, the terpy rings deviate only slightly from planarity within each molecule, the ring twists cause a significant loss of symmetry in the asymmetric unit as a whole. Figure 2 shows a view down the C-axis emphasizing the differences. Table 3 summarises the dihedral angles in both molecules. (Refer to Figure 4.5.1for atomic labeling)

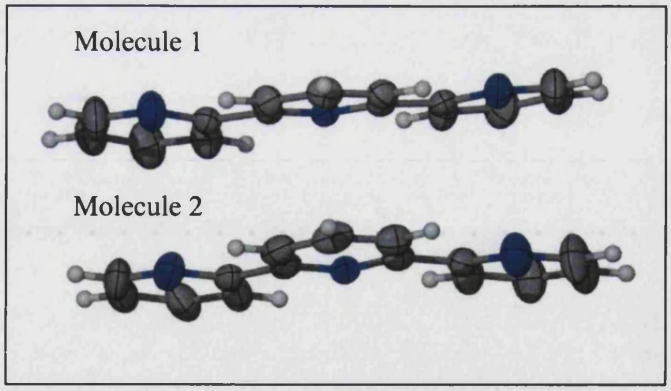

Figure 4.5.2: View down the C-axis

Plane 1	**Plane 2**	**Dihedral Angle (°)**
Molecule 1		
N(1)-C(5)-C(4)	N(2)-C(6)-C(7)	7.33 (4)
N(2)-C(10)-C(9)	N(3)-C(11)-C(12)	3.20(15)
Molecule 2		
N(1')-C(5')-C(4')	N(2')-C(6')-C(7')	2.54 (19)
N(2')-C(10')-C(9')	N(3')-C(11')-C(12')	5.11(18)

Table 4.5.3: Inter-ring dihedral angles

4.5.2 Variable Temperature Study

Table 4.5.4 outlines the changes in the cell dimensions at the various temperatures of data collection.

Temperature (K) **Cell Dimensions**	**250**	**200**	**150**	**100**
a (Å)	11.696(5)	11.6994(2)	11.7070(2)	11.7139(2)
b (Å)	16.071(5)	15.8843(3)	15.7190(3)	15.5770(3)
C (Å)	13.647(5)	13.6337(2)	13.6210(2)	13.6051(3)
β (°)	109.590(5)	109.4290(10)	109.2840(10)	109.1210(10)
Volume ($Å^3$)	2416.7(16)	2389.36(7)	2365.93(7)	2345.53(8)

Table 4.5.4: The cell parameters for the single crystal monoclinic terpyridine at various temperatures

As expected, there is a general decrease in the volume of the cell as the temperature is lowered from 250K to 100K. This decrease averages 23.7 $Å^3$ with a maximum difference of 27.34 Å between the temperatures of 250K and 200K.

This decrease is caused primarily by the reduction in the length of the b-axis. The pairs of terpy molecules are stacked diagonally to this axis and as the temperature is lowered there is a

decrease in the distance between atom pairs is mainly due to the reduction in thermal vibration.

Figure 4.5.3 shows the labelling scheme employed for the centroids while Table 4.5.5 details the centroid-centroid distances at various temperatures.

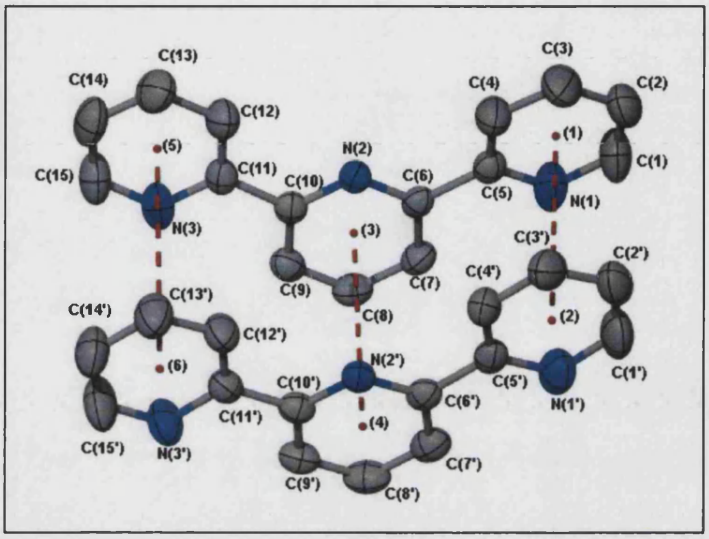

Figure 4.5.3: *Monoclinic* terpy at 250K detailing centroid-centroid distances

Centroids	**100K**	**150K**	**200K**	**250K**
1-2	3.665	3.678	3.692	3.710
3-4	3.666	3.682	3.700	3.723
5-6	4.155	4.169	4.182	4.201

Table 4.5.5: Centroid-centroid distances at various temperatures

4.6 Packing Motifs

Although terpy contains three nitrogen atoms with the potential to act as hydrogen bond acceptors, the formation of hydrogen bonds seem to take less precedence over the C···C and C···H non-bonded interactions[15] which are responsible for the packing arrangements found in both forms of terpy.

4.6.1 Packing Motifs in the *Monoclinic* polymorph of terpy

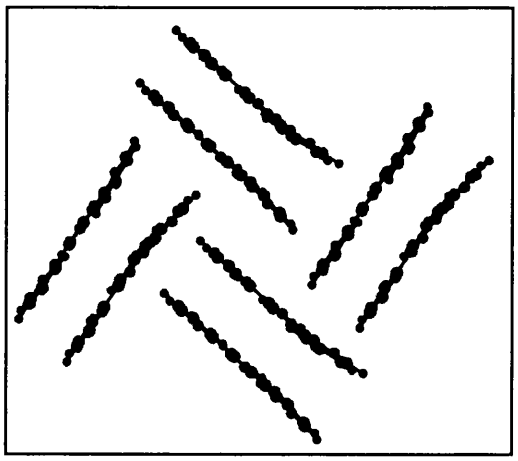

Figure 4.6.1: A view of the packing of *Monoclinic* Terpyridine

The packing of terpy, as displayed in Figure 4.6.1, is typical of a sandwich-herringbone motif,[15] which consists of pairs of molecules parallel to each other and perpendicular to another pair of molecules; i.e. the original herringbone motif made up of sandwich-type diads.[15]

In this formation, the carbon atoms are directed over the centre of an aromatic ring from another pair of parallel molecules. This form of C···H interactions are noted to be most effective between inclined molecules as the inclined arrangement is stabilised by bringing the (+) hydrogen atom of an aromatic ring into close contact with the (-) electron cloud of the adjacent ring[16].

These C-H···π interactions exist in molecule 1 between C(15) and centroid 2 from a neighbouring molecule and also in molecule 2 between C(15') and centroid 1 of the same neighbouring molecule as identified in Fig. 1.6.4.

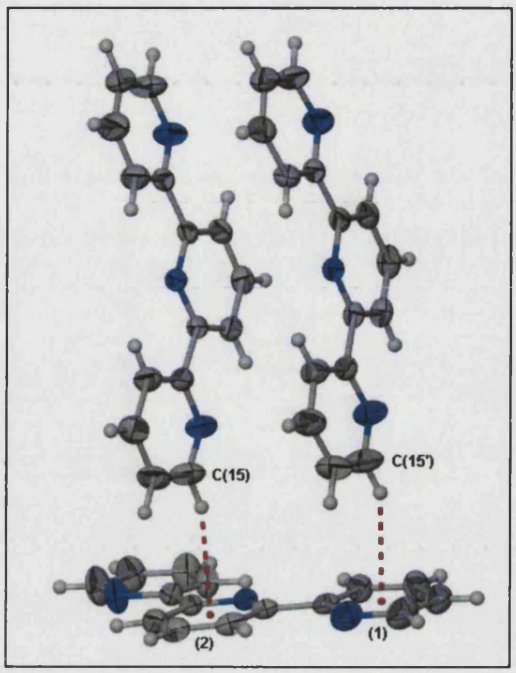

Figure 4.6.2: Orientation of three terpy molecules. C-H···π interactions are shown in red

Temp (K)	**Molecule 1 C···π and C-H···π**		**Molecule 2 C···π and C-H···π**	
	Distances (Å)	Angles (°)	Distances (Å)	Angles (°)
100	3.502 (2.611)	156.39	3.496 (2.635)	151.04
150	3.530 (2.631)	157.95	3.521 (2.657)	151.40
200	3.565 (2.660)	159.45	3.549 (2.682)	152.07
250	3.600 (2.698)	161.03	3.489 (2.720)	153.10
Powder	3.562 (2.603)		3.580 (2.501)	

Table 4.6.1: The C··· π and C-H···π distances in parenthesis and angles for both molecules in single crystal monoclinic terpyridine at variable temperatures.

Table 4.6.1 lists the distances over which C-H···π interactions occur; the C···π distance is most accurate as hydrogen atoms were generated by the refinement program. As expected, there is an increase in these distances as the temperature increases and the atoms experience more thermal vibration.

4.6.2 Packing motifs in the *Orthorhombic* polymorph of terpy

It is instructive to compare the packing in the new *Monoclinic* polymorph with that in the *Orthorhombic* form. This species crystallises in the space group $P2_12_12_1$ with one molecule of terpy in the asymmetric unit and a very short axis of a = 3.9470(10) Å. The discussion of this polymorph is detailed in Churchill et al. (1992).[10]

The crystal packing viewed looking down the a-axis is shown in Figure 4.6.3. The packing is typical of a β-stacking motif where the molecules are stacked at a distance of 3.947 Å down the a-axis.

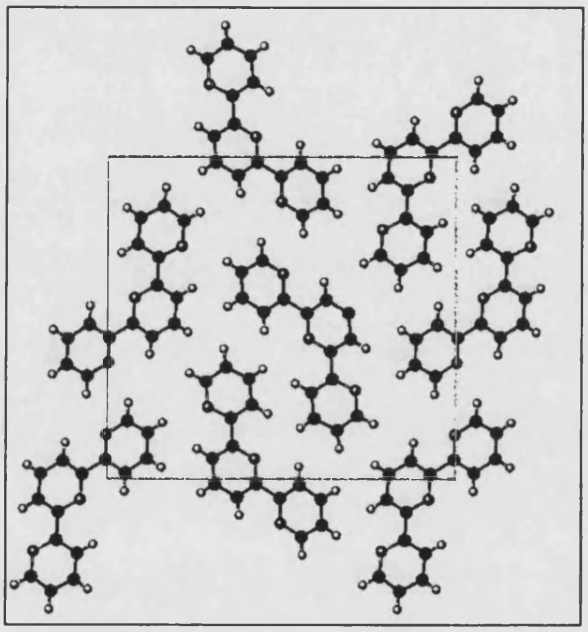

Figure 4.6.3: The packing of molecules in the crystal structure of *Orthorhombic* terpyridine, viewed down the a-axis

Although *C-H*···π interactions are not present in this form, π····π interactions between the planar aromatic rings are dominant. As with typical graphite packing the ring centroid distances are within the range of 3.6 to 4.0 Å, with an offset between the π-stacked ring centroids.

According to *Desiraju et al. (1989)*[15], β-stacking is a result of compounds that are distorted from planarity thus making stacking difficult, although C···C interactions are believed to be important and the non-planar molecule may stack to optimise this interaction. However in order to avoid excessive nonbonded repulsion, a large perpendicular stacking distance and a small degree of lateral offset are necessary; this criteria imply short axes of around 4 Å, which is inline with the packing motif of the *Orthorhombic* polymorph.

[1] E.C. Constable, *Adv. In Inorg Chem and Radiochem.*,1985, **30**, 71.
[2] D.W.Fink and W.E.Ohnesorge, *J. Phys. Chem.* **74**, (1) 74, 1970.
[3] D.R. Kearns, M. A. El-Bayoumi, *J. Chem. Phys.*, **38**, 1508, 1963.
[4] B. Kovac and L. Klasine, *Z. Naturforsch., A* **23A**, 247 1978.
[5] G.B. Deacon, J.M. Patrick, B.W. Skelton, B.W., N.C. Thomas and A.H. White. *Aust. J. Chem.* **37**, 929, 1984.
[6] M.C. Ganorkar, M.H.B Stiddard, *J. Chem. Soc.*, 5346, 1965.
[7] C. C. Adison, R. Davis, N. Logan., *J Chem Soc.*, 2071, 1974.
[8] R.D. Chapman, R.T. Loda, J. P. Riehl, R.W. Schwartz, *Inrog. Chem.*, **7**, 1, 1971.
[9]M. Fréchette, C. Bensimon, *Inorg. Chem.* **34**, 3520, 1995.
[10] C.A. Bessel, R.F. Asee, D. L. Jameson, M.R. Churchill, K.J. Takeuchi, *J. Chem. Soc. Dalton Trans.*, 32, 1992.
[11] M.G.B. Drew, M.J. Hudson, P.B. Iveson , M.L. Russell, J.-O. Liljenzin, M. Sklberg, L. Spjuth and C.J. Madic, *J. Chem. Soc. Dalton. Trans.*1998, 2973-2980.
[12] K. Nakamoto, *J. Chem. Phys.*, 1960, **64**, 1420-1425.
[13] M. Kasha, *Discussions Faraday Soc.*, **9**, 14 1950.
[14] M. Kasha in "Light and Life," W.D.McElroy and B. Glass, Ed., John Hopkins Press, Baltimore, Md., 1961, 31-68.
[15] G.R. Desiraju and A. Gavezzotti, *Acta Crystallogr. Sect. B*, (1989), **B45**, 473-482.
[16] S.K.Burley and G.Petsko, *Science*, (1985) **229**, 23-28.

CHAPTER 5

THE RARE EARTHS

5.0 The Rare Earths

The lanthanides are the series of 14 elements following lanthanum, from cerium (atomic number 58) to lutetium (atomic number 71). Together with the actinides, the lanthanides make up the lower two rows of the Periodic Table and are known as the *f block* or the *f elements.*

Across the lanthanide series, starting at cerium there is a gradual filling in of the *f* orbitals with 14 f electrons. Although lanthanum is formally part of Group III it is often included in discussions of the lanthanide elements. The Lanthanide elements are coloured

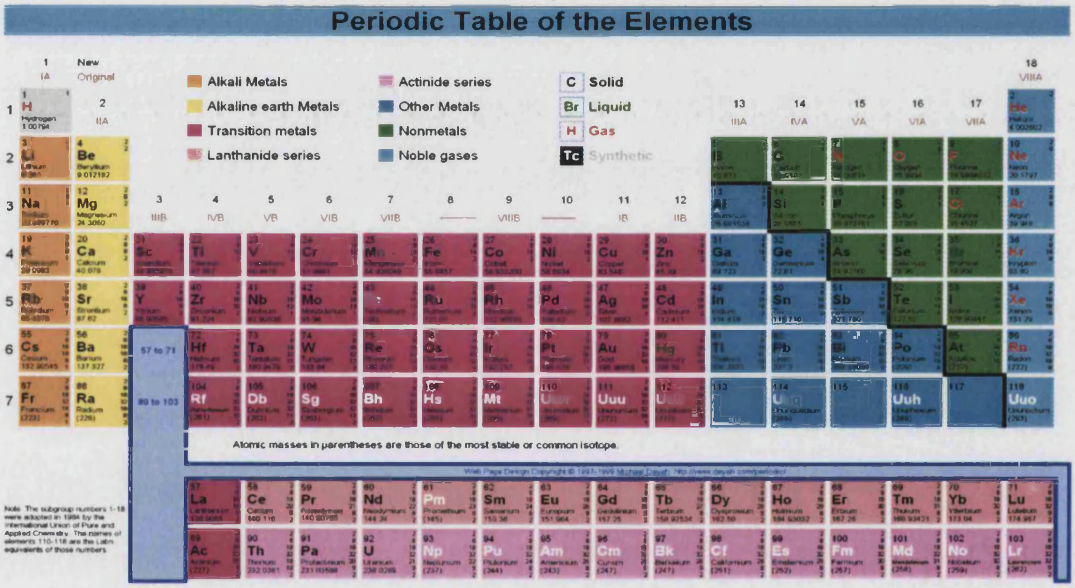

Figure 5.1.1 Periodic table of the Elements [1]

5.1 History of the Lanthanides

5.1.1 Discovery of the Lanthanides

The completion of the lanthanide series spanned over one and a half centuries, beginning first with the discovery of *yttria* in a Ytterby feldspar quarry near Stockholm by Finnish chemist, Johan Gadolin in 1794 and finally coming to a close in 1945 with the discovery of radioactive promethium.[2, 3]

Although Gadolin did not know it at that time, yttria was actually a combination of ten different elements: yttrium, terbium, erbium, ytterbium, scandium, holmium, thulium, gadolinium, dysprosium and lutetium.[2] Later in 1803, Klaproth discovered a somewhat similar yet different compound to yttria and subsequently named it *ceria.* [2]

Many chemists worked on 'purifying' both ceria and yttria and in the early times, proper purification and separation proved challenging. The only known way of separating the strikingly similar elements was via fractional crystallisation. This consisted of repeated crystallisations of the filtrate from which crystals had been removed. This technique produced only partial separations, which were often mistaken for new 'pure' elements. [2]

It did not help that Mendeleev's then current periodic table was based on valency and maximum oxidation states, making nearly all the lanthanides fall in to the Group IIIA category. The confusion was finally resolved with Mosely's determination of atomic numbers and Bohr's theory of the atomic structure based on electronic configurations of the atoms.[4]

By 1907, most of the lanthanides had been characterized except for one element, No. 61 and attempts to isolated it proved to be a laborious. Finally in 1945, promethium was discovered as the elusive by-product of uranium -235 decay.[2]

5.2 Electronic Configuration, Ionisation Potentials and Oxidation States

5.2.1 Electronic Structure of the Lanthanides

The electronic configuration of the lanthanides is characterised by the gradual filling in of the inner $4f$ shell to its capacity of 14 electrons while the outer configuration remains unchanged at $6s^2$ or $5d^1$, $6s^2$.

As the $4f$ shell sits in the core of the atom, well shielded from the outer two shells ($5d$ and $6s$), the nucleus charge consistently increases across the series while the atomic size of the of the atom decreases. Table 5.2.1 lists the trends throughout the entire series.

Given the shape of the f orbitals, they (the $4f$ electrons) do not shield each other efficiently from the growing nuclear charge, this causes the effect known as the *lanthanide contraction*, as the metal and ionic radii decrease across the series.

Element symbol	Atomic number	Outer electron configuration	Density g/cm^3	Ionic radius
La	57	Xe $5d^1 6s^2$	6.162	1.216
Ce	58	Xe $4f^2 6s^2$	6.768	1.196
Pr	59	Xe $4f^3 6s^2$	6.769	1.179
Nd	60	Xe $4f^4 6s^2$	7.007	1.163
Pm	61	Xe $4f^5 6s^2$	-	
Sm	62	Xe $4f^6 6s^2$	7.540	1.132
Eu	63	Xe $4f^7 6s^2$	5.166	1.120
Gd	64	Xe $4f^7 5d^1 6s^2$	7.868	1.107
Tb	65	Xe $4f^9 6s^2$	8.253	1.095
Dy	66	Xe $4f^{10} 6s^2$	8.565	1.083
Ho	67	Xe $4f^{11} 6s^2$	8.799	1.072
Er	68	Xe $4f^{12} 6s^2$	9.058	1.062
Tm	69	Xe $4f^{13} 6s^2$	9.318	1.052
Yb	70	Xe $4f^{14} 6s^2$	6.959	1.042
Lu	71	Xe $4f^{14} 5d^1 6s^2$	9.849	1.032

Table 5.2.1 Physical Data and Properties of the Lanthanides

5.2.2 Oxidation States and Ionisation Energies

Lanthanides have a highly electropositive character that is comparable to that of the alkali and alkaline earth metals.[4] This leads to the predominant formation of ionic compounds.

The most common oxidation state for all the lanthanide metals is the +3 state, although neodymium and dysprosium are known to form tetraflouride complexes, while praseodymium and terbium form both tetraflouride and dioxide complexes. [2, 4] Cerium is also known to form a stable +4 oxidation state in solution while the other tetravalent lanthanide ions are stable only in solid state.

Divalent states of both europium and gadolinium have been extensively studied followed by samarium and thulium.[2] The formation of the +2 oxidation state can be explained by the high third ionisation energies as well as the formation of half-filled *f*-orbitals.

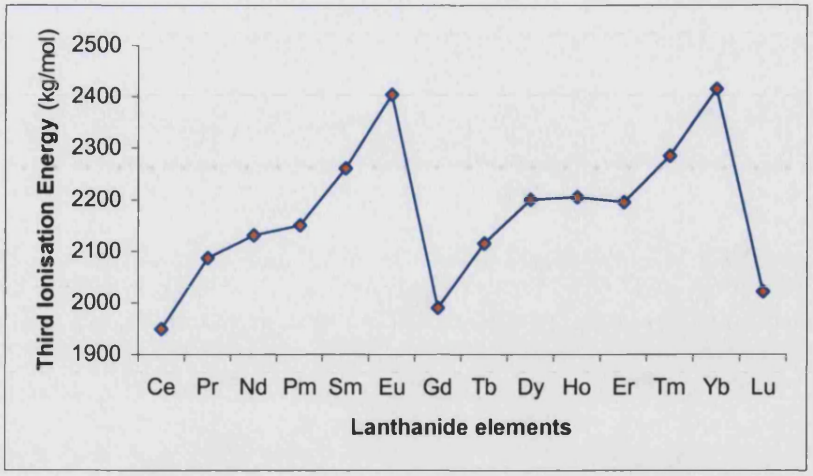

Figure 5.2.1 Third ionisation energy of the Lanthanides[2]

The plot in Figure 5.2.1 shows that both europium and ytterbium have very high third ionisation energies while for gadolinium and lutetium immediately after the two have a markedly lower energy.

For lutetium this can be explained by the fact that Yb^{2+} has the [Xe] $4f^{14}$ configuration and Lu^{2+} would have an additional electron in the $5d$ orbital thus making it less stable and easier to ionise. Similarly for Gd^{2+}, the further ionisation will produce [Xe]$4f^{7}$ with seven electrons in the seven different *f* orbitals with the same spin.

Meanwhile, Eu^{2+} has a stable [Xe]$4f^{7}$ configuration making the third ionisation potentials higher and Yb^{2+} has a fully filled *f* shell ([Xe]$4f^{14}$).

Ionisation energies, optical properties and magnetic moment of numerous lanthanide complexes confirm that the *f*-orbitals are perfectly shielded from the effects of the field of surrounding anions. The 'hidden' orbitals also limit interaction with ligand orbitals.[5] The bonding interaction with ligands is viewed as ionic.

The 18-electron rule does not apply to organolathanide chemistry, particularly as δ-donor and π acceptor bonding is absent. Lanthanides are not known to form classic carbene, carbine or carbon monoxide complexes and Ln=O and Ln≡N bonds have not been observed.[4] However the lack of orbital restrictions allows "symmetry forbidden" reactions.[6]

The ionic character of lanthanide complexes is caused largely by the contracted nature of the 4*f*-orbitals and the poor overlap with the ligand orbitals, as a result the metal-ligand interactions are determined by electrostatic factors. This 'ionic' nature is most obvious in reactions where lanthanide cations interact preferentially with 'hard' ligands forming structures of irregular geometry with a variety of coordination numbers.[4] The geometry of the lanthanide complexes is thus, dominated by ligand-ligand interactions.

5.3 Lanthanide Coordination Chemistry

5.3.1 Features of Lanthanide Coordination Chemistry

Surprisingly, the features of lanthanide coordination are strikingly different from those of the *d* –block elements. The lanthanide cations behave most similarly to the alkaline and alkaline earths. However, because of their size, the lanthanide ions are known to have high coordination numbers between 8 and 12.

Among the key factors to complexation of the lanthanides are:[5]

Each lanthanide cation, Ln^{x+}, has a noble gas configuration in the outer electronic arrangement with the electrons occupying the *4f* orbitals being effectively shielded. Therefore, metal orbitals involved in bonding are restricted to higher energy orbitals while the ligand field stabilisation is correspondingly small.

As the cation is comparatively large, covalent interactions with ligands are also minimised.

With water being a particularly strong ligand, in aqueous media any ligand added is in competition with water for coordination site on the Ln^{3+} ion. Once water is bound to the ion, it is hard to displace it with another ligand unless the ligands are those that are chelating and form complexes of sufficient thermodynamic stability.

As they are kinetically labile, ligand exchange reactions of the lanthanides occur very quickly in solution and this limits the number isolable complexes. It also confines the number of geometrical and/or optical isomers that can be identified.

5.3.2 Types of Donor Atoms and Ligands

Lanthanide ions are classified as 'A' type cations in the Ahrland-Chatt-Davies sense and 'hard' acids in the Pearson sense.[7] As 'hard' acids, lanthanide ions react readily with hard bases such as oxygen or oxygen-nitrogen donors. Most complexes form in aqueous systems contain ligands with oxygen donor sites, in the form of either pure oxygen donors or mixed oxygen-nitrogen donor systems.[6]

The predominance of these oxygen donor species has led some authors to suggest that other atoms either do not behave as donors or do so only very weakly. Moeller,[6] however, suggests that the true situation between donors, is due to competition between donor atoms and to a large degree by the environment in which the reaction is studied. Complexation with 'softer' donors such as nitrogen and phosphorus and sulfur is often facilitated by use of non-aqueous solvents and polydentate donor ligands.

5.3.3 Lanthanide-Nitrogen Complexes

Nitrogen-donor ligands, particularly bi- and tridentate ligands such as bipyridines, phenanthrolines, terpyridines and naphthyridines[8] are well represented in the lanthanide complexes, normally forming complexes with high coordination numbers from 8 to10.

These complexes are mostly either salts or contain coordinated anionic ligands. Due to the somewhat electrostatic nature of the Ln-ligand bond, which results in a large Ln-ligand bond moment, the complexes tend to dissolve only in polar solvents in which they also dissociate.[7]

Nitrogen donor systems of lanthanide trinitrate complexes are reported to be best prepared in non-aqueous solvents of low polarity as weakly basic ligands do not need to compete for a coordination site with the strongly polar water molecule. In an aqueous system the Ln-N complex must have sufficient thermodynamic stability to prevent preferential formation of the highly insoluble hydrous hydroxide.[9]

The lanthanides are known to form complexes with ammonia however they decompose upon addition of water and form hydrous oxides. Thiocyanates and azides complexes have also been synthesized with the pseudohalide acting as a nitrogen donor.[10]

5.3.4 Lanthanide-Oxygen Complexes

Much work has been done on various oxygen donor ligands particularly, in depth studies of fully hydrated lanthanide ions. The lanthanide ions have been found to have nine coordinated water molecules. The coordination numbers and the role of water molecules in complexing the cation however remained a mystery for sometime.[9] The coordination numbers are not known with certainty due to the rapid exchange of bound and unbound water molecules.[2]

Beta-diketonates, amine oxides and carboxylates are also among the well-studied oxide complexes.

By comparison, lanthanide ions complex most readily with phosphine and arsine oxides and other ligands containing the P=O or As=O group than with most other uncharged monodentate ligands.[9] This is most likely to be due to the negative charge on the oxygen atom produced by the P^{+}- O^{-} charge distribution.

Early publications suggest that complexes with Ln-O bonds tend to form preferably compared to Ln-N complexes. However, recent studies (late 1980s-early 1990s) show that the Ln-N interaction involving chelate complexes is stonger than previously believed and N-donor chelators might be playing an unexpected role on Ln (III) behaviour and may be fair competitors with respect to O-donors for lanthanide coordination sites.[11]

It is also likely that while monodentate oxygen donors bind in preference over other monodentate nitrogen donors, polydentate Ln-N interactions with chelate effects form stronger, more stable bonds compared to monodentate Ln-O interactions.

Most lanthanide complexes exhibit high coordination numbers, of nine or greater, and the description of their coordination geometry in terms of regular polyhedra is difficult. Only a few complexes with small ionic ligands approach the idealised geometries of the tricapped trigonal prism for 9-coordination; the bicapped dodecahedron for 10-coordination or the icosahedron for 12-coordination. The observed geometries in chelate complexes, particularly, are highly dependent on factors such as the ligand bite, the ligand geometry and ligand-ligand interactions. Significant deviations from idealised geometries are normal, and descriptions of structures in terms of regular polyhedra are not particularly helpful.

Because of the high coordination number and the non-directional ionic nature of the interaction between the lanthanide ion and the ligands, the ligands can move around the metal centre with ease. However, in solution, the majority of lanthanide complexes are fluxional and even when polydentate chelating ligands are present it is difficult to isolate isomers. When it is possible to run NMR spectra on lanthanum complexes (f^0) the spectra are simply showing that ligands are equivalent, when in the solid state the ligands are shown by crystallography to occupy unequivalent sites.

5.4 Lanthanides and Luminescence

In recent years, the chemistry of multidentate ligands with lanthanide ions has attracted much interest. The popularity of lanthanide ions in complex formation is in part related to their luminescence emission, which is characterised by long decay times and narrow band emission radiation (with linewidths of approximately $1 cm^{-1}$) that provides high chromatic purity.[12, 13] These are sourced as efficient light conversion molecular devices (LCMD) that may find applications as electroluminescent devices.

These characteristics are because the emitting excited state and the ground state have the same f^n electronic configuration (both maximising the number of unpaired electrons). The f orbitals are shielded from the environment by the outer s and p electrons,[14] thus they behave as inner electrons and not valence electrons.[15] Intraconfigurational transitions between states of f^n configuration are parity forbidden and very hard to induce, making molar extinction coefficients extremely low and decay times very long ($\sim 10^{-3}$).[14, 15]

Experimentally however, decay times are of one or two orders of magnitude lower than theoretically predicted suggesting interference of non-radiative decay.[14] Such decay is largely influenced by coupling with vibration modes of the host environment,[12] particularly quenching from –OH, -CH and –NH groups.[16]

In some lanthanide ions, *f-d* transitions can also take place. This generally involves the promotion of a 4*f* electron to a 5*d* orbital.[15] However, not much is known about these

interconfigurational $4f^n \rightarrow 4f^{n-1}5d(f\text{-}d)$ transitions as these transitions generally occur in the ultraviolet (UV) and vacuum-ultraviolet (VUV) regions.[17, 18]

The luminescence properties (intensities and lifetimes) of the lanthanides ions are very much influenced by the coordination environment of its metal centre.[14] Complex formation between lanthanide ions and a ligand set also has a double beneficial effect of protecting the metal ion as well as increasing the light absorption cross section by "antennae effects".[12, 19] In order to obtain strongly luminescent complexes, the ligands that chelate to the lanthanide metal core should be able to a) absorb energy and transfer it efficiently to the central metal b) encapsulate and protect the lanthanide ion from solvent molecules.[14]

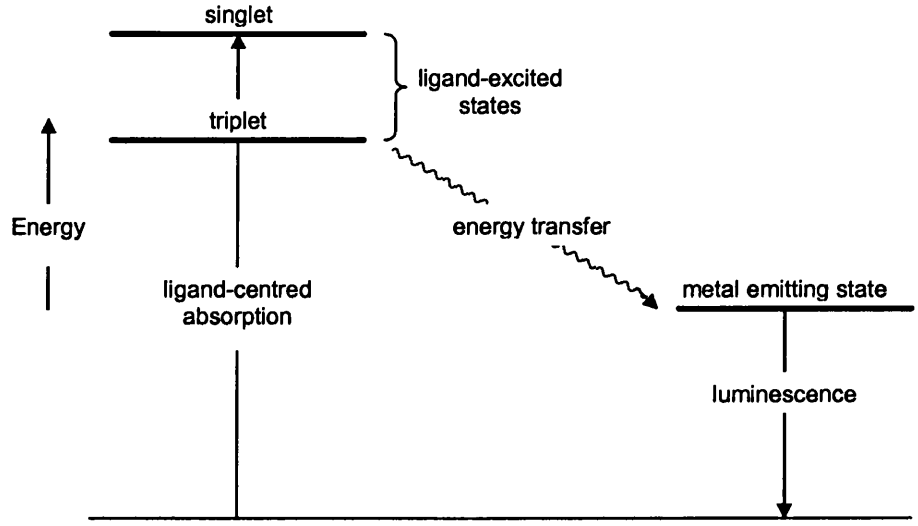

Figure 5.4.1 A schematic representation of the ligand-to-metal energy transfer[14]

Based on these forms of ligand-to-metal charge transfer effects, the intensity of luminescence is dependent on a) the intensity of the ligand absorption, b) the efficiency of the ligand-to-metal energy transfer and c) the efficiency of the metal luminescence.[14]

5.5 Lanthanide Complexes with 2,2':6'2''-Terpyridine (terpy) and 2,4,6-tris(2-pyridyl)-1,3,5-triazine (tptz) Ligands

Lanthanide terpyridine (terpy) complexes were first reported in the mid 1960s first by Sinha (1965) and later by Basile and co-workers (1968).[20] Since then several hydrated lanthanide salts with terpy ligands have been extensively studied and characterised. Terpy is well suited sterically for tridentate coordination to large ions such as those of the lanthanides.[20]

The use of nitrogen heterocycles including 2,2':6'2'' terpyridine and its derivatives have been found to show promise in the separation of lanthanides from americium(III).[21, 22, 23] This is particularly useful in the management of nuclear waste where it is necessary to extract lanthanides from a lanthanide-actinide mixture (in a nitric acid media) in order to ensure the transmutation of long-lived minor actinides (americium) to short-lived isotopes occurs efficiently by neutron irradiation. Lanthanides are able to absorb neutrons more efficiently and therefore, prevent the actinides from undergoing the necessary transmutation.[24] Other tridentate nitrogen-based ligands such as 2,4,6-tris(2-pyridyl)-1,3,5-triazine (tptz) have also generated much interest as it has been found to be more efficient at separation compared to terpyridine at lower pH.[25, 26, 27]

The luminescent properties of terpyridine and its derivatives have also attracted great interest. The inherent fluorescent and potential phosphorescent properties of such ligands make them ideal for the 'antennae effects' necessary to induce the *f-f* transitions in the lanthanides. (Refer to Section 5.4)

The following sections are the results and structural discussions on the reactions of lanthanide metals with both terpy and tptz ligands, followed by relevant luminescence studies.

5.5.1 Lanthanide- 2,2':6'2''-Terpyridine Complexes With Thiocyanate Counterions

The series of crystals of the lanthanide-terpy-thiocyanate complexes can be broadly divided in to two groups. The first ten elements of the series from lanthanum to holmium form complexes with the general formula $Ln(terpy)_2(NCS)_3$, while the following elements form a pair of counterion- complexes with the general formula $\{[Ln(terpy)_2(NCS)_2]^+ [Ln(terpy)(NCS)_4(H_2O)]^- 2EtOH\}$

The structural diversity of this group of the first ten elements, can then be subdivided in to three with lanthanum and cerium crystallising in the *Monoclinic* space group *C 2/c.* This is followed by praseodymium, neodymium and samarium all crystallising in the *Triclinic* space group *P-1*, while europium, gadolinium, terbium, dysprosium and holmium all crystallise in the *Orthorhombic* space group *P can* (a non-standard setting of *P bcn*). These first group of complexes are all nine-coordinate.

Meanwhile, the second group of the lanthanides (Er, Th and Lu) crystallises predominantly in the *Monoclinic* space group $P2_1/c$ with a coordination number of eight at each metal centre. Figure 5.5.1 shows how the lanthanide-terpy-thiocyanate complexes crystallise.

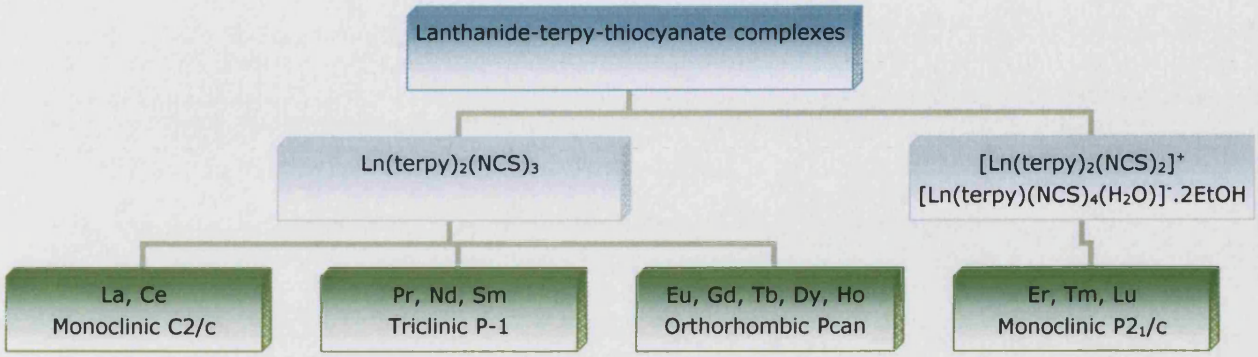

Figure 5.5.1 A schematic breakdown of the Lanthanide-terpy-thiocyanate crystals

Also included in this section are crystals of the formula $La(terpy)(NCS)_3.3MeOH$ (refer Section 5.5.1.1) which were found serendipitously in a batch of $La(terpy)_2(NCS)_3$ and a pseudo polymorph of $Eu(terpy)_2(NCS)_3$ which crystallises with a methanol solvent in the lattice yielding $Eu(terpy)_2(NCS)_3.MeOH$ (refer Section 5.5.1.5).

5.5.1.1 Structural features of La(terpy)$(NCS)_3(MeOH)_3$.2MeOH(1)

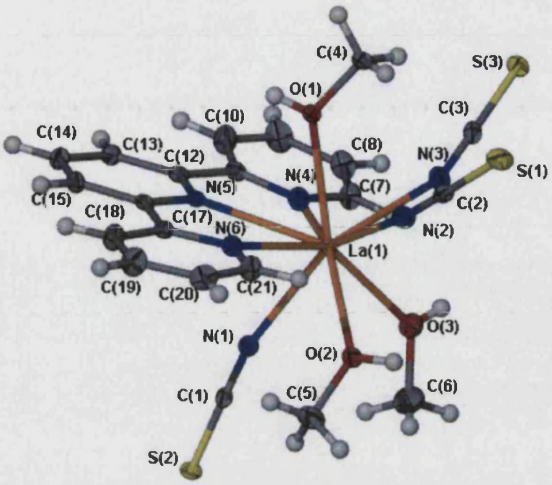

Figure 5.5.2 Structure of La(terpy)$(NCS)_3(MeOH)_3$ (**1**) showing atom-numbering scheme employed. Ellipsoids are drawn at 50% probability level. Solvent molecules have been removed for clarity.

The complex molecule La(terpy)$(NCS)_3(MeOH)_3$ crystallises in the *Orthorhombic* space group *Pbca*. The asymmetric unit contains a discrete [La(terpy)$(NCS)_3(MeOH)_3$] molecule and two solvent molecules.

The molecular structure of La(terpy)$(NCS)_3(MeOH)_3$ (shown in Figure 5.5.2) shows that the lanthanum atoms are nine-coordinate. The metal centre is coordinated to six nitrogen atoms, three from terpy and one from each thiocyanate molecule, and to three oxygen atoms from the three solvent molecules. There are also two free solvent molecules in the asymmetric unit. If the lone terpy ligand is considered to occupy the equatorial plane, then on either side of the trans-axial positions are two thiocyanates, one methanol and two methanol, one thiocyanate groups respectively.

The La-N distances vary from 2.5885(19)Å [La(1)-N(2)]to 2.7343(18)Å [La(1)-N(5)] with the coordinated N from terpy having significantly longer bond distances (average of 2.6973Å) possibly do to the steric hindrance and the rather rigid bite angle of the terpy molecule. The La-O distances range are significantly shorter compared to that of nitrogen from 2.5475(18)Å (La(1)-O(3)) to 2.5868(16)Å [La(1)-O(1)].

The thiocyanate groups are slightly bent with La-N-C angles of between 158.07° (18) to 167.37° (18) and are bound to the lanthanum ion through the nitrogen atoms.

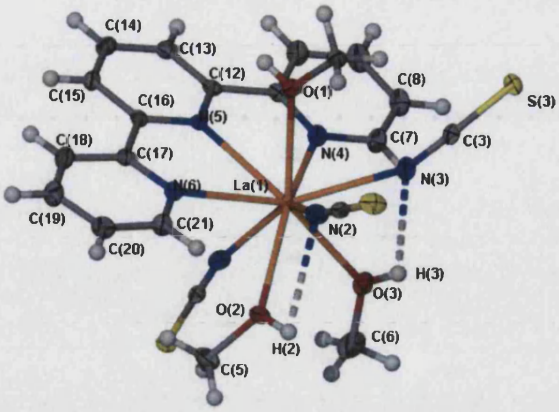

Figure 5.5.3 A graphical representation of the intra-molecular hydrogen bonding

Within the structure the two shortest interactions involving hydrogens are between the bound methanols and the adjacent –NCS groups with O(3)-H(3)···N(3) distances of 2.616Å and an angle of 104.91°, while O(2)-H(2)···N(2) has a distance of 2.791Å and an angle of 90.15° as represented in Figure 5.5.3.

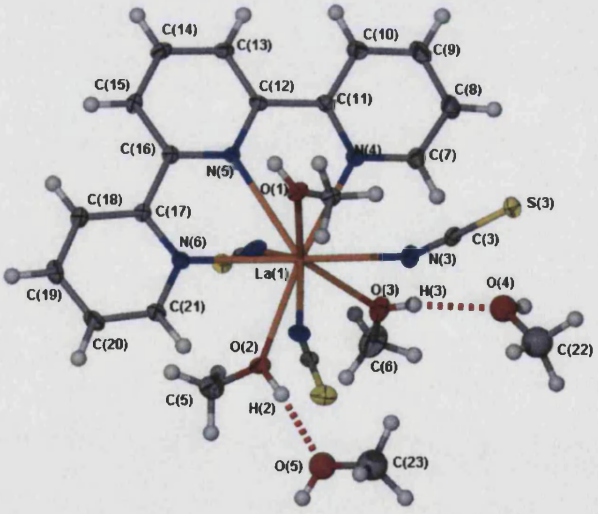

Figure 5.5.4 The inter-molecular hydrogen bonding

Intermolecular hydrogen bonding is also observed between the free solvent molecules and with the end sulphur atoms of the thiocyanate groups as shown in Figure 5.5.4 and Figure 5.5.5. The strongest hydrogen interactions occur between O(2)-H(2)···O(5) and O(3)-H(3)···O(4) with distances of 1.831 Å (170.52°) and 1.8382Å (165.18°) respectively.

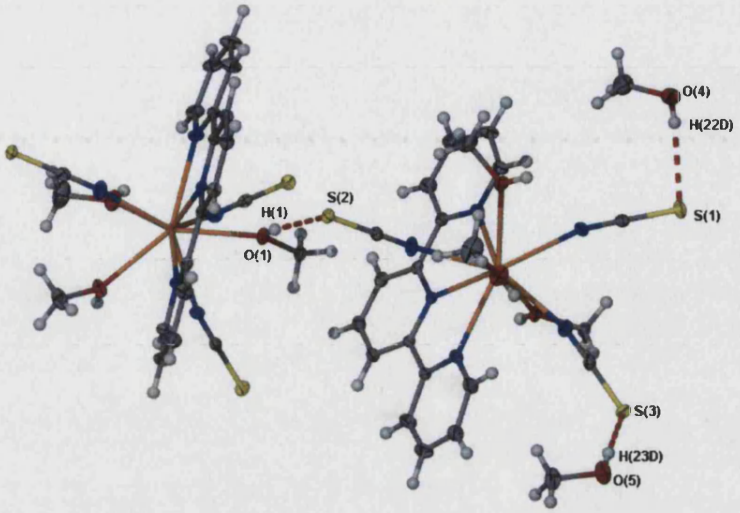

Figure 5.5.5 Weak hydrogen bond interactions between symmetry related molecules

The weaker interactions, shown in Figure 5.5.5 are between O(5)-H(23) ···S(3) (2.472Å, 166.11°) [related by the symmetry operation –x, ½ + y, ½ -z] , O(4)-H(22) ···S(1) (2.465Å, 173.25°) [related by the symmetry operation –x, y-½, ½ -z] and finally O(1)-H(1)…S(2) (2.432Å, 167.50°) [related by the symmetry operation ½ - x, ½ - y, -z].

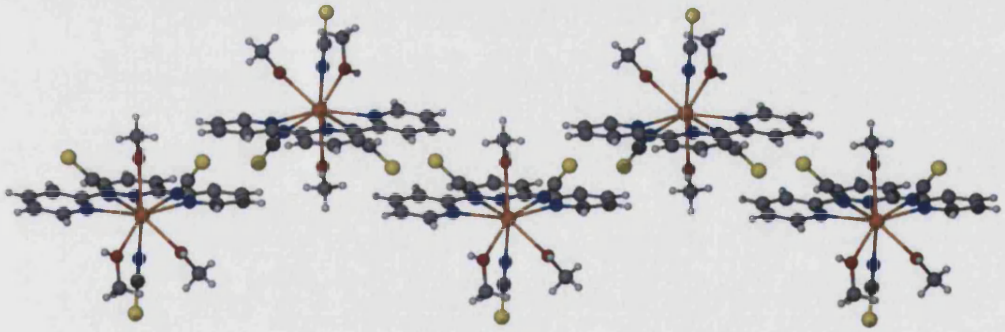

Figure 5.5.6 π-π interactions resulting in a corrugated sheet effect

Figure 5.5.6 shows the weak π-π interactions between the terpy ligands of the La(NCS)-$_3$terpy.3MeOH molecules. The overlap of the end pyridine groups have centroid-centroid distances of 3.905Å (–x, -y-1,1-z) and 3.988Å (–x, -y, 1-z) respectively.

5.5.1.2 Structural Features of $La(terpy)_2(NCS)_3.MeOH$ (2) [Representative of the Ce complex]

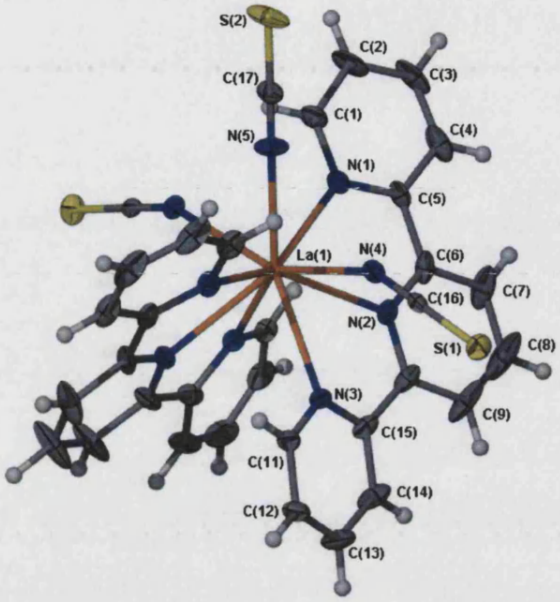

Figure 5.5.7 Structure of $La(terpy)_2(NCS)_3$ (**2**) showing atom-numbering scheme employed. Ellipsoids are drawn at 50% probability level. Solvent molecules have been removed for clarity.

The complex $La(terpy)_2(NCS)_3$ crystallises in the *Monoclinic* space group *C2/c* with a crystallographic two-fold axis through La(1), N(5) C(17) and S(2). Similar to **1**, the lanthanum core also has a coordination number of nine. The metal centre is coordinated to nine nitrogen atoms three each from the two terpy molecules and one from each thiocyante.

The La-N distances vary from 2.575(4)Å [La(1)-N(4)] to 2.734 (4)Å [La(1)-N(2)]. The La-N distances for thiocyanates are shorter than those of the terpy molecules. The metal-thiocyante angles range from a linear 180° (the thiocyanate in a special position on the symmetry axis) to a bent 148.17°.

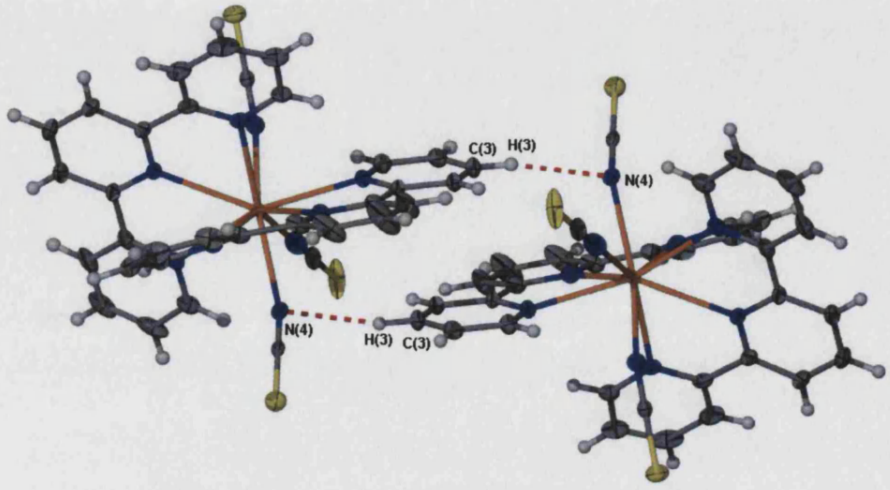

Figure 5.5.8 Intermolecular hydrogen bonding

Hydrogen bonding interactions (Figure 5.5.8) are observed between the aromatic hydrogen on C(3) with N(4), [C(3)-H(3)···N(4)] with distances of 2.485Å and an angle of 165.94° [related by the symmetry operator x, 1-y, z-½].

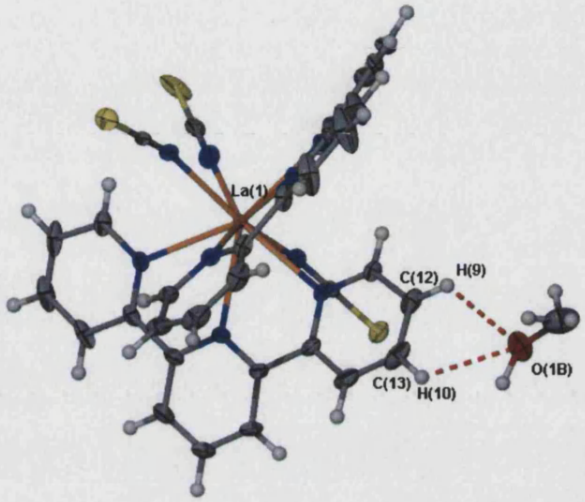

Figure 5.5.9 Hydrogen bonds between the aromatic hydrogens and the solvent molecule

H(9) and H(10), both aromatic hydrogens are weakly hydrogen bonded to O(1b) of the free disordered solvent molecule at distances of 2.588Å (119.24°) and 2.493Å (123.65°) respectively [related by the symmetry operation 1-x, -y, -z] (see Figure 5.5.9).

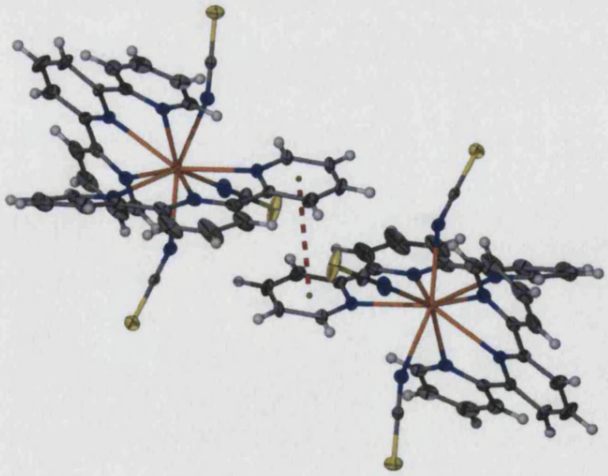

Figure 5.5.10 π-π interactions between pyridine rings

Graphitic π-π interactions are observed with centroid-centroid distances of 3.759 Å, (as shown in Figure 5.5.10) between pyridine rings related by the symmetry operation 1-x, 1-y, -z. The two rings are precisely co-planar by symmetry.

5.5.1.2.1 Discussion and Comparisons between 1 and 2

Although both lanthanum complexes were synthesised using the same method, the resulting crystals differ in that where in **2** there are two terpy ligands and three thiocyanate groups, 1 consists of one terpy ligand and three methanol solvents coordinated to the metal centre. Both molecules crystallise with solvent in the lattice contributing to an extended hydrogen bonding network.

Although unusual, the displacement of one of the two terpy with three methanol molecules seems to be a plausible explanation for the occurrence of **1**. While monodentate oxygen donors often bind preferentially to lanthanide ions over monodentate nitrogen donors, most nitrogen-chelating ligands form more stable bonds compared to the monodentate oxygen donors. However, it is important to note that the formation of solid crystals are not representative of the chemistry in solution and often the crystallisation of lanthanide complexes are based on the fine balance between thermodynamic and kinetic effects at a particular moment in time.

5.5.1.3 Structural Features of $Nd(terpy)_2(NCS)_3$ [28] (3) [Representative of Pr and Sm complexes]

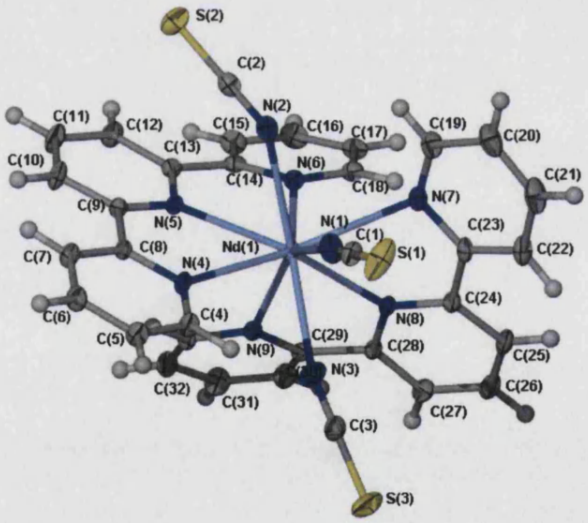

Figure 5.5.11 Structure of $Nd(terpy)_2(NCS)_3$ (**3**) showing atom-numbering scheme employed. Ellipsoids are drawn at 50% probability level. One complex molecule removed for clarity.

The molecule of $Nd(terpy)_2(NCS)_3$ (**3**) crystallises in the *Triclinic* space group *P -1* with two independent but structurally similar molecules in the asymmetric unit. Figure 5.5.11 shows one of the two molecules of the asymmetric unit.

The neodymium metal centre is nine coordinate with bonds to nine nitrogen atoms, three from each of the thiocyanate ligands and six from the two terpy ligands. The Nd-N(thiocyanate) distances average 2.527Å compared with the Nd-N(terpy) distances of 2.638Å. The metal-thiocyanate distances are shorter in comparison with the metal-terpy distances consistent with the variations observed for the isostructural lanthanum complex.

In each of the molecules, two of the thiocyanate groups are bent with average angles of 149°, while one of the thiocyanates groups are close to linear (average angles of 174°).

As expected the terpy rings show significant twisting between adjacent rings with dihedral angles ranging from 5.5° to 46.34° between the rings.

Weak hydrogen bonding occurs between the aromatic hydrogens and the sulphur end groups of the thiocyanates. These are represented in Figure 5.5.12 and Figure 5.5.13.

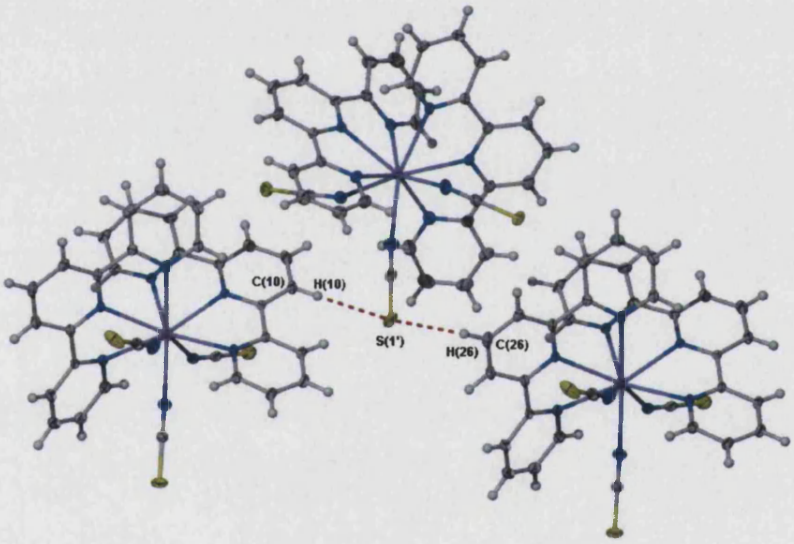

Figure 5.5.12 Hydrogen bonds between aromatic hydrogens and S(1')

The hydrogen interaction observed between the C(10)-H(10)··· S(1') is at a distance of 2.779Å, at an angle of 153.65° (related by the symmetry operator x-1, y, z), while the interaction between C(26)-H(26)···S(1') is 2.749Å at an angle of 169.54° (related by the symmetry operator x-1, y, z-1).

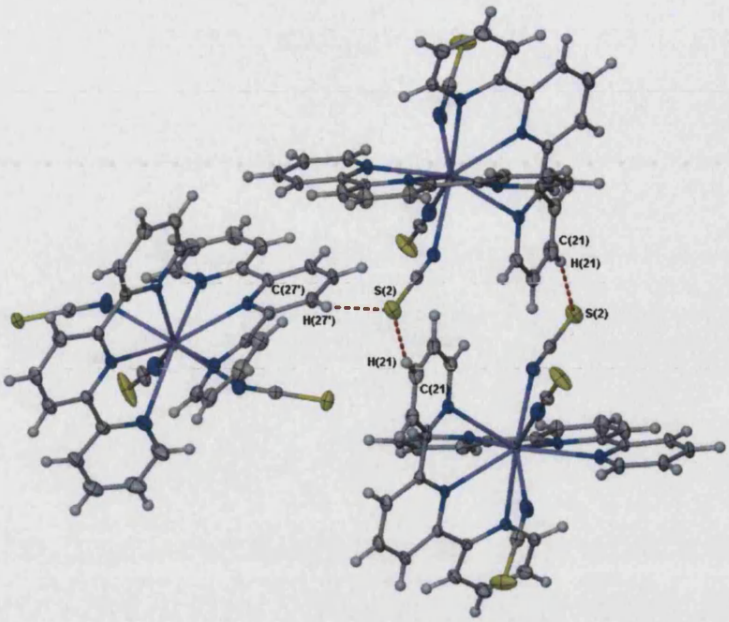

Figure 5.5.13 Hydrogen bonds between aromatic hydrogens and S(2)

Meanwhile the hydrogen interactions between C(21)-H(21)···S(2) are at a distance of 2.846Å and 164.17° (related by the symmetry operator 1-x, 1- y, -z) and C(27')-H(27')···S(2) is 2.821Å apart at an angle of 159.48° (related by the symmetry operator x, y, z).

5.5.1.4 Structural Features of $Eu(terpy)_2(NCS)_3$ (4) [Representative of Gd, Tb, Dy and Ho complexes]

The complex $Eu(terpy)_2(NCS)_3$ crystallises *Orthorhombic* space group *Pcan* shown in Figure 5.5.14. However it also forms a pseudo-polymorph, which crystallises in the *Monoclinic* space group $P\ 2_1/n$, discussed further in Section 5.5.1.5.

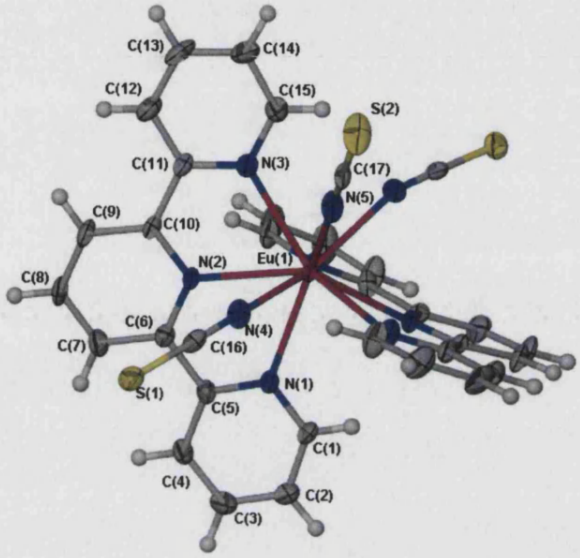

Figure 5.5.14 Structure of $Eu(terpy)_2(NCS)_3$ (**4**) showing atom-numbering scheme employed. Ellipsoids are drawn at 50% probability level.

In the *Orthorhombic* polymorph, there are four molecules in the unit cell. The molecule sits on a crystallographic 2-fold axis that passes through Eu(1), N(5), C(17) and S(2).

The overall geometry is similar to that of the lanthanide complexes discussed in the previous section. The europium complexes are also nine-coordinate with the metal centre coordinated to nine nitrogen atoms, six from the two terpy ligands and one from each thiocyanate molecule.

The Eu-N distances vary from 2.452(4)Å for Eu(1)-N(2) to 2.599(3)Å for Eu(1)-N(5) with shorter Eu-N distances for the thiocyanates (2.452 and 2.504Å respectively). The coordinated nitrogens from the terpy rings have longer bond lengths averaging 2.588Å. In comparison to the lanthanum structures, the overall lengths are shorter than those of La-N bonds consistent with the smaller ionic radius of europium compared with that of the lanthanum, also explained by the lanthanide contraction.

There is a linear thiocyanate group in special positions along the symmetry axis while the other two, mirrored, are bent at an Eu-N-C angle of 155.1(3)°.

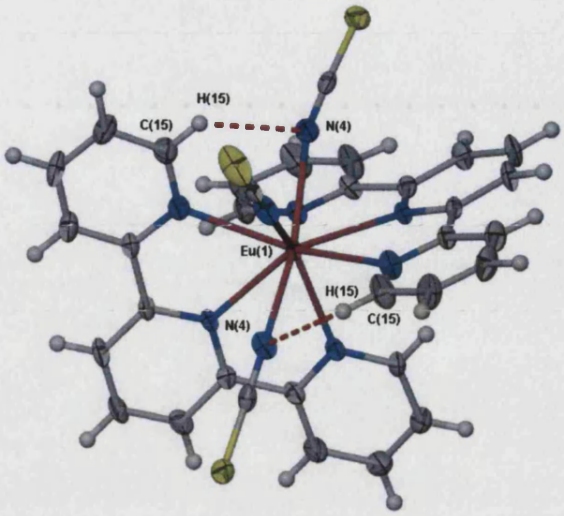

Figure 5.5.15 Intra-molecular hydrogen bonding interactions

Within the structure there are intra-molecular interactions involving hydrogens are between the aromatic hydrogen and a thiocyanate N (C(15)-H(15)...N(4)) with distances of 2.409Å and at an angle of 127.7°. (H15...N4-Eu angle is 86.9° and H15...N4-C15 angle is 113.7°) (shown in Figure 5.5.15)

5.5.1.5 Structural features of $Eu(NCS)_3terpy_2.MeOH$ (5)

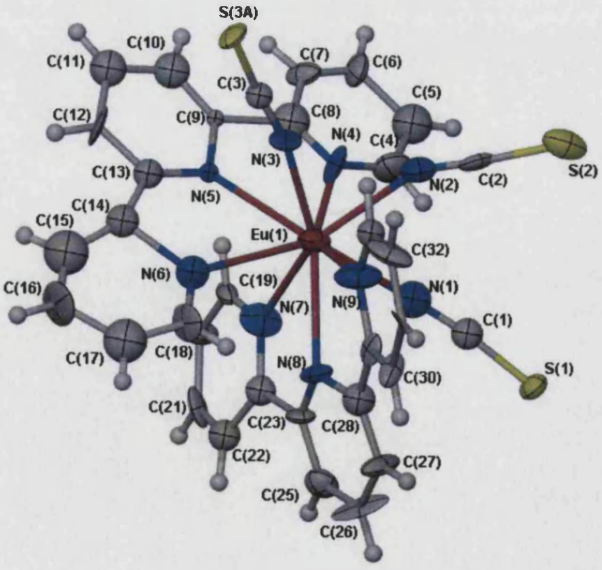

Figure 5.5.16 Structure of $Eu(terpy)_2(NCS)_3$ (**5**) showing atom-numbering scheme employed. Ellipsoids are drawn at 50% probability level. The solvent molecule and a disordered sulphur atom have been removed for clarity.

The unit cell of the second polymorph consists of four europium complexes and methanols which forms in the *Monoclinic* space group $P\ 2_1/n$. Crystals of this polymorph were smaller and the structure was less well determined.

This complex is also nine coordinate with three thiocynates two terpy molecules and a free methanol (solvent) in the lattice. The overall distances for the europium-nitrogen bonds are longer by comparison to the other polymorph at between 2.46(3)Å to 2.62(3)Å
The thiocyanates groups bind with the metal at an average of 2.465Å, while the average terpy distances are 2.58Å. The thiocyanate groups all deviate from linearity with angles less than 170°. The Eu(1)-N(1)-C(1) angle is 155(3)°, Eu(1)-N(2)-C(2) angle is 152(3)° while Eu(1)-N(3)-C(3) is 168(3)°.

The sulphur atom S(2A) is disordered over two sites and individual atomic sites were refined with 70%:30% occupancies and the atomic coordinates and displacement parameters tied together and summed to unity.

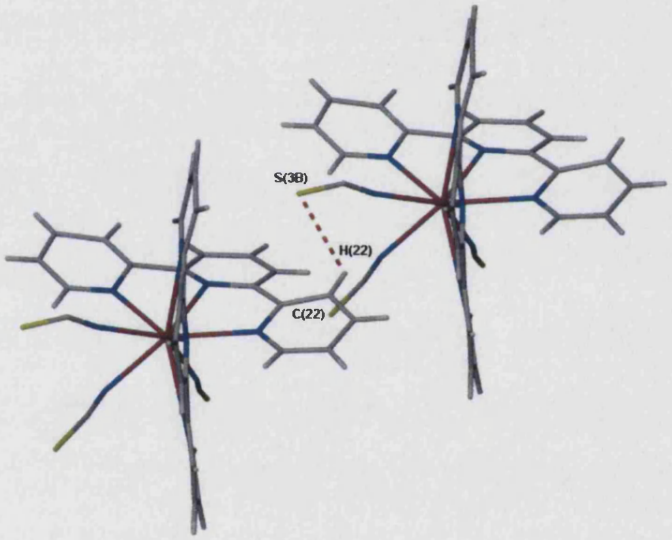

Figure 5.5.17 The inter-molecular hydrogen bond betewen H(22) and S(3B)

Unlike its polymorph, this crystal shows no evidence of intra-molecular hydrogen bonding. However hydrogen bonding does occur between two molecules related by 1+x, y, z, with the aromatic hydrogen on C(22)-H(22)···S(3B) at at distance of 2.671Å and an angle of 115.32°.

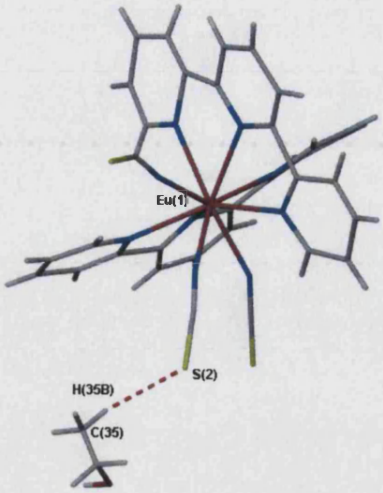

Figure 5.5.18 The interaction between the solvent and a sulphur atom.

Some interaction is also observed between S(2) and the methanolic hydrogen on C35. The interactions are relatively weak at 2.699Å.

5.5.1.6 Structural features of $[Er(terpy)_2(NCS)_2]^+[Er(terpy)(NCS)_4(H_2O)]^-.2EtOH$ (6) [Representative of Tm and Lu]

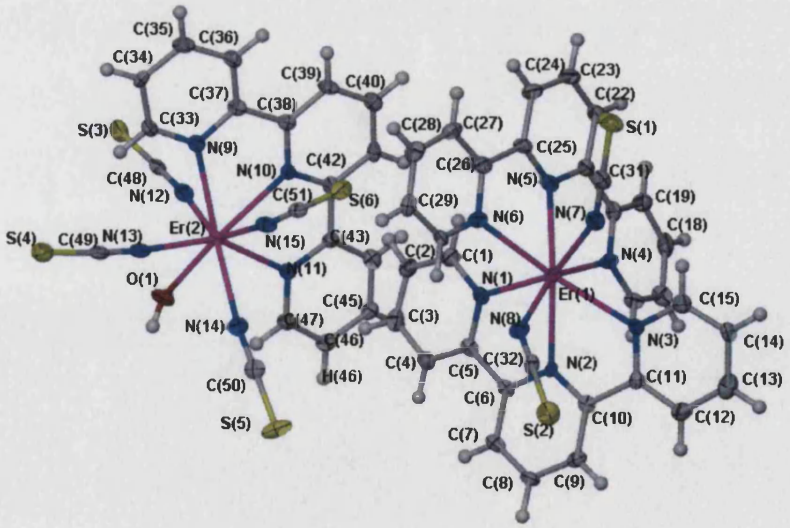

Figure 5.5.19 Structure of $[Er(terpy)_2(NCS)_2]^+[Er(terpy)(NCS)_4(H_2O)]^-.2EtOH$ (**6**) showing atom-numbering scheme employed. Ellipsoids are drawn at 50% probability level. The solvent molecules have been removed for clarity.

The complex molecule $[Er(terpy)_2(NCS)_2]^+[Er(terpy)(NCS)_4(H_2O)]^-.2EtOH$ consists of an ion pair and two ethanol molecules in the crystal lattice as shown in Figure 5.5.19. The

erbium centres are both eight coordinate. One is coordinated to eight nitrogens, six from two terpy ligands and two from the thiocyanates, giving it a formal charge of +1, while the other is coordinated to seven nitrogens from one terpy ligand, four thiocyanates and one oxygen bond to a water molecule, with a formal charge of -1.

The erbium-thiocyanate distances for both molecules range from 2.339(6)Å to 2.396(5)Å 2.344Å and 2.372Å for the cation and anion respectively. Meanwhile the erbium-terpy distances average 2.478Å and 2.506Å for the cation and anion respectively.
With only one terpy molecule on the cation, the average bond lengths are shorter than that of the anion, with less steric bulk around the metal centre.

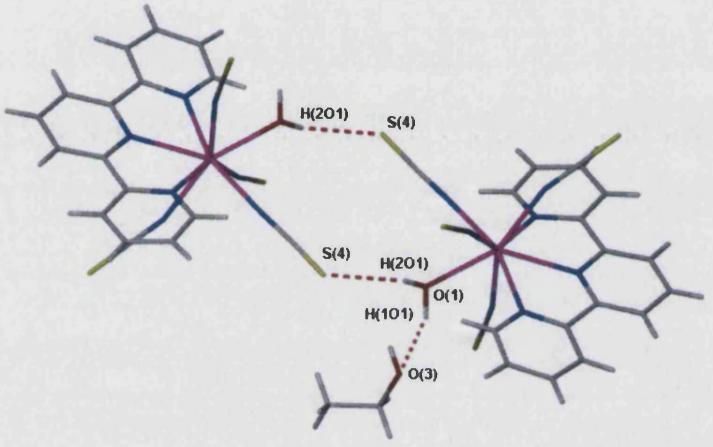

Figure 5.5.20 Hydrogen bonding interactions involving the coordinated water molecule

The coordinated water molecule acts as a hydrogen bond donor to the oxygen of the methanol solvent O(3) and to the sulphur of an adjacent molecule as shown in Figure 5.5.20. The distance between H(101) and O(3) is 1.867Å [O(1)-H(101)···O(3) 2.713Å] at an angle of 154.21°. The two molecules are related by 1+x, ½ -y, z – 1/2 . Meanwhile the distance between H(201) and S(4) is 2.596Å [O(1)-H(201) ···S(4) 3.353Å] at an angle of 163.46° (related by the symmetry operation 2-x, 1-y, -z).

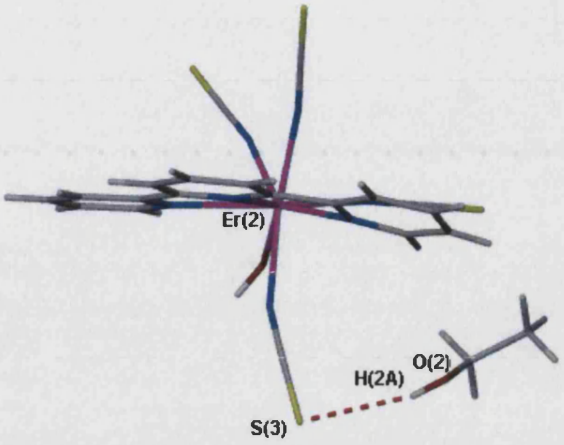

Figure 5.5.21 Hydrogen bond between H(2A) and S(3)

Another interaction is observed between H(2A) and S(3) at a distance of 2.692Å and at an angle of 157.91°. The two molecules are related by 2-x, y-1/2, ½ -z.

5.5.1.7 A Comparison of Bond Lengths in Lanthanide-Terpy-Thiocyanate Complexes

Bond lengths in complexes $Ln(terpy)_2(NCS)_3$																																		
	h01prr12		h01prr14			k02prr17			h02prr10		k01prr46			Bath 41		k01prr52		k01prr16		k01prr13		h01prr66		h01prr63		h01prr64		k01prr60		k03prr12			h03prr12		k03prr10			Bath 59		h03prr13	
	La		La			Ce			Ce		Pr			Nd		Sm		Eu		Eu		Gd		Tb		Dy		Ho		Er			Er		Tm			Lu		Lu	
			1 terpy																																					
Co-ordination number	9		11			10			10		10			10		10		10		10		10		10		10		10		8			8		8			8		8	
Molecule 1																															$[Er(terpy)_2(NCS)_2]$			$[Er(terpy)_2(NCS)_2]$		$[Tm(terpy)_2(NCS)_2]$			$Lu(terpy)_2(NCS)_2$		$[Lu(terpy)_2(NCS)_2]$	
M-N (NCS) (Å)	2.575	4	2.5885	19		2.550	3		2.565	6	2.509	6		2.498	2	2.485	4	2.46	3	2.452	4	2.439	4	2.419	3	2.409	3	2.399	3	2.339	6		2.359	4	2.332	3		2.3254	19	2.334	10
	2.575	4	2.597	2		2.550	3		2.565	6	2.521	6		2.580	2	2.468	4	2.47	4	2.504	3	2.489	2	2.474	2	2.459	2	2.499	2	2.348	6		2.378	4	2.341	3		2.3175	19	2.338	10
	2.623	6	2.597	2		2.596	4		2.595	7	2.584	6		2.516	2	2.514	3	2.47	4	2.504	3	2.489	2	2.474	2	2.459	2	2.499	2	2.344			2.369		2.337			2.321		2.336	
	2.591		2.594						2.575		2.538			2.53133		2.489		2.467		2.487		2.47233		2.45567		2.44233		2.465667												
M-N(terpy) (Å)	2.687	4	2.6778	18		2.668	3		2.664	5	2.597	5		2.5807	19	2.551	3	2.54	3	2.575	3	2.565	2	2.5560	19	2.558	2	2.536	2	2.459	5		2.463	4	2.449	3		2.4785	17	2.451	9
	2.687	4	2.6797	18		2.668	3		2.664	5	2.629	5		2.6111	19	2.578	3	2.55	4	2.575	3	2.565	2	2.5560	19	2.558	2	2.536	2	2.471	5		2.479	3	2.461	3		2.4313	17	2.456	9
	2.694	4	2.7343	18		2.670	3		2.665	5	2.626	5		2.613	2	2.593	3	2.60	3	2.590	3	2.578	2	2.5707	19	2.563	2	2.547	2	2.476	5		2.482	4	2.463	3		2.4415	17	2.470	10
	2.694	4				2.670	3		2.665	5	2.689	6		2.672	2	2.663	4	2.61	4	2.590	3	2.578	2	2.5707	19	2.563	2	2.547	2	2.476	5		2.485	3	2.468	3		2.4461	17	2.484	10
	2.734	4				2.705	3		2.699	5	2.624	5		2.6068	19	2.569	3	2.61	3	2.599	3	2.587	2	2.5679	19	2.546	2	2.554	2	2.488	5		2.496	4	2.476	3		2.4463	16	2.487	10
	2.734	4				2.705	3		2.699	5	2.691	6		2.696	2	2.660	4	2.62	3	2.599	3	2.587	2	2.5679	19	2.546	2	2.554	2	2.500	6		2.509	4	2.490	3		2.4611	17	2.493	10
Average M-N (terpy) (Å)	2.705								2.676		2.643			2.62993		2.602		2.588		2.588		2.577		2.56487		2.556		2.546		2.478			2.486		2.468			2.451		2.474	
Co-ordination number																														7			7			7			7		7	
Molecule 2																														$[Er(terpy)(NCS)_4]^-$			$[Er(terpy)(NCS)_4]^-$		$[Tm(terpy)(NCS)_4]^-$			$[Lu(terpy)(NCS)_4]^-$		$[Lu(terpy)(NCS)_4]^-$	
M-N (NCS) (Å)											2.537	6		2.518	2	2.488	4													2.352	7		2.382	4	2.354	3		2.3605	19	2.349	11
											2.522	6		2.523	2	2.495	4												2.388	6		2.385	4	2.374	3		2.3654	19	2.374	11
											2.545	6		2.526	2	2.474	4												2.396	5		2.393	4	2.378	3		2.3397	18	2.394	12
																													2.352	7		2.404	4	2.389	3		2.3542	18	2.397	11
																													2.372			2.391		2.3738			2.3550			
M-N(terpy) (Å)			La-O (MeOH)																										2.487	6		2.484	4	2.480	3		2.4655	17	2.470	9
											2.648	6		2.628	2	2.619	4												2.498	5		2.493	4	2.484	3		2.4599	17	2.471	10
			2.5475	18							2.657	5		2.637	2	2.622	3												2.534	5		2.537	4	2.524	3		2.5120	17	2.537	10
			2.5645	16							2.69	6		2.639	2	2.652	4												2.506			2.505		2.496			2.479		2.493	
			2.5969	16							2.663	5		2.645	2	2.6250	3																								
											2.648	5		2.651	2	2.6060	3																								
Average M-N (terpy) (Å)											2.638	5		2.674	2	2.6050	3																								
$M\text{-}OH_2$ (Å)	1 disordered		MeOH			1 disordered																																				
	MeOH		3 attached			MeOH																																				
Average $M\text{-}OH_2$ (Å)			2 in lattice			in lattice																																			
Ionic radius in CN9	1.216		1.216			1.196			1.196		1.179			1.163		1.132		1.120		1.120		1.107		1.095		1.083		1.072		1.062			1.062		1.052					1.032	
Cell Dimensions	Monoclinic		Orthorhombic			Monoclinic			Monoclinic		Triclinic			Triclinic		Triclinic		Monoclinic		Orthorhombi		Orthorhombi		Orthorhombic		Orthorhombic		Orthorhombic		Monoclinic			Monoclinic		Monoclinic			Monoclinic		Monoclinic	
	C2/c		P 222			C2/c			C2/c		P(-1)			P(-1)		P(-1)		P21/n		P(can)		P(can)		P(can)		Pcan		Pcan		P21/c			P21/c		P21/c			P21/c		P21/c	
a	19.572	4	15.5708	1		19.6470	3		19.6714	5	12.5331	2		12.5114	4	12.4706	2	9.6984	7	10.4043	3	10.3749	1	10.3593	1	10.3535	2	10.3477	2	12.954	5		12.9270	2	12.9453	1		12.912	3	12.9270	2
b	12.915	3	16.5161	2		12.9100	3		12.8883	4	15.2988	2		15.3681	5	15.3968	3	13.2538	12	16.7646	5	16.7192	2	16.7021	3	16.6842	3	16.6695	4	27.708	5		27.6790	2	27.6894	2		27.648	6	27.6790	2
c	16.816	3	23.6877	2		16.8090	3		16.8029	5	16.8222	3		16.7776	5	16.7210	3	28.613	3	18.9281	7	18.8998	3	18.9212	3	18.9222	4	18.9414	4	16.178	5		16.1340	6	16.1581	1		16.118	3	16.1340	6
α	90		90			90			90.0000		81.9370	10		81.827	2	81.6760	10	90.000	3	90.000	1	90.000		90.00		90.00		90.00		90.0000			90.0000		90.0000			90.00		90.0000	
β	121.66	3	90			121.644			121.7450	10	89.2600	10		89.147	2	89.0730	10	99.397	3	90.000	1	90.000		90.00		90.00		90.00		96.696	5		96.6510	10	96.6343	3		96.60	3	96.651	1
γ	90		90			90			90.0000		89.4360	10		89.338	2	89.2960	10	90.000	3	90.000	1	90.000		90.00		90.00		90.00		90.0000			90.0000		90.0000			90.00		90.0000	
V	3618.0	13	6091.74	10		3629.39	12				3193.26	9		3192.67	19	3176.16	10	3628.6	6	3301.51	18	3278.36	7	3273.79	8	3268.62	11	3267.22	12	5767.3	2		5734.0	2	5753.05	7				5734.0	2
mosaicity			0.645																																					
GOOF	1.371		1.04			1.145			1.042		1.036			1.025		0.955		1.253		1.022		1.196		1.025		1.040		1.082		1.007			0.977		1.038			1.049		0.977	
R obs	0.0433		0.0287			0.0465			0.0590		0.0597			0.0312		0.0411		0.1897		0.0356		0.0259		0.0237		0.0242		0.0269		0.0543			0.0552		0.0295			0.0217		0.0552	

5.5.1.8 Luminescence Studies on Lanthanide-Terpy-Thiocyanate Complexes

A number of the lanthanide complexes (samarium, europium, terbium and dysprosium) were found to luminesce under ultra-violet (UV) irradiation and as a result, attempts to try to identify the transitions responsible for the emissions were made.

While absorption studies were not able to be carried out on the complexes, due to their highly insoluble nature and preliminary reflectance studies did not provide sufficient information, the nature of the complexes and their chromophoric ligands based on a theoretical understanding of how lanthanide luminescence worked (refer Section 5.4) enabled emission measurements (phosphorescence and fluorescence) to be carried out.

The measurements were carried out in the solid state and the excitation wavelength was based on the ligand excitation at both 313nm and 365nm. It was found that the emission spectra for all the complexes excited at both wavelengths were identical and reported below are the spectra excited at only one of the two wavelengths.

5.5.1.8.1 Emission Spectra of $Sm(terpy)_2(NCS)_3$

The emission of $Sm(terpy)_2(NCS)_3$ is characterised by a yellowy-orange emission under UV light. In both phosphorescence and fluorescence spectras the $^4G_{5/2}$ transitions to $^6H_{5/2}$ and $^6H_{9/2}$ are comparable while the transitions to $^6H_{7/2}$ are much greater for phosphorescence.

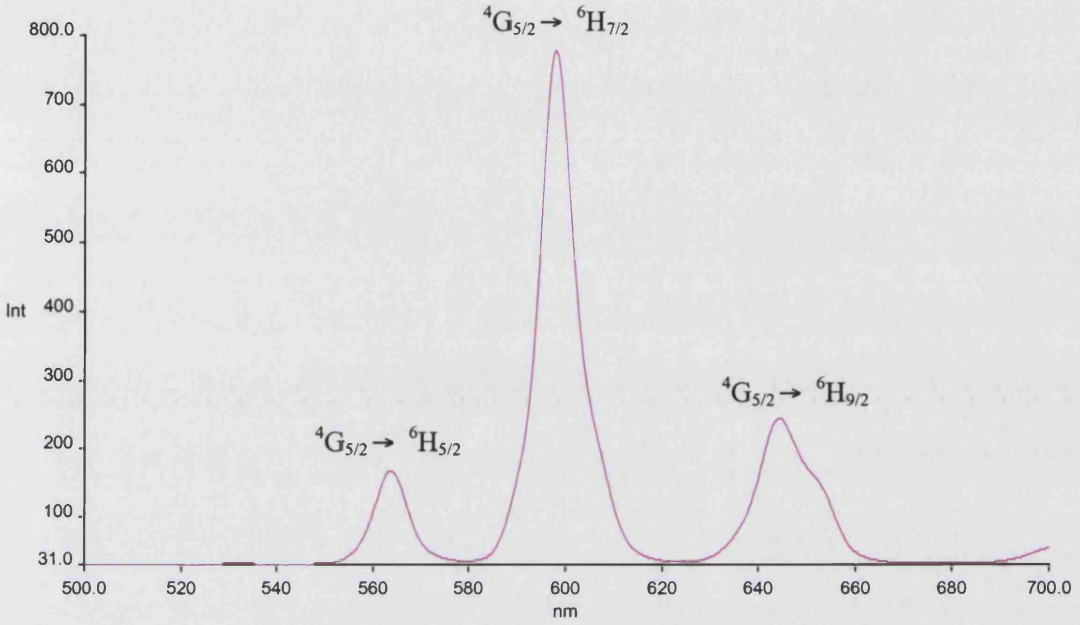

Figure 5.5.22 Phosphorescence spectra for $Sm(terpy)_2(NCS)_3$ (λ_{ex} = 365nm)

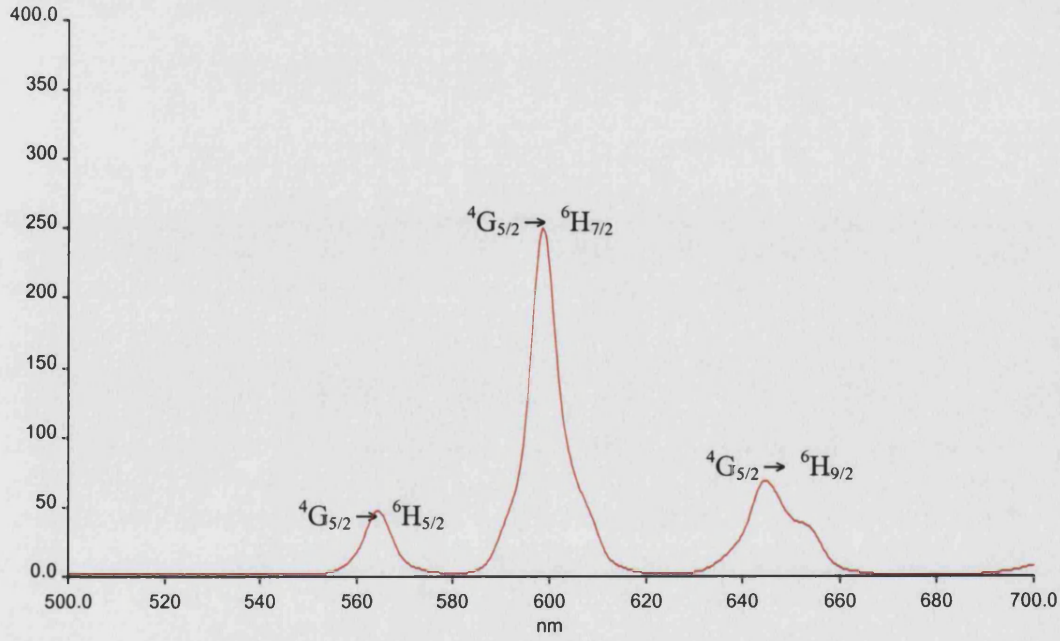

Figure 5.5.23 Flourescence spectra for $Sm(terpy)_2(NCS)_3$ (λ_{ex} = 365nm)

5.5.1.8.2 Emission Spectra of $Eu(terpy)_2(NCS)_3$

The emissions for $Eu(terpy)_2(NCS)_3$ are characterised by the typical $^5D_0 \rightarrow {}^7F_J$ (J = 0 - 4) transitions. The emission are an intense red under the UV light. As the $^5D_0 \rightarrow {}^7F_2$ transitions is more intense than that of $^5D_0 \rightarrow {}^7F_1$, this shows that Eu^{3+} ion does not lie on a centrosymmetric coordination site.[29] In the fluorescence spectra there are some remains of the ligand-centred luminescence.

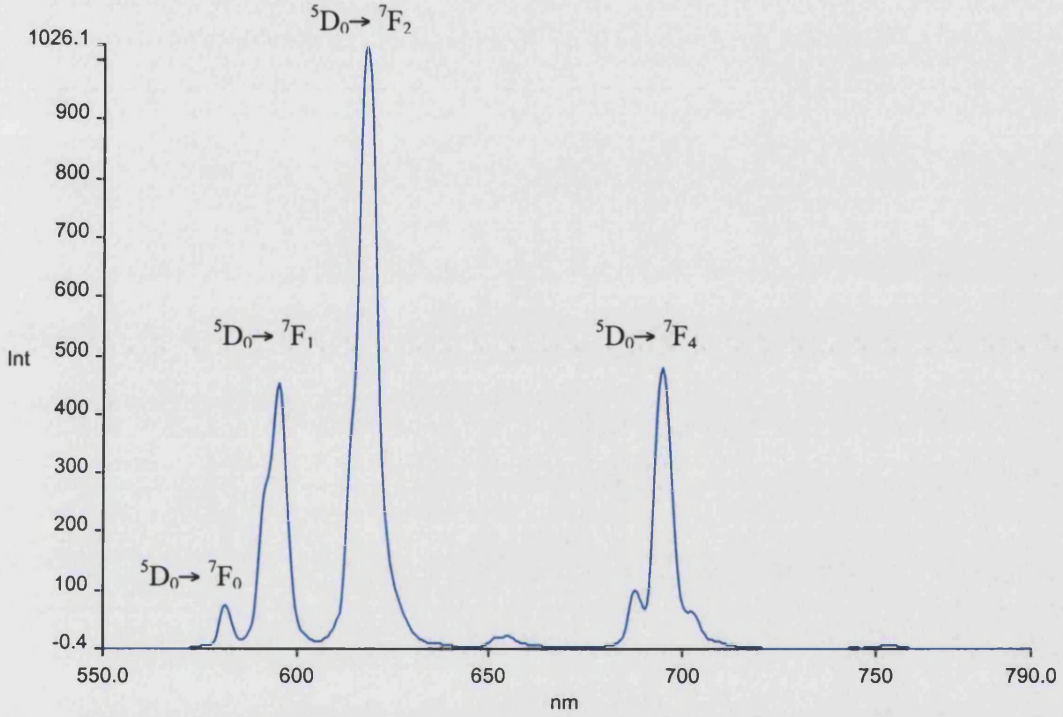

Figure 5.5.24 Phosphorescence spectra for $Eu(terpy)_2(NCS)_3$ (λ_{ex} = 365nm)

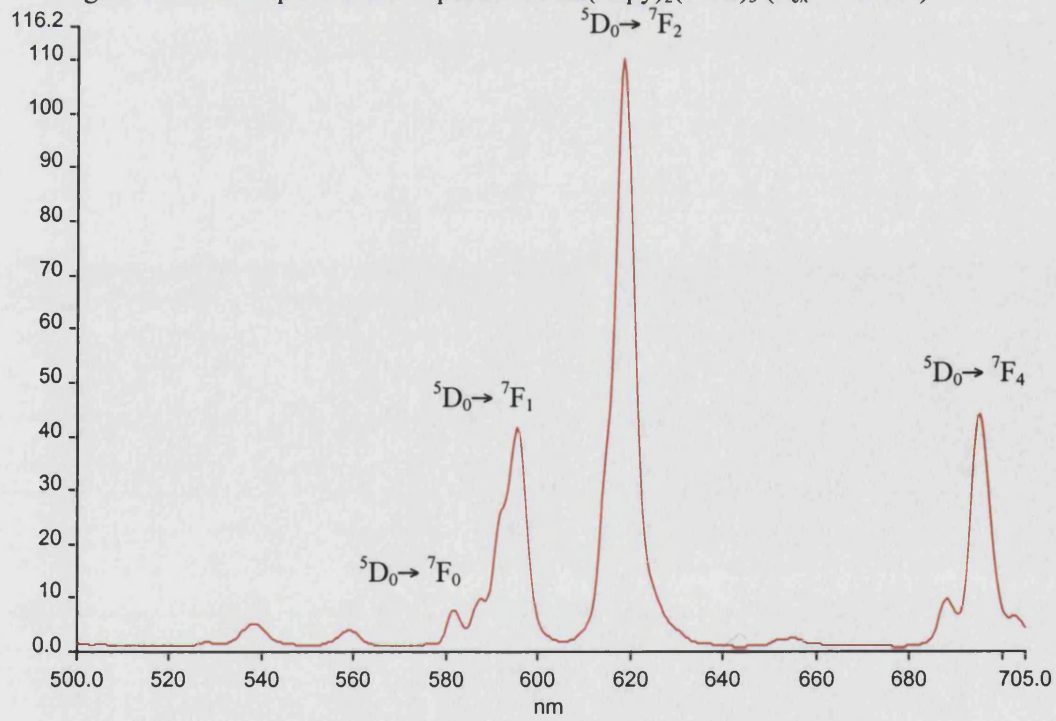

Figure 5.5.25 Flourescence spectra for $Eu(terpy)_2(NCS)_3$ (λ_{ex} = 365nm)

5.5.1.8.3 Emission Spectra of $Tb(terpy)_2(NCS)_3$

Both fluorescence and phosphorescence spectra of $Tb(terpy)_2(NCS)_3$ are the typical five-fingered spectra of the Tb^{3+} ion, characterised by an intensely green emission under UV light. Both flourescence and phosphorescence spectra are identical with typical $^5D_4 \rightarrow 7F_J$ transitions

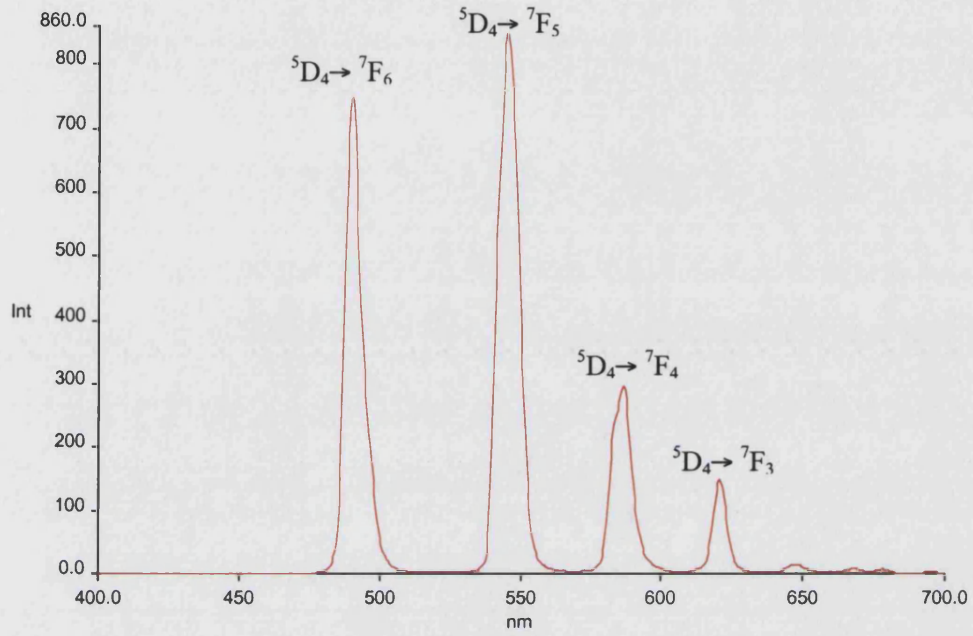

Figure 5.5.26 Phosphorescence spectra for $Tb(terpy)_2(NCS)_3$ (λ_{ex} = 313nm)

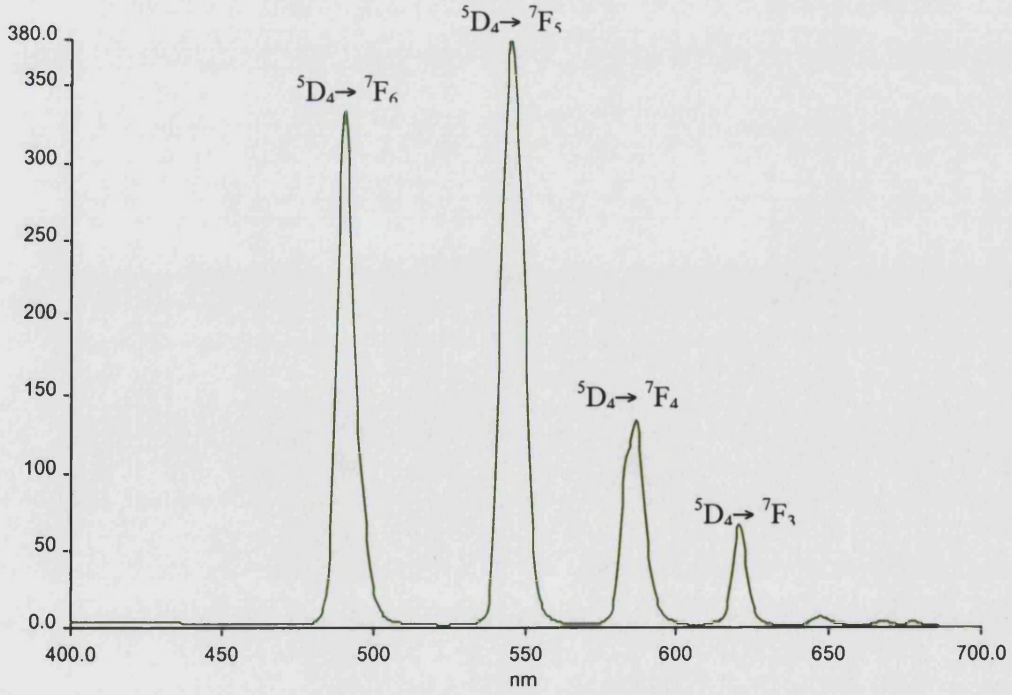

Figure 5.5.27 Flourescence spectra for $Tb(terpy)_2(NCS)_3$ (λ_{ex} = 313nm)

5.5.1.8.4 Emission Spectra of $Dy(terpy)_2(NCS)_3$

The emissions of $Dy(terpy)_2(NCS)_3$ are characterised by a yellowy-orange glow under UV light. Both the fluorescence and phosphorescence spectra are inequvalent with only two peaks in the fluorescence spectra, although the same peaks are observed in the phosphorescence spectra.. While only $^4F_{9/2} \rightarrow {}^6H_{15/2}$, $^4F_{9/2} \rightarrow {}^6H_{13/2}$, $^4F_{9/2} \rightarrow {}^6H_{11/2}$ transitions are assigned based those previously reported [33], the other transitions have been assigned by analogy.

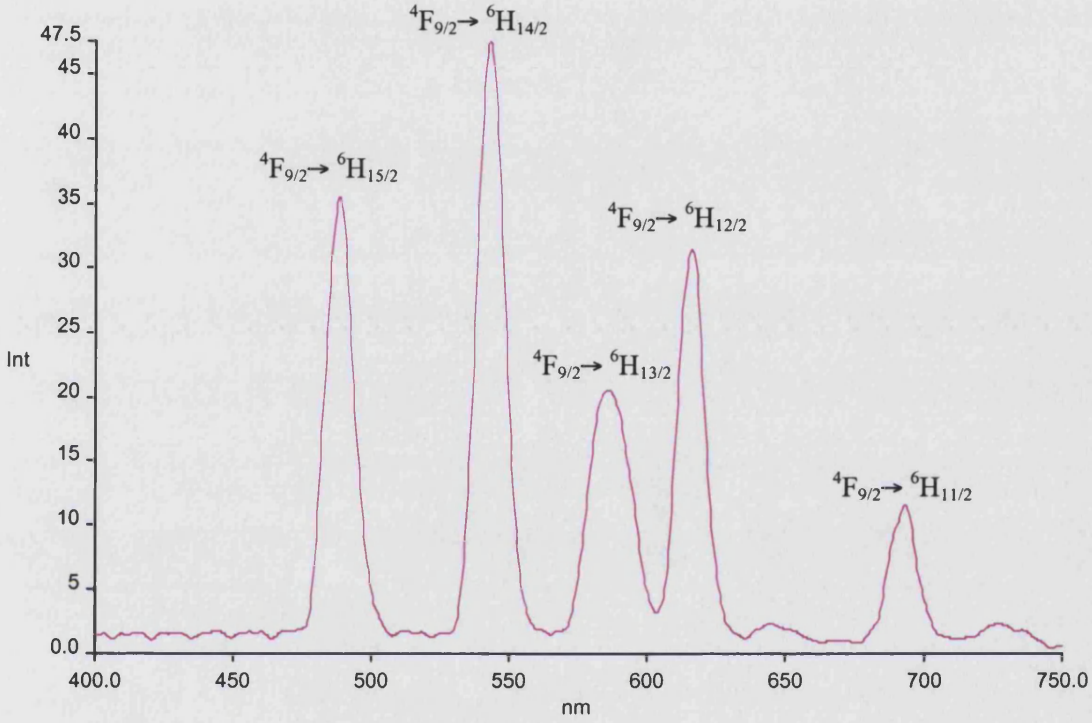

Figure 5.5.28 Phosphorescence spectra for $Dy(terpy)_2(NCS)_3$ (λ_{ex} = 365nm)

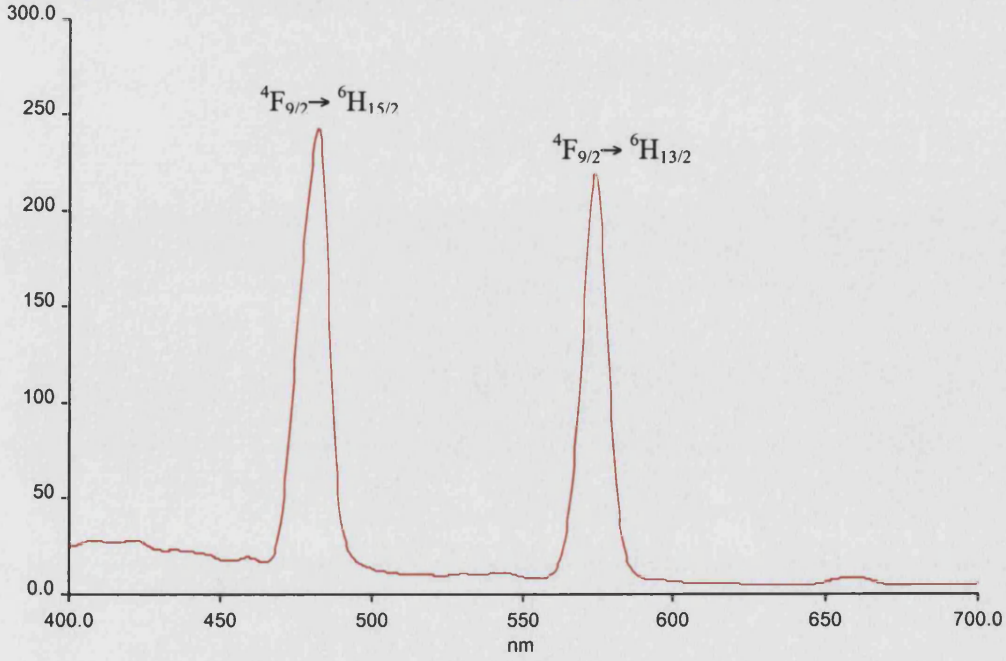

Figure 5.5.29 Flourescence spectra for $Dy(terpy)_2(NCS)_3$ (λ_{ex} = 365nm)

5.5.1.9 Discussions and Conclusions on Lanthanide-Terpy-Thiocyanate Complexes

The thiocyanate complexes of the lanthanides have been studied in some detail and have been known to crystallise in a variety of ionic forms including $[M(NCS)_6]^{3-}$,$[M(NCS)_7]^{4-}$, $[M(NCS)_7(H_2O)]^{4-}$ and $[M(NCS)_8]^{5-}$, [30] less however, is known about the neutral complexes.

The formation of the lanthanide-terpy-thiocyanate complexes can be broadly divided in to two. The first ten elements form the neutral $Ln(NCS)_3terpy_2$ with no crystallisation solvent while the from erbium onwards an ion pair of $Ln(terpy)_2(NCS)_2]^+[Ln(terpy)(NCS)_4(H_2O)]^-$ crystallises with two ethanol solvents in the lattice. Although it was not possible to crystallise the ytterbium analogue, it is believed to form isostructurally to the later lanthanide crystals.

Across the series, the first set of lanthanides is nine-coordinate while the latter are eight-coordinate with a progressive reduction in the bond lengths. The contracting sphere of the later elements would explain the lower coordination number along with the steric hindrance of fitting two bulky terpy ligands around a smaller metal sphere.

The thiocyanate ligands while, mostly all linear, show significant bending at the nitrogens, especially the equatorial –NCS groups. As the bonding in lanthanide complexes are essentially ionic and non-directional, the bending of these groups helps reduce the steric crowding but does not greatly weaken the bond. A search in the Cambridge Structural Database[31] shows that the bending of thiocyanate ligands in lanthanoid complexes is a common feature, whereas in transition metal thiocyanates they remain close to linear. [32]

The formation of ion pairs while not common, is not unprecedented and in the later elements of the $Ln(terpy)(NO_3)_3$ series, the solvolysis of a nitrate occurs stereoselectively.[28, 32]

While the luminescence measurements were only carried out on the complexes which showed emissions under UV light, it is likely that if measured nearly all the complexes would show some form of luminescence due to the chromophoric ligands. The phosphorescence measurements due to the lack of sensitivity on the spectrophotometer are those of only the very long-lived triplet states which are able to be picked up by the machine.

The overall emission spectra show a strong metal-based luminescence suggesting that the overall efficiency of the ligand-to-metal charge transfers appear to be quite high, although quantum yields were not able to be calculated. Assignments of the electronic transitions were, where possible based on published literature.[33, 34, 35, 36, 37, 38, 39]

5.6 Lanthanide-1,3,5-tri-(2-pyridyl)-2,4,6-triazine (tptz) Complexes

The lanthanide-tptz complexes is a complete series that consists of the lanthanide metals coordinated to one tptz ligand with three nitrates with the general formula $Ln(tptz)(NO_3)(H_2O).xEtOH$

5.6.1 Lanthanide-1,3,5-tri-(2-pyridyl)-2,4,6-triazine (tptz) Complexes with Nitrate Counterions

The complexes all crystallise in the *Triclinic* space group *P-1* and can be broadly divided in to two groups. The asymmetric units of the complexes contain a single $Ln(tptz)(NO_3)_3$ unit with either a bound water or an ethanol molecule and one or two ethanol solvent molecules in the lattice. Although all complexes are nearly isostructural and crystallise in the same space group, the unit cell dimensions are not equivalent.

The first group, from lanthanum to ytterbium are ten-coordinate with three nitrogen bonds to the three thiocyante molecules, seven oxygen bonds to the six nitrate molecules and to one water molecule. Although yttrium is not formally a lanthanide, it is often included in the series. In this case, it was found to be isostructural to the early lanthanides, although its ionic size is closer to that of the later lanthanides.

Interestingly, the ytterbium complex crystallises in both forms, possibly as a transitory metal between the ten and the nine coordinate metals. The lutetium complex is nine-coordinate, with three bonds to nitrogen atoms from the thiocyantes and six oxygen-bonds. Four of the oxygen-bonds are to bidentate nitrates, while there is one bond each from a monodentate nitrate and one coordinated ethanol solvent molecule. With the smaller Lu^{3+} ion, it is believed the ten-coordinate cannot be achieved with the ligand set and one nitrate becomes monodentate to relieve the steric strain. Again the change in coordination number is related to the reduction in the size of the metal ion. Figure 5.6.1 shows a breakdown of how the lanthanide-tptz-nitrate complexes crystallise.

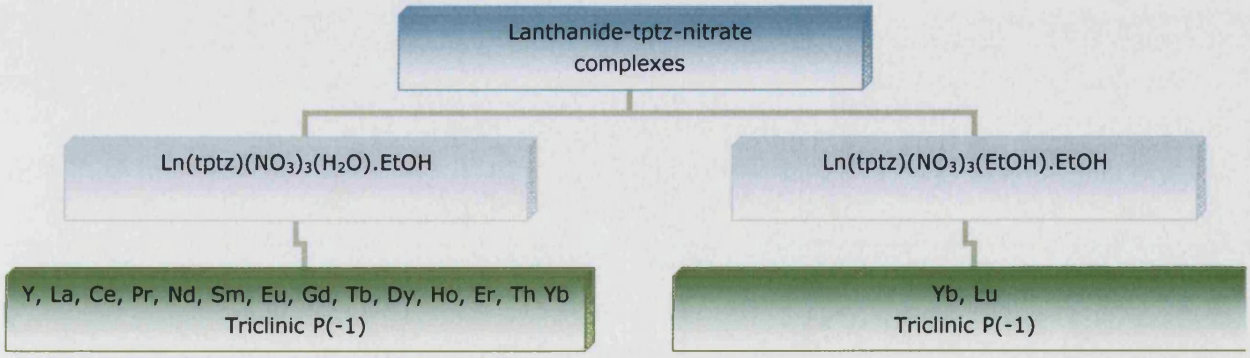

Figure 5.6.1 A schematic breakdown of the Lanthanide-tptz-nitrate crystals

Also included in this section is a discussion on a variety of and lutetium tptz complexes which were crystallised from different solvents in section 5.6.1.6.

5.6.1.1 Structural features of $Ce(tptz)(NO_3)_3(H_2O).xEtOH$ (7) [Representative of Y, La, Ce, Pr, Nd, Sm, Eu, Gd, Tb, Dy, Ho, Er, Tm, Yb complexes]

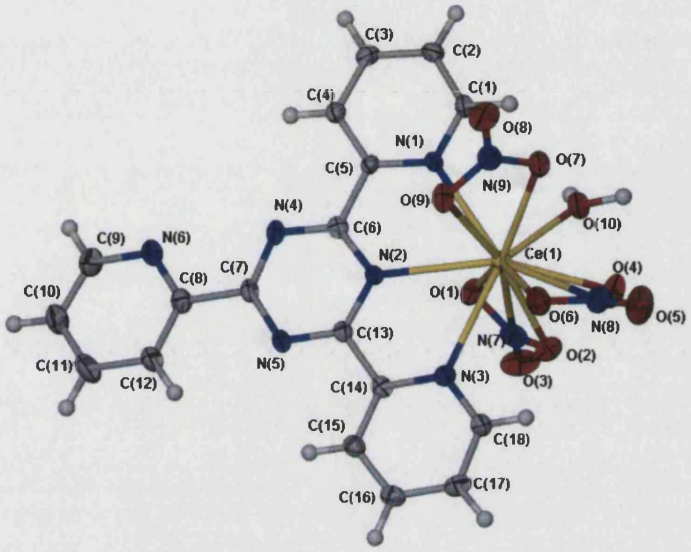

Figure 5.6.2 Structure of $Ce(tptz)(NO_3)_3(H_2O).2EtOH$ (**7**) showing atom-numbering scheme employed. Ellipsoids are drawn at 50% probability level. Solvent molecules have been removed for clarity.

The complex $Ce(tptz)(NO_3)_3(H_2O).2EtOH$ (**7**) is coordinated to three nitrogen atoms, from the single tptz ligand and seven oxygen atoms; two each from the three nitrates and one from the coordinated water molecule.

The Ce-N distances vary from 2.660(4)Å [Ce(1)-N(1)]to 2.696(4)Å [Ce(1)-N(3)] for the tptz ligand, while the Ce-O distances for the nitrate groups vary from 2.549(4)Å [Ce(1)-O(1)] to 2.618(4)Å [Ce(1)-O(6)] averaging 2.588Å. The shortest Ce-O bond is that of the coordinated water molecule at 2.424(4)Å.

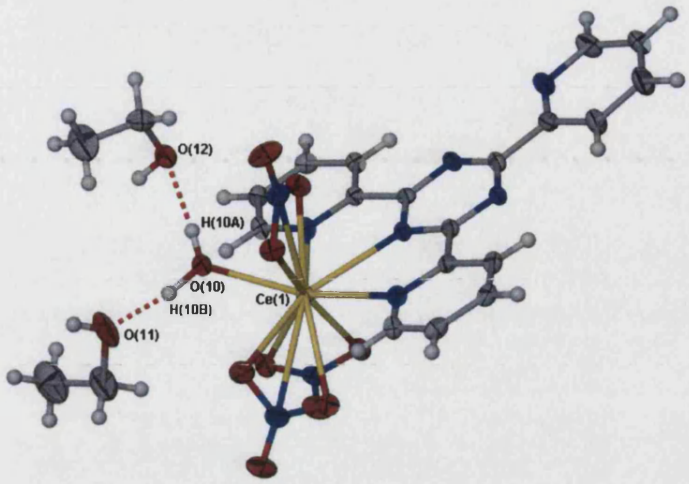

Figure 5.6.3 Hydrogen bond interactions between the bound water molecule and the solvent molecules.

While there are no intra-molecular interactions, inter-molecular hydrogen interaction occurs between the complex and the solvent molecules (refer to Figure 5.6.3). The water hydrogen H(10A) forms a hydrogen bond with an ethanolic oxygen O(12) (O(10)-H(10A)···O(12)) at distances of 1.839Å and an angle of 173°, while the other hydrogen H(10B) interacts with the other ethanolic oxygen O(11) [O(10)-H(10b)···O(11)] at a distance of 1.650Å and an angle of 168.84°. Both ethanols are related by the symmetry operation 1-x, -y, 1-z.

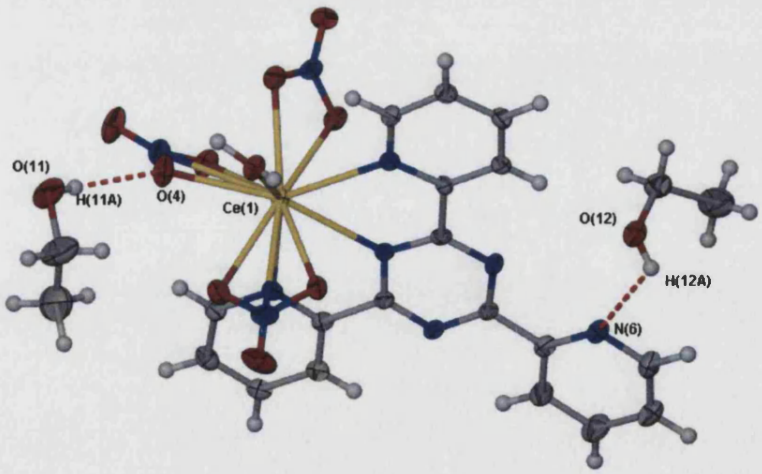

Figure 5.6.4 Other hydrogen interactions involving the solvent molecules

Meanwhile the ethanolic hydrogen H(11A) forms an interaction with O(4) from the nitrate group [O(11)-H(11A)···O(4)] with a distance of 2.059Å and at an angle of 153.66°. They are related by the symmetry operator 1+x, y, z. The other ethanolic hydrogen H(12A) also forms

a hydrogen bond, but with a pyridine nitrogen [O(12)-H(12A_d)···N(6)] at a distance of 2.287Å and an angle of 119.05° related by the symmetry operation x, y, 1+z.

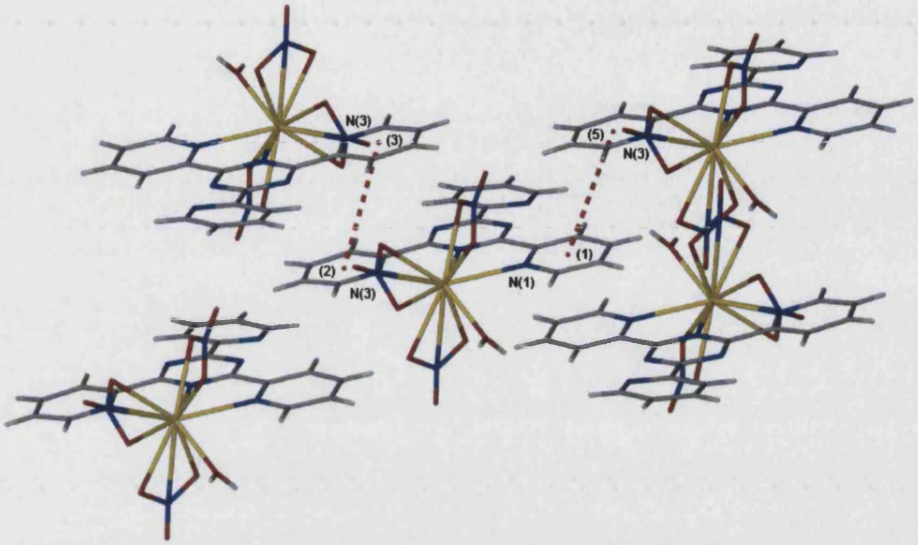

Figure 5.6.5 π-π interactions between the pyridine rings. Solvent molecules have been removed for clarity.

Some weak graphitic π-π interactions were also observed between the pyridine end groups of the tptz ligand as shown in Figure 5.6.5. The distances between centroid (2) and (3) is 4.003Å (related by the symmetry operator -x, 1-y, -z) while that between centroid (1) and (5) is 4.084Å (related by the symmetry operator x, y, z).

5.6.1.2 Structural Features of $Lu(tptz)(NO_3)_3(EtOH).EtOH$ (8) [Representative of the Yb complex]

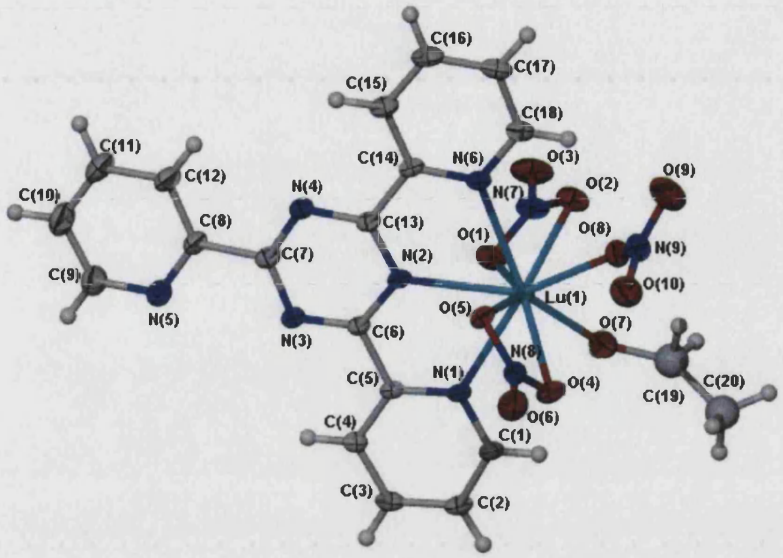

Figure 5.6.6 Structure of $Lu(tptz)(NO_3)_3(EtOH).EtOH$ (**8**) showing atom-numbering scheme employed. Ellipsoids are drawn at 50% probability level. Solvent molecules have been removed for clarity.

Unlike the other lanthanide tptz complexes, the Lu complex is nine-coordinated with bonds to the three nitrogen atoms from the single tptz ligand and to six oxygen atoms, two from the two bidentate nitrates and one each from the monodentate nitrate and the coordinated ethanol molecule. The initially bidentate nitrogen (in the earlier elements of the series) is replaced by a monodentate nitrate and an ethanol molecule.

The free ethanol molecule in the lattice (not shown in the figure) is disordered over two positions. Individual atomic sites were refined with 66%:34% occupancies and the atomic coordinates and displacement parameters tied together and summed to unity.

The Lu-N distances vary from 2.453(3)Å [Lu(1)-N(2)]to 2.510(3)Å [Lu(1)-N(6)] for the tptz ligand, while the Lu-O distances for the nitrate groups vary from 2.269(3)Å [Lu(1)-O(8)], the monodentate nitrate to 2.464(4)Å [Lu(1)-O(2)] averaging 2.371Å. The coordinated ethanol molecule is the second shortest bond at 2.271(3)Å [Lu(1)-O(7)].

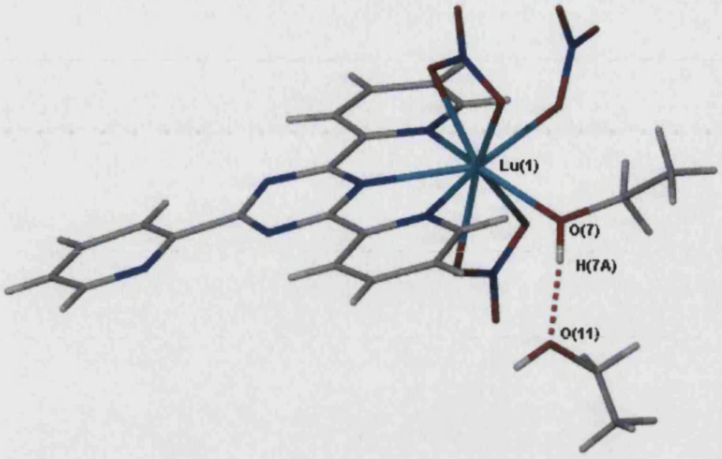

Figure 5.6.7 Hydrogen bond between the two ethanol molecules

The only observed inter-molecular interaction is between the free ethanolic oxygen O(11) and H(7A) on the bound ethanol at a distance of 1.792Å and an angle of 172.31° (related by the symmetry operator 1-x, -y, 1-z) as shown in Figure 5.6.7.

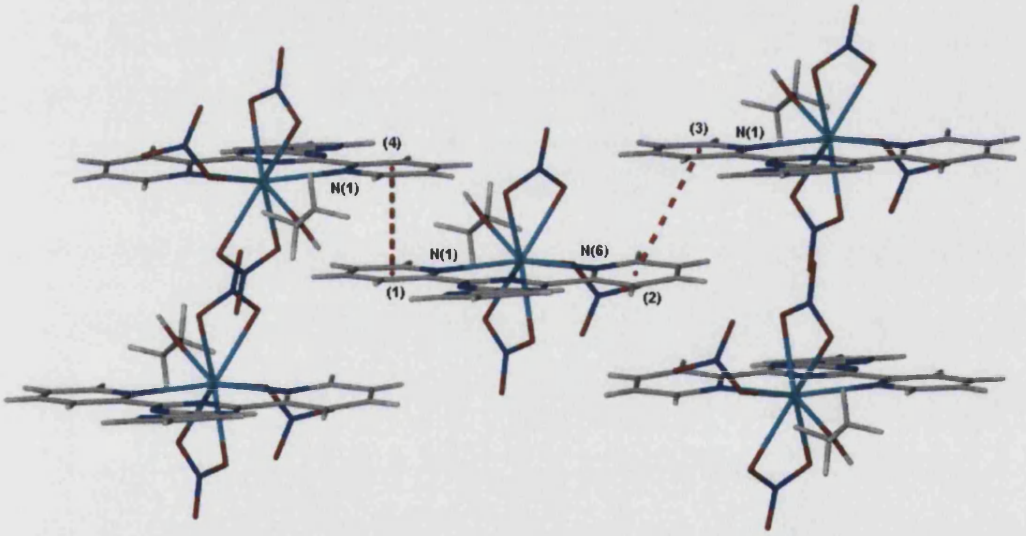

Figure 5.6.8 π-π interactions between the pyridine rings. Solvent molecules have been removed for clarity.

As observed with the earlier group of lanthanides (refer Section 5.6.1.1), there is also some evidence of weak graphitic packing between the pyridine rings of the tptz ligands. The centroid-centroid distances are 4.167Å between (1) and (4) (related by the symmetry operator 1-x, -y, 1-z) and 3.978 between (2) and (3) (related by the symmetry operator x, y, z).

5.6.1.3 A Comparison of Bond Lengths in Lanthanide-Tptz-Nitrate Complexes

Bond lengths in complexes $Ln(tptz)_x(NO_3)_3 \cdot xH_2O$	h01prr59		h02prr13		k02prr14		Bath70		k01prr20		k01prr1		k01prr21		k01prr44		h01prr41		k00prr13		h01prr19		h01prr69		h01prr60		h01prr40		k01prr56		k01prr43		h01prr42		k01prr27		h01prr24	
			1 mono NO_3		(microwave/acetone)																																	
	Y		La		La		La		Ce		Pr		Nd		Sm		Eu		Eu		Gd		Tb		Dy		Ho		Er		Tm		Yb		Yb		Lu	
x	1		1		1		1		1		1		1		1		1		1		1		1		1		1		1		1		0		0	
Co-ordination number	10		10		10		10		10		10		10		10		10		10		10		10		10		10		10		10		9		9	
M-N(tptz) (Å)	2.529	2	2.723	2	2.674	4	2.667	15	2.660	4	2.63	3	2.614	3	2.593	2	2.576	2	2.577	4	2.5674	18	2.545	2	2.534	2	2.5365	15	2.513	2	2.508	4	2.510	2	2.456	5	2.453	3
	2.539	2	2.761	2	2.699	4	2.6911	14	2.678	4	2.644	3	2.629	3	2.603	2	2.579	2	2.577	4	2.5688	18	2.555	2	2.547	2	2.5238	15	2.528	2	2.508	4	2.490	2	2.500	5	2.490	3
	2.578	2	2.790	2	2.721	4	2.7031	14	2.679	4	2.668	3	2.658	3	2.629	2	2.6185	19	2.623	4	2.6066	19	2.592	2	2.582	2	2.5734	16	2.562	3	2.519	3	2.541	2	2.517	5	2.510	3
Average M-N (tptz) (Å)	2.5487		2.7580		2.6980		2.6871		2.6723		2.6473		2.6337		2.6083		2.5912		2.5923		2.5809		2.5640		2.5543		2.5446		2.5343		2.5117		2.5137		2.4910		2.4843	
M-O (NO3) (Å)	2.412	2	2.569	2	2.555	4	2.5700	13	2.549	4	2.524	3	2.506	3	2.4809	19	2.4648	16	2.470	4	2.4559	17	2.439	2	2.426	2	2.4162	14	2.401	3	2.404	3	2.3770	19	2.273	5	2.269	3
	2.441	2	2.592	2	2.574	4	2.5881	15	2.565	4	2.546	3	2.534	3	2.505	2	2.4901	19	2.496	3	2.4818	17	2.464	2	2.451	2	2.4415	15	2.429	3	2.409	3	2.399	2	2.350	5	2.345	3
	2.442	2	2.612	2	2.580	4	2.5952	13	2.585	4	2.556	3	2.541	3	2.5105	19	2.4955	16	2.497	4	2.4854	17	2.467	2	2.453	2	2.4417	14	2.432	3	2.437	3	2.4125	18	2.368	5	2.367	3
	2.505	2	2.691	2	2.605	4	2.6171	14	2.598	4	2.583	3	2.568	3	2.5462	19	2.5361	17	2.540	4	2.5315	18	2.520	2	2.515	2	2.5058	15	2.495	3	2.520	3	2.482	2	2.406	5	2.408	3
	2.508	2	2.714	2	2.633	4	2.6312	14	2.611	4	2.592	3	2.584	3	2.5573	19	2.5437	17	2.552	4	2.5375	18	2.552	19	2.516	2	2.5121	15	2.503	3	2.528	3	2.504	2	2.464	5	2.464	3
	2.538	2			2.658	4	2.6314	14	2.618	4	2.594	3	2.584	3	2.5663	19	2.5580	17	2.560	4	2.5548	17	2.523	2	2.545	2	2.5435	15	2.544	3	2.542	3	2.567	2					
Average M-O (NO3) (Å)	2.4743		2.6356		2.6008		2.6055		2.5877		2.5658		2.5528		2.5277		2.5147		2.5192		2.5078		2.494		2.4843		2.4768		2.4673		2.4733		2.4569		2.3722		2.3706	
			2 attached MeOH																																1attached EtOH		1attached EtOH	
M-OH_2 (Å)	2.299	2	2.6029	19	2.477	4	2.4523	13	2.424	4	2.412	3	2.400	3	2.368	2	2.3494	18	2.352	3	2.337	18	2.322	2	2.3109	19	2.3026	15	2.292	2	2.262	3	2.270	2	2.271	5	2.271	3
			2.615	2																																		
Ionic radius in CN9			1.216		1.216		1.216		1.196		1.179		1.163		1.132		1.120		1.12		1.107		1.095		1.083		1.072		1.062		1.052		1.042		1.042		1.032	
In Lattice:	.2EtOH		-		.1(CH3)2CO		.2EtOH		.2EtOH		.2EtOH		.2EtOH		.2EtOH		.2EtOH		.2EtOH		.2EtOH		.2EtOH		.2EtOH		.2EtOH		.2EtOH		.2EtOH		.EtOH		.EtOH	
Cell Dimensions																																						
	P(-1)		P(-1)		P(-1)		P(-1)		P(-1)		P(-1)		P(-1)		P(-1)		P(-1)		P(-1)		P(-1)		P(-1)		P(-1)		P(-1)		P(-1)		P(-1)		P(-1)		P(-1)		P(-1)	
a	9.6081	7	9.9621	1	9.6214	3	9.6254	19	9.6076	3	9.6117	5	9.6125	2	9.6111	2	9.6085	2	9.6100	3	9.61040	10	9.6116	2	9.60830	10	9.6090	10	9.6004	2	9.6124	3	9.6053	2	9.53830	10	9.52900	10
b	108969	3	10.4472	2	10.4431	3	11.041	2	11.0114	4	10.9783	7	10.9669	2	10.9431	2	10.9303	3	10.9290	4	10.91860	2	10.9088	2	10.89760	10	10.8960	10	10.8858	3	10.8791	3	10.8858	2	12.1048	2	12.10240	10
c	14.2605	3	14.0540	2	13.9299	5	14.439	3	14.4695	6	14.4323	10	14.4121	4	14.3639	3	14.3252	3	14.3380	6	14.31480	2	14.2875	3	14.2920	2	14.2560	2	14.2428	4	14.2773	7	14.2006	3	13.7600	2	13.7520	2
α	79.9340	10	75.9520	10	86.8560	10	79.299	3	79.538	2	79.7630	3	79.8105	9	79.9330	10	79.9680	10	79.9200	10	79.92300	10	79.9300	10	79.9130	10	79.9400	10	79.8680	10	79.8060	10	79.7250	10	112.3226	10	112.3020	10
β	81.8570	10	74.3710	10	85.9510	10	82.405	3	82.414	2	82.223	3	82.1513	9	82.1280	10	82.0140	10	81.9900	10	81.98700	10	81.9270	10	81.8550	10	81.8280	10	81.7670	10	81.7140	10	81.7190	10	101.8953	9	101.9110	10
γ	86.7340	10	65.4340	10	73.0910	10	89.683	3	88.734	2	87.995	5	87.5897	12	87.3240	10	87.1660	10	87.0890	10	86.96600	10	86.8660	10	86.7110	10	86.6400	10	86.6890	10	84.4740	10	86.5100	10	99.1145	7	99.0980	10
V	1454.45	6	1266.75	3	1334.92	7	1494.3	5	1492.15	9	1484.78	16	1481.09	6	1473.05	5	1466.63	6	1467.64	9	1463.84	4	1459.67	5	1455.63	3	1453.50	3	1449.36	6	1445.20	9	1444.84	5	1388.06	4	1385.87	3
mosaicity	0.598	2	0.424	1	0.434	2			1.116	3	1.737	3	0.532	2	0.823	1	0.892	2	1.180	3	0.4530	10	0.547	2	0.5260	10	0.5260	10	0.809	2	1.381	2	0.784	2	0.490	2	0.4800	10
GOOF	0.926		1.288		1.006		1.078		1.046		1.048		1.066		1.099		0.966		1.24		0.985		1.027		1.045		1.049		1.052		1.141		1.003		1.200		1.071	
R obs	0.045		0.0239		0.05		0.0211		0.0484		0.0329		0.037		0.0311		0.034		0.0421		0.0296		0.0294		0.0285		0.023		0.0302		0.0375		0.0367		0.0422		0.037	

Table 5.6.1 Table of Comparisons between Lanthanide-Tptz-Nitrate Complexes

5.6.1.4 Luminescence Studies on Lanthanide-Tptz-Nitrate Complexes

A smaller number of the lanthanide complexes (samarium, europium, and terbium) were found to luminesce under ultra-violet (UV) irradiation compared to the terpy-thiocyanate complexes. With no emissions observed for lanthanum, dysprosium and gadolinium.

As with the lanthanide-terpy-thiocyanate complexes, absorption studies were also not able to be carried out on the complexes, due to their highly insoluble nature. Given the structural similarities between tptz and terpy, a similar chromophoric behaviour was assumed and emission measurements (phosphorescence and fluorescence) carried out.

The measurements were carried out in the solid state and the excitation wavelength was based on the ligand excitation, both also at 313nm and 365nm. It was found that the emission spectra for all the complexes excited at both wavelengths were identical and reported below are the spectra excited at only one of the two wavelengths.

5.6.1.4.1 Emission Spectra of $Sm(tptz)(NO_3)_3$

While the phosphorescence of $Sm(tptz)(NO_3)_3$ was extremely weak, bordering on non-existent, the fluorescence spectra is characterised by the $^4G_{5/2} \rightarrow {}^6H_{5/2}$, $^4G_{5/2} \rightarrow {}^6H_{7/2}$ and $^4G_{5/2} \rightarrow {}^6H_{9/2}$ transitions.

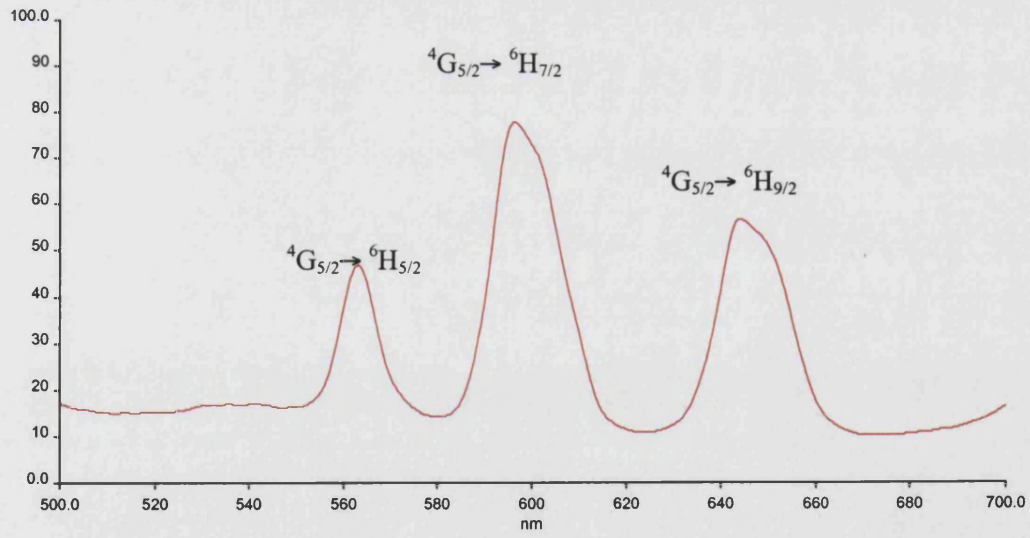

Figure 5.6.9 Flourescence spectra for $Sm(tptz)(NO_3)_3$ (λ_{ex} = 365nm)

5.6.1.4.2 Emission Spectra of $Eu(tptz)(NO_3)_3$

As with most europium-centred luminescence, this complex emits an intense red luminescence under UV irradiation with typical $^5D_0 \rightarrow {}^7F_J$ transitions where both phosphorescence and fluorescence spectra are almost identical.

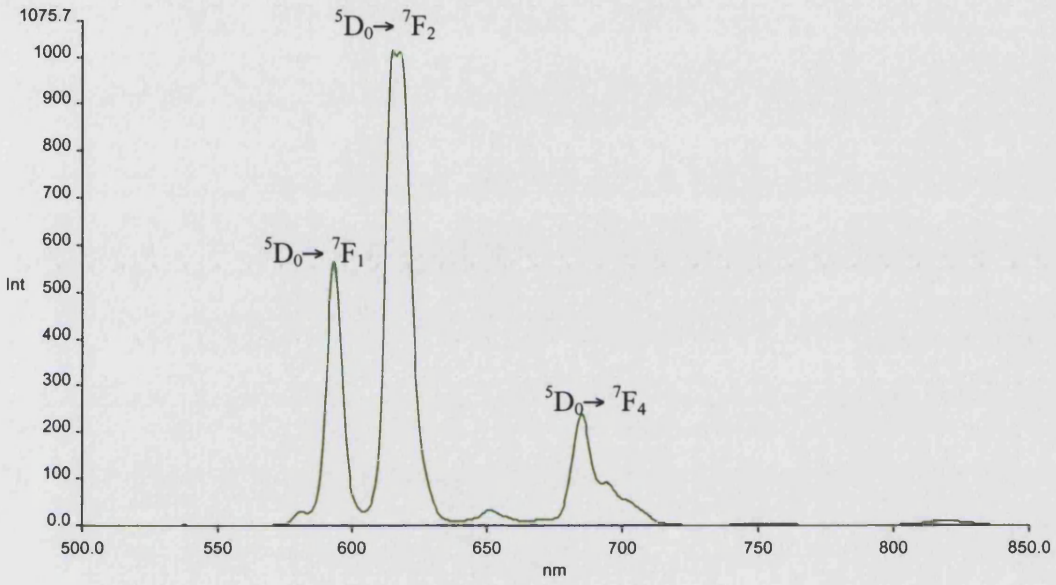

Figure 5.6.10 Phosphorescence spectra for $Eu(tptz)(NO_3)_3$ (λ_{ex} = 365nm)

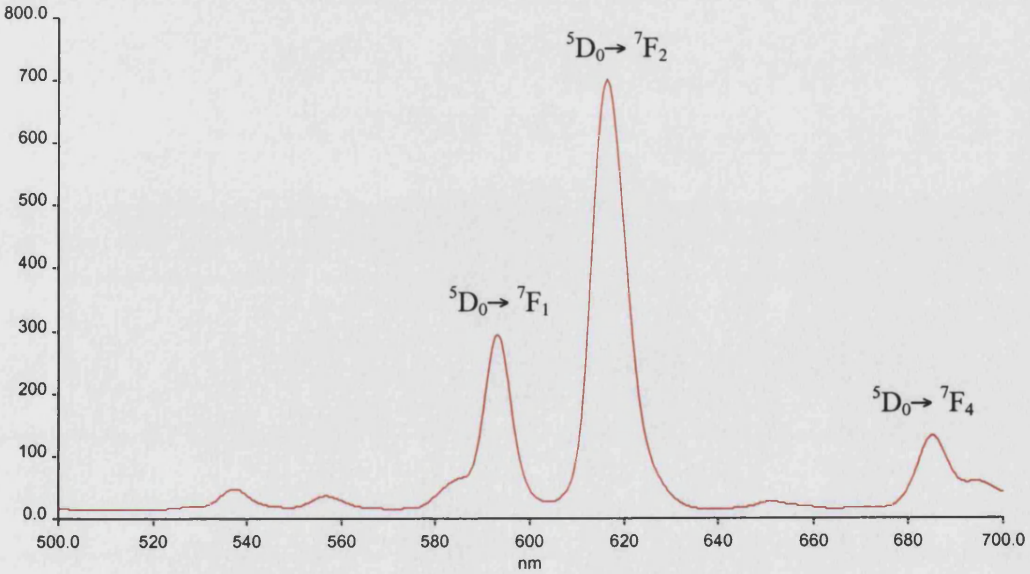

Figure 5.6.11 Flourescence spectra for $Eu(tptz)(NO_3)_3$ (λ_{ex} = 365nm)

5.6.1.4.3 Emission Spectra of $Tb(tptz)(NO_3)_3$

Again the emissions of $Tb(tptz)(NO_3)_3$ are typical of the five-fingered Tb^{3+} ion luminescence and the emissions are characteristically green under UV irradiation. Both the fluorescence and phosphorescence spectra are also nearly identical.

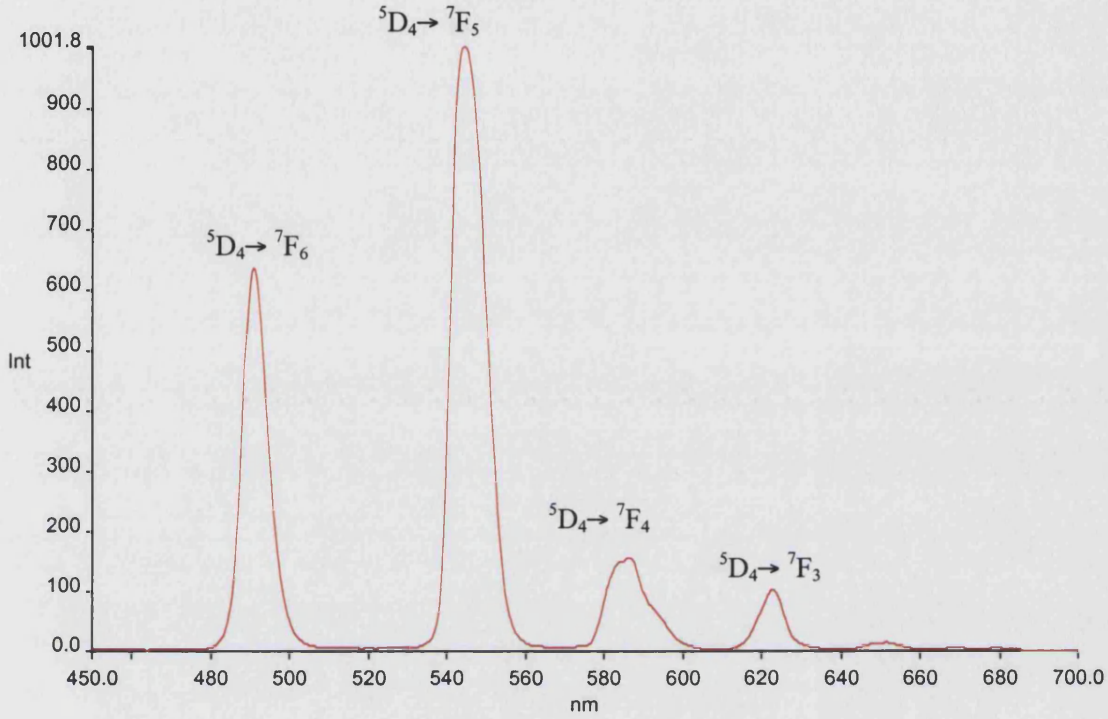

Figure 5.6.12 Phosphorescence spectra for $Tb(tptz)(NO_3)_3$ (λ_{ex} = 313nm)

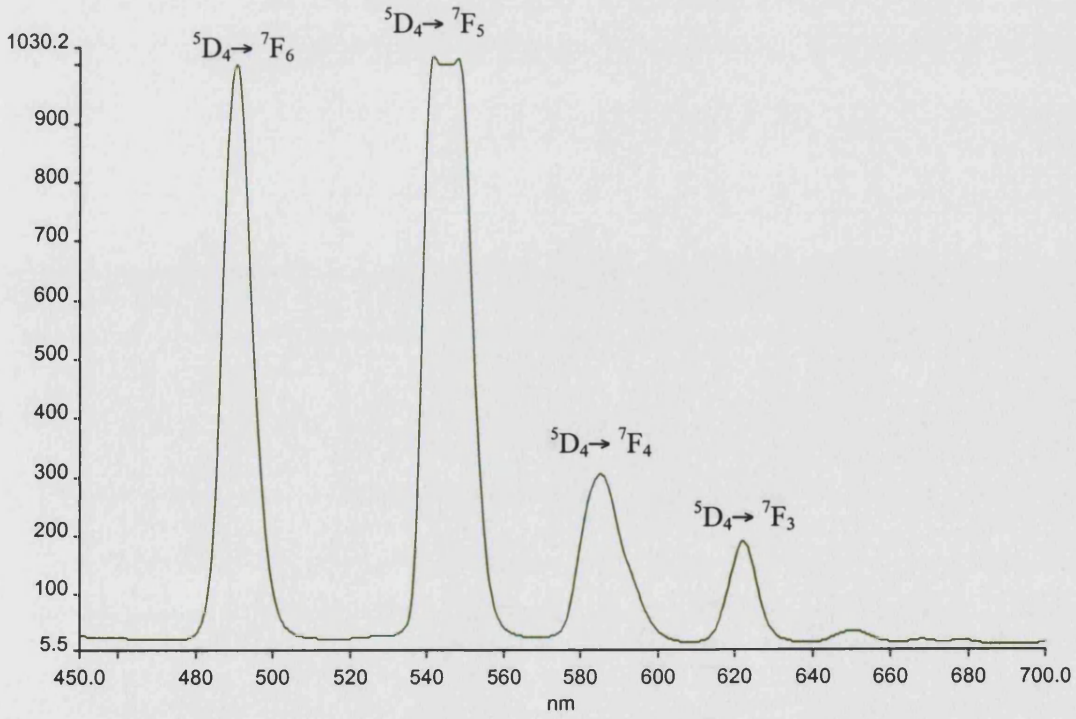

Figure 5.6.13 Flourescence spectra for Eu(tptz)(NO3)3 (λ_{ex} = 365nm)

5.6.1.5 Discussions and Conclusions on Lanthanide-Tptz-Nitrate Complexes

The formation of the lanthanide-tptz-nitrate complexes can again be broadly divided in to two. The first twelve elements, and the yttrium and lanthanum complexes form $Ln(tptz)(NO_3)_3(H_2O).EtOH$ while ytterbium and lutetium form $Ln(tptz)(NO_3)_3(EtOH).EtOH$.

Across the series, the first set of lanthanides is ten-coordinate with the last two of the series becoming nine-coordinate with a monodentate nitrate group attached to the metal centre. The contracting sphere of the later elements might explain the lower coordination number although it is unusual that the change in the coordination sphere did not occur earlier in the series.

The luminescence of the lanthanide-tptz-nitrate series are generally not as efficient compared to terpy-thiocyanates. This is possibly due to quenching from the bound solvent molecules. The presence of H_2O unfortunately cannot be completely eradicated due to the use of hydrated lanthanide salts in the initial synthesis.

As with the terpy-thiocyanates, the overall emission spectra of the lanthanide-tptz-nitrate also show a strong metal-based luminescence. However, the overall efficiency of the ligand-to-metal charge transfers would probably not be as high as with the terpy-thiocyanates.

5.6.1.6 A Case Study: Solvent Effects on the Crystallisation of Lu(tptz)(NO3)3

A brief study was carried out on the solvent effects of crystallisation. Three different lutetium complexes were obtained by varying the solvent in which the reaction was carried out. $[Lu(tptz)(NO_3)_3(EtOH)].EtOH$ (discussed earlier in Section 5.6.1.2) and $[Lu(tptz)(NO_3)_3(H_2O)].MeCN$, both contain two bidentate nitrate groups, a monodentate nitrate group and a co-ordinated solvent molecule, while $[Lu(tptz)(NO_3)_3.(H_2O)_2]^+ (NO_3)^-.3MeOH$ has two bidentate nitrate groups and two co-ordinated water molecules.

Although the solvents used were not pre-dried, the presence of water from the hydrated metal salts would have also contributed to the water content in the reaction.

5.6.1.6.1 Structural Features of $Lu(tptz)(NO_3)_3(H_2O).MeCN$ (9)

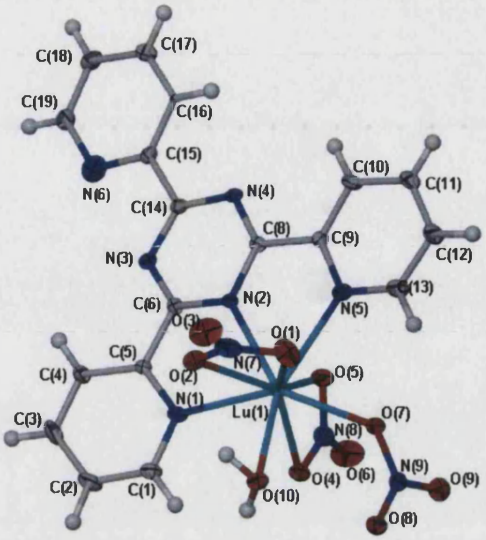

Figure 5.6.14 Structure of $Lu(tptz)(NO_3)_3.H_2O.MeCN$ (**9**) showing the atom-numbering scheme employed. Ellipsoids are drawn at 50% probability level. The solvent molecule has been removed for clarity.

The complex molecule $Lu(tptz)(NO_3)_3.H_2O.MeCN$ (**9**) closely resembles $Lu(tptz)(NO_3)_3.(C_2H_5OH)$ (**8**)(refer to Section 5.6.1.2) in having a tridentate tptz ligand, two bidentate nitrates, one monodentate nitrate and a co-ordinated oxygen atom from a neutral donor.

The average lengths of the lutetium-nitrogen bonds are 2.455 Å, while the lutetium-oxygen bonds range from 2.370(3)Å to 2.447(3)Å for the bidentate nitrates and the lutetium-monodentate nitrate bond length is 2.270(3) Å. The lutetium-oxygen distance for the coordinated water molecule is comparable to that of the coordinated ethanol in **8** at 2.293(3)Å.

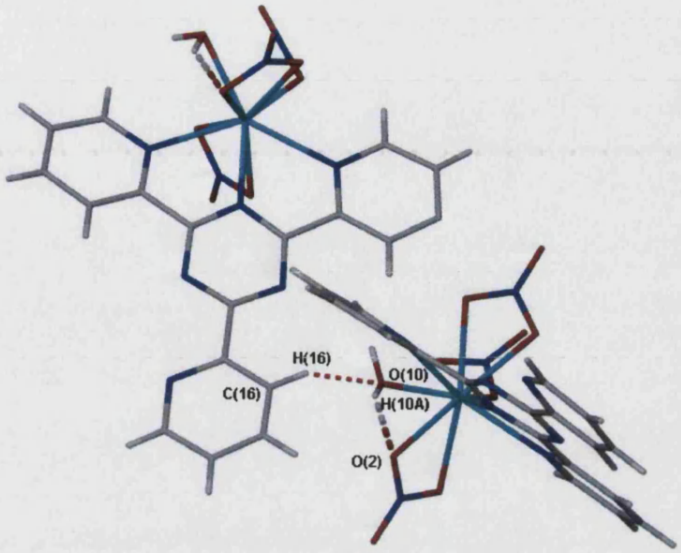

Figure 5.6.15 Hydrogen bonds involving O(10)

Hydrogen bonds contribute to the packing of the molecules in solid state with intra- and intermolecular interactions involving O(10) (see Figure 5.6.15). O(10) acts as a hydrogen bond acceptor in an interaction with the aromatic hydrogen H(16) at a distance of 1.874Å and an angle of 151.42° (related by x- ½, ½ -y, z- ½), while H(10A) is a hydrogen bond donor to the intramolecular O(2) at a distance of 2.152Å and an angle of 147.52°.

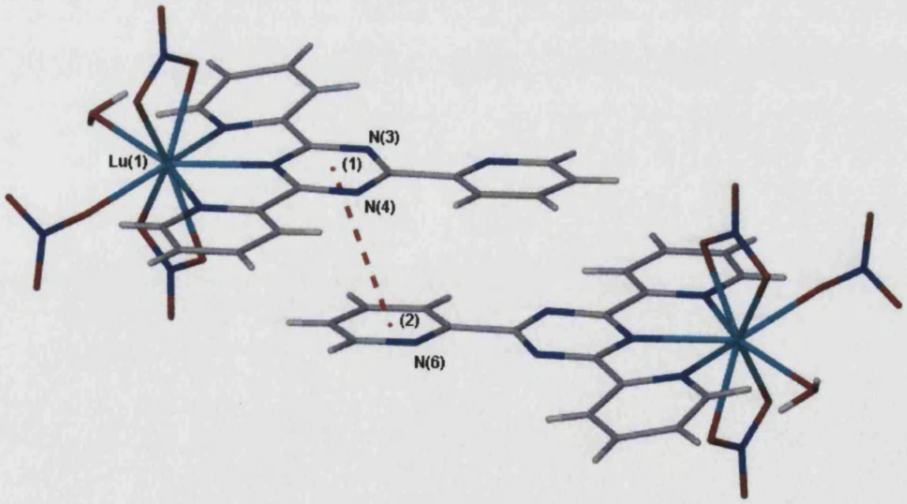

Figure 5.6.16 Graphitic π-π interactions between the aromatic rings

The observed graphitic stacking in Figure 5.6.16 between the aromatic rings are at a distance of 3.789Å apart.

5.6.1.7 Structural Features of $[Lu(tptz)(NO_3)_3.(H_2O)_2]^+ (NO_3)^-$. 3MeOH (10)

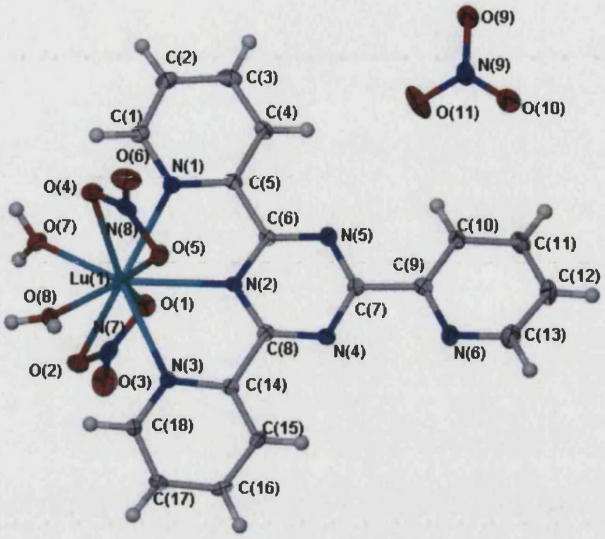

Figure 5.6.17 Structure of $[Lu(tptz)(NO_3)_3.(H_2O)_2]^+ (NO_3)^-$. 3MeOH (**10**) showing the atom-numbering scheme employed. Ellipsoids are drawn at 50% probability level. The solvent molecules have been removed for clarity.

When methanol is used as the solvent, the complex molecule $[Lu(tptz)(NO_3)_3.(H_2O)_2]^+ (NO_3)^-$. 3MeOH (**10**) is formed. This compound differs from the other two lutetium complexes in having an ionic structure (see Figure 5.6.17) in which the complete solvolysis of a co-ordinated nitrate group has taken place. The cation containing two bidentate nitrate groups and two co-ordinated water molecules, strongly resembles that found in $[Lu(terpy)(NO_3)_2.(H_2O)_2]$. $NO_3.2H_2O$ [40] and terpy analogues with other heavy lanthanides. As in the case of the terpy complexes, it is the nitrate situated trans- to the terpy ligand that has undergone solvolysis.

Corresponding average bond lengths (values for the tptz complex first) are :- Lu-N 2.488 and 2.472 Å, Lu-O (nitrate) 2.400 and 2.411 Å and Lu-O(water) 2.266 and 2.266 Å.

The average lengths of the lutetium-nitrogen bonds are 2.488Å for the tptz ligand, while the lutetium-oxygen bonds range from 2.368(3)Å to 2.445(3)Å for the bidentate nitrates, averaging 2.401Å. The lutetium-oxygen distance for the coordinated water molecules are 2.258(3)Å and 2.274(4)Å comparable to that of the other coordinated solvent molecules.

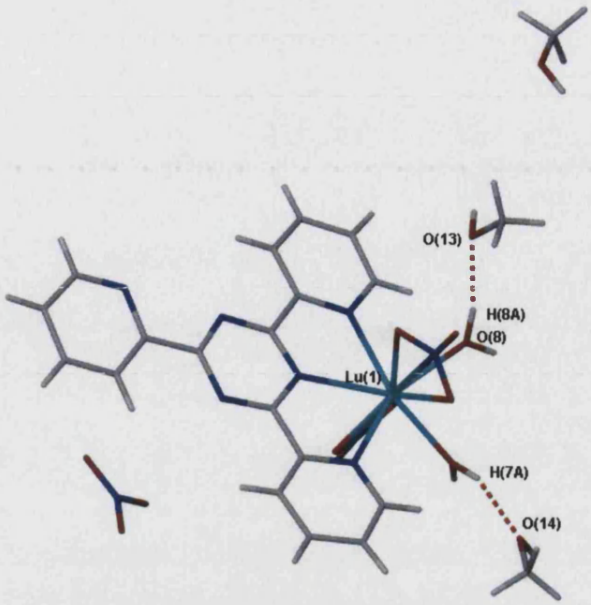

Figure 5.6.18 A hydrogen bonding network within the asymmetric unit

The free uncoordinated solvent molecules within the crystal lattice contribute to extensive hydrogen bonding. The methanolic oxygens O(13) and O(14) both act as hydrogen bond donors to the coordinated water molecules. The interactions between O(13)···H(8A) and O(14)···H(7A) are 1.803Å (163.34°) and 1.918Å (153.11°) respectively.

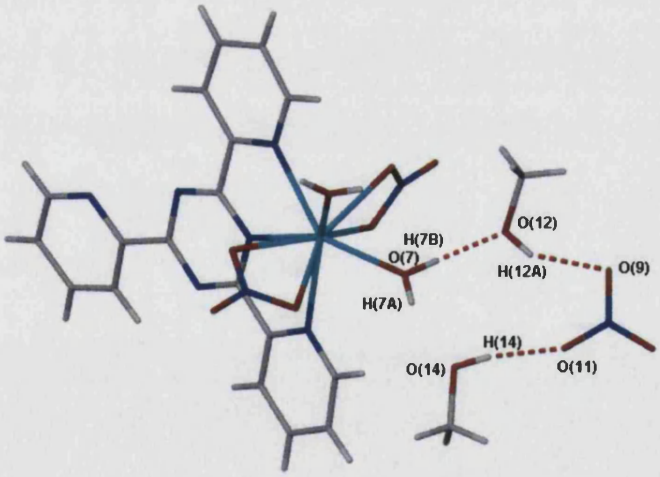

Figure 5.6.19 Hydrogen bonds involving symmetry related molecules

Meanwhile, the symmetry related nitrate anion acts as a hydrogen bond acceptor to two methanol solvent molecules. The distances between H(12A) and O(9) is 2.075Å at an angle of 150.91° (related by 1-x, 1-y, 1-z), while O(11) and H(14) is 2.049Å apart, at an angle of 148.30° (related by 1-x, -y, 1-z). The hydrogen H(7B) on the coordinated O(7) acts as a hydrogen bond donor to O(12) with distances between O(12) and H(7B) at 1.808Å and at an angle of 176.35° (related by x, y-1, z).

5.6.1.7.1 A Comparison of Bond lengths in Lu(tptz)$(NO_3)_3$ Complexes

	h01prr24		k02prr15		k02prr5	
crystallised:	from EtOH		from MeOH		from MeCN	
	Lu		Lu		Lu	
Co-ordination number	9		9		9	
M-N(tptz) (Å)	2.453	3	2.454	4	2.410	3
	2.490	3	2.493	4	2.461	3
	2.510	3	2.518	4	2.495	4
Average M-N (tptz) (Å)	2.484		2.488		2.455	
M-O (NO3) (Å)	2.269	3	2.368	3	2.270	3
	2.345	3	2.378	3	2.370	3
	2.367	3	2.411	3	2.375	3
	2.408	3	2.445	3	2.394	3
	2.464	3			2.447	3
Average M-O (NO3) (Å)	2.3706		2.4005		2.3712	
	1attached EtOH		2 attached H_2O		1 attached H_2O	
M-OH_2 (Å)	2.271	3	2.258	3	2.293	3
			2.274	4		
Ionic radius in CN9	1.032		1.032		1.032	
In Lattice:	.EtOH		.3 MeOH		.MeCN	
Cell Dimensions	Triclinic		Triclinic		Monoclinic	
	P(-1)		P(-1)		$P2_1/n$	
a	9.5290	1	9.6852	2	9.2814	2
b	12.1024	1	11.9769	2	15.5441	4
c	13.7520	2	13.4392	3	17.5975	4
α	112.302	1	90.460	1	90	0
β	101.911	1	107.242	1	98.3080	2
γ	99.098	1	100.531	1	90	0
V	1385.87	3	1460.58	5	2512.17	10
mosaicity	0.4800	10	0.760	2	0.747	2
GOOF	1.071		1.158		1.047	
R obs	0.037		0.0293		0.0322	

Table 5.6.2 Table of Comparisons between Lu(tptz) complexes

5.6.1.7.2 Discussions and Conclusions on the Solvent Effects on the Crystallisation of $Lu(tptz)(NO_3)_3$

The complexes of lutetium with tptz ligands are all nine-coordinate with one tridentate ligand, while the variation lies in the nitrate groups and the coordinated solvent molecules.

For the complexes synthesised in EtOH and MeCN, all the nitrate groups are coordinated to the metal centre although one is monodentate with one other solvent attached to the metal core (MeCN). However, the complexes synthesised in MeOH, the monodentate nitrate has been displaced by solvolysis with two H_2O molecules.

While a change in solvent causes a change in the complexes that crystallise out of solution, it is difficult to draw firm conclusions as to the sort of effects of the varying solvents. Undoubtedly the nature of competiting solvent and the free water molecules play a large role in determining the outcome of the final structure in solid state.

5.7 Lanthanides with 1, 10-Phenanthroline (phen) Ligands

Lanthanide complexes with phen ligands were first synthesised in the mid-1960s by Laming and Hart [41, 42] in studies related to the metal-ligand ratio of the lanthanide ions. The first known complexes were synthesised with the lanthanide nitrates under anhydrous conditions.

Akin to 2,2':6'2''-terpyridine, phen is also able to form a closed protective sphere around the metal centre, as well as transfer absorbed energy to a metal as an antennae ligand. Its photophysical properties especially when coordinated to luminescent lanthanides, particularly europium and terbium, has long interested chemists.[43, 44, 45, 46]

The following sections describe some structural and luminescence studies on a variety of lanthanide-phen complexes.

5.7.1 Lanthanide-1,10-Phenanthroline Complexes with Thiocyanate Counterions

All of the lanthanide-phen thiocyanate complexes all crystallise in the *Triclinic* space group, *P-1*. They can be broadly divided in to two groups of which the first six elements of lanthanum, cerium, praseodymium, neodymium, samarium and europium form one group, while the next eight elements, gadolinium, terbium, dysprosium, holmium, erbium, thullium, ytterbium and lutetium form the other. Unlike in the series of the lanthanide-tptz-nitrate complexes where the yttrium is isostructural to the early lanthanides, in this series, the yttrium complex shares the same coordination sphere as the later lanthanides.

The asymmetric units of the first group contain a single complex molecule with the general formula $Ln(phen)_3(NCS)_3.EtOH$. The complexes are isostructural, with the lanthanide ions coordinated to nine nitrogen atoms, three from the thiocyanates and two each from the three phen ligands.

The asymmetric units of the second group of complexes however, contain a single complex molecule and a free phen molecule in the lattice, with the general formula Ln(phen)2(NCS)3(MeOH).phen. They are also isostructural with a coordination number of eight at the metal core. The complexes bond to three nitrogens from the thiocyanates, four nitrogens from the two phen ligands and to an oxygen atom from a solvent molecule. Figure 5.7.1 represents a schematic breakdown of the lanthanide-phen-thiocyanate complexes and their crystal systems.

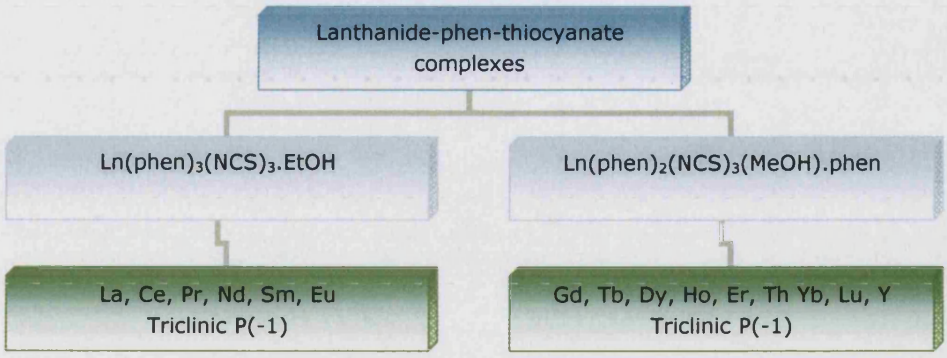

Figure 5.7.1 A schematic breakdown of the Lanthanide-phen-thiocyanate crystals

The structural change from nine-coordinate to eight-coordinate occurs between europium and gadolinium, and is likely to be related to the decrease in size of the Ln^{3+} ion as the series is crossed. The later lanthanides appear unable to sustain the coordination of three phen ligands and one phen is lost from the coordination sphere, although it is retained in the crystal and participates in hydrogen bonding and π-stacking. In the later members of the series, a single solvent molecule replaces the two coordination sites occupied in the early part of the series by the phen ring. Overall, the structures are determined by ligand-ligand interactions.

5.7.1.1 Structural features of $Ce(phen)_3(NCS)_3$. EtOH (11) [Representative of La, Ce, Pr, Nd, Sm, Eu]

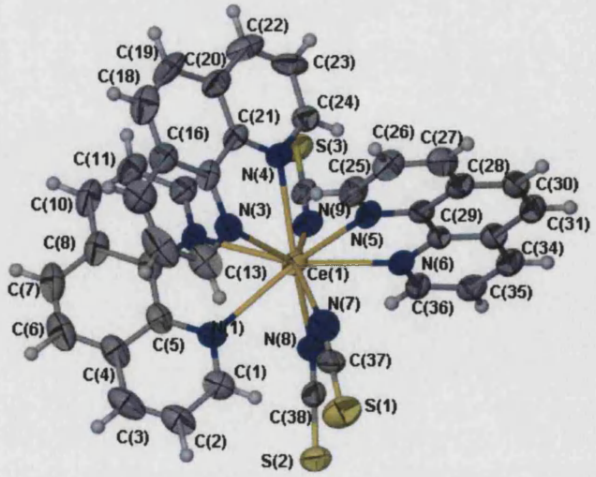

Figure 5.7.2 Structure of $Ce(phen)_3(NCS)_3$.EtOH (**11**) showing atom-numbering scheme employed. Ellipsoids are drawn at 50% probability level. The solvent molecule has been removed for clarity.

The complex molecule $Ce(phen)_3(NCS)_3.EtOH$ (**11**) is coordinated to nine nitrogen atoms, six from the three phen ligands and one from each thiocyanate molecule. The methanol solvent in the lattice is disordered over two positions. Individual atomic sites were refined with 60%:40% occupancies and the atomic coordinates and displacement parameters tied together and summed to unity.

The Ce-N distances vary from 2.534(7)Å [Ce(1)-N(9)]to 2.724Å [Ce(1)-N(2)] with shorter Ce-N distances for the thiocyanates at 2.534Å(7)Å, 2.536(7)Å and 2.549(8)Å respectively. The coordinated nitrogens from the phen ligands have longer bond lengths averaging 2.713Å.

All three thiocyante groups are slightly bent at angles of Ce(1)-C(37)-N(7) 166.9(7)°, Ce(1)-C(38)-N(8) at 155.6(6)° and Ce(1)-C(39)-N(9) at 156.6(6)°.

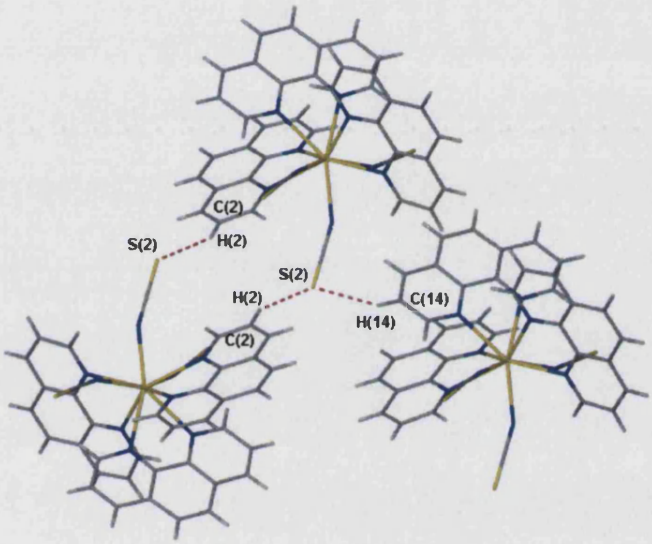

Figure 5.7.3 Hydrogen bond interactions between S(2) and the aromatic hydrogens.

While there are no intra-molecular interactions, there are some weak hydrogen interactions between the molecules. There are hydrogen interactions between the aromatic hydrogens of C(2)-H(2)···S(2) at a distance of 2.822Å and an angle of 150.66° (related by the symmetry operator -x, 1-y, -z) and C(14)-H(14)···S(2) at a distance of 2.844Å and an angle of 152.68° (related by the symmetry operator 1+x, y, z) (both shown in Figure 5.7.3). Another weak hydrogen interaction is between H(11) and S(1) where the C(11)-H(11)···S(1) distance is 2.718Å at an angle of 144.59° (related by the symmetry operator x, y-1, z , as shown in Figure 5.7.4)

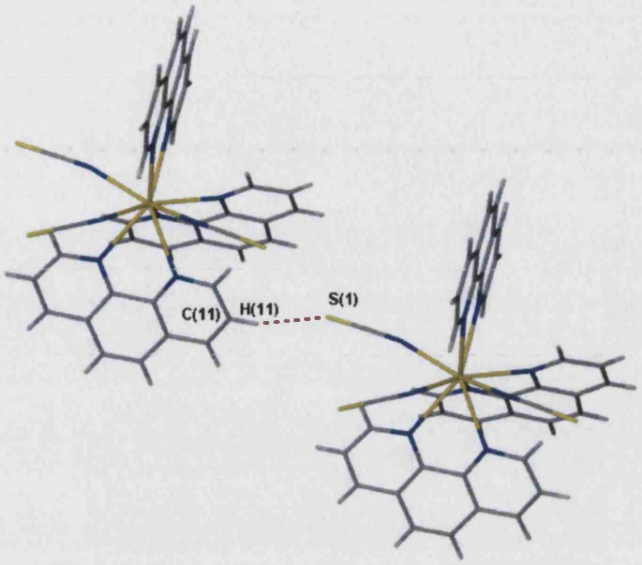

Figure 5.7.4 Hydrogen bond interactions between S(1) and H(11).

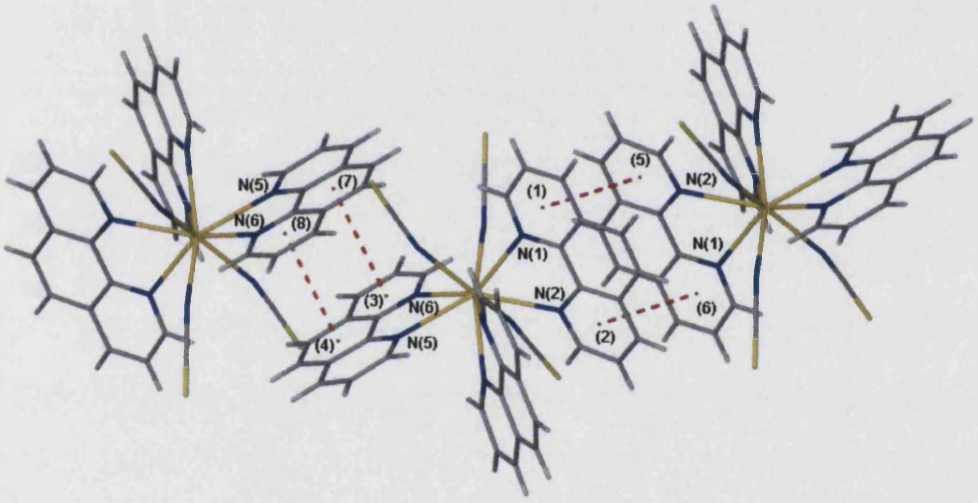

Figure 5.7.5π-π interactions between the rings. Solvent molecules have been removed for clarity.

Graphitic π-π stacking was observed between the phen ligands which would contribute significantly to the packing arrangements in the lattice. The rings are directly parallel with centroid distances between (7) and (3), and (8) and (4) being equivalent at 3.694Å. The two molecules are related by the symmetry operation -x, 1-y, 1-z. While centroids (1) and (5), and (2) and (6) are also equivalent with distances of 3.708Å. The molecules are related by the symmetry element x,y,z.

5.7.1.2 Structural features of $Dy(phen)_2(NCS)_3(phen)(MeOH)$ (12) [Representative of Gd, Tb, Dy, Ho, Er, Th Yb, Lu, Y]

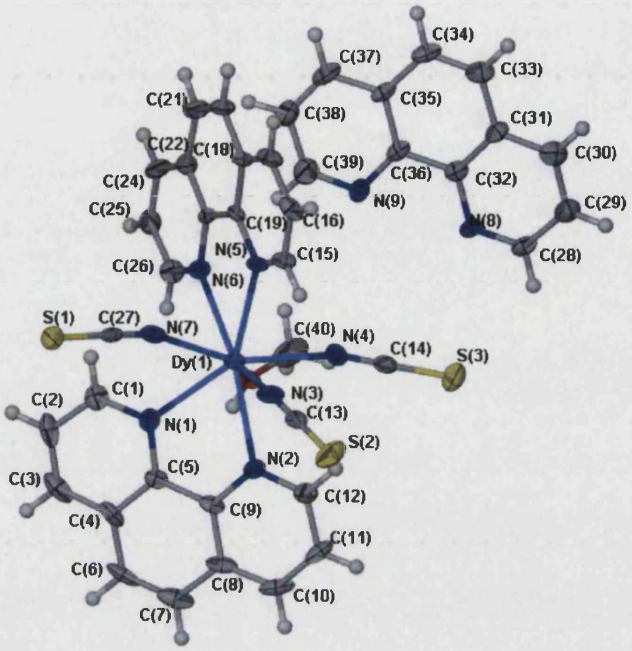

Figure 5.7.6 Structure of $Dy(phen)_2(NCS)_3(phen)(MeOH)$ (**12**) showing atom-numbering scheme employed. Ellipsoids are drawn at 50% probability level.

The dysprosium complex $Dy(phen)_2(NCS)_3(phen)(MeOH)$, (**12**) is coordinated to seven nitrogen atoms, four from the two phen ligands, one from each thiocyanate molecule and to one oxygen atom from a coordinated methanol solvent molecule.

The Dy-N distances vary from 2.361(5)Å [Dy(1)-N(3)]to 2.576(4)Å [Dy(1)-N(6)]. Akin to the earlier lanthanides, discussed in Section 5.7.1.1, the Dysprosium-thiocyanate bond lengths are shorter compared to that of the phen ligands at 2.361(5)Å, 2.375(4)Å and 2.402(5)Å respectively. The coordinated nitrogens from the phen ligands have longer bond lengths, averaging 2.544Å.

The three thiocyante groups are slightly bent at angles of Dy(1)-C(13)-N(3) 163.6(5)°, Dy(1)-C(14)-N(4) at 165.3(4)° and Dy(1)-C(27)-N(7) at 164.1(4)°.

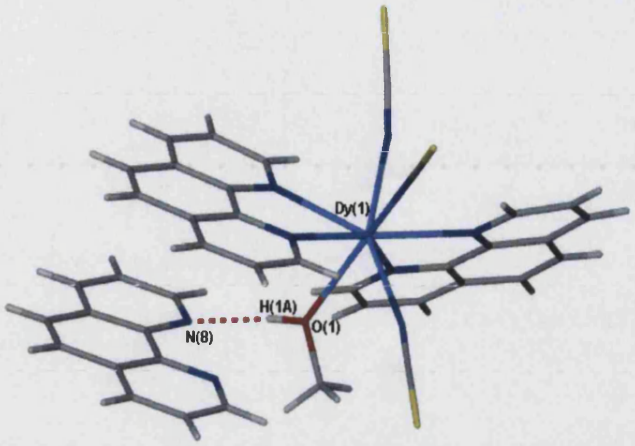

Figure 5.7.7 Hydrogen bonding between methanolic hydrogen and nitrogen.

Although there is not evidence of intra-molecular hydrogen bonding, an inter-molecular interaction is observed between a phen nitrogen, N(8) and methanolic hydrogen H(1A) at a distance of 1.938Å and an angle of 165.34°. The two molecules are related by the symmetry operator -x, -y, 1-z.

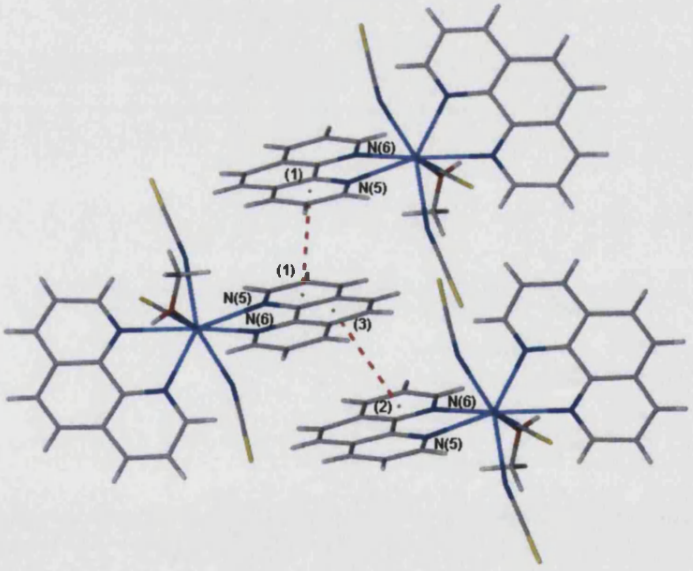

Figure 5.7.8 Graphitic π-π stacking between the coordinated phen ligands

Graphitic packing is observed between the coordinated phen ligands with N(5) and N(6) (as depicted Figure 5.7.8). The centroid-centroid distances between the rings as labelled (1)-(1) and (2)-(3) are 3.458Å (related by x, y ,z) and 3.872 Å(related by 1-x, 1-y, 1-z) respectively.

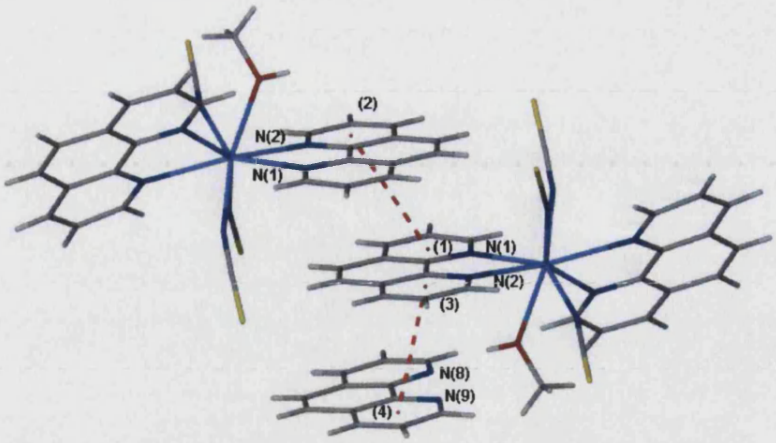

Figure 5.7.9 Graphitic π-π stacking between the coordinated phen ligands and the free phen

π-π interactions between the phen ligands with N(1) and N(2) and the free phen (as shown in Figure 5.7.9) are also observed. The centroid-centroid distances for (1)-(2) is 3.924Å, while that for (3)-(4) is 3.583Å. Both molecules are related by x, y, z symmetry.

5.7.1.3 A Comparison of Bond Lengths in Lanthanide-Phen-Thiocyanate Complexes

Bond lengths in complexes $Ln(phen)_x(NCS)_3(EtOH)_n$

		free phen						2.5NCS 0.5Cl		2 units in cell							
		k01prr41		h01prr22		Bath 53		k01prr30		k02prr8				h01prr11		k01prr8	
	Sc	Y		Y		La		La		La1		La2		Ce		Pr	
x		2		2		3		3		3		3		3		3	
Co-ordination number		8		8		9		9		9		9		9		9	
M-NCS (Å)		2.373	3	2.371	4	2.551	3	2.55	3	2.528	14	2.547	13	2.534	7	2.504	4
		2.384	4	2.376	4	2.568	3	2.574	5	2.555	14	2.551	14	2.536	7	2.507	4
		2.386	4	2.394	4	2.587	3	2.580	5	2.567	14	2.592	14	2.549	8	2.513	4
Average M-NCS (Å)		2.381		2.380				2.568		2.550		2.563		2.540		2.508	
M-N (phen) (Å)		2.521	3	2.539	3	2.747	3	2.736	4	2.698	13	2.730	15	2.702	6	2.679	3
		2.524	3	2.544	3	2.751	3	2.736	4	2.713	14	2.736	12	2.706	6	2.691	3
		2.539	3	2.517	3	2.758	3	2.741	4	2.723	12	2.744	12	2.712	6	2.698	3
		2.543	3	2.517	3	2.758	3	2.753	4	2.731	14	2.746	12	2.713	6	2.716	3
						2.755	3	2.760	4	2.745	14	2.755	14	2.723	6	2.718	3
						2.741	3	2.775	4	2.763	14	2.770	14	2.724	6	2.723	3
Average M-N (phen) (Å)		2.532		2.529		2.752		2.750		2.729		2.747		2.713		2.704	
M-EtOH (Å)		H_2O 2.394	3	2.391	3			no solvent		no solvent				no solvent		no solvent	
						0.5 MeOH		0.5 EtOH in latt		1 EtOH in latt.						1EtOH in latt	
Ionic radius in CN9								1.216		1.216		1.216		1.196		1.179	
										data not good							
Cell Dimensions		Triclinic		Triclinic		Triclinic		Triclinic		Triclinic				Triclinic		Triclinic	
		P(-1)		P(-1)		P(-1)		P(-1)		P(-1)				P(-1)		P(-1)	
a		10.4934	3	10.4704	2	10.9153	4	10.8352	4	10.9110	3			10.9028	4	10.9021	6
b		12.4999	4	12.5023	2	12.5126	9	12.3577	5	18.2759	7			12.2506	5	12.2410	8
c		15.0514	4	15.0597	4	14.8200	8	15.4396	7	20.8950	9			15.5545	7	15.5055	11
α		95.940	1	96.0400	#	95.891	2	97.064	2	101.594	3			97.432	2	97.388	3
β		104.045	2	104.2080	#	102.751	2	102.134	2	91.985	3			102.631	2	102.351	3
γ		104.312	1	104.1120	#	103.919	3	101.705	2	105.974	1			100.977	2	101.312	2
V		1827.5	9	1824.61	7	1890.11	#	1949.27	14	3906.1	2			1958.22	14	1950.4	2
mosaicity		0.690	2	0.491	2			1.434	3	1.043	2			1.178	3	0.977	4
		150K		150K		150K		150K		150K				150K		150K	
GOOF		1.047		1.312		1.058		1.073		0.962				1.039		0.918	
R obs		0.054		0.0511		0.0374		0.515		0.111				0.0423		0.0814	

	pr9960		h01prr21		h01prr62		k01prr2		pr0018		k01prr57		h01prr10		h01prr53	
	Nd		Sm		Sm		Eu		Gd		Tb		Dy		Ho	
x	3		3		3		3		2		2		2		2	
Co-ordination number	9		9		9		9		8		8		8		8	
M-NCS (Å)	2.488	4	2.469	5	2.460	2	2.442	4	2.395	4	2.404	4	2.361	5	2.368	3
	2.493	4	2.476	5	2.463	2	2.449	4	2.407	4	2.392	3	2.389	4	2.375	3
	2.498	4	2.503	5	2.466	2	2.421	4	2.421	4	2.416	4	2.402	5	2.383	3
Average M-NCS (Å)	2.493		2.483		2.463		2.437		2.408		2.404		2.384		2.375	
M-N (phen) (Å)	2.655	3	2.625	5	2.680	2	2.615	3	2.565	3	2.542	3	2.507	4	2.516	3
	2.661	4	2.634	5	2.681	2	2.621	3	2.568	3	2.545	3	2.547	4	2.519	3
	2.679	3	2.657	5	2.627	2	2.644	3	2.583	3	2.564	3	2.552	4	2.536	3
	2.694	3	2.679	5	2.632	2	2.67	3	2.595	3	2.559	3	2.576	4	2.537	3
	2.701	3	2.687	5	2.705	2	2.672	3								
	2.705	3	2.700	5	2.657	2	2.699	3								
Average M-N (phen) (Å)	2.683		2.664		2.664		2.654		2.578		2.553		2.546		2.527	
M-EtOH (Å)	no solvent		no solvent		no solvent		no solvent		(MeOH) 2.421	3	(MeOH) 2.424	2	(MeOH) 2.391	4	(MeOH) 2.382	3
	1EtOH in latt				1EtOH in latt		1 MeOH in latt									
Ionic radius in CN9	1.163		1.132		1.132		1.120		1.107		1.095		1.083		1.072	
Cell Dimensions	Triclinic		Triclinic		Triclinic		Triclinic		Triclinic		Triclinic		Triclinic		Triclinic	
	P(-1)		P(-1)		P(-1)		P(-1)		P(-1)		P(-1)		P(-1)		P(-1)	
a	10.9237	6	10.9008	2	10.9407	2	10.9438	2	10.3873	15	10.4657	2	10.4874	2	10.4752	2
b	12.1738	6	12.1271	3	12.1095	2	12.0944	3	12.4723	15	12.4734	2	12.5040	3	12.4918	3
c	15.5675	8	15.5914	4	15.6573	3	15.6508	4	15.7312	18	15.1688	4	15.0373	4	15.0572	4
α	97.7220	10	97.8500	10	98.0330	10	98.0360	10	96.514	9	95.8940	10	95.9510	10	95.9700	10
β	101.8720	10	101.7250	10	101.5610	10	101.6080	10	106.41	9	104.0340	10	103.9680	10	104.1110	10
γ	101.3930	10	101.1310	10	101.1310	10	101.0420	10	102.125	7	104.0830	10	103.2670	10	104.2370	10
V	1952.68	18	1946.70	8	1959.41	6	1957.02	8	1878.7	4	1835.62	7	1835.92	7	1823.76	7
mosaicity			0.707	2	0.8140	10	0.387	2			0.921	2	0.445		1.320	2
	180K		150K		150K		150K		150K		150K		150K		150K	
GOOF	1.102		1.103		0.878		1.017		0.98		1.118		0.984		1.02	
R obs	0.0625		0.0511		0.0317		0.0381		0.0629		0.0348		0.0488		0.0354	

	pr0029		pr0030		h02prr2		h02prr3		h01prr56		pr0022		pr0020		k01pr	
	Er		Er		Er		Er		Tm		Yb		Yb		Lu	
x	2		2		2		2		2		2		2			
Co-ordination number	8		8		8		8		8		8		8			
M-NCS (Å)	2.340	5	2.333	4	2.337	6	2.348	4	2.343	5	2.325	4	2.327	3	2	
	2.362	4	2.362	4	2.356	7	2.372	4	2.355	4	2.342	5	2.334	3	2	
	2.364	4	2.369	4	2.365	7	2.380	4	2.359	5	2.343	5	2.339	3	2	
Average M-NCS (Å)	2.355		2.355		2.353		2.367		2.352		2.337		2.333		2	
M-N (phen) (Å)	2.499	4	2.508	3	2.498	6	2.502	3	2.490	3	2.483	4	2.497	3	2	
	2.507	4	2.513	3	2.499	6	2.517	4	2.496	3	2.489	4	2.498	3	2	
	2.530	4	2.532	3	2.524	6	2.527	3	2.518	3	2.507	4	2.517	3	2	
	2.531	4	2.537	4	2.531	6	2.530	3	2.516	2	2.510	4	2.521	3	2	
Average M-N (phen) (Å)	2.517		2.523		2.513		2.519		2.505		2.497		2.508		2	
	0 5water 0.5MeOH										from ortep					
M-EtOH (Å)	from Ortep 2.399		from Ortep 2.378		(MeOH) 2.391		(MeOH) 2.405	11	(MeOH) 2.377	2	(MeOH) 2.377		(MeOH) 2.356	3	(MeOH) 2	
Ionic radius in CN9	1.062		1.062		1.062		1.062		1.052		1.042		1.042		1	
Cell Dimensions	Triclinic		Triclinic		Triclinic		Triclinic		Triclinic		Triclinic		Triclinic		Triclin	
	P(-1)		P(-1)		P(-1)		P(-1)		P(-1)		P(-1)		P(-1)		P(-1)	
a	10.4960	15	10.3654	12	10.4836	4	10.4850	3	10.4645	2	10.5010	18	10.3438	9	10.4	
b	12.497	2	12.4613	18	12.4721	5	12.4720	4	12.4745	3	12.487	2	12.4417	15	12.4	
c	15.130	3	15.744	2	15.0583	8	15.0620	5	15.0749	4	15.1183	15	15.7646	15	15.	
α	96.066	8	96.789	6	95.9590	10	95.946	2	96.049	1	96.072	9	96.858	6	95	
β	104.232	10	106.764	7	104.1940	10	104.215	2	104.421	1	104.383	9	106.999	6	104	
γ	104.310	9	102.177	7	104.271	2	104.283	1	104.097	1	104.376	6	102.071	6	104	
V	1834.5	5	1868.3	4	1821.41	14	1821.84	10	1819.36	7	1830.3	5	1861.6	3	18	
mosaicity					0.491	3	1.017	3	1.139	2					1	
	180K		180K		150K		150K		150K		180K		180K		150K	
GOOF	0.968		0.992		1.071		1.071		0.926		0.966		1.021		1	
R obs	0.0656		0.0593		0.0388		0.0388		0.0306		0.0404		0.0405		0.0	

Table 5.7.1 Table of Comparisons between Lanthanide-Phen-Thiocyanate Complexes

Bond Lengths in Lanthanide-Phen-Thiocyanate Complexes

(EtOH)$_n$

phen						2.5NCS 0.5Cl		2 units in cell							
prr41		h01prr22		Bath 53		k01prr30		k02prr8				h01prr11		k01prr8	
		Y		La		La		La1		La2		Ce		Pr	
2		2		3		3		3		3		3		3	
8		8		9		9		9		9		9		9	
2.373	3	2.371	4	2.551	3	2.55	3	2.528	14	2.547	13	2.534	7	2.504	4
2.384	4	2.376	4	2.568	3	2.574	5	2.555	14	2.551	14	2.536	7	2.507	4
2.386	4	2.394	4	2.587	3	2.580	5	2.567	14	2.592	14	2.549	8	2.513	4
2.381		2.380				2.568		2.550		2.563		2.540		2.508	
2.521	3	2.539	3	2.747	3	2.736	4	2.698	13	2.730	15	2.702	6	2.679	3
2.524	3	2.544	3	2.751	3	2.736	4	2.713	14	2.736	12	2.706	6	2.691	3
2.539	3	2.517	3	2.758	3	2.741	4	2.723	12	2.744	12	2.712	6	2.698	3
2.543	3	2.517	3	2.758	3	2.753	4	2.731	14	2.746	12	2.713	6	2.716	3
				2.755	3	2.760	4	2.745	14	2.755	14	2.723	6	2.718	3
				2.741	3	2.775	4	2.763	14	2.770	14	2.724	6	2.723	3
2.532		2.529		2.752		2.750		2.729		2.747		2.713		2.704	
2.394	3	2.391	3			no solvent		no solvent				no solvent		no solvent	
				0.5 MeOH		0.5 EtOH in latt		1 EtOH in latt						1EtOH in latt	
						1.216		1.216		1.216		1.196		1.179	
								data not good							
clinic		Triclinic		Triclinic		Triclinic		Triclinic				Triclinic		Triclinic	
1)		P(-1)		P(-1)		P(-1)		P(-1)				P(-1)		P(-1)	
0.4934	3	10.4704	2	10.9153	4	10.8352	4	10.9110	3			10.9028	4	10.9021	6
2.4999	4	12.5023	2	12.5126	9	12.3577	5	18.2759	7			12.2506	5	12.2410	8
5.0514	4	15.0597	4	14.8200	8	15.4396	7	20.8950	9			15.5545	7	15.5055	11
95.940	1	96.0400	#	95.891	2	97.064	2	101.594	3			97.432	2	97.388	3
04.045	2	104.2080	#	102.751	2	102.134	2	91.985	3			102.631	2	102.351	3
04.312	1	104.1120	#	103.919	3	101.705	2	105.974	1			100.977	2	101.312	2
1827.5	9	1824.61	7	1890.11	#	1949.27	14	3906.1	2			1958.22	14	1950.4	2
0.690	2	0.491	2			1.434	3	1.043	2			1.178	3	0.977	4
)K		150K		150K		150K		150K				150K		150K	
1.047		1.312		1.058		1.073		0.962				1.039		0.918	
0.054		0.0511		0.0374		0.515		0.111				0.0423		0.0814	

pr9960		h01prr21		h01prr62		k01prr2		pr0018		k01prr57		h01prr10		h01prr53	
Nd		Sm		Sm		Eu		Gd		Tb		Dy		Ho	
3		3		3		3		2		2		2		2	
9		9		9		9		8		8		8		8	
2.488	4	2.469	5	2.460	2	2.442	4	2.395	4	2.404	4	2.361	5	2.368	3
2.493	4	2.476	5	2.463	2	2.449	4	2.407	4	2.392	3	2.389	4	2.375	3
2.498	4	2.503	5	2.466	2	2.421	4	2.421	4	2.416	4	2.402	5	2.383	3
2.493		2.483		2.463		2.437		2.408		2.404		2.384		2.375	
2.655	3	2.625	5	2.680	2	2.615	3	2.565	3	2.542	3	2.507	4	2.516	3
2.661	4	2.634	5	2.681	2	2.621	3	2.568	3	2.545	3	2.547	4	2.519	3
2.679	3	2.657	5	2.627	2	2.644	3	2.583	3	2.564	3	2.552	4	2.536	3
2.694	3	2.679	5	2.632	2	2.67	3	2.595	3	2.559	3	2.576	4	2.537	3
2.701	3	2.687	5	2.705	2	2.672	3								
2.705	3	2.700	5	2.657	2	2.699	3								
2.683		2.664		2.664		2.654		2.578		2.553		2.546		2.527	
no solvent		no solvent		no solvent		no solvent		(MeOH) 2.421	3	(MeOH) 2.424	2	(MeOH) 2.391	4	(MeOH) 2.382	3
1EtOH in latt				1EtOH in latt		1 MeOH in latt									
1.163		1.132		1.132		1.120		1.107		1.095		1.083		1.072	
Triclinic		Triclinic		Triclinic		Triclinic		Triclinic		Triclinic		Triclinic		Triclinic	
P(-1)		P(-1)		P(-1)		P(-1)		P(-1)		P(-1)		P(-1)		P(-1)	
10.9237	6	10.9008	2	10.9407	2	10.9438	2	10.3873	15	10.4657	2	10.4874	2	10.4752	2
12.1738	6	12.1271	3	12.1095	2	12.0944	3	12.4723	15	12.4734	2	12.5040	3	12.4918	3
15.5675	8	15.5914	4	15.6573	3	15.6508	4	15.7312	18	15.1688	4	15.0373	4	15.0572	4
97.7220	10	97.8500	10	98.0330	10	98.0360	10	96.514	9	95.8940	10	95.9510	10	95.9700	10
101.8720	10	101.7250	10	101.5610	10	101.6080	10	106.41	9	104.0340	10	103.9680	10	104.1110	10
101.3930	10	101.1310	10	101.1310	10	101.0420	10	102.125	7	104.0830	10	103.2670	10	104.2370	10
1952.68	18	1946.70	8	1959.41	6	1957.02	8	1878.7	4	1835.62	7	1835.92	7	1823.76	7
		0.707	2	0.8140	10	0.387	2			0.921	2	0.445		1.320	2
180K		150K		150K		150K		150K		150K		150K		150K	
1.102		1.103		0.878		1.017		0.98		1.118		0.984		1.02	
0.0625		0.0511		0.0317		0.0381		0.0629		0.0348		0.0488		0.0354	

pr0029		pr0030		h02prr2		h02prr3		h01prr56		pr0022		pr0020		k01prr6		Bath 72	
Er		Er		Er		Er		Tm		Yb		Yb		Lu		Lu	
2		2		2		2		2		2		2		2		2	
8		8		8		8		8		8		8		8		8	
2.340	5	2.333	4	2.337	6	2.348	4	2.343	5	2.325	4	2.327	3	2.320	12	2.319	2
2.362	4	2.362	4	2.356	7	2.372	4	2.355	4	2.342	5	2.334	3	2.345	13	2.334	3
2.364	4	2.369	4	2.365	7	2.380	4	2.359	5	2.343	5	2.339	3	2.378	12	2.339	3
2.355		2.355		2.353		2.367		2.352		2.337		2.333		2.348		2.331	
2.499	4	2.508	3	2.498	6	2.502	3	2.490	3	2.483	4	2.497	3	2.485	11	2.475	2
2.507	4	2.513	3	2.499	6	2.517	4	2.496	3	2.489	4	2.498	3	2.489	11	2.480	2
2.530	4	2.532	3	2.524	6	2.527	3	2.518	3	2.507	4	2.517	3	2.491	10	2.491	2
2.531	4	2.537	4	2.531	6	2.530	3	2.516	2	2.510	4	2.521	3	2.492	10	2.496	2
2.517		2.523		2.513		2.519		2.505		2.497		2.508		2.489		2.486	
0.5water 0.5MeOH										from ortep							
from Ortep 2.399		from Ortep 2.378		(MeOH) 2.391		(MeOH) 2.405	11	(MeOH) 2.377	2	(MeOH) 2.377		(MeOH) 2.356	3	(MeOH) 2.344	10	(MeOH) 2.37	2
1.062		1.062		1.062		1.062		1.052		1.042		1.042		1.032		1.032	
Triclinic		Triclinic		Triclinic		Triclinic		Triclinic		Triclinic		Triclinic		Triclinic		Triclinic	
P(-1)		P(-1)		P(-1)		P(-1)		P(-1)		P(-1)		P(-1)		P(-1)		P(-1)	
10.4960	15	10.3654	12	10.4836	4	10.4850	3	10.4645	2	10.5010	18	10.3438	9	10.4544	7	10.4661	9
12.497	2	12.4613	18	12.4721	5	12.4720	4	12.4745	3	12.487	2	12.4417	15	12.4631	11	12.4378	11
15.130	3	15.744	2	15.0583	8	15.0620	5	15.0749	4	15.1183	15	15.7646	15	15.0536	13	15.0603	13
96.066	8	96.789	6	95.9590	10	95.946	2	96.049	1	96.072	9	96.858	6	95.890	4	95.998	2
104.232	10	106.764	7	104.1940	10	104.215	2	104.421	1	104.383	9	106.999	6	104.625	3	104.432	2
104.310	9	102.177	7	104.271	2	104.283	1	104.097	1	104.376	6	102.071	6	104.221	3	104.311	2
1834.5	5	1868.3	4	1821.41	14	1821.84	10	1819.36	7	1830.3	5	1861.6	3	1811.1	3	1810.6	3
				0.491	3	1.017	3	1.139	2					1.732	4		
180K		180K		150K		150K		150K		180K		180K		150K			
0.968		0.992		1.071		1.071		0.926		0.966		1.021		1.003		1.020	
0.0656		0.0593		0.0388		0.0388		0.0306		0.0404		0.0405		0.0893		0.0240	

Table 5.7.1 Table of Comparisons between Lanthanide-Phen-Thiocyanate Complexes

5.7.1.4 Luminescence studies Lanthanide-Phen-Thiocyanate Complexes

The lanthanide complexes (samarium, terbium and dysprosium) were found to luminesce under ultra-violet (UV) irradiation, almost comparable to the terpy-thiocyanate series. (The europium complex which also luminesces was not available for emission measurements)

Akin to the other two lanthanides series, absorption studies were also not able to be carried out on the complexes, due to their highly insoluble nature. However, based on literature of other emission studies on lanthanide-phen complexes, emission measurements (phosphorescence and fluorescence) carried out at the excitation wavelength 355nm.

The measurements were carried out in the solid state and the excitation wavelength was based on the ligand excitation. It was found that the emission spectra for all the complexes excited at both wavelengths were identical and reported below are the spectra excited at only one of the two wavelengths.

5.7.1.4.1 Emission Spectra of $Sm(phen)_3(NCS)_3$

The emission spectra, both phosphorescence and fluorescence of $Sm(phen)_3(NCS)_3$ is similar to that of the other samarium complexes with the same transitions observed.

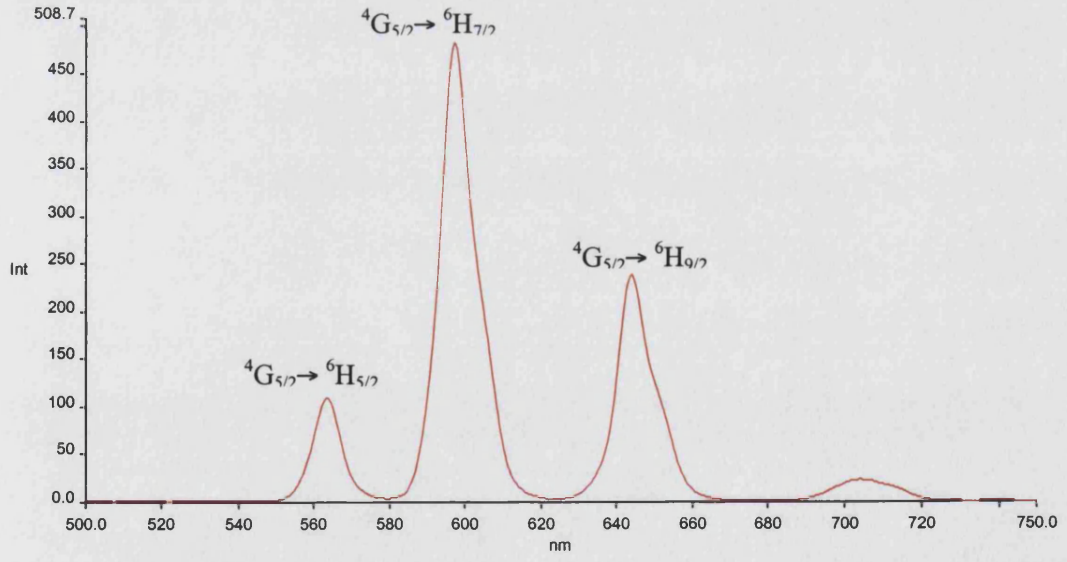

Figure 5.7.10 Phosphorescence spectra for $Sm(phen)(NO_3)_3$ (λ_{ex} = 355nm)

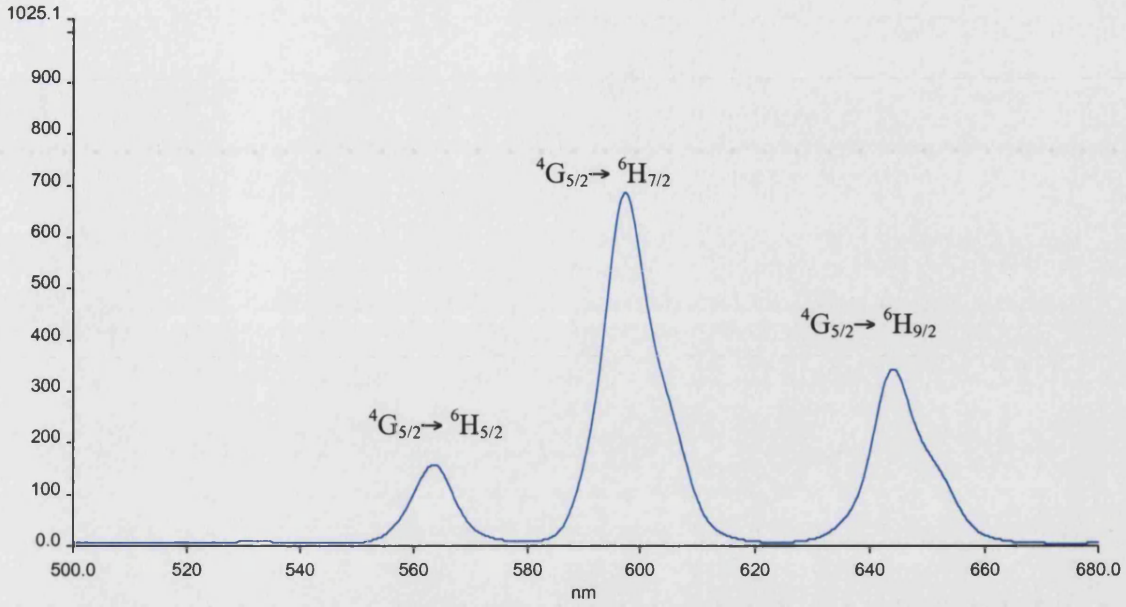

Figure 5.7.11 Flourescence spectra for $Sm(phen)(NO_3)_3$ (λ_{ex} = 355nm)

5.7.1.4.2 Emission Spectra of $Tb(phen)_3(NCS)_3$

Again as with the previous two lanthanide series, this $Tb(phen)_3(NCS)_3$ complex has the typical five-fingered Tb^{3+} luminescence spectra, also characterised by the intensely green emissions. Both fluorescence and phosphorescence spectra are equivalent.

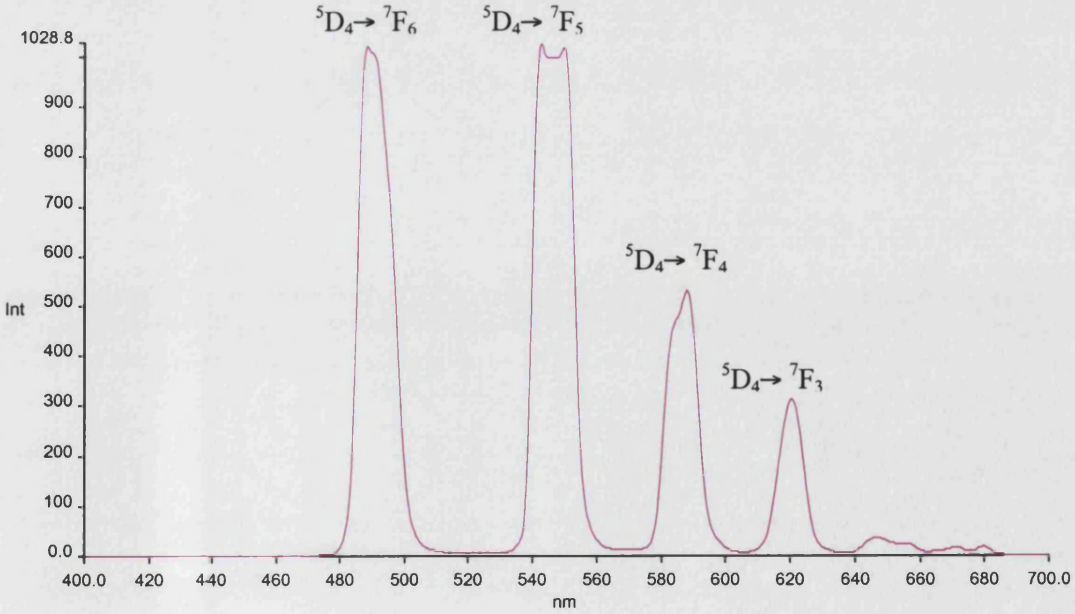

Figure 5.7.12 Phosphorescence spectra for $Tb(phen)(NO_3)_3$ (λ_{ex} = 355nm)

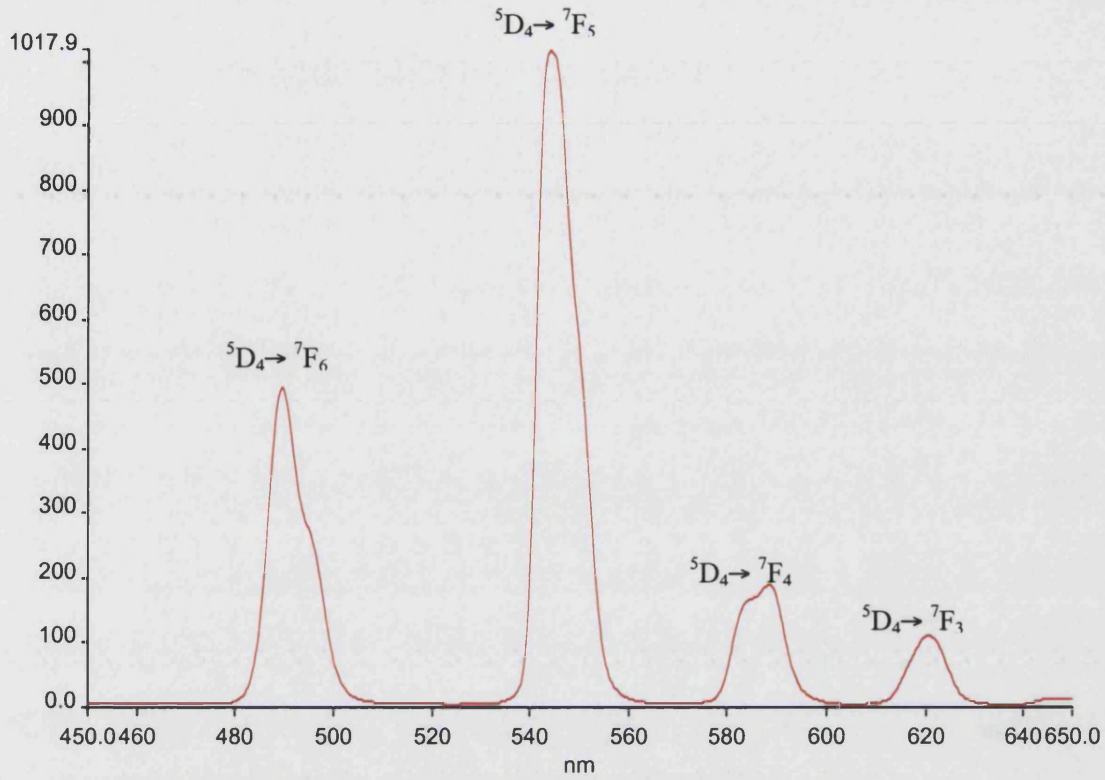

Figure 5.7.13 Flourescence spectra for $Tb(phen)(NO_3)_3$ (λ_{ex} = 355nm)

5.7.1.4.3 Emission Spectra of $Dy(phen)_3(NCS)_3$

The phosphorescence spectra of $Dy(phen)_3(NCS)_3$ was extremely weak with only minor peaks not corresponding to the metal-centred luminescence, which might be attributed to impurities. However, the flourescence emission is similar to that observed for the $Dy(terpy)_2(NCS)_3$ complex.

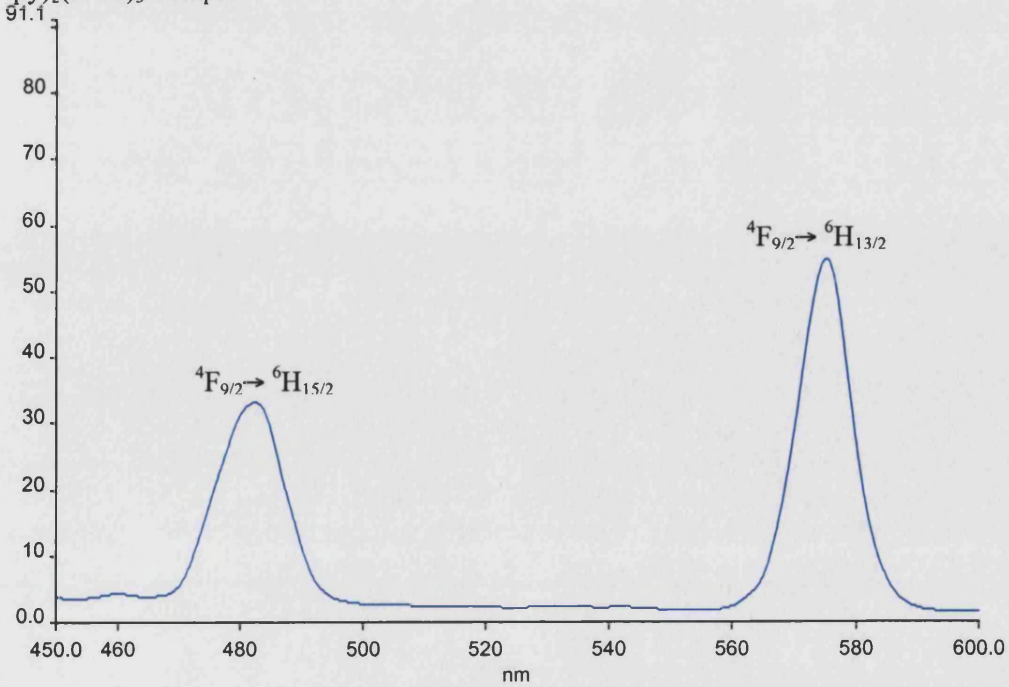

Figure 5.7.14 Flourescence spectra for $Dy(phen)(NO_3)_3$ (λ_{ex} = 355nm)

5.7.1.5 Discussions and Conclusions on Lanthanide-Phen-Thiocyanate Complexes

The lanthanide-phen-thiocyanate complexes can also divided into two $Ln(phen)_3(NCS)_3.EtOH$ for the first six elements of the series including lanthanum and $Ln(phen)_2(NCS)_3(MeOH).phen$ for the latter half of the series including yttrium.

In the early lanthanides, the coordination spheres were large enough to accommodate three phen ligands with three thiocyanates, however in the later lanthanides due to the contracting sphere the number of coordinated phen ligands is reduced to two with the uncoordinated phen held within the lattice by π-π interactions. In the later elements of the series there is also a coordinated solvent molecule.

The luminescence properties of this series are similar, with a few exceptions, to the terpy-thiocyanates. As with the terpy-thiocyanates, the overall emission spectra of the lanthanide-phen-thiocyanates also show a strong metal-based luminescence indicating an efficient energy transfer from the ligand to the metal.

5.7.1.6 Lanthanide- 1, 10-Phenanthroline Complexes with Thiocyanate and Nitrate Counterions

All the complexes with the general formula $Ln(phen)_2(NCS)_2(NO_3)(MeOH)$ crystallise in the *Triclinic* space group *P-1*. Unlike the previous series of $Ln(phen)_3(NCS)_3.EtOH$ (Section 5.7.1) in which the coordination number changes from nine to eight between europium and gadolinium, the complexes of terbium and holmium in this series are isostructural to the larger lanthanide metals.

The asymmetric units of this series consists of two phen molecules bound to the lanthanide ion with two thiocyanate groups and a single nitrate group attached. There is also a coordinated alcohol solvent molecule. Although there is no significant structural change across the series the Ln-N and Ln-O bonds become progressively shorter, consistent with the decrease in the radius of the lanthanide ion.

Attempts to synthesise the complexes of Eu, Gd, Tm, Yb and Lu in the two thiocyanate to one nitrate ratios were all unsuccessful, all yielding the crystals of the three thiocyanates (refer to Section 5.7.1).

Interestingly, while it was possible to synthesise the erbium complex in a one thiocyanate to two nitrate ratio to yield $Er(phen)_2(NCS)(NO_3)_2$, multiple attempts to synthesise the equivalent $Er(phen)_2(NCS)_2(NO_3)$ failed. As it was not possible to synthesise the rest of the later lanthanides in either ratios, it is hard to predict what form the crystals would take. Although one might expect it to form isostructurally to the erbium complex, it is important to note that while the ionic radius of yttrium is closer to that of the later lanthanides, its complex was found to be isostructural to that of the early elements of the series $[Ln(phen)_2(NCS)_2(NO_3)(MeOH)]$. Figure 5.1.1 briefly outlines the breakdown of the structures of this series.

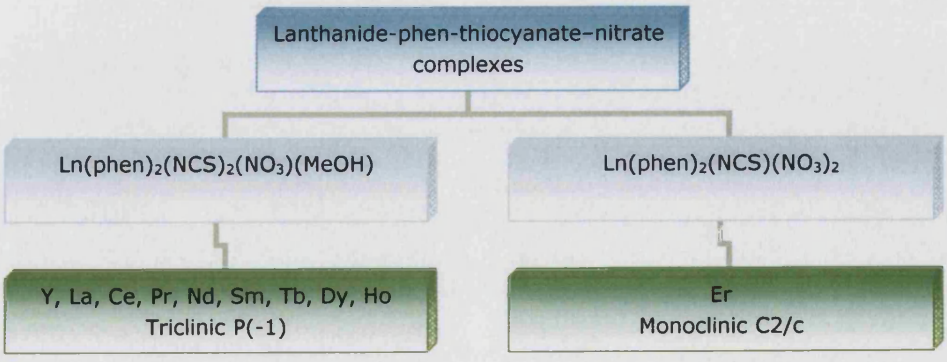

Figure 5.7.15 A schematic breakdown of the Lanthanide-phen-thiocyanate-nitrate crystals

Also included in this section are discussions on $Pr(phen)_2(NO_3)_3$ (Section 5.7.1.9) and $Er(phen)_2(NO_3)_3$ (Section 0). A table of comparisons between $Er(phen)_2(NCS)_3$ $Er(phen)_2(NCS)(NO_3)_2$ and $Er(phen)_2(NO_3)_3$ and between $Pr(phen)_2(NCS)_3$ $Pr(phen)_2(NCS)_2(NO_3)$ and $Pr(phen)_2(NO_3)_3$ is included in Section 5.7.1.12.

5.7.1.7 Structural features of $Tb(phen)_2(NCS)_2(NO_3)(MeOH)$ (13) (representative of Y, La, Ce, Pr, Nd, Sm, Tb, Dy, Ho)

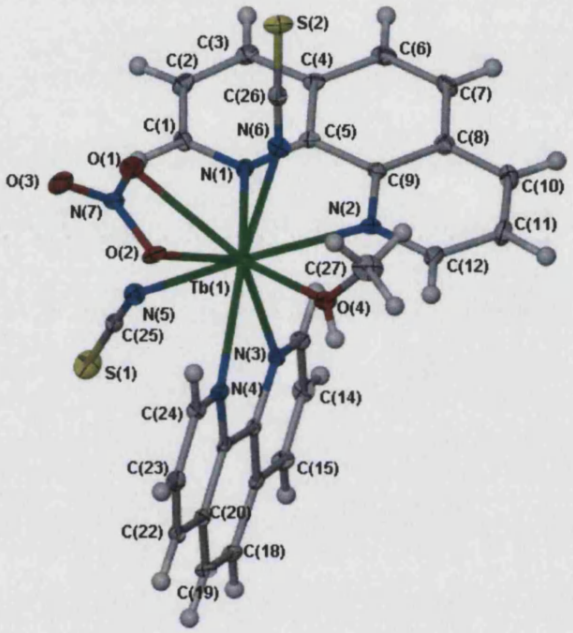

Figure 5.7.16 Structure of $Tb(phen)_2(NCS)_2(NO_3)(MeOH)$ (**13**) showing atom-numbering scheme employed. Ellipsoids are drawn at 50% probability level.

The complex molecule $Tb(phen)_2(NCS)_2(NO_3)(MeOH)$ is coordinated to six nitrogen atoms, from the two phen ligands and two thiocyantes. It is also coordinated to three oxygen atoms, two from the nitrate and one from a coordinated methanol.

The terbium-nitrogen distances for the phen ligands vary from 2.540(2)Å [Tb(1)-N(1)]to 2.584(3)Å [Tb(1)-N(2)] averaging 2.563Å. The terbium-thiocyanate bonds are shorter compared with those of the phen ligands with the distances for the two thiocyanate groups at 2.404(3)Å [Tb(1-N(5)] and 2.456(3)Å [Tb(1)-C(6)]respectively. The thiocyanate ligands are bent at angles of 143.7(3)° [Tb(1)-N(5)-C(25)] and 161.4(3)° [Tb(1)-N(6)-C(26)].

Meanwhile, the terbium-oxygen bond lengths vary from 2.426(2)Å [Tb(1)-O(2)] to 2.661(2)Å [Tb(1)-O(1)] for both nitrate oxygen atoms while the coordinated methanol solvent is 2.429(2)Å.

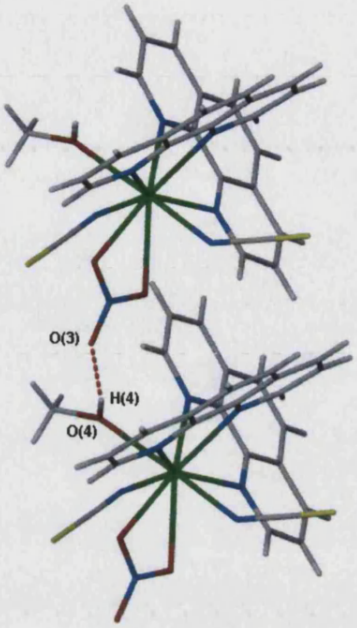

Figure 5.7.17 Hydrogen bond between H(4) and O(3)

While there are no intra-molecular interactions, inter-molecular hydrogen interaction occurs between one of the nitrate ligands and the coordinated solvent molecule. The methanolic hydrogen H(4) interacts with a the nitrate oxygen O(3) at a distance of 2.086Å and an angle of 168.44°. Both molecules are related by the symmetry operation x-1, y, z.

5.7.1.8 Structural Features of $Er(phen)_2(NCS)(NO_3)_2$ (14)

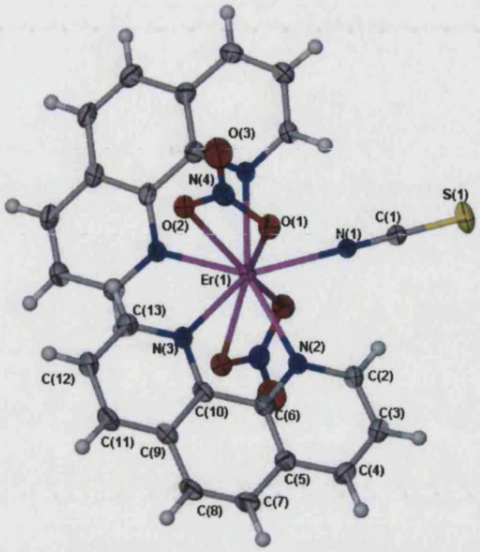

Figure 5.7.18 Structure of $Er(phen)_2(NCS)(NO_3)_2$ (**14**) showing atom-numbering scheme employed. Ellipsoids are drawn at 50% probability level.

The complex molecule $Er(phen)_2(NCS)(NO_3)_2$ (**14**) crystallises in the *Monoclinic* space group *C2/c*. The molecule sits on a crystallographic 2-fold axis that passes through Er(1), N(1), C(1) and S(1).

The erbium metal centre is coordinated to five nitrogen and four oxygen atoms. The five nitrogens are from the two phen ligands and one thiocyanate, while the oxygens are contributions from the nitrate ligands.

The lone thiocyanate is bonded at a distance of 2.354(6)Å from the erbium centre while the erbium-phen distances average 2.512Å. The erbium-oxygen bonds range from 2.398(4)Å to 2.462(4)Å averaging 2.423Å while the erbium-nitrogen bonds average 2.508Å.

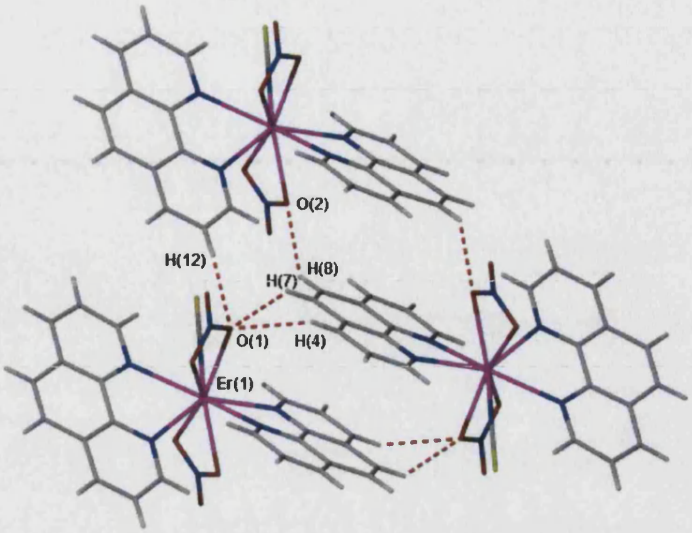

Figure 5.7.19 Hydrogen bonding interactions to the nitrate oxygens

A number of hydrogen bonding interactions hold the molecules in place (see Figure 5.7.19). The aromatic hydrogen H(8) acts as a donor to O(2) at a distance of 2.470Å with the C(8)-H(8)···O(2) angle at 139.23° (related by x, 1-y, z- ½). Meanwhile, three different aromatic hydrogens interact with O(1). H(4) and H(7) form interactions at distance of 2.643Å and 2.550Ä and angles of 130.77° and 134.54° respectively. The molecules involved in this interaction are related by ½ -x, ½ -y, -z. O(1) also acts as a hydrogen bond acceptor to the aromatic hydrogen H(12) at a distance of 2.478Å and an angle of 174.45°.

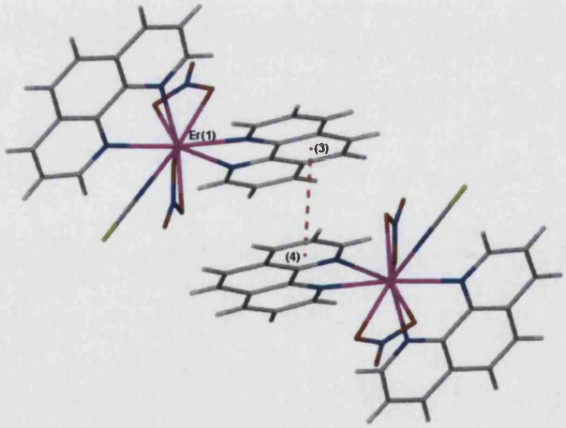

Figure 5.7.20 π-π interactions between the phen rings

A typical graphitic π-π stacking is observed between the phen rings of two molecules related by 3/2 –x, ½ -y, 1-z. The centroid-centroid distance between (3) and (4) is 3.559Å. (as shown in Figure 5.7.20).

5.7.1.9 Structural features of $Er(phen)_2(NO_3)_3$ (15)

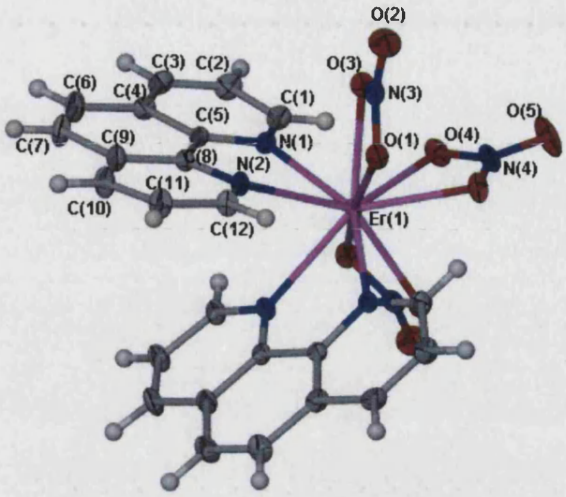

Figure 5.7.21 Structure of $Er(phen)_2(NO_3)_3$ (**15**) showing atom-numbering scheme employed. Ellipsoids are drawn at 50% probability level.

The complex molecule $Er(phen)_2(NO_3)_3$ (**15**) also crystallises in the *Monoclinic* space group *C2/c*. As with the the related $Er(phen)_2(NCS)(NO_3)_2$, the molecule sits on a crystallographic 2-fold axis that passes through Er(1), N(4) and O(5).

The erbium metal centre is ten-coordinate, to six oxygen atoms from the three nitrates and to four nitrogen atoms of the two phen ligands. The erbium-nitrogen bonds are an average of 2.500Å while the erbium-oxygen bonds range from 2.434(3)Å to 2.509(3)Å with an average length of 2.463Å.

Hydrogen bonding and staggered π-π interactions hold the molecules in place in the crystal lattice. An aromatic hydrogen H(2) acts as a hydrogen bond donor to an oxygen of one of the nitrates (see Figure 5.7.22). The H(2)···O(5) distance is 2.468Å while the C(2)-H(2)···O(4) angle is 152.04°.

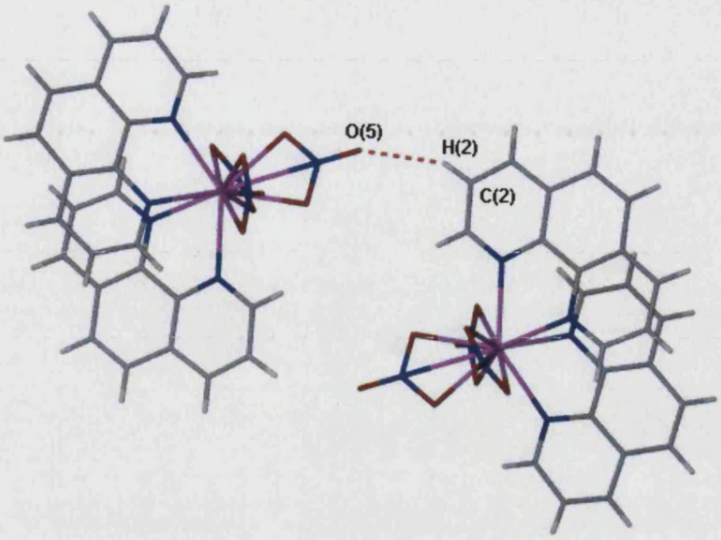

Figure 5.7.22 Hydrogen bonding between H(2) and O(5)

The graphitic π-π stacking is observed between the phen rings (see Figure 5.7.23). The distance between (1) and (2) is 3.746Å, related by the symmetry element, ½ -x , ½ -y, -z.

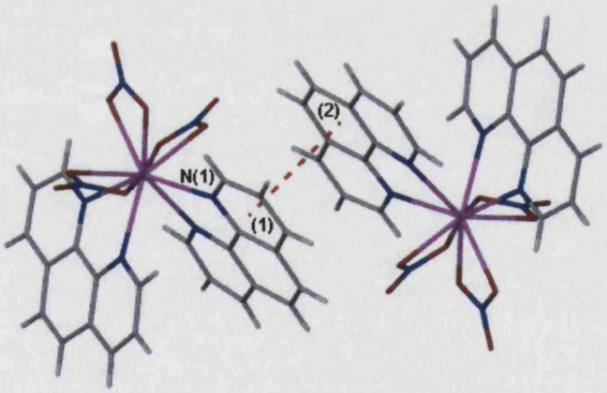

Figure 5.7.23 π-π interactions between the phen ligands

5.7.1.10 Structural features of $Pr(phen)_2(NO_3)_3$ (16)

As with the erbium analogue, $Pr(phen)_2(NO_3)_3$ (**16**) is also ten-coordinate with two phen ligands and three nitrate groups (see Figure 5.7.24). It crystallises in the *Monoclinic* space group $P2_1/c$ with one whole molecule in the asymmetric unit. The loss of symmetry compared with the erbium molecule might be attributed to the slightly larger metal centre to which the ligands might not pack as efficiently compared to the smaller erbium metal core.

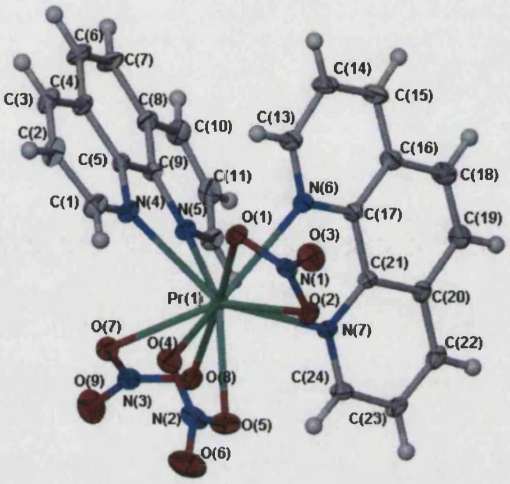

Figure 5.7.24 Structure of $Pr(phen)_2(NO_3)_3$ (**16**) showing atom-numbering scheme employed. Ellipsoids are drawn at 50% probability level.

The praseodymium-nitrogen bond lengths range from 2.605(3)Å to 2.661(3)Å averaging 2.631Å, while the praseodymium-oxygen lengths range from 2.545(3)Å to 2.585(3)Å with an average of 2.561Å.

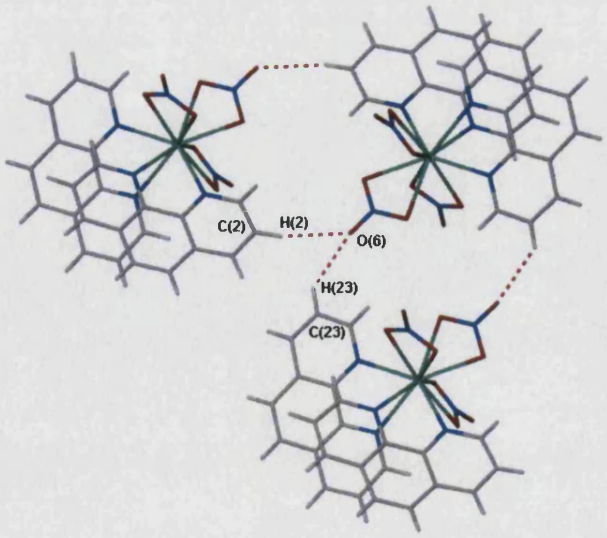

Figure 5.7.25 Hydrogen bond interactions between aromatic hydrogens and O(6)

Extensive hydrogen bonding between aromatic hydrogens and the nitrate oxygens contribute to holding the molecules in place. Among the interactions are C(2)-H(2)···O(6) at a distance of 2.553Å and at an angle of 168.75° (related by –x, -y, -z) and C(23)-H(23)···O(6) at a distance of 2.443Å and an angle of 134.47° (relate by –x, -y, 1-z) (see Figure 5.7.25).

O(7) is also involved in some weak hydrogen interactions (see Figure 5.7.26). The hydrogen bonding distances and angles are 2.496Å (155.79°) and 2.686Å (138.23°) for C(10)-H(10)···O(7) (related by ½ -x, y- ½, ½ -z) and C(22)-H(22)···O(7) (related by ½ +x, ½ -y, z - ½) respectively.

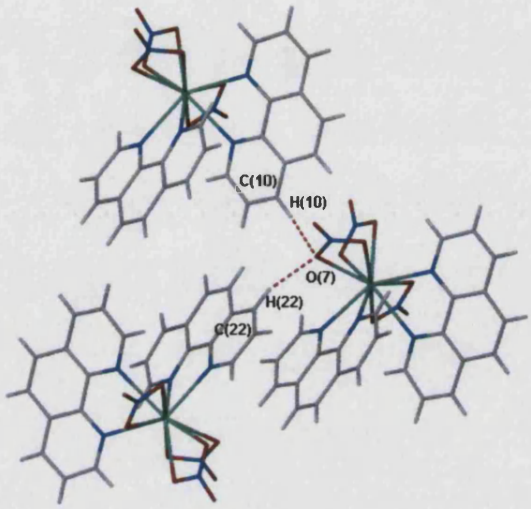

Figure 5.7.26 Hydrogen bond interactions between aromatic hydrogens and O(7)

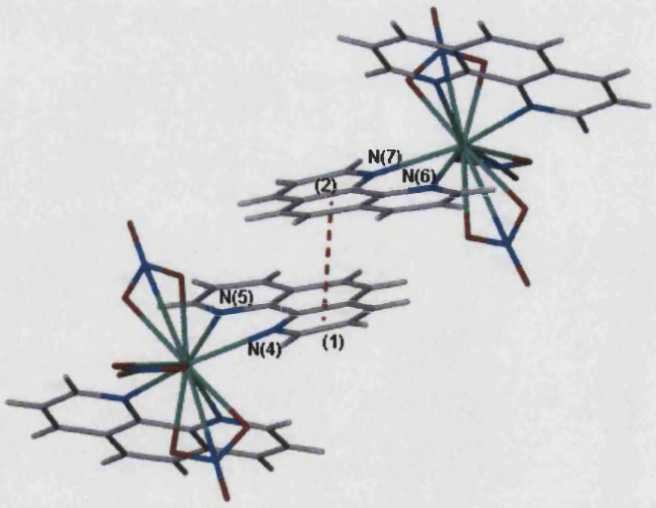

Figure 5.7.27 π-π interactions between the phen ligands

The π-π interactions between the phen ligands are shown in Figure 5.7.27 with the centroid-centroid distances between (1) and (2) at 3.766Å (related by x, y, z).

5.7.1.11 A Comparison of Bond Lengths in Lanthanide-Phen-Nitrate-Thiocyanate Complexes

Bond lengths in complexes $Ln(phen)_2(NCS)_2NO_3(EtOH)$																								
	pr0027		h01prr57		k02prr6		pr0023		pr0019		k03prr11		k03prr14		k01prr58		k01prr9		k03prr25		k00prr16	
	Y		La		La		La		Ce		Pr		Nd		Sm		Tb		Dy		Ho	
x																						
Co-ordination number	9		9		9		9		9		9		9		9		9				9	
M-NCS (Å)	2.378	3	2.526	3	2.586	8	2.538	5	2.498	3	2.489	2	2.472	2	2.442	4	2.404	3	2.380	3	2.385	5
	2.424	4	2.594	4	2.615	8	2.593	5	2.573	4	2.550	2	2.534	2	2.494	4	2.456	3	2.437	4	2.441	6
Average M-NCS (Å)	2.401		2.560		2.601		2.566		2.536		2.520		2.503				2.430				2.413	
M-N (phen) (Å)	2.514	3	2.661	3	2.690	7	2.658	4	2.635	3	2.6192	18	2.601	2	2.599	3	2.540	2	2.520	3	2.519	6
	2.537	3	2.682	3	2.694	6	2.672	4	2.659	3	2.6398	18	2.6261	19	2.613	3	2.557	2	2.553	3	2.546	5
	2.554	3	2.698	3	2.696	6	2.707	4	2.679	3	2.6588	18	2.643	2	2.633	4	2.569	2	2.570	3	2.551	5
	2.570	3	2.725	3	2.740	7	2.718	4	2.688	3	2.6801	19	2.662	2	2.576	3	2.584	3	2.588	3	2.578	5
Average M-N (phen) (Å)	2.544		2.692		2.705		2.689		2.665		2.649		2.633		2.605		2.563		2.558		2.549	
M-ONO_2 (Å)	2.395	3	2.561	2	2.581	6	2.555	3	2.543	2	2.5243	15	2.5044	17	2.48	3	2.426	2			2.408	5
	2.660	3	2.696	2	2.720	6	2.703	4	2.692	2	2.6737	16	2.6614	18	4.647	3	2.661	2			2.662	5
Average M-ONO_2 (Å)	2.5275		2.6285		2.6505		2.629		2.6175		2.599		2.5829		3.5635		2.5435				2.535	
	MeOH (ortep)						EtOH (ortep)															
M-EtOH (Å)	2.403		2.532	3	2.576	6	2.531		2.514	3	2.4979	17	2.4812	18	2.457	3	2.429	2	2.410	3	2.413	5
Ionic radius in CN9			1.216		1.216		1.216		1.196		1.179		1.163		1.132		1.095		1.083		1.072	
Cell Dimensions	Triclinic		Triclinic		Triclinic		Triclinic		Triclinic		Triclinic		Triclinic		Triclinic		Triclinic		Triclinic		Triclinic	
	P(-1)		P(-1)		P(-1)		P(-1)		P(-1)		P(-1)		P(-1)		P(-1)		P(-1)		P(-1)		P(-1)	
a	7.4939	15	7.5964	1	7.5964		7.610	2	7.5945	9	7.4713	1	7.5611	1	7.5476	2	7.4810	1	7.5390	1	7.4740	2
b	9.435	2	9.5735	2	9.5735		9.576	15	9.5711	15	9.5678	1	9.5665	1	9.5609	2	9.4450	2	9.5250	2	9.4340	2
c	19.743	5	20.1846	4	20.1846		19.743	6	20.180	3	20.1035	3	20.0651	3	19.9883	5	19.7330	5	19.8850	4	19.6890	5
α	91.804	11	91.600	1	91.600		91.331	15	91.318	6	91.325	1	91.283	1	91.2880	10	91.9610	10	91.246	1	91.8530	10
β	93.551	12	93.594	1	93.594		93.693	12	93.735	9	93.664	1	93.714	1	93.8420	10	93.3000	10	94.136	1	93.4220	10
γ	109.375	11	109.806	1	109.806		109.821	15	109.928	9	110.075	1	110.126	1	110.1150	10	109.4230	10	109.998	1	109.4420	10
V	1312.4	5	1376.47	4	1376.47		1382.5	6	1374.5	3	1363.59	3	1358.34	3	1349.77	6	1310.65	5	1336.69	4	1304.76	6
mosaicity															0.833	2	0.461	2	0.542	2	0.512	2
GOOF	1.020		1.062		1.062		0.985		1.035		1.036		1.092		1.054		1.045		1.060		1.181	
R obs	0.0470		0.0365		0.0365		0.045		0.0334		0.0276		0.0244		0.0332		0.0308		0.0359		0.0374	

Table 5.5.1 Table of Comparisons between Lanthanide- Phen-Nitrate-Thiocyanate Complexes

5.7.1.12 A Comparison of Bond lengths in Er-Phen and Pr-Phen Complexes

Bond lengths in complexes $Er(phen)_z(NCS)_x(NO_3)_{3-x}$,phen												
	pr0030		h02prr2		h02prr3		h01prr58		h02prr9		h02prr1	
	3NCS		3NCS		3NCS		1NCS 2NO_3		1NCS 2NO_3		3NO_3	
	Er		Er		Er		Er		Er		Er	
x	2		2		2		1		1		0	
Co-ordination number	8		8		8		10		10			
M-NCS (Å)	2.333	4	2.337	6	2.348	4	2.364	5	2.354	6		
	2.362	4	2.356	7	2.372	4						
	2.369	4	2.365	7	2.380	4						
Average M-NCS (Å)	2.355		2.353		2.367							
M-N (phen) (Å)	2.508	3	2.498	6	2.502	3	2.500	4	2.497	4	2.468	3
	2.513	3	2.499	6	2.517	4	2.500	4	2.497	4	2.468	3
	2.532	3	2.524	6	2.527	3	2.524	4	2.519	4	2.532	3
	2.537	4	2.531	6	2.530	3	2.524	4	2.519	4	2.532	3
Average M-N (phen) (Å)	2.523		2.513		2.519		2.512		2.508		2.500	
M-NO_3 (Å)							2.838	4	2.852	5	2.861	5
							2.838	4	2.852	5	2.901	4
											2.901	4
M-ONO_2 (Å)							2.394	3	2.398	4	2.434	3
							2.394	3	2.398	4	2.434	3
							2.451	3	2.462	4	2.445	3
							2.451	3	2.462	4	2.445	3
											2.509	3
											2.509	3
Average M-ONO_2 (Å)							2.4225		2.430		2.463	
M-MeOH (Å)	from Ortep 2.378		(MeOH) 2.391		(MeOH) 2.405	11	-		-			
Ionic radius in CN9	1.062		1.062		1.062		1.062		1.062		1.062	
Cell Dimensions	Triclinic		Triclinic		Triclinic		Monoclinic		Monoclinic		Monoclinic	
	P(-1)		P(-1)		P(-1)		C2/c		C2/c		C2/c	
a	10.3654	12	10.4836	4	10.4850	3	10.4620	3	10.4550	3	10.9960	3
b	12.4613	18	12.4721	5	12.4720	4	15.2810	3	15.2890	4	17.8130	4
c	15.744	2	15.0583	8	15.0620	5	15.8420	6	15.8710	4	12.9740	4
α	96.789	6	95.9590	10	95.946	2	90.0000	13	90		90	
β	106.764	7	104.1940	10	104.215	2	98.1810	12	98.494	2	100.529	1
γ	102.177	7	104.271	2	104.283	1	90.0000	14	90		90	
V	1868.3	4	1821.41	14	1821.84	10	2506.88	13	2509.10	12	2498.45	12
mosaicity			0.491	3	1.017	3	1.198	3	1.282	2		
	180K		150K		150K		150K		150K			
GOOF	0.992		1.071		1.071		0.963		1.136		1.186	
R obs	0.0593		0.0388		0.0388		0.0385		0.0326		0.257	

Bond lengths in complexes $Pr(phen)_x(NCS)_y(NO3)_{3-y}$						
	k01prr8		k03prr11		k02prr7	
	3NCS		2NCS 1NO3		3NO_3	
	Pr		Pr		Pr	
x	3		2		2	
y	3		2		0	
Co-ordination number	9		9			
M-NCS (Å)	2.506	10	2.489			
	2.509	9	2.550			
	2.520	9				
Average M-NCS (Å)	2.512		2.520			
M-N (phen) (Å)	2.659	9	2.6192	18	2.605	3
	2.692	9	2.6398	18	2.608	3
	2.701	8	2.6588	18	2.649	3
	2.704	8	2.6801	19	2.661	3
	2.717	8				
	2.721	8				
Average M-N (phen) (Å)	2.699		2.649		2.631	
M-ONO_2 (Å)			2.5243	15	2.581	3
			2.6737	16	2.564	3
					2.569	3
					2.546	3
					2.545	3
					2.585	3
Average M-ONO2 (Å)					2.561	
M-EtOH (Å)			2.4979		-	
	1 EtOH in latt					
Ionic radius in CN9	1.062		1.062		1.062	
Cell Dimensions	Triclinic		Triclinic		Monoclinic	
	P(-1)		P(-1)		P21/c	
a	10.9021	6	7.4713	1	11.1236	2
b	12.2410	8	9.5678	1	17.9711	4
c	15.5055	11	20.1035	3	13.0164	3
α	97.388	3	91.325	1	90	
β	102.351	3	93.664	1	100.4840	1
γ	101.312	2	110.075	1	90	
V	1950.4	2	1363.59	3	2558.58	9
mosaicity	0.977	4				
GOOF	0.918		1.036		1.14	
R obs	0.0814		0.0276		0.0391	

Table 5.7.3 Table of Comparisons between Er-Phen and Pr-Phen Complexes

5.8 Overall Conclusions

Based on the studies of the various ligands and anions across the lanthanide series', a general trend in line with the lanthanide contraction can be observed where there is a diminishing number of coordination sites progressively across the series. However the coordination number of each lanthanide metal is not fixed and varies in accordance with the ligands, presumably determined by both the ligand-ligand interactions and the sterics surrounding the metal centre.

While crystallography is a very useful tool in lanthanide chemistry, given the problems in redissolving precipitates and crystals once formed, it is important bear in mind that crystals in solid state are not always representative of the chemistry in solution and that while it is a convenient assumption, one crystal in a batch is not always representative of the bulk.

The luminescence studies have given an insight in to the effects of coordinated solvent and ligand variation on lanthanide luminescence. They have been found to be analogous to other lanthanide-metal based luminescence and can be explained with a photophysical model, accounting for the sensitisation pathway is based on the absorption of light in to the first excited singlet state of the antennae chromophore, the intersystem crossing to the antennae triplet state and finally the energy transfer to the lanthanide ion.

Although actual experimental energy-transfer efficiencies can be calculated[14] based on the efficiency of the singlet-to-triplet conversion in the antennae chromophore and the efficiency of the triplet-to-metal energy transfer step, this often requires luminescence measurements to be carried out in solution and the quantum efficiencies calculated.

For future work, it would be interesting to compare ligand-metal energy transfers based on theoretical models describing energy transfer between ligand and lanthanide ion[47, 48, 49, 50] with the experimental values.

5.9 Lanthanide polymers

To date, little is known about lanthanide polymers although corresponding transition metal polymers gain wide attention. This may in part be due to the difficulty in characterising the polymers given that the majority of simple lanthanide complexes either do not dissolve in non-polar solvents or simply dissociate in most polar solvents.

However, among the studied polymeric systems, the chelate system of beta-diketonates in lanthanides is interesting in that it can be used to efficiently 'pump energy' from the organic molecule to the metal ion to enhance fluorescence.[51] This is different from the conventional system where pump energy is absorbed directly by the lanthanide ion. The basis of the study by Okamoto and co-workers, was due in part to reducing the probability of dissociation in these complexes by using a polymer matrix. By which they hoped that the solid polymer complexes would be locked in to a specific configuration.

Reported electro luminescent (EL) devices using conjugated organic polymers have attracted attention due to their favourable light emitting properties. It is also possible to tune the emission colour of these polymer systems by modifying certain substituents.[52]

Recent luminescent lanthanide compounds have been found to have potential as emitters as well, however as the emission intensity of the lanthanide ions is usually very weak hindering their applications in EL displays.[53] However with the appropriate ligands the f $\rightarrow$f emission intensity can be enhanced.[51]

These provide an insight in to the possibility of synthesizing luminescent lanthanide complex polymers, which are likely to have novel properties, which will enhance emission intensity, as well as being able to be deposited on substrates for use as EL devices. The self-assembly processes that are involved in the formation of lanthanide-containing co-ordination polymers and array materials, are often directed by hydrogen bonds or metal-ligand ligation that gives rise to supramolecular systems with novel topologies[54].

It has also been shown that the electronic properties can be tailored depending on the ligand sets present and on the level of aggregation present in the systems. Examples of ligand systems that have been used successfully include those shown in Figure 5.9.1.[55, 56, 57, 58, 59]

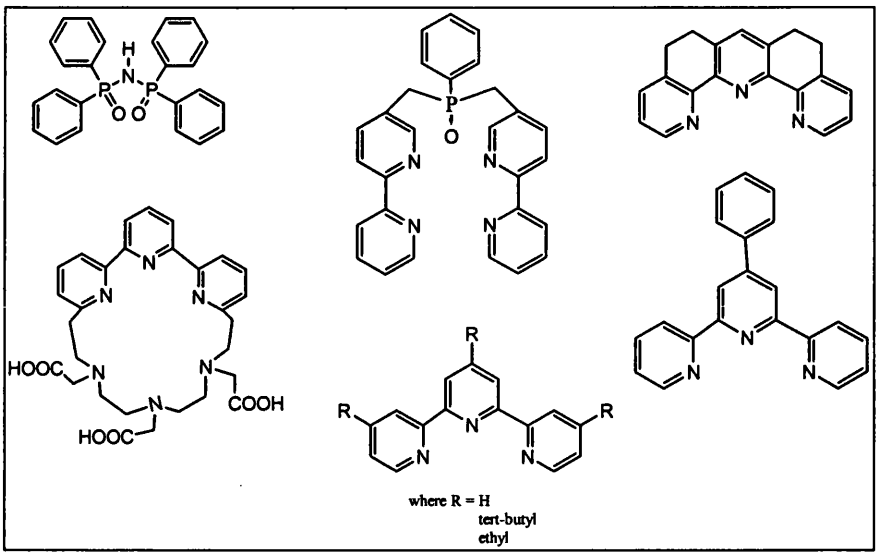

Figure 5.9.1 Multidentate ligand systems that have been shown to co-ordinate to lanthanide centers.

The use of benzoic multicarboxylates and pyridine ligands have also often been employed for the purpose of building large polymeric complexes with lanthanide centers due to their various bridging abilities[60] and their propensity to form hydrogen bonds and other intermolecular interactions[61].

The following section details the structural properties of $[La(O_2CPh)_3(CH_3OH)_3(H_2O)]$ (Section 5.9.1) and $[La(O_2CPh)_3(H_2O)_2.bipy]$ (Section 5.9.2). (2,2'-bipyridine = bipy)

5.9.1 Structural Features of $La(O_2CPh)_3(CH_3OH)_2(H_2O)_n$ (17)

The structure of **17** is isostructural with the previously published terbium analogue[53]. The asymmetric unit of compound **17,** shown in Figure 5.9.2, consists of an eight-coordinate lanthanum ion bound to eight oxygen atoms forming a distorted square anitprism (Figure 5.9.3). The ligands consist of five oxygens from three benzoate ligands, two methanol molecules and a single coordinated water molecule.

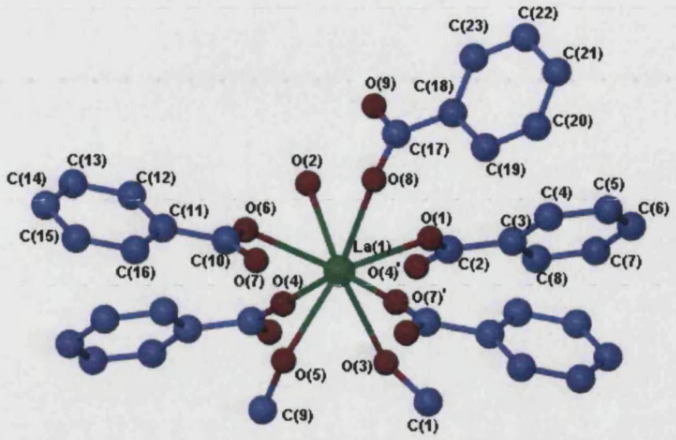

Figure 5.9.2 Structure of $[La(O_2CPh)_3(CH_3OH)_2(H_2O)]$ (**17**) showing atom-numbering scheme employed.

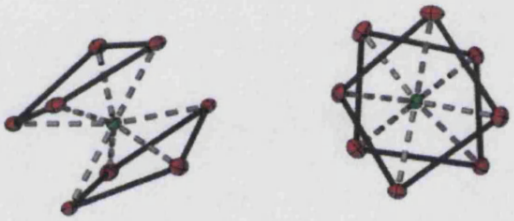

Figure 5.9.3 The distorted square antiprism geometry of the lanthanum centre

The La-O bond lengths vary from 2.4206 (17)Å for La(1)-O(4) to 2.6246 (18)Å for La(1)-O(2), in contrast to the equivalent Tb-O distances[53] ranging from 2.276(2) to 2.481(3)Å which is consistent with the lanthanide contraction. The published covalent radii for lanthanum and terbium are 1.69Å and 1.59Å respectively.

Extensive hydrogen bonding, both inter and intramolecular as well as inter-chain interactions constrains the polymer to form fairly rigid chains with interchain separations in the range of 7.787Å to 8.722Å.

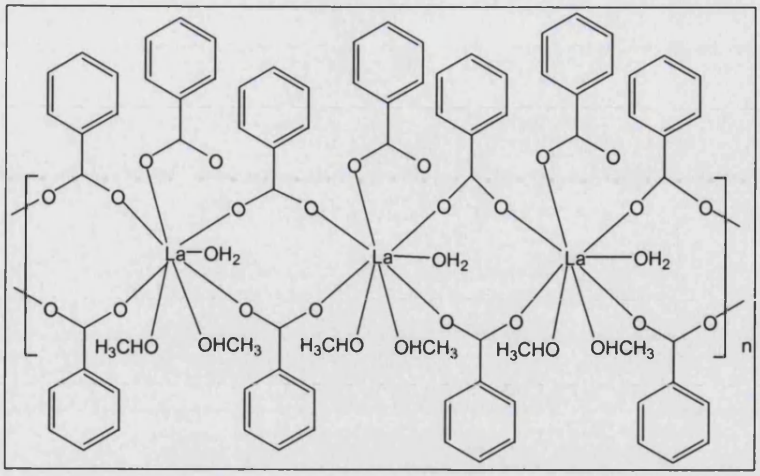

Figure 5.9.4 A schematic drawing of the polymeric chains

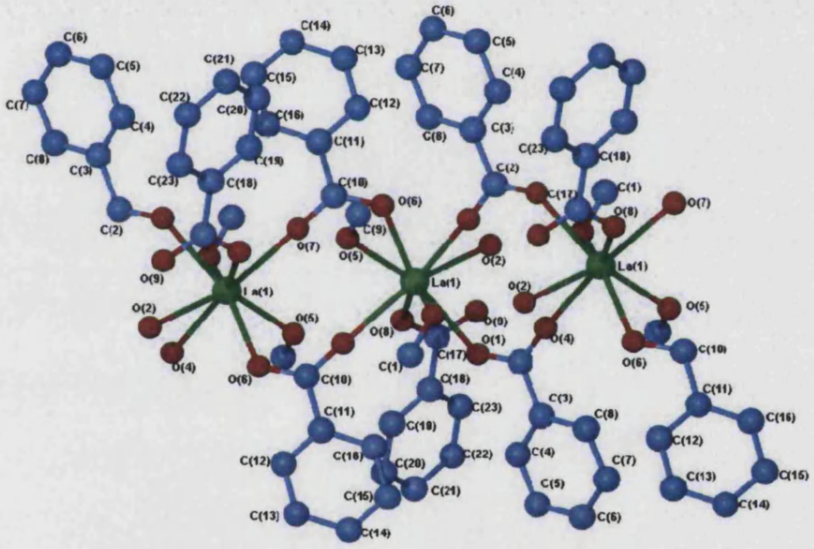

Figure 5.9.5 The polymeric chains of **17**

Two of the three benzoate ligands are involved in bidentate bridging thus forming a 1-D chain with La-La distances of 4.840Å and 5.158Å repectively. The La(1B)-La(1A)-La(1D) angle is 167.22° making it an almost linear chain (see Figure 5.9.5).

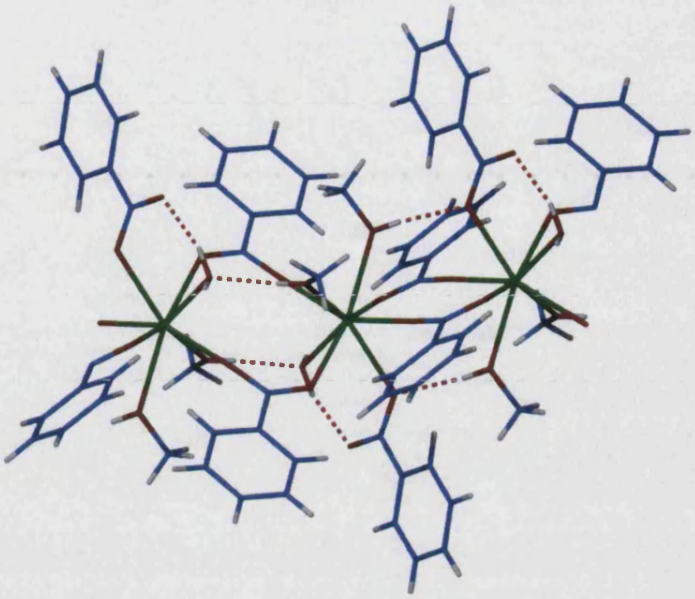

Figure 5.9.6 Intramolecular hydrogen bonding within the lanthanum chain

The third benzoate ligand is terminal and forms an intramolecular hydrogen bond through the free carbonyl oxygen atom with the coordinated H_2O with a O(9)...O(2) distances of 2.633(1)Å, O(2)-H(2B)...O(9) 162.84° (3.89)and an interchain interaction at distances of O(9)...O(2) 2.915Å, O(2)-H(2B)...O(9) 162.34° respectively (see Figure 5.9.6). The benzoate rings are also not planar with the COO^- moiety with dihedral angles ranging from 12.02(16)° to 17.66(15)°.

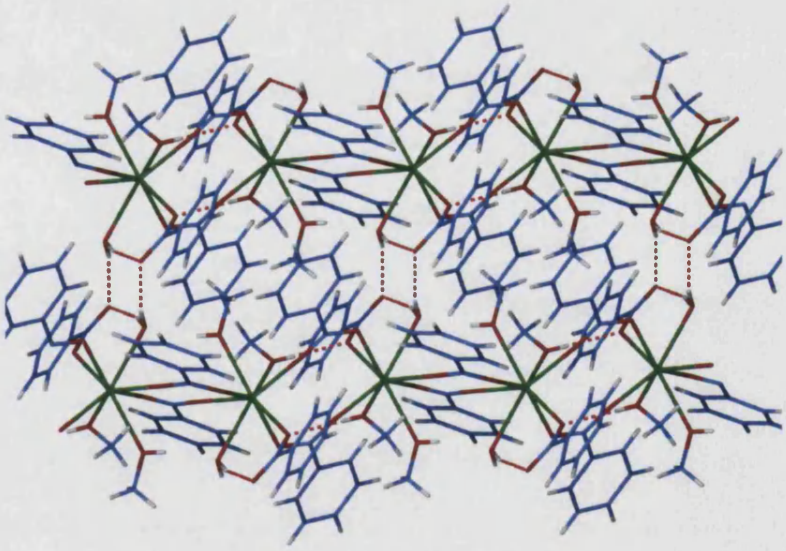

Figure 5.9.7 Intermolecular hydrogen bonding

Both coordinated methanol molecules are also involved in intermolecular hydrogen bonding forming a 3D polymeric structure, with one methanol interacting with the benzoate oxygen at a distance of O(5)...O(8b) 2.774(3)Å, O(5)-H(5O)...O(8b) 172.98° (4.14) (b= -x+2,-y,-z+1) and the other interacting with a H_2O molecule with distances of O(3)...O(2c) 2.696(3)Å, O(3)-H(30)...O(2) 168.27° (5.10) (c=-x+2,-y+1,-z+1). The attached H_2O molecule functions both as a hydrogen bond donor and acceptor. (Figure 5.9.7)

5.9.2 Structural Features of $(La(O_2CPh)_3(H_2O)_2.bipy)_n$ (18) (2,2'-bipyridine = bipy)

The crystal structure of **18** differs from those of related lanthanide species in that a free bipy molecule is present in the lattice. This molecule is involved in the hydrogen-bonding network within the crystal. The asymmetric unit of **18**, with a crystallographically imposed 2-fold rotation axis along *C* through the molecule, consists of a lanthanum metal core co-ordinated to four oxygen atoms, one derived from a chelating benzoate ligand, two from two bridging benzoates, and one from a water molecule, within the asymmetric unit, there is also an uncoordinated bipy (see Figure 5.9.8).

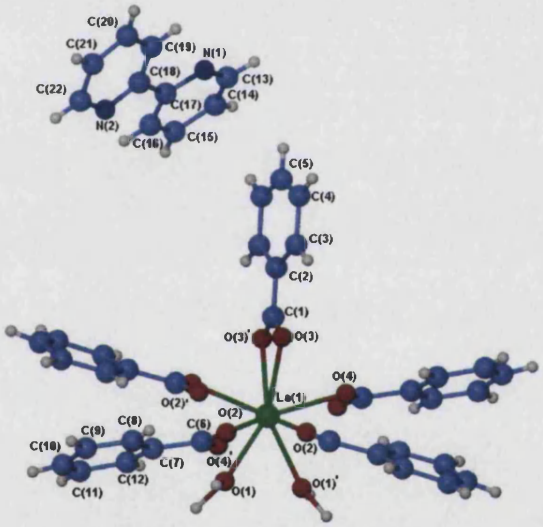

Figure 5.9.8 Structure of $[La(O_2CPh)_3(H_2O)_2.bipy]_n$ (**18**) showing atom-numbering scheme employed.

Figure 5.9.9 The distorted square antiprism geometry of the lanthanum centre

As with **17**, the core of compound 18 also forms a distorted square antiprism (see Figure 5.9.9). However, unlike **17**, in which the benzoate ligands are mostly bridging, each metal core of **18** consists of four bridging and one chelating benzoate for every La metal.

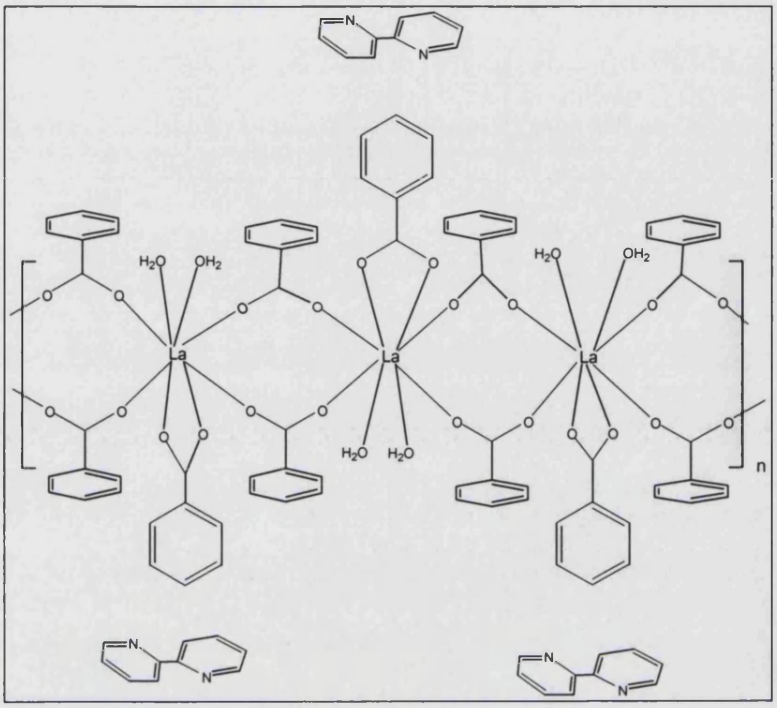

Figure 5.9.10 A schematic representation of **20**

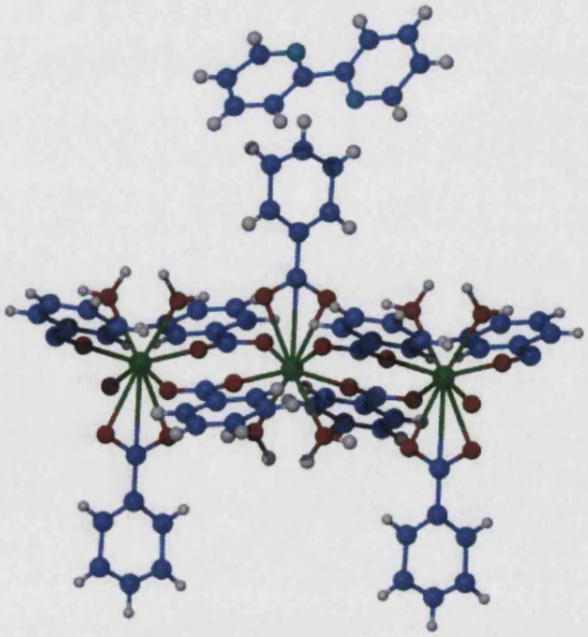

Figure 5.9.11 The polymeric chains of **18**

The four bridging benzoate ligands link the La metal centers, forming a 1-D polymeric chain with neighbouring La-La distances of 4.901 Å. The La-O distances vary from 2.405 (4)Å for La(1)-O(2) to 2.575(4)Å for La(1)-O(3) with the average La-O distance being 2.515Å. (see Figure 5.9.11)

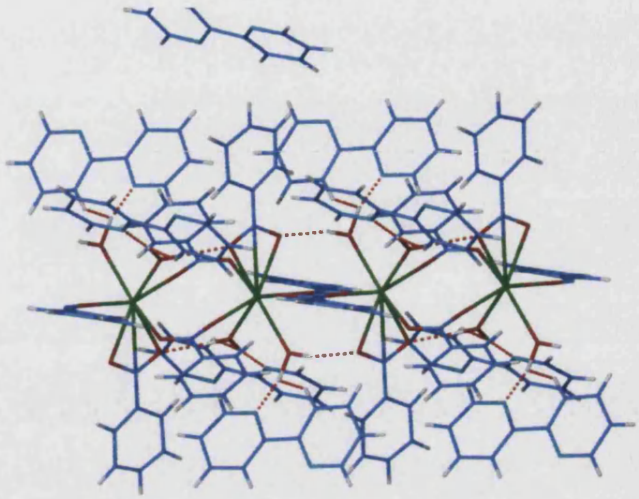

Figure 5.9.12 Intramolecular hydrogen bonds

Weak intramolecular hydrogen bonds between the coordinated water molecule and the chelating benzoate ligand O-H…O distances of O(1)…O(3) 2.788 (7)Å, at an angle of O1-H1B…O3 157.15 (6.17) help hold the polymer rigid producing a significantly planar La(B)-La(A)-La(D) angle of 179.96°. (see Figure 5.9.12)

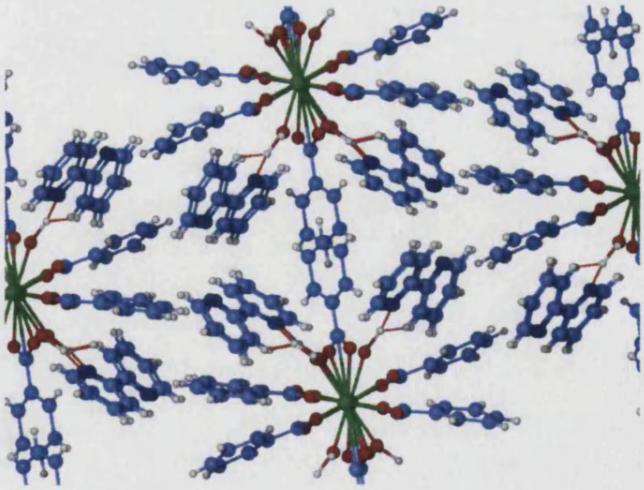

Figure 5.9.13 Intermolecular hydrogen bonding

Hydrogen bonding between the bipy moiety and the coordinated water molecules give rise to a 3-D system in which the La polymer layers interspaced with bipy ligands (see Figure 5.9.13).

The bipy moiety is anchored between the polymeric layers through hydrogen bonds formed between a N on the bipy ligand and the coordinated water molecule with distances of O1...N1 2.832 (8) at an angle of O1-H1A...N 161.88 (7.17). The planes of the pyridine rings are slightly twisted at 11.48° (28).

The benzoate rings in **18** are also slightly twisted away from planarity with the carboxylate moiety at angles of 12°(0.32) and 14.85° (0.64) respectively.

5.9.3 Discussion and Comparisons Between the Two Polymers

There are three main binding modes for carboxylate moieties, chelating, bridging and chelating-bridging.[62, 63] The bridging and chelating-bridging modes tend be most common among the rare earth carboxylates, although we observed only bridging in **17** and bridging and chelating in **18**.

Both **17** and **18** consists of two pairs of bridging carboxylate ligands, although the final carboxylate ligand in **17** is terminal with a non-bonded C=O bond, while **18** has a chelating carboxylate group. The chelate only binding mode, although is less common in related structures is not unknown.[64, 65]

It is suggested in a reported structure of cerium- 3,5 di-nitrobenzoate dihydrate that the single mode coordination, i.e. bridging, was due to the occurance of two nitro groups on the phenyl ring, however, this is not the case for **17** which has no other functional groups on the phenyl ring.[66]

It should be noted that the bound solvent molecules, MeOH and water in **17**, and only water in **18**, play a vital role in determining both the intra- and interchain interactions, thereby influencing the packing effects within the crystal structures.

In comparing the two structures, the linearity of the polymeric chain in **18** is greater with angles approximating to 180° (179.96°) compared to 167.22° in **17**. The chelated benzoate group in **18** is kept rigid through interactions with water molecules on either side (see Figure 5.9.14).

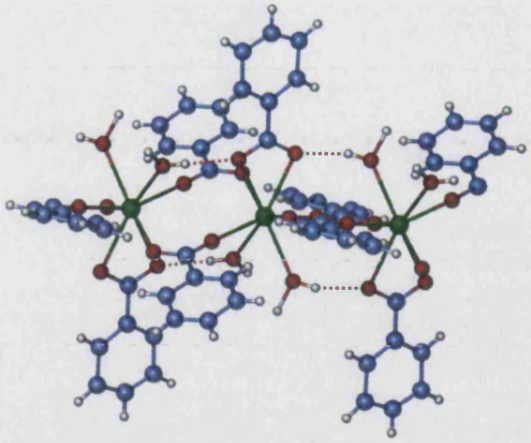

Figure 5.9.14 Interactions with the bound water in **20**

While in **17** there is a very slight corrugated effect, due to the interactions between MeOH and water on one side and water and a bridged benzoate oxygen on the other as shown in Figure 5.9.15.

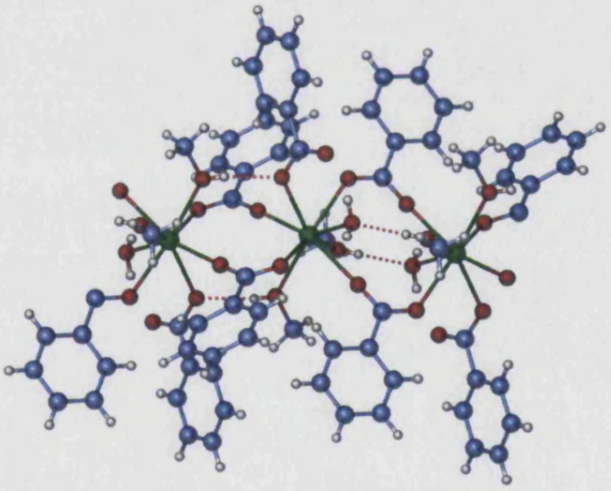

Figure 5.9.15 Interactions between the bound water and MeOH solvent in **17**

The differences between the type of co-ordinated solvents, MeOH and water are likely to be influenced by the pH conditions within the environment. Both reactions were performed in alkaline solutions with the addition of KOH.

In other related lanthanoid structures with bipy ligands, the ligands tend to be terminally chelated on dimers [67, 68] synthesized in pH environments of between 6 and 7. A free non-

chelated bipy moiety as in **18** is unprecendented. This could be due to the relatively weak affinity of nitrogen for Ln^{3+} compared to oxygen, [69, 70] and/or the basic nature of the reaction solution.

[1] Source: www.dayah.com/periodic

[2] M.M. Woyski and R.E. Harris, The Rare Earths and Rare-Earth Compounds in Treatise on Analytical Chemistry Part II, Analytical Chemistry of the Elements, 1963, **8**, 4-5.

[3] N.Kaltsoyannis and P. Scott, *The f elements*, Oxford Chemistry Primers, 1999, 1-2.

[4] Lanthanides and Actinitdes, The Open University, The Trinity Press, 1977

[5] R. Anwander and W.A Herrmann, *Features of Organolanthanide Complexes* in Topics in Current Chemistry, **179**, Eds J.D. Dunitz *et al.*, 1996, Pg 6-10 and references therein

[6] T. Moeller in J.C. Bailar *et al.*, Comprehensive Inorganic Chemistry, Vol. 4, Pergamon, Oxford, Chap 44. 19

[7] T. Moeller Complexes of the Lanthanides in H.J. Emelius MTP International Review of Science Lanthanides and Actinides, , 1972 Series 1, Volume1.

[8] G. Wilkinson *et al.*, Comprehensive Coordination Chemistry, 1987 **1**: 1068-1073

[9] T. Moeller and H.E. Kremers, Chem. Rev., 1945, **37**, 97.

[10] F.A. Hart, Scandium Yttrium and the lanthanides in G. Wilkinson et al., Comprehensive Coordination Chemistry 1987, **3** 1069

[11] M. Frechette and C. Bensimon, *Inorg. Chem.* 1995, **34** 3520-3527.

[12] V. Bekiari and P. Lianos, *Adv. Mater.* 1998, **10**, 1455-1458.

[13] V. Bekiari, P. Lianos and P. Judeinstein, *Chem. Phy. Lett.*, 1999, **307**, 310-316.

[14] N.Sabbatini, M. Guardigli, and J-M. Lehn, *Coord. Chem. Rev.* 1993, **123**, 201.

[15] A.Vogler and H, Kunkely, Luminescent Metal Complexes: Diversity of Excited States in Topics in Current Chemistry: Transition Metal and Rare Earth Compounds- Excited States, Transitions and Interactions I, 2001, **213**, 143-182.

[16] S.W. Magennis, S. Parsons, A. Corval, J.D. Woollins and Z, Pikramenou, *J. Chem. Soc. Chem. Comm.* 1999, 61-62.

[17] L. van Pieterson, M.F. Reid, R.T. Wegh, S. Soverna and A. Meijerink, *Phys. Rev. B.*, 2002, **65**, 1-13.

[18] G.W. Burdick and M.C. Downer, *J. Chem Phys.*, 1989, **91**, 1511-1520.

[19] V. Balzani, R. Ballardini, F. Bolletta, M.T. Gandolfi, A. Juris, M. Maestri, M.F. Manfrin, L. Moggi and N. Sabbatini, *Coord. Chem Rev.*, 1993, **125**, 75-88.

[20] D.A. Durham, G.H. Frost and F.A. Hart, *J. Inorg Nucl. Chem*, 1969, **31**, 833-838 and references therein.

[21] M.J. Hudson, M.G.B. Drew, M.R. S. Foreman, C. Hill, N. Huet, C. Madic and T.G.A. Youngs, *J. Chem. Soc. Dalton Trans.*, 2003, 1675-1685.

[22] P. Byers, G.Y.S. Chan, M.G.B. Drew and M.J. Hudson, *Polyhedron*, 1996, **15**, 2845-2849.

[23] G.Y.S. Chan, M.G.B. Drew, M.J. Hudson, M.J. Hudson, N.S. Isaacs and P. Byers, 1996, *Polyhedron*, **15** 3385-3398.

[24] M.G.B. Drew, P.B. Iveson, M.J. Hudson, J.O. Liljenzin, L. Spjuth, P.-Y. Cordier, A. Enarsson, C. Hill and C. Madic, *J. Chem. Soc. Dalton Trans.*, 2000, 821-830.

[25] M.G.B. Drew, M.J. Hudson, P.B. Iveson and C. Madic, *Acta Cryst. C.*, 2000, **56**, 434-435.

[26] M.G.B. Drew, M.J. Hudson, P.B. Iveson, M.L. Russell, J.O. Liljenzin, M. Skålberg, L. Spjuth and C. Madic *J. Chem. Soc. Dalton Trans.*, 1998, 2973-2982.

[27] M.G.B. Drew, M.J. Hudson, P.B. Iveson, M.L. Russell and C. Madic, *Acta Cryst. C.*, 1998, **54**, 985-987.

[28] S.A. Cotton, V. Franckevicius, R. E. How, B. Ahrens, L.-L. Ooi, M.F.Mahon, P.R. Raithby, S.J. Teat, *Polyhedron*, 2003, **22**, 1489-1497.

[29] X.P. Yang, C.-Y, Su, B.-S. Kang, S.-L. Feng, W.-L. Xiao and H-Q. Liu, *J. Chem. Soc. Dalton Trans.*, 2000, 3253-3260.

[30] N. Matsumura, T. Takeguchi, A. Ouchi, *Bull. Chem. Soc. Jpn.*, 1990, **63**, 620 and references therein.

[31] F.H. Allen, O. Kennard, *Chem. Des. Automat. News 8*, 1993, **1**, 31.

[32] B. Ahrens, S.A. Cotton, N. Feeder, O.E. Noy, P.R. Raithby and S.J. Teat, *J. Chem. Soc. Dalton Trans.*, 2002, 2027-2030.

[33] L.P. Wan, PhD. Thesis, Synthesis, Structural Characterisation and Photophysical Properties of Lanthanide Complexes Containing Polydentate Amide Ligands, 2001, Hong Kong.

[34] C. Galaup, J. Azema, P. Tisnes, C. Picard, P. Ramos, O. Juanes, E. Brunet and J. C. Rodriguez-Ubis, *Helv. Chim. Acta*, 2002, **85**, 1613-1625.

[35] C. Galaup, J.M. Couchet, C. Picard and P. Tisnes, *Terahedron. Lett.*, 2001, **42**, 6275-6278.

[36] M. Sun, H. Xin, K.-Z, Wang, Y.-A, Zhang, L.-P. Jin and C.-H Huang, *J. Chem. Soc. Chem. Comm.*, 2003, 702-703.

[37] M.E. Cooper and P.G. Sammes, *J. Chem. Soc. Perkin Trans. 2*, 2000, **8**, 1695-1700.

[38] G. Blasse, G.J. Dirksen, N. Sabbatini, S. Perathoner, J.M. Lehn and B.Alpha, *J. Phys. Chem.*, 1988, **92**, 2419-2422.

[39] X. Li, X. Zheng, L. Jin, S. Lu and J. Zhang, *J. Mol. Struct.*, 2001, **559**, 341-346.

[40] L.I. Semenova and A.H. White, *Aust. J. Chem.*, 1999, **52**, 507

[41] F.A. Hart and F.P. Laming, *J. Inorg. Nucl. Chem.*, 1965, **27**, 1605.

[42] F.A. Hart and F.P. Laming, *J. Inorg. Nucl. Chem.*, 1965, **27**, 1825.

[43] A.G. Mirochnik, B.V. Buknetskii, P.A. Zhikhareva and V.E. Karasev, *Russ. J. Coord. Chem.*, 2001, **6**, 475-480.

[44] Y.-Q. Zheng, L.-X. Zhou and J.-L. Lin, Z. *Anorg. Allg. Chem*, 2001, **627**, 1643-1646.

[45] A.K. Boudalis, V. Nastopoulos, S.P. Perlepes, C.P. Raptopoulou and A. Terzis, *Trans. Metal Chem.*, 2001, **26**, 276-281.

[46] N. Armaroli, L. de Cola, V. Balzani, J.-P. Sauvage, C.O. Dietrich-Burchercker, J. –M. Kern, *J. Chem., Soc. Faraday Trans.*,1992, **88**, 553-556.

[47] W.M. Faustimo, G.B. Rocha, F.R. Gonçalves e Silva, O.L. Malta, H.F. G.F. de Sá and A.M. Simas, *J. Mol. Struct.*, 2000, 245-251.

[48] A.V.M. de Andrade, N.M. da Costa, R.L. Longo, O.L. Malta, A. M. Simas and G.F. de Sá, *Mol. Eng.*, 1997, **7**, 293.

[49] O.L. Malta, *J. Lumin.*, 1997, **71**, 229.

[50] O.L. Malta, H.F. Brito, J.F.S. Menezes, F.R. Gonçalves e Silva, S. Alves Jr., F.S. Farias Jr. and A.V.M. Andrade, *J. Lumin*, 1997, **75**, 255.

[51] Y. Okamoto et al. Synthesis, characterisation and Applications of Rare Earth Metal ion Chelating Polymers in J.E. Sheats and C.E. Arraher, Jr. and C.U. Pittman, Jr. Metal –containing Polymeric Systems, 1985, 425

[52] C.P Shipley, S.Capecchi, O.V. Salata, M. Etchells, P.J. Dobson and V.Christou, *Adv. Mater.* 1999, **11** (7) 533-536

[53] C.Seward, N, Hu and S.Wang, *J. Chem. Soc., Dalton Trans.*, 2001, 134-137.

[54] L. Ma, O. R. Evans, B. M. Foxman, and W. Lin, *Inorg. Chem.*, 1999, **38**, 5837.

[55] L. J. Charbonniere, R. Ziessel, M. Montalti, L. Prodi, N. Zaccheroni, C. Boehme, and G. Wipff, *J. Am. Chem. Soc.*, 2002, **124**, 7779.

[56] S. W. Magennis, S. Parsons, A. Corval, J. D. Woollins, and Z. Pikramenou, *J. Chem. Soc Chem. Comm.*, 1999, 61.

[57] C. Galaup, J. M. Couchet, C. Picard, and P. Tisnes, *Tetrahedron Lett.*, 2001, **42**, 6275.

[58] M. E. Cooper and P. G. Sammes, *J. Chem., Soc. Perkin 2*, 2000, 1695.

[59] H. R. Murner, E. Chassat, R. P. Thummel, and J. C. G. Bunzli, *J. Chem. Soc. Dalton Trans.*, 2000, 2809.

[60] D. Sun, R. Cao, Y. Liang, Q. Shi, and M. Hong, *J. Chem. Soc. Dalton Trans.* 2002, 1847.

[61] Ma, B.-Q, Gao, S, Sun H.-L, Xu G.-X, *Cryst. Eng. Comm.*, 2001, **35**, 1-5.

[62] J. F. Ma, Z. S. Jin, and J. Z. Ni, *Acta Cryst. C.*, 1994, **50**, 1008.

[63] J. F. Ma, Z. S. Jin, and J. Z. Ni, *Acta Cryst. C.*, 1994, **50**, 1010.

[64] L. Ma, O. R. Evans, B. M. Foxman, and W. Lin, *Inorg. Chem.*, 1999, **38**, 5837.

[65] D. Sun, R. Cao, Y. Liang, Q. Shi, and M. Hong, *J. Chem. Soc. Dalton Trans.*, 2002, 1847.

[66] M. N. Tahir, D. Uelkue, C. Uenaleroglu, and E. M. Moevsuemov, *Acta Cryst. C*, 1996, **52**, 1449.

[67] L. Jin and S. Lu, *Polyhedron*, 1996, **15**, 4069.

[68] L. Jin, R. Wang, L. Li, S. Lu. S. Huang , *Polyhedron*, 1999, **18**, 487.

[69] T. Moeller, in J.C. Bailar, *et al* Comprehensive Inorganic Chemistry, Vol.4, Pergamon, Oxford, Chap 44, 19

[70] T. Moeller, *Complexes of the Lanthanides* in H.J. Emelius *MTP International Review of Science Lanthanides and Actinides,* 1972, Series 1 Volume 1.

CHAPTER 6

EXPERIMENTAL METHODS

6.0 Experimental Methods

6.1 Reactions of Os3(μ-H)2(CO)10 with 1,4-bis(3-thiophenyl)butadiyne and 1,3-bis(3-thiophenyl)butadiyne.

Materials. The parent osmium cluster $[H_2Os_3(CO)_{10}]$ and 2-and 3-thienyl substituted butadiyne ligands were prepared by literature methods[1, 2, 3]and purified using thin layer (TLC) and column chromatography. Spectroscopic data for the ligands were in agreement with those reported earlier. All reagents were of analytical grade and were used as received. The reactions were carried out under nitrogen using freshly distilled solvents. All manipulations of the products were performed in air.

Chromatography. Thin layer chromatography was performed on commercial 20 x 20 cm plates (Aldrich) covered with Merck silica gel 60 F254 to 0.25 or 1.0 mm thickness. Column chromatography separations were performed using 2x40 cm column and SG 60 silica gel (Aldrich).

Spectroscopic Studies. Infrared spectra were measured using a Nicolet Avatar 360 FTIR spectrometer from dichloromethane solutions. ^1H NMR spectra were recorded at room temperature on a Bruker 300 MHz spectrometer using $CDCl_3$ as a solvent. Elemental analysis was performed on an Exeter Analytical Inc. CE-440 Elemental Analyser.

6.1.1 Preparation of $[Os_3(\mu\text{-}H)(CO)_{10}\{(\mu\text{-}\eta\text{-}(C_4H_3S)(C_8H_4S)\}]$ (1)

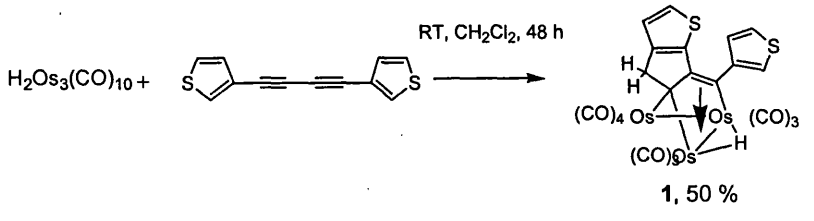

1, 50 %

$[H_2Os_3(CO)_{10}]$ (143 mg, 0.17 mmol) and 1,4-bis(3-thiophenyl)butadiyne (40 mg, 0.19 mmol) were added to dichloromethane (40 mL) and stirred under nitrogen at room temperature. The reaction was allowed to proceed for 48 hours and was monitored by TLC spot tests. The resulting yellow solution was concentrated under reduced pressure, and separated by TLC (eluent: dichloromethane/hexane 1:6). Apart from a small amount of starting material, the major yellow product was identified as $[Os_3(\mu\text{-}H)(CO)_{10}\{(\mu\text{-}\eta\text{-}(C_4H_3S)(C_8H_4S)\}]$ (**1**). It was recrystallised from chloroform at –20°C to yield yellow crystals, which were subsequently analysed by single crystal X-ray diffraction.

IR (CH_2Cl_2), ν_{CO}/cm^{-1}: 2110(m), 2081(vs), 2056(vs), 2024(vs), 2001(s), 1974(sh). ^1H NMR δ 7.37 (dd, 1 H, ^3J=4.8, ^4J=3.0), 7.28 (d, 1 H, ^3J=4.8), 7.01 (dd, 1 H, ^3J=4.8, ^4J=1.2), 6.93 (d, 1 H, ^3J=4.8), 6.77 (dd, 1 H, ^4J=3.0, ^4J=1.5), 4.24 (d, 1 H, ^2J=21.6), 4.04 (d, 1 H, ^2J=21.6), –

16.9 (s, 1 H). FAB MS (m/z) obs. center of isotopic envelope 1068, calc. 1068. Anal. Calcd for $C_{22}H_8O_{10}S_2Os_3$: C, 24.7; H, 0.75. Found: C, 24.8; H, 0.8.

6.1.2 Thermal decarbonylation of 2

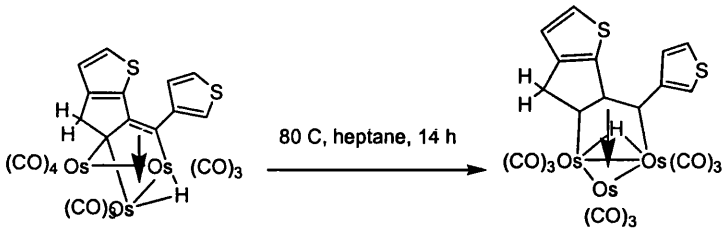

1 **2**, 79 %

1 (100 mg, 0.09 mmol) was dissolved in heptane (35 mL) and heated at 80°C for 14 hours under nitrogen. The resulting yellow solution was cooled to room temperature and the solvent removed under reduced pressure. Separation by TLC (eluent: dichloromethane/hexane 1:4) and subsequent crystallization from dichlorometane solution yielded pale yellow crystals (77 mg, 79 %), characterized as $[Os_3(\mu\text{-}H)(CO)_9\{(\mu_3\text{-}\eta^3\text{-}(C_4H_3S)(C_8H_4S)\}]$ (**2**), also analysed by single crystal X-ray diffraction.

2 was also formed (in approximately 30 % yield) when **1** was refluxed in toluene (40 mL) under hydrogen for 14 hours. The reaction mixture also contained some starting material, **1**, a small amount of $[Os_3(\mu\text{-}H)_2(CO)_{10}]$, and a dark-brown decomposition product.

IR (CH_2Cl_2), ν_{CO} /cm^{-1}: 2097(s), 2071(vs), 2045(s), 2016(sh), 2002(s), 1991(sh). ^{1}H NMR δ 7.49 (dd, 1 H, ^3J=4.80, ^4J=3.20), 7.20 (d, 1 H, ^3J=4.80), 7.17 (dd, 1 H, ^3J=4.80, ^4J=1.20), 7.03 (dd, 1 H, ^4J=2.70, ^4J=1.20), 6.81 (d, 1 H, ^3J=4.8), 3.60 (d, 1 H, ^2J=22.20), 3 .30 (d, 1 H, ^2J=22.20), −18.72 (s, 1 H). FAB MS (m/z) obs. 1040, calc. 1040. Anal. Calcd for $C_{21}H_8O_{10}S_2Os_3$: C, 24.3; H, 0.78. Found: C, 24.7; H, 0.9.

6.1.3 Synthesis of $[Os_3(\mu\text{-}H)(CO)_{10}\{(\mu\text{-}\eta\text{-}(C_4H_3S)(C_8H_4S)\}]$ (3) and $[Os_3(\mu\text{-}H)(CO)_{10}\{(\mu_3\text{-}\eta^2\text{-}\eta^1\text{-}\eta^1\text{-}(SC_7H_4)C(SC_4H_3)\}]$ (4a and 4b)

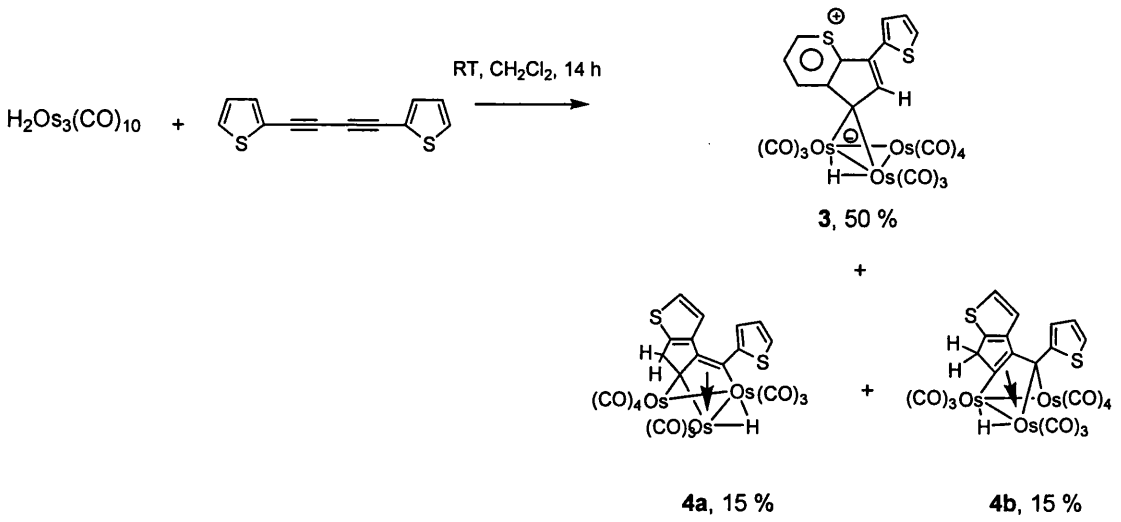

This was prepared essentially by the literature method,[4] as follows:
$[H_2Os_3(CO)_{10}]$ (200mg, 0.21 mmol) and 1,4-bis(2-thiophenyl)butadiyne (47mg, 0.22 mmol) were dissolved in dichloromethane (40 mL) and the resulting dark green solution was stirred at room temperature for 12 hours under nitrogen. The reaction mixture was separated using TLC (eluent: hexane/dichloromethane 3:1) after reducing the volume. The green main product, collected from the middle of the plate was characterized as $[Os_3(\mu\text{-}H)\ (CO)_{10}\{(\mu\text{-}\eta\text{-}(C_4H_3S)(C_8H_4S))\}]$ (**3**, yield 55 %). Evaporation of a dichloromethane solution of **3** yielded dark green crystals suitable for single crystal X-ray diffraction.

IR (CH_2Cl_2), ν_{CO}/cm^{-1}: 2095(s), 2086(sh), 2060(vs), 2052(vs), 2039(sh), 2007(vs), 1998(sh), 1976(m). ^1H NMR δ 9.65 (s, 1 H), 8.27 (d, 1 H, ^3J=8.54), 7.93 (d, 1 H, ^3J=7.60), 7.88 (dd, 1 H, ^3J=8.54, ^3J=7.62) 7.54 (dd, 1 H, ^3J=3.62, ^4J=0.95) 7.40 (dd, 1 H, ^3J=5.09, ^4J=0.95) 7.19 (dd, 1 H, ^3J=5.07, ^4J=3.62) –14.82 (s, 1 H). FAB MS (m/z) obs. 1068, calc. 1068. Anal. Calcd for $C_{22}H_8O_{10}S_2Os_3$: C, 24.7; H, 0.75. Found: C, 24.8; H, 0.8.

A minor yellow band separated from the top of the TLC plate was analysed and subsequently identified as a pair of isomeric products, $[Os_3(\mu\text{-}H)(CO)_{10}\{(\mu_3\text{-}\eta^2\text{-}\eta^1\text{-}\eta^1\text{-}(SC_7H_4)C(SC_4H_3)\}]$ (**4a** and **4b**, combined yield 35%). Attempts at the chromatographic separation of these isomers were unsuccessful, however, compound **4a** could be selectively recrystallised from dichloromethane/hexane solution at –20°C, yielding light yellow crystals suitable for single crystal X-ray diffraction, which allowed the full characterization of both isomers.

4a: IR (CH_2Cl_2), ν_{CO}/cm^{-1}: 2111(w), 2083(m), 2058(vs), 2027(vs), 2006(s), 1983(sh). ^1H NMR δ 8.27 (d, 1 H, ^3J=5.04), 7.02 (dd, 1 H, ^3J=3.39, ^3J=5.21), 6.98 (dd, 1 H, ^3J=5.24, ^4J=1.15), 6.82 (dd, 1 H, ^3J=3.42, ^4J=1.15), 5.98 (d, 1 H, ^3J=5.06), 4.35 (d, 1 H, ^2J=22.01),

4.21 (d, 1 H, ^2J=22.01), –16.93 (s, 1 H). FAB MS (m/z) obs. 1040, calc. 1068. Anal. Calcd for $C_{22}H_8O_{10}S_2Os_3$: C, 24.7; H, 0.75. Found: C, 24.6; H, 0.9 .

4b: IR (CH_2Cl_2), ν_{CO}/cm^{-1}: 2099(w), 2083(m), 2066(vs), 2055(sh), 2033(m), 2018(m), 1998(mw). ^{1}H NMR δ 8.27 (d, 1 H, ^3J=5.08), 7.36 (dd, 1 H, ^3J=4.35, ^3J=0.88), 7.17 (dd, 1 H, ^3J=3.50, ^4J=0.86), 7.01 (dd, 1 H, ^3J=4.35, ^4J=3.46), 6.51 (d, 1 H, ^3J=5.06), 3.76 (d, 1 H, ^2J=22.53), 3.48 (d, 1 H, ^2J=22.53), –17.18 (s, 1 H). FAB MS (m/z) obs. 1040, calc. 1068.

6.1.4 Thermal decarbonylation of 3

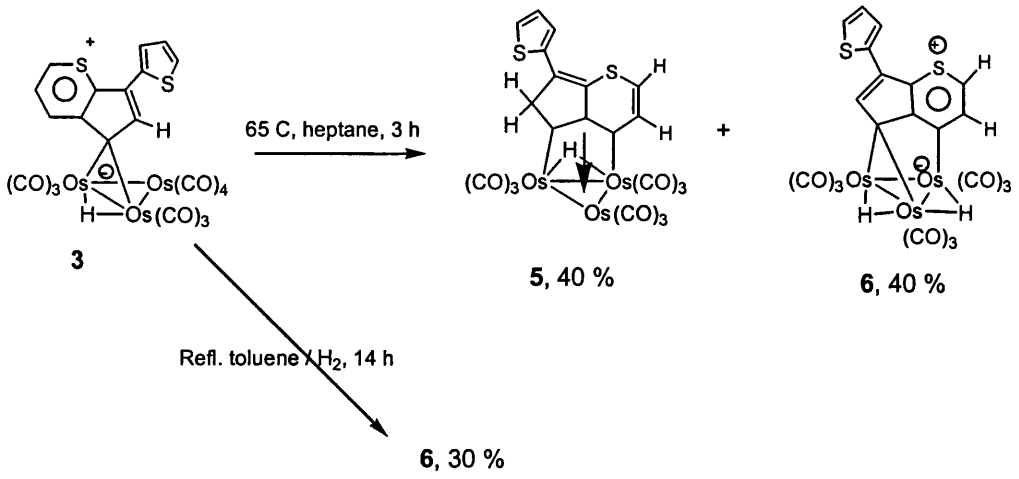

3 (60 mg, 0.056 mmol) was dissolved in heptane (35 mL) and was heated to 65°C under nitrogen for 3 hours. The resulting orange solution was cooled to room temperature and the solvent removed under reduced pressure. Work up of the crude products by TLC (eluent: dichloromethane/hexane 3:7) recovered approximately equal amounts of orange and red products.

The orange product (yield 40 %) (with a high Rf value,) was recrystallised from dichloromethane as a microcrystalline solid that was characterized by spectroscopic methods and single crystal X-ray diffraction as $[Os_3(\mu\text{-}H)(CO)_9\{(\mu_3\text{-}\eta^3\text{-}(C_4H_3S)(C_8H_4S)\}]$ (**5**).

IR (CH_2Cl_2), ν_{CO} /cm^{-1}: 2096(s), 2069(vs), 2047(vs), 2016(m), 2001(m), 1986(sh). ^{1}H NMR δ 7.31 (dd, 1 H, ^3J=5.07, ^4J=1.05), 7.13 (dd, 1 H, ^3J=3.66, ^3J=5.07), 7.10 (dd, 1 H, ^3J=3.65, ^4J=1.1.05), 7.04 (d, 1 H, ^3J=9.64), 6.44 (d, 1 H, ^3J=9.62), 3.68 (d, 1 H, ^2J=22.98), 3.52 (d, 1 H, ^2J=22.98), –18.58 (s, 1 H). FAB MS (m/z) obs. 1040, calc. 1040. Anal. Calcd for $C_{21}H_8O_{10}S_2Os_3$: C, 24.2; H, 1.21. Found: C, 24.8; H, 1.66.

The second product yielded dark red crystals from the slow evaporation of a chloroform solution at –20°C. Spectroscopic studies and single crystal X-ray diffraction of the crystals led to the identification of this product as $[Os_3(\mu\text{-}H)_2(CO)_9\{(\mu_3\text{-}\eta^1\text{-}\eta^1\text{-}(C_4H_3S)(C_8H_3S)\}]$ (**6**).

IR (CH_2Cl_2), ν_{CO} /cm^{-1}: 2103(m), 2071(vs), 2043(vs), 2025(m), 1996(m), 1982(sh), 1963(m). ^{1}H NMR δ 8.46 (d, 1 H, ^3J=8.56), 7.96 (d, 1 H, ^3J=8.57), 7.84 (s, 1 H), 7.51 (dd, 1 H, ^3J=3.68,

^4J=1.06), 7.38 (dd, 1 H, ^3J=5.10, ^4J=1.06), 7.15 (dd, 1 H, ^3J=3.65, ^3J=5.10), –14.38 (s, 1 H), –15.58 (s, 1 H). FAB MS (m/z) obs. 1040, calc. 1040. Anal. Calcd for $C_{21}H_8O_{10}S_2Os_3$: C, 24.2; H, 1.21. Found: C, 24.1; H, 1.5.

6 was also formed (in approximately 20 % yield) when **3** (36 mg, m mol) was refluxed in toluene (40 mL) under hydrogen for 14 hours. TLC separation of the reaction mixture showed the presence of dark brown immobile decomposition product and on the top of the silica plate a small amount of the dihydride carbonyl cluster $[Os_3(\mu\text{-}H)_2(CO)_{10}]$, but no trace of cluster **5**.

6.1.5 Thermal decarbonylation of 4a and 4b

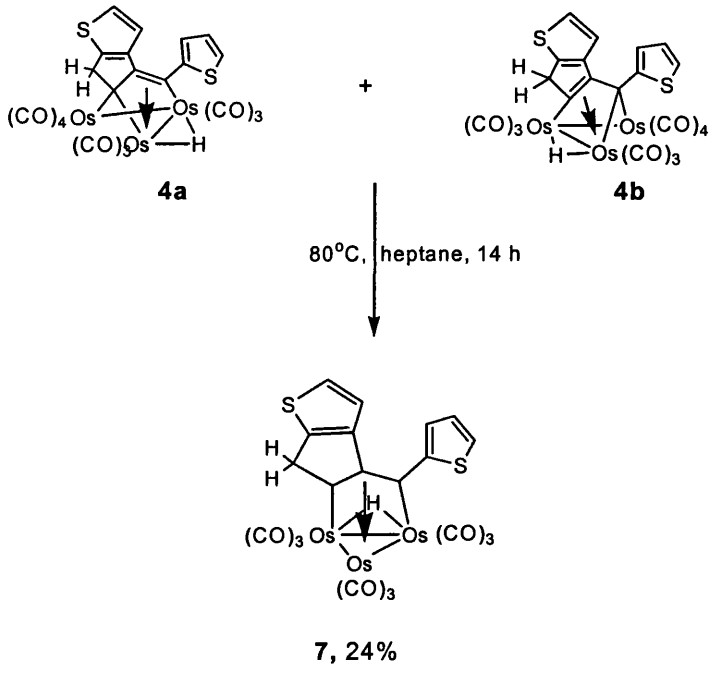

The isomeric mixture **4a** and **4b** (30 mg, 0.03 mmol) was dissolved in heptane (30 mL) and heated to 90°C under nitrogen. The reaction was quenched after 27 hours, when the IR sample showed strong ν(CO) absorptions indicating the presence of a new cluster carbonyl species. The resulting yellow solution was cooled to room temperature, and the solvent removed under reduced pressure. In addition to the unreacted isomeric mixture of 4a and 4b (6mg, 20%), work up by TLC (eluent: dichloromethane/hexane 1:4) yielded a decarbonylated yellow product characterized by spectroscopic techniques as $[Os_3(\mu\text{-}H)(CO)_9\{(\mu_3\text{-}\eta^3\text{-}(C_4H_3S)(C_8H_4S)\}]$ (**7**) (7mg, 24 %). Crystals suitable for single crystal X-ray diffraction were grown by solvent diffusion from a dichloromethane/heptane mixture.

IR (CH_2Cl_2), ν_{CO} / cm^{-1}: 2097(s), 2072(vs), 2045(s), 2018(sh), 2004(s), 1990(sh). ^1H NMR δ 7.49 (dd, 1 H, ^3J=4.80, ^4J=3.20), 7.20 (d, 1 H, ^3J=4.80), 7.17 (dd, 1 H, ^3J=4.80, ^4J=1.20), 7.03 (dd, 1 H, ^4J=2.70, ^4J=1.20), 6.81 (d, 1 H, ^3J=4.8), 3.60 (d, 1 H, ^2J=22.20), 3 .30 (d, 1 H, ^2J=22.20), –18.72 (s, 1 H). FAB MS (m/z) 1040, calc. 1040. Owing to the small amount of the product, elemental analysis was not acquired for cluster **7**.

6.1.6 Reaction of cluster 1 with trifluoroacetic acid

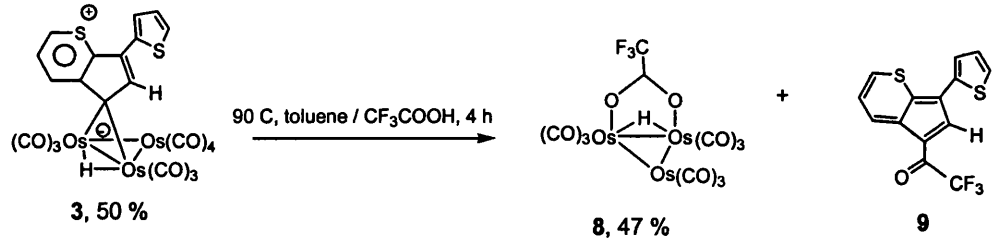

3, 50 %

8, 47 %

9

5, 6 % + **6**, 20 %

Triflouroacetic acid (CF_3COOH) (99 %, 1.5 mL) was added dropwise to a toluene solution (50 mL) of **3** (50 mg, 0.05 mmol). The resulting dark green mixture was heated to 90°C under nitrogen and the reaction monitored by TLC spot tests. It was quenched after 3 hours when starting cluster was consumed. The resulting dark reddish-violet solution was cooled to room temperature, and the solvent removed under reduced pressure. Work up by TLC (eluent: dichloromethane/hexane 1:3) yielded small amounts of the expected decarbonylated clusters **5** (3 mg, 6.1 %), and **6** (10 mg, 20.5 %), as well as a yellow product (high Rf) characterized as $[Os_3(\mu\text{-}H)(CO)_{10}(O_2CCF_3)]$ (8) (21 mg, 47 %). The spectroscopic data for **8** were in accordance with the previously reported values.[5] Crystals suitable for single crystal X-ray diffraction were grown by slow evaporation from a dichloromethane solution at –20°C.

A fourth, intensely deep blue coloured product **9** (10 mg) was separated from the bottom of the TLC plate. Spectroscopic analysis and single crystal X-ray diffraction identified the compound as the organic fragment cleaved from the parent cluster. Crystals suitable for single crystal X-ray diffraction were grown from slow evaporation of dichloromethane and chloroform solutions under nitrogen at –20°C.

9 IR (CH_2Cl_2), ν_{CO}/cm^{-1}:not observed; ν_{COO}/cm^{-1}: 1662(m). ^1H NMR δ 9.34 (d, 1 H, ^3J=8.11), 8.28 (m, 1 H), 8.24 (d, 1 H, ^3J=8.71), 7.71 (dd, 1 H, ^3J=8.11, ^3J=8.71, 7.40 (dd, 1 H, ^3J=3.60, ^4J=0.90), 7.29 (dd, 1 H, ^3J=4.95, ^4J=0.60), 7.12 (dd, 1 H, ^3J=4.95, ^4J=3.60). FAB MS (m/z) obs. 312, calc. 312 for $C_{12}H_7S_2CF_3CO$.

6.2 Thermolysis/ Pyrolysis Reactions of $Ru_3(CO)_{12}$ Clusters under Microwave Irradiation

Materials. All reagents were of analytical grade obtained from commercial suppliers and were used as received. The reactions were performed under nitrogen using pre-dried solvents. All manipulations of the products were also carried out in air. Microwave reaction tubes were rinsed with DCM and dried under nitrogen prior to use.

Chromatography. Thin layer chromatography (TLC) was performed on commercial 20 x 20 cm plates (Aldrich) covered with Merck silica gel 60 F254 to 0.25 or 1.0 mm thickness.

Microwave irradiation was carried out on a CEM MDS2000 Microwave Cavity.

6.2.1 Synthesis of $Ru_6C(CO)_{14}[\eta^6-(C_6H_5)CH_3]$ (10)

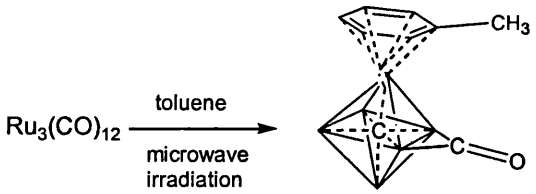

$Ru_3(CO)_{12}$ (25mg, 0.039mmol) was stirred in toluene (4 mL) for 30 minutes in a sealed reaction tube under nitrogen. This was then irradiated at 300W for 60 minutes at 230°C.
The resultant solution was a deep red colour with a small amount of black precipitate and a shiny metallic precipitate on the tube walls, presumed to be metallic ruthenium. The reaction mixture was concentrated under reduced pressure and separated using TLC (eluent: hexane/DCM 1:1). The deep red product obtained from the middle of the plate was recrystallised from DCM affording single crystals suitable for X-ray analysis (Yield: 10mg, 46.5%)

6.2.2 Synthesis of $Ru_6C(CO)_{17}$ (11)

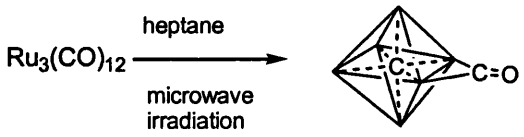

This reaction was based on previously reported methods carried out in an autoclave[6, 7].
The reaction tubes were first flushed with nitrogen and then with ethylene gas. $Ru_3(CO)_{12}$ (32mg, 0.05 mmol) was stirred in heptane (5 mL) for 15 minutes in the sealed reaction-tube under ethylene gas.

The microwave-irradiation occurred in a three-step process. First, it was irradiated at 200W for 30 minutes at 80°C, this was then increased to 300W for 60 minutes at 150°C. Finally the temperature was increased to 180°C and held for another 60 minutes.

The resultant solution was a deep red colour with a small amount of deep red precipitate and some orange starting material. The reaction mixture was concentrated under reduced pressure and separated using TLC (eluent: hexane/DCM 1:1). The deep red product obtained from the middle of the plate was recrystallised from DCM affording single crystals suitable for X-ray analysis (Yield: 20mg, 73%)

6.2.3 Synthesis of $Ru_3(\mu_2\text{-}CO)_2(CO)_8$(bipy) (12)

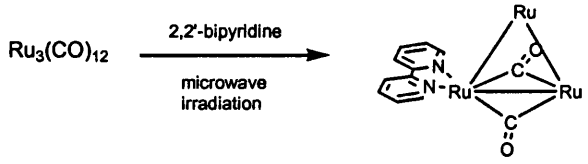

This reaction was based on previously reported methods carried out by reflux[8].
$Ru_3(CO)_{12}$ (0.040mg, 0.063 mmol) and 2,2'-bipyridine (10mg, 0.063 mmol) was stirred in cyclohexane (5 mL) for 15 minutes in the sealed reaction tube under nitrogen.

The microwave-irradiation occurred in a two-step process. First, it was irradiated at 200W for 5 minutes at 50°C, this was then increased to 300W for 10 minutes at 100°C.

The resultant solution was dark brown with a small amount of black precipitate. The reaction mixture was reduced under pressure and separated using TLC (eluent: hexane/DCM 1:1). The reddish-brown product obtained was recrystallised from dicholoromethane affording single crystals suitable for X-ray analysis (Yield: 36mg, 77.3 %)

6.3 Lanthanide Coordination Complexes

Materials. All reagents were of analytical grade obtained from commercial suppliers and were used as received. The reactions were performed in air using solvents as obtained, unless stated otherwise. All manipulations of the products were also carried out in air.

Spectroscopic Studies. Infrared spectra were measured using a Nicolet Avatar 360 FTIR spectrometer from nujol mulls. Elemental analysis was performed on an Exeter Analytical Inc. CE-440 Elemental Analyser. Luminescence measurements were carried out on a Perkin Elmer LS55 Spectrophotometer.

Microanalyses of the lanthanide compounds were carried out but the analyses tended to be misleading. With the facilities available, limited precautions could be taken in handling the compounds prior to microanalysis and it is believed that loss of solvent, methanol, ethanol and water occurred (in some cases unprotected crystals rapidly deteriorated upon exposure to air).

6.3.1 Lanthanide 2,2': 6'2'' terpyridine (terpy) complexes

6.3.1.1 A) Synthesis of $[Ln(terpy)_2(NCS)_3]$; Ln = La, Ce, Pr, Nd, Sm, Eu, Gd, Tb, Dy, Ho
B) Synthesis of $\{[Ln(terpy)_2(NCS)_2]^+ [Ln(terpy)(NCS)_4(H_2O)]^- 2EtOH\}$ Ln= Er, Tm, Lu

Solutions of $LnCl_3.xH_2O$ (0.4 mmol), KNCS (0.117 g; 1.2 mmol) and terpy (0.187 g; 0.8mmol) were warmed in ethanol (5 mL). KNCS was added to the $LnCl_3.xH_2O$ solution followed by terpy. A pale white precipitate was formed almost immediately. After stirring for 15 minutes, the precipitate was collected by filtration over Whatman's No.6 filter paper. The air-dried precipitate was then dissolved in boiling methanol (30 mL) and left to crystallise whereupon crystals of the corresponding metal $[Ln(terpy)_2(NCS)_3]$ and $\{[Ln(terpy)_2(NCS)_2]^+ [Ln(terpy)(NCS)_4(H_2O)]^- .2EtOH\}$ were obtained.

6.3.2 Lanthanide 1,3,5-tri-(2-pyridyl)-2,4,6-triazine (tptz) complexes

6.3.2.1 Synthesis of $[Ln(tptz)(NO)_3.xEtOH]$ {x=2, Ln= La, Ce, Pr, Nd, Sm, Eu, Gd, Tb, Dy, Ho, Er, Tm, Yb; *x*=1, Ln= Yb, Lu}

This was prepared essentially by the literature method,[9] as follows. A hot solution of $Ln(NO_3)_3.xH_2O$ (0.18 mmol) in ethanol (5 mL) was mixed with a solution of 2, 4, 6-tri-α-pyridyl-1,3,5-triazine (0.05 g; 0.16 mmol) in ethanol (25 mL) and allowed to stand overnight, when corresponding crystals of $[Ln(tptz)(NO)_3.xEtOH]$ were obtained.

6.3.3 Lanthanide 1,10-phenanthroline (phen) complexes

6.3.3.1 Synthesis of $[Ln(phen)_3(NCS)_3]$; {Ln = Y, La, Ce, Pr, Nd, Sm and Eu}

A solution of $Ln(NO_3)_3.xH_2O$ (0.38 mmol) in ethanol (2 mL) was mixed with a solution of KNCS (0.12 g; 1.24 mmol) in ethanol (5 mL). After standing for 15 minutes, the solution was filtered to remove the crystals of KNO_3 and heated to approximately 70 °C. It was mixed with a hot solution of phen (0.21 g; 1.16 mmol) in ethanol (60 mL) and allowed to crystallise overnight, whereupon crystals of the corresponding metal $[Ln(phen)_3(NCS)_3.xEtOH]$ were obtained.

6.3.3.2 Synthesis of $[Ln(phen)_2(NCS)_3.MeOH].phen$; {Ln= Gd, Tb, Ho, Er, Tm, Yb and Lu}

A solution of $Ln(NO_3)_3.xH_2O$ (0.38 mmol) in methanol (2 mL) was mixed with a solution of KNCS (0.12 g; 1.24 mmol) in methanol (5 mL). After standing for 15 minutes, the solution was filtered to remove the crystals of KNO_3 and heated to approximately 70 °C. It was mixed with a hot solution of phen (0.21 g; 1.16 mmol) in methanol (60 mL) and allowed to crystallise overnight, whereupon corresponding crystals of {$[Ln(phen)_2(NCS)_3.EtOH].phen$} were obtained.

6.3.3.3 Synthesis of $[Ln(phen)_2(NCS)_2(NO_3).EtOH]$ {Ln =Y, La, Ce, Pr, Nd, Sm, Tb, Dy, Ho}

A solution of $Ln(NO_3)_3.xH_2O$ (0.38 mmol) in ethanol (2 mL) was mixed with a solution of KNCS (0.074 mg, 0.76 mmol) in ethanol (5 mL); after standing for 15 minutes, the solution was filtered to remove the crystals of KNO_3 and heated to ~70 °C. It was mixed with a hot solution of phen (0.137 g; 0.76 mmol) in ethanol (60 mL) and allowed to crystallise overnight, whereupon corresponding crystals of {$[Ln(phen)_2(NCS)_3.EtOH].phen$} were obtained.

6.3.4 Lanthanum Polymers

Full spectroscopic characterization of the polymers was not possible because of their insolubility in common solvents.

6.3.4.1 Synthesis of $[La(O_2CPh)_3(CH_3OH)_3(H_2O)]_n$

Benzoic acid (1.8g, 14.73 mmol) and KOH (2 ml, 1M) in water (10 mL) was stirred at room temperature for 15 minutes. This was then added to a warm solution of $LaCl_3.7H_2O$(1.82g, 4.91 mmol) in methanol (10 mL). A white precipitate was formed immediately. The precipitate was filtered and washed with methanol (5mL) and diethyl ether (5 mL). The product was dissolved in hot methanol (10 mL) for crystallization and colourless single

crystals suitable for single crystal X-ray diffraction were obtained upon slow evaporation of the solvent.

6.3.4.2 Synthesis of $[La(O_2CPh)_3(H_2O)_2\ bpy]_n$ (2,2' bipyridine = bpy)

Benzoic acid (1.8g, 14.73 mmol) and KOH (2 ml, 1M) in water was stirred at room temperature for 15 minutes and then added to a mixture of 2,2' bipyridine (0.77g, 4.91 mmol) and $LaCl_3.7H_2O$(1.82g, 4.91 mmol) in methanol (10 mL). A white precipitate was formed immediately. The precipitate was filtered and washed with methanol (5 mL) and diethyl ether (5 mL). The product was dissolved in hot methanol (10 mL) for crystallisation and colourless single crystals suitable for single crystal X-ray diffraction were obtained upon slow evaporation of the solvent.

6.4 Single Crystal X-ray Crystallography

6.4.1 Experimental

Data Collection and Processing - Single crystal data collection was carried out on a Bruker Nonius Kappa CCD diffractometer using graphite monochromated Mo-Kα radiation or a Bruker AXS SMART diffractometer on Station 9.8 Daresbury on the CLRC Daresbury synchrotron. Both were equipped with an Oxford Cryostream cooling apparatus. The data sets were corrected for Lorentz and polarisation effects and for absorption using SORTAV[10] or SADABS[11]. Structure solution was achieved either by direct methods using Sir-92[12], Sir-97[13] or by Patterson methods using Dirdiff-99[14] and refined by full-matrix least-squares on F^2 (SHELXL 97 [15]) with all non-hydrogen atoms assigned anisotropic displacement parameters. Hydrogen atoms attached to carbon atoms were placed in idealised positions and allowed to ride on the relevant carbon atom. The hydrides on the metal clusters (Chapter 3) were based on calculated positions by XHYDEX[16]. In the final cycles of refinement a weighting scheme that gave a relatively flat analysis of variance was introduced and refinement continued until convergence was reached.

[1] H.D. Kaesz, *Inorg. Synth.*, 1990, **28**, 238.
[2] Sarkar, A.; Talvar, S. S. *J. Chem. Soc., Perkin Trans.* 1998, 4141.
[3] Sarkar, A.; Okada, S.; Nakanishi, H.; Matsuda, H. *Helv. Chim. Acta.* 1999, **82**, 138
[4] Lionel Clarke; PhD Thesis; The Chemistry of Osmium and Ruthenium Diyne Clusters; 1997; Cambridge.
[5] E.G. Bryan, B.F.G. Johnson, J. Lewis, *J. Chem. Soc., Dalton Trans.*, 1977, 1328.
[6] G.Freeman, S.L. Ingham, B.F.G. Johnson, M. McPartlin and I.J. Scowen, *J. Chem Soc Dalton Trans.*, 1997, 2705.
[7] D. Braga, F. Grepioni, P.J. Dyson, B.F.G. Johnson, P. Frediani, M. Bianchi and F. Piacenti, *J. Chem Soc Dalton Trans.*, 1992, 2565.
[8] Michael I. Bruce, Mark G. Humphrey, Michael R. Snow, Edward R. T. Tiekink and Robert C. Wallis, *J. Organometallic Chem.*, 1986, **314**, 311.
[9] D.A.Durham, G.H.Frost and F.A.Hart, *J. Inorg. Nucl. Chem.*, 1969, **31**, 571
[10] R.H. Blessing, *Acta Crystallogr. Sect. A*, 1995, **51**, 33.
[11] S.P. Sinha, Z. *Naturforsch., Teil. A,* 1965, **20**, 1661.
[12] SIR-92 -A. Altomare, G. Cascarano, C. Giacovazzo and A. Guagliardi, *J. Appl. Crystallogr.* 1993, **26**, 343.
[13] SIR-97 - Altomare A., Burla M.C., Camalli M., Cascarano G.L., Giacovazzo C., Guagliardi A., Moliterni A.G.G., Polidori G.,Spagna R., *J. Appl. Cryst.*, 1999, **32**, 115.
[14] DIRDIF96 program system. P. T. Beurskens, G. Beurskens, W. P. Bosman, R. de Gelder, S. Garcia-Granda, R. O. Gould, R. Israel and J. M. M. Smits, Crystallography Laboratory, University of Nijmegen, The Netherlands. 1996.
[15] G.M. Sheldrick, SHELXL A program for crystal structure refinement, University of Göttingen, 1986.
[16] XHYDEX - A. G. Orpen, *J. Chem. Soc. Dalton Trans.* 1980, 2509

APPENDIX I

CRYSTAL STRUCTURE DATA

Identification code	h01prr5	k01prr36	k01prr62	k02prr3
Empirical formula	C22 H8 O10 Os3 S2	C21 H8 O9 Os3 S2	C22 H10 Cl2 O9 Os3 S2	C22 H11 Cl2 O9 Os3 S2
Formula weight	1067.00	1038.99	1123.92	1124.93
Temperature	150(2) K	299(2) K	150(2) K	150(2) K
Wavelength	0.71073 Å	0.71073 Å	0.71073 Å	0.71073 Å
Crystal system	Monoclinic	Triclinic	Monoclinic	Triclinic
Space group	P $2_1/c$	P -1	P $2_1/n$	P -1
Unit cell dimensions	a = 9.58200(10) Å	a = 9.79140(10) Å	a = 10.13450(10) Å	a = 8.0318(1) Å
	b = 12.8410(2) Å	b = 9.8672(2) Å	b = 10.08430(10) Å	b = 13.0303(2) Å
	c = 20.8926(3) Å	c = 14.7041(3) Å	c = 24.6832(3) Å	c = 13.3423(2) Å
	α= 90°.	α= 101.2340(10)°.	α= 90°.	α= 93.248(1)°.
	β= 99.6670(10)°.	β= 96.8400(10)°.	β= 92.7790(10)°.	β= 97.560(1)°.
	γ = 90°.	γ = 115.9360(10)°.	γ = 90°.	γ = 101.826(1)°.
Volume	2534.17(6) $Å^3$	1218.98(4) $Å^3$	2519.64(5) $Å^3$	1349.80(3) $Å^3$
Z	4	2	4	2
Density (calculated)	2.797 Mg/m^3	2.831 Mg/m^3	2.963 Mg/m^3	2.768 Mg/m^3
Absorption coefficient	15.223 mm^{-1}	15.817 mm^{-1}	15.522 mm^{-1}	14.487 mm^{-1}
F(000)	1920	932	2032	1018
Crystal size	0.30 x 0.30 x 0.30 mm^3	0.30 x 0.10 x 0.05 mm^3	0.25 x 0.13 x 0.10 mm^3	0.18 x 0.13 x 0.05 mm^3
Theta range for data collection	2.98 to 27.47°.	3.71 to 30.09°.	2.94 to 28.68°.	3.60 to 27.54°.
Index ranges	-12<=h<=12, -15<=k<=16, -27<=l<=27	-13<=h<=13, -13<=k<=13, -20<=l<=20	-13<=h<=13, -13<=k<=13, -33<=l<=33	-10<=h<=10, -16<=k<=16, -17<=l<=17
Reflections collected	34765	21119	31649	29766
Independent reflections	5794 [R(int) = 0.0776]	7117 [R(int) = 0.0798]	6015 [R(int) = 0.1118]	6187 [R(int) = 0.0817]
Completeness to theta = 25.00°	99.8 %	99.3 %	92.6 %	99.4 %
Absorption correction	Multiscan	Multiscan	Multiscan	Multiscan
Max. and min. transmission	0.0919 and 0.0919	0.470 and 0.074	0.3059 and 0.1125	0.510 and 0.289
Refinement method	Full-matrix least-squares on F^2	Full-matrix least-squares on F^2	Full-matrix least-squares on F^2	Full-matrix least-squares on F^2
Data / restraints / parameters	5794 / 0 / 334	7117 / 0 / 321	6015 / 0 / 343	6187 / 0 / 355
Goodness-of-fit on F^2	1.115	1.037	1.152	1.033
Final R indices [I>2sigma(I)]	R1 = 0.0382, wR2 = 0.1009	R1 = 0.0508, wR2 = 0.1300	R1 = 0.0425, wR2 = 0.1126	R1 = 0.0399, wR2 = 0.1005
R indices (all data)	R1 = 0.0433, wR2 = 0.1036	R1 = 0.0601, wR2 = 0.1378	R1 = 0.0527, wR2 = 0.1319	R1 = 0.0472, wR2 = 0.1052
Largest diff. peak and hole	2.253 and -1.294 $e.Å^{-3}$	3.198 and -4.161 $e.Å^{-3}$	1.907 and -6.440 $e.Å^{-3}$	4.127 and -3.960 $e.Å^{-3}$

Identification code	k02prr1	k01prr61	bath34
Empirical formula	C21 H8 O9 Os3 S2	C12 H F3 O12 Os3	C14 H7 F3 O S2
Formula weight	1038.99	964.73	312.32
Temperature	150(2) K	150(2) K	293(2) K
Wavelength	0.71073 Å	0.71073 Å	0.68410 Å
Crystal system	Monoclinic	Orthorhombic	Monoclinic
Space group	P 2_1/c	P bca	P 2_1/n
Unit cell dimensions	a = 7.1181(1) Å	a = 14.4142(3) Å	a = 5.1020(6) Å
	b = 9.3994(2) Å	b = 16.1384(4) Å	b = 13.007(2) Å
	c = 35.2309(7) Å	c = 14.1976(4) Å	c = 18.958(2) Å
	α= 90°.	α= 90°.	α= 90°.
	β= 95.504(1)°.	β= 90°.	β= 95.236(2)°.
	γ = 90°.	γ = 90°.	γ = 90°.
Volume	2346.29(8) $Å^3$	3302.68(14) $Å^3$	1252.8(3) $Å^3$
Z	4	8	4
Density (calculated)	2.941 Mg/m^3	3.880 Mg/m^3	1.656 Mg/m^3
Absorption coefficient	16.435 mm^{-1}	23.129 mm^{-1}	0.452 mm^{-1}
F(000)	1864	3392	632
Crystal size	0.25 x 0.03 x 0.03 mm^3	0.13 x 0.10 x 0.08 mm^3	0.04 x 0.02 x 0.01 mm^3
Theta range for data collection	3.00 to 27.35°.	3.79 to 31.34°.	3.46 to 29.20°.
Index ranges	-9<=h<=9, -12<=k<=12, -45<=l<=45	-17<=h<=18, -20<=k<=20, -21<=l<=21	-6<=h<=7, -18<=k<=17, -21<=l<=27
Reflections collected	24322	22773	8683
Independent reflections	5248 [R(int) = 0.1446]	4301 [R(int) = 0.0900]	3504 [R(int) = 0.0329]
Completeness to theta = 25.00°	99.0 %	79.4 %	92.1 %
Absorption correction	Multiscan	Multiscan	SADABS
Max. and min. transmission	0.737 and 0.234	0.2591 and 0.1530	0.9955 and 0.9821
Refinement method	Full-matrix least-squares on F^2	Full-matrix least-squares on F^2	Full-matrix least-squares on F^2
Data / restraints / parameters	5248 / 0 / 315	4301 / 0 / 275	3504 / 0 / 187
Goodness-of-fit on F^2	1.120	1.003	1.045
Final R indices [I>2sigma(I)]	R1 = 0.0506, wR2 = 0.1129	R1 = 0.0402, wR2 = 0.0848	R1 = 0.0526, wR2 = 0.1412
R indices (all data)	R1 = 0.0852, wR2 = 0.1423	R1 = 0.0643, wR2 = 0.0944	R1 = 0.0596, wR2 = 0.1471
Largest diff. peak and hole	3.205 and -4.159 $e.Å^{-3}$	3.509 and -3.654 $e.Å^{-3}$	1.050 and -0.544 $e.Å^{-3}$

Identification code	k02prr21	k03prr5	h03prr7
Empirical formula	C22 H8 O14 Ru6	C18 O17 Ru6	C20 H8 N2 O10 Ru3
Formula weight	1102.70	1094.60	739.49
Temperature	150(2) K	150(2) K	150(2) K
Wavelength	0.71073 Å	0.71073 Å	0.71073 Å
Crystal system	Orthorhombic	Monoclinic	Monoclinic
Space group	P nam	P 2_1/n	P2_1/n
Unit cell dimensions	a = 12.4692(3) Å	a = 9.1192(2) Å	a = 7.7321(1) Å
	b = 14.2112(5) Å	b = 31.8826(6) Å	b = 25.7473(3) Å
	c = 14.8738(4) Å	c = 9.4987(2) Å	c = 11.6511(1) Å
	α= 90°.	α= 90°.	α= 90°.
	β= 90°.	β= 112.2350(10)°.	β= 107.897(1)°.
	γ = 90°.	γ = 90°.	γ = 90°.
Volume	2635.67(13) $Å^3$	2556.33(9) $Å^3$	2207.27(4) $Å^3$
Z	4	4	4
Density (calculated)	2.779 Mg/m^3	2.844 Mg/m^3	2.225 Mg/m^3
Absorption coefficient	3.423 mm^{-1}	3.536 mm^{-1}	2.088 mm^{-1}
F(000)	2064	2032	1416
Crystal size	0.15 x 0.13 x 0.05 mm^3	0.13 x 0.10 x 0.03 mm^3	0.40 x 0.08 x 0.08 mm^3
Theta range for data collection	3.27 to 30.02°.	2.93 to 25.00°.	2.92 to 27.48°.
Index ranges	-16<=h<=17, -19<=k<=20, -20<=l<=20	-10<=h<=10, -37<=k<=37, -11<=l<=11	-10<=h<=10, -33<=k<=33, -15<=l<=15
Reflections collected	21546	13174	35859
Independent reflections	3983 [R(int) = 0.1096]	4010 [R(int) = 0.0551]	5040 [R(int) = 0.0573]
Completeness to theta = 25.00°	99.8 %	89.0 %	99.9 %
Absorption correction	Multiscan	Multiscan	Multiscan
Max. and min. transmission	0.845 and 0.721	0.903 and 0.795	0.858 and 0.716
Refinement method	Full-matrix least-squares on F^2	Full-matrix least-squares on F^2	Full-matrix least-squares on F^2
Data / restraints / parameters	3983 / 0 / 205	4010 / 0 / 370	5040 / 0 / 316
Goodness-of-fit on F^2	0.990	1.181	1.229
Final R indices [I>2sigma(I)]	R1 = 0.0456, wR2 = 0.0795	R1 = 0.0353, wR2 = 0.0750	R1 = 0.0258, wR2 = 0.0682
R indices (all data)	R1 = 0.1121, wR2 = 0.1007	R1 = 0.0533, wR2 = 0.0978	R1 = 0.0385, wR2 = 0.0973
Largest diff. peak and hole	1.614 and -1.460 $e.Å^{-3}$	1.182 and -1.159 $e.Å^{-3}$	0.963 and -2.286 $e.Å^{-3}$

Identification code	h01prr14	h01prr12	bath41	k01prr13
Empirical formula	C23 H31 La N6 O5 S3	C35 H30 La N9 O2 S3	C33 H22 N9 Nd S3	C33 H22 Eu N9 S3
Formula weight	706.63	843.77	785.02	792.74
Temperature	100(2) K	100(2) K	150(2) K	180(2) K
Wavelength	0.71073 Å	0.71073 Å	0.68670 Å	0.71073 Å
Crystal system	Orthorhombic	Monoclinic	Triclinic	Orthorhombic
Space group	P bca	C 2/c	P -1	P can
Unit cell dimensions	a = 15.57080(10) Å	a = 19.572(4) Å	a = 12.5114(4) Å	a = 10.4043(3) Å
	b = 16.5161(2) Å	b = 12.915(3) Å	b = 15.3681(5) Å	b = 16.7646(5) Å
	c = 23.6877(2) Å	c = 16.816(3) Å	c = 16.7776(5) Å	c = 18.9281(7) Å
	α= 90°.	α= 90°.	α= 81.827(2)°.	α= 90.000(1)°.
	β= 90°.	β= 121.66(3)°.	β= 89.147(2)°.	β= 90.000(1)°.
	γ = 90°.	γ = 90°.	γ = 89.338(2)°.	γ = 90.000(1)°.
Volume	6091.74(10) $Å^3$	3618.0(13) $Å^3$	3192.67(17) $Å^3$	3301.51(18) $Å^3$
Z	8	4	4	4
Density (calculated)	1.541 Mg/m^3	1.549 Mg/m^3	1.633 Mg/m^3	1.595 Mg/m^3
Absorption coefficient	1.649 mm^{-1}	1.400 mm^{-1}	1.862 mm^{-1}	2.128 mm^{-1}
F(000)	2848	1696	1564	1576
Crystal size	0.25 x 0.20 x 0.05 mm^3	0.25 x 0.20 x 0.16 mm^3	0.02 x 0.02 x 0.02 mm^3	0.35 x 0.35 x 0.20 mm^3
Theta range for data collection	2.92 to 30.02°.	2.00 to 30.01°.	1.94 to 30.47°.	3.15 to 27.47°.
Index ranges	-21<=h<=21, -23<=k<=23, -33<=l<=33	-27<=h<=27, -18<=k<=16, -23<=l<=23	-17<=h<=17, -20<=k<=21, -23<=l<=23	-10<=h<=13, -16<=k<=21, -24<=l<=24
Reflections collected	102313	19967	33113	14118
Independent reflections	8880 [R(int) = 0.0739]	5294 [R(int) = 0.0447]	17421 [R(int) = 0.0329]	3758 [R(int) = 0.0796]
Completeness to theta = 25.00°	99.9 %	99.8 %	89.7 %	99.3 %
Absorption correction	Multiscan	Multiscan	SADABS	None
Max. and min. transmission	0.9221 and 0.6832	0.8071 and 0.7211	0.9637 and 0.9637	0.6755 and 0.5229
Refinement method	Full-matrix least-squares on F^2	Full-matrix least-squares on F^2	Full-matrix least-squares on F^2	Full-matrix least-squares on F^2
Data / restraints / parameters	8880 / 0 / 387	5294 / 5 / 257	17421 / 0 / 829	3758 / 0 / 210
Goodness-of-fit on F^2	1.043	1.371	1.025	1.022
Final R indices [I>2sigma(I)]	R1 = 0.0289, wR2 = 0.0597	R1 = 0.0433, wR2 = 0.1335	R1 = 0.0312, wR2 = 0.0747	R1 = 0.0356, wR2 = 0.0725
R indices (all data)	R1 = 0.0510, wR2 = 0.0653	R1 = 0.0521, wR2 = 0.1542	R1 = 0.0414, wR2 = 0.0787	R1 = 0.0716, wR2 = 0.0827
Largest diff. peak and hole	0.704 and -0.855 $e.Å^{-3}$	0.817 and -2.194 $e.Å^{-3}$	1.224 and -1.008 $e.Å^{-3}$	0.541 and -1.137 $e.Å^{-3}$

Identification code	k01prr16	k03prr12	k01prr20	h01prr24
Empirical formula	C34 H25 Eu N9 O0.50 S3	C55 H47 Er2 N15 O3 S6	C22 H26 Ce N9 O12	C22 H24 Lu N9 O11
Formula weight	815.77	1492.96	748.64	762.45
Temperature	396(2) K	150(2) K	150(2) K	150(2) K
Wavelength	0.71073 Å	0.71073 Å	0.71073 Å	0.71073 Å
Crystal system	Monoclinic	Monoclinic	Triclinic	Triclinic
Space group	P $2_1/n$	P $2_1/c$	P -1	P -1
Unit cell dimensions	a = 9.6984(7) Å	a = 12.954(5) Å	a = 9.6076(3) Å	a = 9.5290(1) Å
	b = 13.2538(12) Å	b = 27.708(5) Å	b = 11.0114(4) Å	b = 12.1024(1) Å
	c = 28.613(3) Å	c = 16.178(5) Å	c = 14.4695(6) Å	c = 13.7520(2) Å
	α= 90.000(3)°.	α= 90.000(5)°.	α= 79.538(2)°.	α= 112.302(1)°.
	β= 99.397(3)°.	β= 96.696(5)°.	β= 82.414(2)°.	β= 101.911(1)°.
	γ = 90.000(3)°.	γ = 90.000(5)°.	γ = 88.734(2)°.	γ = 99.098(1)°.
Volume	3628.6(6) $Å^3$	5767(3) $Å^3$	1492.15(9) $Å^3$	1385.87(3) $Å^3$
Z	4	4	2	2
Density (calculated)	1.493 Mg/m^3	1.719 Mg/m^3	1.666 Mg/m^3	1.827 Mg/m^3
Absorption coefficient	1.940 mm^{-1}	3.166 mm^{-1}	1.600 mm^{-1}	3.637 mm^{-1}
F(000)	1628	2952	750	750
Crystal size	0.23 x 0.09 x 0.09 mm^3	0.10 x 0.05 x 0.03 mm^3	0.18 x 0.14 x 0.02 mm^3	0.33 x 0.15 x 0.05 mm^3
Theta range for data collection	3.62 to 21.50°.	2.92 to 27.47°.	3.15 to 27.55°.	2.96 to 29.80°.
Index ranges	-9<=h<=9, -13<=k<=13, -29<=l<=29	-16<=h<=16, -35<=k<=35, -20<=l<=21	-12<=h<=12, -14<=k<=14, -18<=l<=18	-13<=h<=13, -16<=k<=16, -19<=l<=19
Reflections collected	10729	89161	23722	36103
Independent reflections	3963 [R(int) = 0.0945]	13185 [R(int) = 0.1528]	6816 [R(int) = 0.0762]	7829 [R(int) = 0.0572]
Completeness to theta = 25.00°	95.3 %	99.9 %	98.8 %	98.7 %
Absorption correction	Multiscan	Multiscan	Multiscan	Multiscan
Max. and min. transmission	0.8448 and 0.6639	0.801 and 0.714	0.9687 and 0.7616	0.8391 and 0.3799
Refinement method	Full-matrix least-squares on F^2	Full-matrix least-squares on F^2	Full-matrix least-squares on F^2	Full-matrix least-squares on F^2
Data / restraints / parameters	3963 / 0 / 334	13185 / 0 / 736	6816 / 0 / 405	7829 / 0 / 366
Goodness-of-fit on F^2	1.253	1.007	1.046	1.071
Final R indices [I>2sigma(I)]	R1 = 0.1897, wR2 = 0.4180	R1 = 0.0543, wR2 = 0.0695	R1 = 0.0484, wR2 = 0.1095	R1 = 0.0370, wR2 = 0.1051
R indices (all data)	R1 = 0.2150, wR2 = 0.4303	R1 = 0.1362, wR2 = 0.0854	R1 = 0.0865, wR2 = 0.1284	R1 = 0.0425, wR2 = 0.1081
Largest diff. peak and hole	4.653 and -5.486 $e.Å^{-3}$	1.137 and -0.994 $e.Å^{-3}$	1.013 and -0.987 $e.Å^{-3}$	1.981 and -2.829 $e.Å^{-3}$

Identification code	k02prr5	k02prr15	h01prr11	h01prr10
Empirical formula	C20 H17 Lu N10 O10	C21 H28 Lu N9 O14	C41 H30 Ce N9 O S3	C39.50 H28 Dy N9 O S3
Formula weight	732.41	805.49	901.04	903.39
Temperature	150(2) K	150(2) K	150(2) K	150(2) K
Wavelength	0.71073 Å	0.71073 Å	0.71073 Å	0.71073 Å
Crystal system	Monoclinic	Triclinic	Triclinic	Triclinic
Space group	P $2_1/n$	P -1	P -1	P -1
Unit cell dimensions	a = 9.2814(2) Å	a = 9.6852(2) Å	a = 10.9028(4) Å	a = 10.4874(2) Å
	b = 15.5441(4) Å	b = 11.9769(2) Å	b = 12.2506(5) Å	b = 12.5040(3) Å
	c = 17.5975(4) Å	c = 13.4392(3) Å	c = 15.5545(7) Å	c = 15.0373(4) Å
	α= 90°.	α= 90.460(1)°.	α= 97.432(2)°.	α= 95.951(1)°.
	β= 98.308(2)°.	β= 107.242(1)°.	β= 102.631(2)°.	β= 103.968(1)°.
	γ = 90°.	γ = 100.531(1)°.	γ= 100.977(2)°.	γ = 103.267(1)°.
Volume	2512.17(10) $Å^3$	1460.58(5) $Å^3$	1958.22(14) $Å^3$	1835.92(7) $Å^3$
Z	4	2	2	2
Density (calculated)	1.936 Mg/m^3	1.832 Mg/m^3	1.528 Mg/m^3	1.634 Mg/m^3
Absorption coefficient	4.006 mm^{-1}	3.463 mm^{-1}	1.368 mm^{-1}	2.252 mm^{-1}
F(000)	1432	800	906	900
Crystal size	0.25 x 0.05 x 0.05 mm^3	0.20 x 0.05 x 0.03 mm^3	0.20 x 0.14 x 0.05 mm^3	0.15 x 0.08 x 0.04 mm^3
Theta range for data collection	2.96 to 27.50°.	1.59 to 27.46°.	2.94 to 20.58°.	2.94 to 25.20°.
Index ranges	-12<=h<=12, -20<=k<=20, -22<=l<=22	-12<=h<=12, -15<=k<=15, -17<=l<=17	-10<=h<=10, -12<=k<=12, -15<=l<=15	-12<=h<=12, -14<=k<=14, -17<=l<=17
Reflections collected	29333	31549	20710	26992
Independent reflections	5729 [R(int) = 0.0600]	6688 [R(int) = 0.0627]	3916 [R(int) = 0.0777]	6209 [R(int) = 0.1177]
Completeness to theta = 25.00°	99.3 %	99.9 %	98.5 %	93.8 %
Absorption correction	Multiscan	Multiscan	Multiscan	Multiscan
Max. and min. transmission	0.8248 and 0.4341	0.9032 and 0.5443	0.963 and 1.047	0.976 and 1.029
Refinement method	Full-matrix least-squares on F^2	Full-matrix least-squares on F^2	Full-matrix least-squares on F^2	Full-matrix least-squares on F^2
Data / restraints / parameters	5729 / 0 / 371	6688 / 0 / 412	3916 / 0 / 475	6209 / 0 / 490
Goodness-of-fit on F^2	1.047	1.158	1.044	0.947
Final R indices [I>2sigma(I)]	R1 = 0.0322, wR2 = 0.0666	R1 = 0.0293, wR2 = 0.0812	R1 = 0.0426, wR2 = 0.0961	R1 = 0.0470, wR2 = 0.0559
R indices (all data)	R1 = 0.0532, wR2 = 0.0752	R1 = 0.0431, wR2 = 0.1090	R1 = 0.0641, wR2 = 0.1052	R1 = 0.1103, wR2 = 0.0654
Largest diff. peak and hole	1.044 and -1.251 $e.Å^{-3}$	0.965 and -2.700 $e.Å^{-3}$	1.057 and -0.468 $e.Å^{-3}$	0.681 and -0.818 $e.Å^{-3}$

Identification code	k01prr9	h02prr9	h02prr1	k02prr7
Empirical formula	C27 H20 Cl0 N7 O4 S2 Tb	C25 H16 Er N7 O6 S	C24 H16 Er N7 O9	C24 H16 N7 O9 Pr
Formula weight	729.54	709.77	713.70	687.35
Temperature	150(2) K	150(2) K	150(2) K	150(2) K
Wavelength	0.71073 Å	0.71073 Å	0.71073 Å	0.71073 Å
Crystal system	Triclinic	Monoclinic	Monoclinic	Monoclinic
Space group	P -1	C 2/c	C 2/c	P 2_1/n
Unit cell dimensions	a = 7.48100(10) Å	a = 10.4550(3) Å	a = 10.9960(3) Å	a = 11.1236(2) Å
	b = 9.4450(2) Å	b = 15.2890(4) Å	b = 17.8130(4) Å	b = 17.9711(4) Å
	c = 19.7330(5) Å	c = 15.8710(4) Å	c = 12.9740(4) Å	c = 13.0164(3) Å
	α= 91.961(1)°.	α= 90°.	α= 90°.	α= 90°.
	β= 93.300(1)°.	β= 98.494(2)°.	β= 100.529(1)°.	β= 100.484(1)°.
	γ = 109.423(1)°.	γ = 90°.	γ = 90°.	γ = 90°.
Volume	1310.65(5) $Å^3$	2509.10(12) $Å^3$	2498.45(12) $Å^3$	2558.58(9) $Å^3$
Z	2	4	4	4
Density (calculated)	1.849 Mg/m^3	1.879 Mg/m^3	1.897 Mg/m^3	1.784 Mg/m^3
Absorption coefficient	2.908 mm^{-1}	3.485 mm^{-1}	3.429 mm^{-1}	1.972 mm^{-1}
F(000)	720	1388	1396	1360
Crystal size	0.32 x 0.18 x 0.08 mm^3	0.20 x 0.10 x 0.08 mm^3	0.23 x 0.10 x 0.04 mm^3	0.33 x 0.25 x 0.05 mm^3
Theta range for data collection	3.62 to 27.47°.	2.96 to 27.48°.	3.59 to 25.35°.	2.93 to 27.48°.
Index ranges	-9<=h<=9, -12<=k<=12, -25<=l<=25	-13<=h<=13, -19<=k<=19, -20<=l<=20	-13<=h<=12, -19<=k<=21, -15<=l<=13	-14<=h<=14, -23<=k<=23, -16<=l<=16
Reflections collected	15300	19410	9574	26139
Independent reflections	5961 [R(int) = 0.0548]	2873 [R(int) = 0.0647]	2290 [R(int) = 0.0601]	5856 [R(int) = 0.0543]
Completeness to theta = 25.00°	99.2 %	99.7 %	99.7 %	99.8 %
Absorption correction	Multiscan	Multiscan	Multiscan	Multiscan
Max. and min. transmission	0.8007 and 0.4564	0.7679 and 0.5424	0.8750 and 0.5060	0.995 and 0.894
Refinement method	Full-matrix least-squares on F^2	Full-matrix least-squares on F^2	Full-matrix least-squares on F^2	Full-matrix least-squares on F^2
Data / restraints / parameters	5961 / 0 / 374	2873 / 0 / 183	2290 / 0 / 187	5856 / 0 / 370
Goodness-of-fit on F^2	1.045	1.136	1.186	1.151
Final R indices [I>2sigma(I)]	R1 = 0.0308, wR2 = 0.0674	R1 = 0.0326, wR2 = 0.0812	R1 = 0.0257, wR2 = 0.0603	R1 = 0.0375, wR2 = 0.0860
R indices (all data)	R1 = 0.0373, wR2 = 0.0702	R1 = 0.0463, wR2 = 0.1023	R1 = 0.0339, wR2 = 0.0726	R1 = 0.0565, wR2 = 0.0917
Largest diff. peak and hole	1.092 and -1.381 $e.Å^{-3}$	0.824 and -1.465 $e.Å^{-3}$	0.783 and -1.859 $e.Å^{-3}$	0.968 and -1.383 $e.Å^{-3}$

Identification code	bath31	bath29
Empirical formula	C23 H25 La O9	C41 H35 La N4 O8
Formula weight	584.34	850.64
Temperature	150(2) K	150(2) K
Wavelength	0.71073 Å	0.69040 Å
Crystal system	Triclinic	Monoclinic
Space group	P -1	C 2/c
Unit cell dimensions	a = 8.9379(3) Å	a = 27.691(3) Å
	b = 9.9350(4) Å	b = 14.1822(15) Å
	c = 14.7534(6) Å	c = 9.8010(11) Å
	α= 92.092(1)°.	α= 90°.
	β= 95.497(1)°.	β= 93.583(2)°.
	γ = 114.300(1)°.	γ = 90°.
Volume	1184.34(8) $Å^3$	3841.5(7) $Å^3$
Z	2	4
Density (calculated)	1.639 Mg/m^3	1.471 Mg/m^3
Absorption coefficient	1.853 mm^{-1}	1.170 mm^{-1}
F(000)	584	1720
Crystal size	0.12 x 0.04 x 0.02 mm^3	0.20 x 0.01 x 0.01 mm^3
Theta range for data collection	2.26 to 29.86°.	2.52 to 28.91°.
Index ranges	-11<=h<=11, -13<=k<=13, -20<=l<=20	-26<=h<=38, -19<=k<=18, -13<=l<=13
Reflections collected	11496	12708
Independent reflections	6114 [R(int) = 0.0168]	5029 [R(int) = 0.0450]
Completeness to theta = 25.00°	89.6 %	91.0 %
Absorption correction	SADABS	SADABS
Max. and min. transmission	0.9639 and 0.8082	0.9884 and 0.7998
Refinement method	Full-matrix least-squares on F^2	Full-matrix least-squares on F^2
Data / restraints / parameters	6114 / 0 / 314	5029 / 0 / 158
Goodness-of-fit on F^2	0.976	1.055
Final R indices [I>2sigma(I)]	R1 = 0.0257, wR2 = 0.0626	R1 = 0.0665, wR2 = 0.1936
R indices (all data)	R1 = 0.0278, wR2 = 0.0629	R1 = 0.0992, wR2 = 0.2086
Largest diff. peak and hole	1.264 and -0.422 $e.Å^{-3}$	1.296 and -0.834 $e.Å^{-3}$

APPENDIX II

SERVICE CRYSTALS

No.	Molecular Formula	Crystal Structure	Crystal Code
1.	C24 H19 Au Br P S	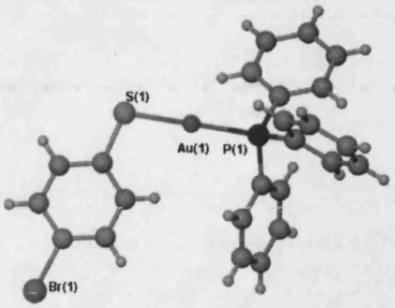	K03prr24 H03prr29
2.	C10 H7 O3	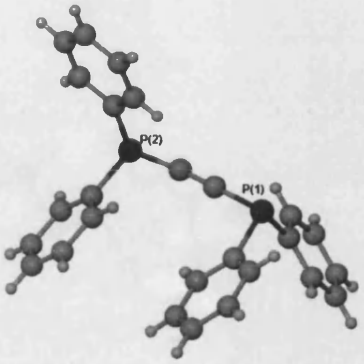	H01prr13
3.	C26 H0 P2	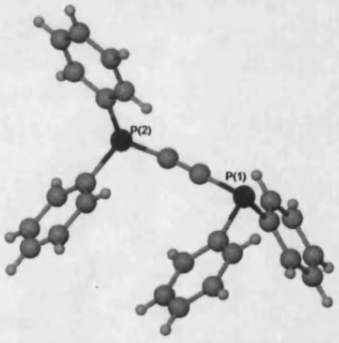	H02prr12
4.	C24 H18 Fe2	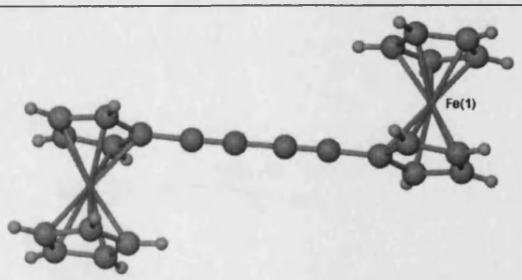	H03prr21

5.	C36.5 H32 O2.5 P2	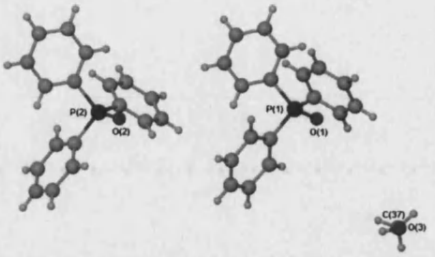	K02prr18
6.	C52 H40 N4	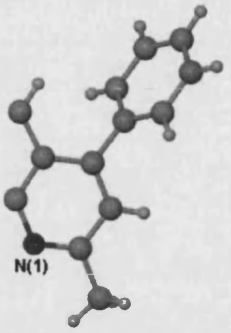	K02prr23
7.	C24 H54 Cl2 P2 Pt	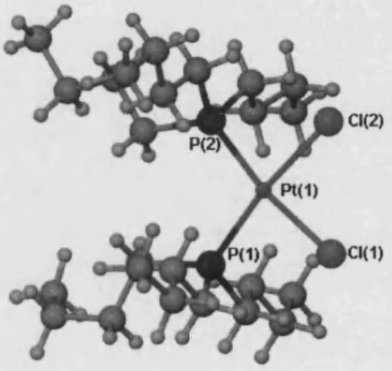	K02prr24
8.	C32 H59 Cl P2 Pt	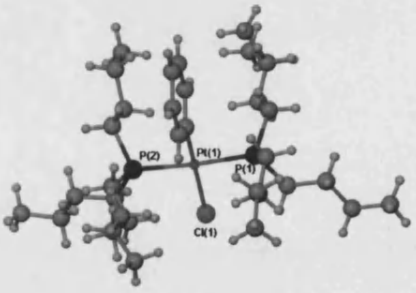	K03prr15
9.	C14.5 H10.5 Fe1 N0.5	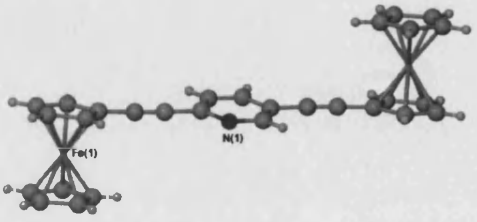	K03prr23

10.	C122 H98 P Pt2	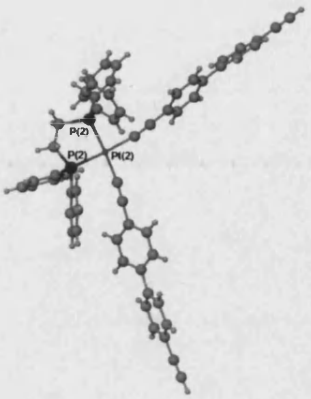	K03prr32
11.	C33 H22 B N O2	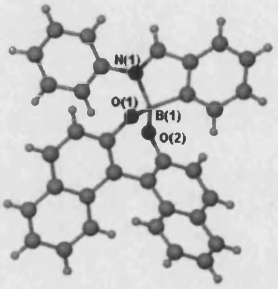	H01tdj3
12.	C34 H26 B N O2	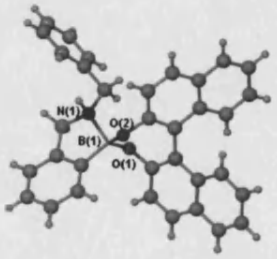	H01tdj4
13.	C35 H25 B Cl3 N O2	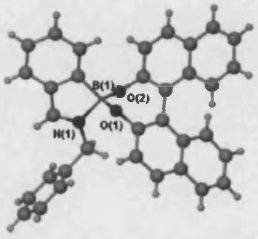	K01tdj5
14.	C20 H20 B N O6	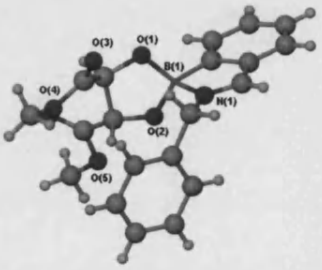	K02tdj1

APPENDIX III

LIST OF PUBLICATIONS

1. Diop, C.A.K, Mahon, M.F., Molloy, K.C., Ooi, L., Raithby, P.R., Venter, M. M. and Teat, S.J. 'Supramolecular lattices built from di- and tri-tetrazoles: the structures of 1,3,5-tritetrazol-5-ylbenznen bis-dioxane monohydrate and ditetrazol-5-ylmethane; Cyst. Eng. Comm., 2002, 4(76), 462-466.

2. Cotton,S.A., Franckevicius, V., How, R.E., Ahrens, B., Ooi, L., Mahon, M.F., Raithby, P.R. and Teat S.J. 'Synthesis of complexes of 2,2':6'2" – terpyridine and 1,10-phenanthroline with lanthanide thiocyanates; the molecular structures of [Ln(terpy)2(NCS)3] (Ln= Pr, Nd), [Nd(terpy)2(NCS)3].EtOH and [Ln(phen)3(NCS)3].EtOH (Ln = Pr, Nd); Polyhedron, 2003, 22 (11), 1489-1497.

3. Chawdhury, N., Long, N.J., Mahon, M.F., Rooke, S., Ooi, L., Raithby, P.R., White, A.J.P., Williams D. J. and Younus, M. Synthesis and Characterisation of Aromatic Ethynyl Bridged Ferrocenes; J. Organometal. Chem.; Submitted.

4. Ooi, L., Raithby, P.R., Monge, C.M. 'Unprecedented formation of some interesting polymeric lanthanum complexes'; Cryst. Eng. Comm. In preparation

5. Griffin, A., Ooi, L., Raithby, P.R., Sparkes, H.A., Bowes, K., Cole, J., 'Structural Study of Terpyridine'; In preparation.

1. Diop, C.A.K, Mahon, M.F., Molloy, K.C., Ooi, L., Raithby, P.R., Venter, M. M. and Teat, S.J. 'Supramolecular lattices built from di- and tri-tetrazoles: the structures of 1,3,5-tritetrazol-5-ylbenznen bis-dioxane monohydrate and ditetrazol-5-ylmethane; Cyst. Eng. Comm., 2002, 4(76), 462-466.

2. Cotton,S.A., Franckevicius, V., How, R.E., Ahrens, B., Ooi, L., Mahon, M.F., Raithby, P.R. and Teat S.J. 'Synthesis of complexes of 2,2':6'2" – terpyridine and 1,10-phenanthroline with lanthanide thiocyanates; the molecular structures of [Ln(terpy)2(NCS)3] (Ln= Pr, Nd), [Nd(terpy)2(NCS)3].EtOH and [Ln(phen)3(NCS)3].EtOH (Ln = Pr, Nd); Polyhedron, 2003, 22 (11), 1489-1497.

3. Chawdhury, N., Long, N.J., Mahon, M.F., Rooke, S., Ooi, L., Raithby, P.R., White, A.J.P., Williams D. J. and Younus, M. Synthesis and Characterisation of Aromatic Ethynyl Bridged Ferrocenes; J. Organometal. Chem.; Submitted.

4. Ooi, L., Raithby, P.R., Monge, C.M. 'Unprecedented formation of some interesting polymeric lanthanum complexes'; Cryst. Eng. Comm. In preparation

5. Griffin, A., Ooi, L., Raithby, P.R., Sparkes, H.A., Bowes, K., Cole, J., 'Structural Study of Terpyridine'; In preparation.